University of Glasgow

Investigating the interaction between PDE4D7 and DHX9 in the progression of prostate cancer

Tara Simone Busiau
BSc (Hons) Biomedical Sciences

Submitted in fulfilment of the requirements for the Degree of Philosophy

Institute of Cardiovascular and Medical Sciences
College of Medical, Veterinary and Life Sciences

University of Glasgow
June 2020

Abstract

Prostate cancer (PC) is the most commonly diagnosed disease in men, and is considered the second most likely cause of cancer-related death in the Western male population behind lung cancer. In recent years, the rate of disease detection has significantly increased in part due to the successful implementation of the prostate specific antigen (PSA) testing in clinics. Currently, PC is positively diagnosed when PSA levels are detected to be over 4.0 ng/mL in the blood plasma. However, increasing evidence has shown that this number is often misleading and inaccurate. The prostate is known to have a very good blood supply, therefore small amounts of PSA can always be detected. Furthermore, the PSA reflects the state of the whole gland itself rather than indicating the presence of a tumour at this site. As the availability of PSA testing increases, this has also resulted in the detection of false positives as some men have naturally higher levels of PSA than others. On the other hand, some cancers can go undetected as it may have progressed so far that it no longer expresses PSA. Following a positive diagnosis, the most common course of treatment prescribed is androgen deprivation therapy (ADT). ADT refers to the treatments that aim to reduce the effects of testosterone and other androgens by surgically or chemically preventing their production. Although ADT is known as the gold standard in PC treatment, approximately 15% of men fail to respond to this form of therapy. Furthermore, after a mean time of 13-19 months, some men become castration resistant and no longer respond to ADT.

There is currently a need to identify novel biomarkers in order to accurately diagnose and stage the disease. Furthermore, new drug targets need to be identified in order to provide the best course of treatment. Previous work by the Baillie laboratory, in collaboration with Philips Diagnostics, recently identified phosphodiesterase 4D7 (PDE4D7) to be a novel prognostic marker for disease. PDE4D7 expression was shown to be decreased in PC cell lines and primary tumours as the disease progressed to the hormone independent state. The 3',5'-cyclic adenosine monophosphate (cAMP) and protein kinase A (PKA) are known to play a role in disease progression as they mediate downstream signalling pathways that can promote cell growth and disease progression. PDE enzymes

are the only known enzyme family to hydrolyse cAMP, and loss of PDE4D7 expression, in particular, during PC correlates with disease progression. Interestingly, DHX9 has recently been identified as a novel interacting partner for PDE4D7. Work by Dr Ashleigh Byrne identified DHX9 as a novel interactor by using mass spectrometry, and since then DHX9 has become a subject of increased interest in the area of cancer research. DHX9 is an RNA/DNA helicase that is involved in multiple cellular processes, including transcription and maintaining genome stability. DHX9 expression is known to increase as cancers, such as lung and colorectal, progress towards their metastatic stages. Previous work by other lab groups have demonstrated that DHX9 is linked to multiple signalling pathways that are involved in cancer development, such as the mTOR and p53 pathway. Interestingly, DHX9 maps to the PC susceptibility locus, making it an interesting protein to study in the context of PC disease progression and metastasis.

Work in this thesis provides further evidence that PDE4D7 and DHX9 proteins are novel interactors in PC. By using a series of biochemical techniques, PDE4D7 was shown to interact with DHX9 in androgen sensitive PC cell line. By using peptide array technology, I was able to map where this interaction took place and define docking sites on both protein partners. DHX9 was found to bind within the newly identified FLY multi docking site within the upstream conserved region-1 (UCR1) of PDE4D7. Furthermore, PDE4D7 was found to bind within DHX9's helicase core domain, suggesting that it may play a role in regulating its activity. I was able to further validate these binding sites by designing cell permeable peptides designed to disrupt protein binding *in vitro*.

Considering that many PKA substrates are found in complex with PDEs, DHX9 was found to be a PKA substrate *in vitro*. By using biochemical techniques, such as immunoprecipitations and proximity ligations assay, DHX9 was found to be readily phosphorylated by PKA, and this was significantly increased when cells were pre-treated with the adenylate cyclase activator forskolin and the general PDE inhibitor IBMX. By using peptide array technology and bioinformatic predictions, serine 449 within the helicase core of DHX9 was found to be in a PKA motif and phosphorylated by PKA. Interestingly, this serine can be found upstream of the PDE4D7 binding site. Disruption of the interaction between

PDE4D7 and DHX9 led to a significant increase in DHX9 phosphorylation, supporting the idea that PDE4D7 binding regulated DHX9 phosphorylation. Using the information gained in the peptide arrays, a phospho-specific antibody against DHX9 was raised. The newly synthesised antibody was able to detect phosphorylated DHX9 by western blotting and immunofluorescence with confocal microscopy.

Although DHX9 is known to be differentially expressed in multiple cancers, little is known about its function in PC. Silencing of DHX9 expression using siRNA technology significantly inhibited PC cell growth. Interestingly, previous work by Erzikhan et al (2009) demonstrated that inhibiting DHX9's oncogenic activity, by disrupting DHX9's interaction with EWS-FL1 using YK-4-279, significantly decreased growth when assessed by xCELLigence technology. Unfortunately, disruption of this interaction between PDE4D7 and DHX9 did not alter the growth of PC cells following treatment with the cell permeable disruptor peptide. However, the disruption of the interaction between PDE4D7 and DHX9 significantly decreased DHX9's ability to promote R-loop formation when assessed by immunofluorescence and confocal microscopy. Using RPPA analysis, I was also able to show that the loss of DHX9 expression in PC cells can potentially affect the mTOR signalling pathway.

To conclude, this thesis provides further evidence that PDE4D7 and DHX9 form a signalling complex that may be relevant in PC. I was able to map where these interactions took place and design cell permeable peptides that were able to disrupt this interaction. I was also able to show that DHX9 can be readily phosphorylated *in vitro*, and its phosphorylation is partly regulated by its interaction with PDE4D7. Loss of DHX9 expression, and interaction with EWS-FL1, significantly decreases cell growth, and this may partly be due to changes in mTOR pathways. However, future work on this topic is still needed. Unfortunately, due to time constraints, the functional implications of DHX9 phosphorylation was not studied in this thesis and I was not able to use relevant human samples to further validate the relevance of my findings.

Table of Contents

List of Tables

List of Figures

Conferences, Presentations, and Publications

Conferences

2018 Gordon Research Seminar and Conference on Cyclic Nucleotide Phosphodiesterases, Maine, USA.

2018, British Association for Cancer Research Student Conference, Francis-Crick Institute, London, UK

2019, National Cancer Research Institute Conference, SECC, Glasgow, UK.

Poster Presentations

Busiau, T., Findlay, J., MacQuaide, N., Hoffman, R., Baillie, G.S (2018). 'Investigating the role of PDE4D7 in the progression of Prostate Cancer' GRS and GRC conference, Maine, USA.

Busiau, T., Findlay, J., MacQuaide, N., Hoffman, R., Baillie, G.S (2018). 'Investigating the role of PDE4D7 in the progression of Prostate Cancer'. BACR Student Conference, London

Busiau, T., Findlay, J., MacQuaide, N., Edwards, J., Hoffman, R., Baillie, G.S (2018). 'Investigating the interaction between phosphodiesterase 4D7 (PDE4D7) and DHX9 in the progression of Prostate Cancer'. NCRI Conference, Glasgow

Oral Presentations

2017, 3 Minute Thesis Competition, MVLS Heats. "Molecular Role of Phosphodiesterase 4D7 in Prostate Cancer".
https://www.youtube.com/watch?v=B7HKJHexD_M

Publications

Gormley, D. West, K., Busiau, T., Spatt, L.,Priest, R., Osuch, I. (2017) 'Generation of CD46, CD55 and CD59 CRISPR/Cas9 knockout cell lines', Molecular Immunology, 89, p. 169. doi: 10.1016/j.molimm.2017.06.145.

Tibbo, A. J., Busiau, T. and Baillie, G. S. (2019) 'Methods to Investigate Arrestins in Complex with Phosphodiesterases', 1957, pp. 121–137.

Acknowledgements

I would firstly like to thank my supervisor, Prof George Baillie. Thank you so much for all your help and your advice throughout these three year. Thank you so much for believing in me, despite the couple (dozens) of panic attacks I've had in your office. You clearly thought that I could do this despite all the tears I have shed. I will miss your really (bad) dad jokes and the Friday afternoon whiskey tasting when I leave. I don't think I would be the scientist that I am today without your guidance from these last three year. I can't thank you enough for giving me this great opportunity and welcoming me with open arms into your lab. Long live the praying mantis!

Thank you to my secondary supervisor, Prof Joanne Edwards. Although you may have joined this project late, your prostate cancer knowledge has been invaluable! Thank you so much for your support over the past two years. Thank you for being a role model for women in science. Seeing you talk at the recent NCRI conference and being so supportive to your staff was so inspiring to me.

I would also like to thank Dr Ralf Hoffmann for his invaluable contribution to this project. Although we may have met a handful of times in person, our conversations (by email or in person) were always interesting and pushed me to achieve more. Thank you to Philips Research for funding this project and allowing me to be part of this team.

I would also like to thank all the past and present members of the Baillie, Freeman and Fuller lab for making my time in the lab so entertaining. Thank you to Dr Ella Whitely, Dr Bracy Fertig, Alice Main, Jack Beazer, Dr Oom Patanapirunhakit, Xuan Gao, and Dr Dilys Freeman for these past three years. Thank you to Dr Gillian Borland, Dr Gonzalo Sanchez Tejeda, Dr Angie Sin, and Dr Denise Hough for acting as my third supervisors and keeping me on the path of success. My PhD experience has been extremely entertaining, and it has been great to learn alongside like-minded people. Special thanks to my partner in crime, and fellow graduate, Dr Amy J Tibbo. I thank my lucky stars every day that you decided to join the Baillie lab and slot yourself right into my life. Thank you, a million times, for scraping me off the pavement after my many panic attacks and pushing me to get through this. You have made these three years so

memorable, and I don't think I could have gotten through this without you. I will really miss all the fun times we had in the office and can't imagine how it will feel like not working alongside you. Thank you for guiding me through this journey and acting as my life guru, but you're also stuck with me now! To Fiona Jordan, thank you for taking me in as your own adoptive daughter. Your silly jokes and chats in the office have made me feel so welcome in this country I am happy to call home.

Lastly, I would like to thank the members of my family for being supportive of me since day 1. To my mum and dad, Masako and Luc Busiau, for always believing in me despite me being clueless most of my childhood. Seeing you both accomplish so much during my lifetime only pushed me to achieve my own goals. Thank you for supporting me morally (and financially) during my whole education, and I would not be in this position now without your support. To my sister, Mei Busiau, who I have named after one of my all-time favourite movie "Totoro", thank you for being there. Thank you for, almost, always picking up the phone when I call and being supportive, and always giving me great fashion advice. To Kieran Irvine, you have been my rock these past two years. Thank you for keeping me sane even when I am shouting absolute gibberish at you. Thank you for always making me laugh even when I'm feeling sorry for myself. To Toby the Cat, you're the best napping partner.

Author's Declaration

I hereby declare that the following thesis is my own composition and is a record of my own work. Contributions from other members of the Baillie lab have been clearly referenced and included in this thesis with their permission.

This work has not previously been submitted for other degrees and was supervised by Prof George S. Baillie, Prof Joanne Edwards, and Dr Ralf Hoffmann.

Tara S. Busiau

Abbreviations

AC	Adenylyl Cyclase
ACTH	adrenocorticotropin hormone
ADP	Adenosine diphosphate
ADT	Androgen Deprivation Therapy
AF-1	Activation function 1
AF-2	Activation function 1
AI	Androgen Insensitive
AKAP	A-Kinase anchoring protein
AMPK	5' AMP-activated protein kinase
AR	Androgen receptor
AS	Androgen sensitive
ATM	Ataxia telangiectasia mutated
ATP	Adenosine triphosphate
BSA	Bovine serum albumin
CBP	CREB binding protein
CDK	Cyclin-D kinase
CI	Cell index
CNG	Cyclin nucleotide gated channel
CPP	Cell permeable peptide
CREB	cAMP response element-binding protein
CRISPR	Clustered regularly interspaced short palindromic repeats
CRPC	Castration resistant prostate cancer
ctDNA	Circulating tumour DNA
DBD	DNA binding domain
DHEA	Dehydroepiandrosterone
DHT	Dihydrotestosterone
DHX9	DExH-Box Helicase 9
DMSO	Dimethyl sulfoxide
DNA	Deoxyribonucleic acid
DRE	Digital rectal examination
dsRBD	Double stranded RNA binding domain
DTT	Dithiothreitol

EBRT	External Beam Radiation Therapy
ECL	Enhanced Chemiluminescence
EDTA	Ethylenediaminetetraacetic acid
EGF	Epidermal growth factor
EGFR	Epidermal growth factor receptor
EGTA	Ethylene-bis(oxyethylenenitrilo)tetraacetic acid
EPAC	Exchange protein activated by cAMP
ER	Oestrogen receptor
ERG	ETS-related gene
ERK	extracellular signal-regulated kinases
ESFT	Ewing's Sarcoma family tumours
ETS	Erythroblast Transformation Specific transcription factor
EWS	Ewing's Sarcoma
FAK	Focal adhesion kinase
FBS	Foetal bovine serum
FISH	Fluorescent In Situ Hybridization
FL	Full length
FMOC	Fluorenyl methoxycarbonyl protecting group
FP	Fluorescent Polarization
FRET	Fluorescence resonance energy transfer
FSH	Follicle-stimulating hormone
GDP	Guanosine diphosphate
GEF	Guanine nucleotide exchange factors
GEM	Genetically Modified Mice
GPCR	G protein coupled receptor
GST	Glutathione-S-transferase
GTP	Guanosine triphosphate
HA2	Helicase associated domain 2
H&E	Haematoxylin and eosin
HRP	Horse radish peroxidase
IBMX	3-isobutyl-1-methylxanthine
ICC	Immunocytochemistry
IF	Immunofluorescence
IGF	Insulin-like growth factor
IL-6	Interleukin-6

IP	Immunoprecipitation
IPTG	Isopropyl ß- d-1-thiogalactopyranoside
IV	Intravenous
KRAS	Kirsten rat sarcoma
LB	Lysogeny broth
LBD	Ligand binding domain
LH	Luteinizing hormone
LHRH	Luteinizing hormone-releasing hormone
LMB	Leptomycin B
LR1	Linker region 1
LR2	Linker region 2
MAP	Mitogen activated protein
MAPK	Mitogen activated protein kinase
MEK	Mitogen-activated protein kinase kinase
MFI	Mean fluorescence intensity
mP	Millipolarisation
MRI	Magnetic resonance imaging
mRNA	Messenger RNA
MTAD	Minimal transactivation domain
NES	Nuclear export signal
NLS	Nuclear localization signal
NO	Nitric oxide
NPB	Nuclear preparation buffer
NPC	Nuclear pore complex
NTD	Nucleoside diphosphate
NTP	Nucleoside triphosphate
OB-fold	Oligonucleotide/oligosaccharide-binding fold
PAGE	Polyacrylamide gel
PBS	Phosphate-buffered saline
PC	Prostate cancer
PCE	Post-translational control element
PCR	Polymerase chain reaction
PDE	Phosphodiesterase
PDE4D	Phosphodiesterase isoform 4D
PDE4D7	Phosphodiesterase isoform 4D7

PDSM	Phosphorylation-Dependent SUMOylation
PI3KK	Phosphatidylinositol 3-kinase-related kinases
PIN	Prostatic Intraepithelial Neoplasia
PK	Protein Kinase
PKA	Protein Kinase A
PKC	Protein Kinase C
PKG	Protein Kinase G
PLA	Proximity ligation assay
POPDC	Popeye-domain-containing protein
PPI	Protein-protein interaction
PRMT	Protein arginine methyltransferase
PSA	Prostate specific antigen
PTEN	Phosphatase and tensin homolog deleted on chromosome 10
PTM	Post-translational modification
RHA	RNA Helicase A
RNA	Ribonucleic acid
RPM	Rounds per minute
RPPA	Reverse Phase Protein Array
RT	Room temperature
RTCA	Real time cell analyser
SCID	Severe combined immunodeficiency
SDS	Sodium dodecyl sulphate
SEM	Standard error of the mean
SFPQ	Splicing Factor Proline And Glutamine Rich
SHBG	Sex hormone binding globulin
SIM	SUMO interacting motif
SOX	sex determining region Y
SPR	Surface plasmon resonance
TBS	Tris-buffer saline
TBST	Tris-buffer saline with Tween20
TGF	Transforming growth factor
TMPRSS2	Transmembrane Serine Protease 2
TRAMP	Transgenic adenocarcinoma of the mouse prostate
UCR1	Upstream conserved Region 1
UCR2	Upstream conserved Region 2

WB	Western blot
WCL	Whole cell lysate
WGA	Wheat Germ Agglutinin

Chapter 1 Introduction

1.1 Advances in cancer research and treatment

Since the 1970s, a dramatic reduction in the mortality rates of certain cancers has been observed, thanks to the use of classic therapeutic strategies such as chemotherapy, radiotherapy, and surgery (Alvarez and Besa, 2000). Despite this detection and treatment of cancer is increase in almost every country, becoming the most significant public health challenge in the 21st century (Bray *et al.*, 2018). Although cancer is the second leading cause of death in high income counties, the 5 year survival rate following treatment has increased to 70 % in 2020, compared to 49 % in the 1970s (Schilsky *et al.*, 2020). The complexity of cancer at a cellular and molecular level is often considered an obstacle to achieve important changes in the understanding of basic cellular and molecular changes that allow a cell to become cancerous (Alvarez and Besa, 2000). However, in the past decade, many researchers have focused on finding new drug targets and therapeutic strategies to overcome these obstacles (Pucci, Martinelli and Ciofani, 2019).

1.1.1 Precision medicine

Ove the past decade, it has become widely accepted that traditional cancer therapies are ineffective and expensive, often leading to unnecessary side effects. Current therapies do not take into the fact that no two patient cancers are the same, leading to different responses to treatments such as chemotherapy or radiation (Krzyszczyk *et al.*, 2018). Recently, a shift from organ-centric treatment to a more personalised approach for treatment has greatly modernized the field. Tools such as next generation sequencing and RNA sequence has helped to identify novel druggable target for the treatment of different cancers (Gambardella *et al.*, 2020). In recent years, RNA sequencing has become one of the most important tools for transcriptomic profiling. The revolutions from bulk RNA sequencing to single-cell sequencing has enabled researchers to identify novel biomarkers and characterise different types of cancer (Hong *et al.*, 2020). To date, precision medicine has been proved to be highly successful in the identification of new targets in breast, and lung cancer, and in melanoma (Gambardella *et al.*, 2020). Identifying specific molecular

changes, somatic or germline mutations, or gene fusions using these next generations techniques would allow doctors to tailor treatment to their specific cancer, resulting in better patient outcome (Kimmelman and Tannock, 2018). Precision medicine provides the best personalised therapies for cancer patients (Pucci, Martinelli and Ciofani, 2019).

1.1.2 Novel Cancer Therapies

During the last decade, traditional cancer therapy mainly consisted of chemotherapy which maximised damaged to the rapidly dividing cells. But this would often come at the expense of normal cells, leading to a poor quality of life to the patient. The development of new anticancer drugs has rapidly changed this, thanks to a greater understanding of tumour biology and cancer cells (Ramaswami, Harding and Newsom-Davis, 2013). These novel approaches aim to limit the damage to healthy normal cells, while enhacing tumour destruction (Shariff *et al.*, 2019).

One of these novel therapies aims to inhibit the epidermal growth factor receptor (EGFR). EGFR's role in the body is to regulate epithelial tissue development and homeostasis. However, in cancer, EGFR is a driver of tumorigenesis, often caused by mutations, transcriptional upregulation, or ligand overproduction. (Sigismund, Avanzato and Lanzetti, 2018). EGFR is a tyrosine kinase receptor consisting of an extracellular ligand-binding domain, a transmembrane anchoring region, and an intracellular tyrosine kinase. Upon ligand binding, the receptor dimerises, leading to its phosphorylation. This in turn creates a docking site for numerous effector proteins such as PI3K (Gerber, 2008). In recent years, EGFR has increasingly been recognised as a biomarker of resistance in tumours. Mutations and amplification of this receptor has been found to increase under drug pressure (Sigismund, Avanzato and Lanzetti, 2018). The identification of this novel biomarker has greatly impacted the treatment of non-small cell lung cancer (NSCLC). However, the introduction of EGFR inhibitors has greatly improved disease outcome (Gerber, 2008). First generation EGFR inhibitors, such as gefitinib and erlotinib, binds reversibly to the MgATP binding site within the EGFR tyrosine kinase catalytic domain. Studies have shown that binding of these drugs results in reduced cellular proliferation, increased apoptosis, and inhibition of cell migration (Lenz, 2006). Inhibition of the tyrosine

kinase region of EGFR leads to the greatest duration of disease control, the longest overall survival, and the best quality of life (Le and Gerber, 2019).

In addition to inhibiting EGFR, immunotherapy has revolutionised the management of metastatic cancers (Le Saux *et al.*, 2020). Immunotherapies against existing cancers include various approaches, ranging from stimulating the immune system to counteracting inhibitory and suppressive mechanisms (Farkona, Diamandis and Blasutig, 2016). Over the last decade, the primary approach to activate host T-cells against tumour antigens has been through therapeutic cancer vaccination, such as the vaccination against human papillomavirus (Mellman, Coukos and Dranoff, 2011). Alternatively, oncolytic viruses can be engineered in order to selectively replicate in and kill cancer cells (Kaufman, Kohlhapp and Zloza, 2015). These viruses can reduced tumour sizes by causing tumour cell infections, promoting cell lysis, or by inducing the antitumour immunity (Farkona, Diamandis and Blasutig, 2016). However, the most promising of the immunotherapies is the use of chimeric antigen receptor (CAR) engineered T-cells. CAR T-cell therapy involves genetically modifying a T-cell to specifically express a chimeric antigen for a specific tumour antigen, the re-infused back into the patient. These engineered cells are then re-infused back into the patient (Miliotou and Papadopoulou, 2018). CAR T-cells has largely been successful in the treatment of haematological malignancies. Over the last 10 years, clinical trial involving CAR T-cells engineered to express CD19 have shown high and durable response rate in patients suffering from acute lymphoblastic leukaemia and aggressive B-cell non-Hodgkin lymphomas (Leon, Ranganathan and Savoldo, 2020).

1.1.3 Peptide mimetics for the treatment of cancer

In addition to precisions medicine and immunotherapy, peptide therapeutic has become a promising field for emerging anti-cancer agents (Boohaker *et al.*, 2012). Protein-protein interaction have been recognised as key mediators of biological processes and the progression of certain cancers. So far, over 650 000 disease relevant interactions have been identified, and the large majority of these have been deemed “undruggable” due to their highly dynamic nature. However, due to technological improvement, these interactions have slowly emerged as highly interesting drug targets (Mabonga and Kappo, 2020). By

identifying interacting regions that contain hot spots, defined as the residues which are crucial for interaction, researchers have been able to develop novel small molecule inhibitors to block interactions that are known to drive disease (Ma and Nussinov, 2014). Currently, there are over 60 approved peptide drugs for the treatment of different diseases, four of which have been approved for the treatment of cancer (Thundimadathil, 2012). Use of peptide in the treatment of cancer will be discussed in section 3.4.3.

1.2 The human male prostate gland

The prostate gland plays an important role in male reproduction. It contains a system of branching ducts composed of pseudo-stratified epithelium surrounded by a fibromuscular stroma. This gland secretes lipids, enzymes, amines, and metal ions that are essential in the normal function of spermatozoa. The gland itself is the source of some of the most common medical problems of men over the age of 40 (Toivanen and Shen, 2017). Benign inflammation of the prostate occurs in more than 50% of men within this age group, and post-mortem autopsies revealed that 31% of Caucasians and 51 % of African-American men between the age of 70-79 were found to have tumours within their prostate (Jahn, Giovannucci and Stampfer, 2015). Due to high occurrence of benign inflammation, the prostate is susceptible to oncogenic transformation at a significantly higher frequency than that of other accessory glands (Toivanen and Shen, 2017).

The prostate surrounds the urethra at the neck of the urinary bladder. It is the size of a large walnut with a wide base on top. The gland is located underneath the floor of the bladder, and it's narrow apex is directed towards the urogenital diaphragm (Aschoff *et al.*, 2011). The prostatic gland is composed of two distinctive compartments: the epithelium and the stroma. These two compartments interact with each other via androgen receptors (AR) and this interplay is important in the development and differentiation of the prostate (Krušlin, Ulamec and Tomas, 2015). Structurally, it is organised anatomically into four zones: the peripheral (70%), central (25%), transition (5%), and anterior fibromuscular zones (Sidelsky, Setia and Vourganti, 2017) (Figure 1.1).

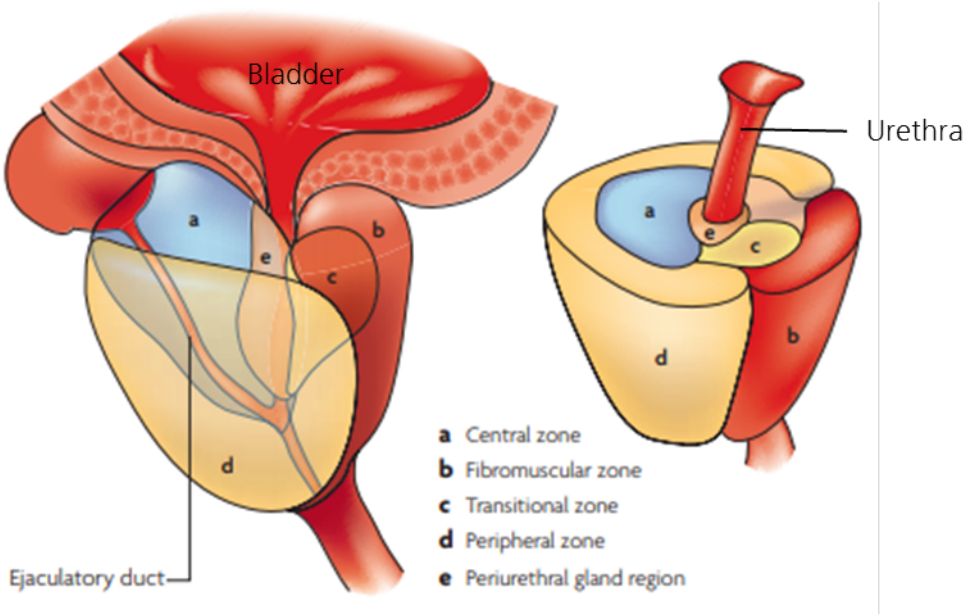

Figure 1.1 Structural organization of the prostate. The prostate is distributed into the peripheral, central, transition, and anterior fibromuscular zones. (Image adapted from Marzo et al. 2007).

The main function of the stromal compartment of the prostate gland is to ensure an appropriate microenvironment for the epithelial compartment. It provides many supportive signals to retain or restore gland homeostasis in healthy conditions or during regeneration processes. In addition, the prostate epithelium has a glandular function as it secretes prostatic fluid that constitutes approximately one fifth to one third of the volume of the entire ejaculate. Prostatic fluid contains a number of factors that control the ejaculation process and regulate the proteins required to activate sperm maturation (Verze, Cai and Lorenzetti, 2016).

1.3 Modelling human prostate cancer using mice

Over the years, mouse models have been used for human cancer research as they have proven to be a useful tool due to their similar genomic and physiological characteristics of tumour biology between mice and humans (Lampreht Tratar, Horvat and Cemazar, 2018). These mouse models have played a central role in the study of disease aetiology, prevention, and treatment of PC. Although multiple cell models have been developed, they do not take into account the numerous cellular interactions within the tumour environment that play a key role in disease initiation and progression (Ittmann *et al.*, 2013). Although the gross anatomy of the mouse prostate is different to that of

humans, the prostate of both species is composed of glands and ducts of similar organisation (Parisotto and Metzger, 2013). Mouse models for PC can be divide into two categories: xenograft models or genetically engineered models (GEM). In xenograft models, PC cell lines are directly implanted into immunocompromised host mice either subcutaneously or injected orthotopically into the prostate (Ittmann *et al.*, 2013). Different PC cell lines have been used to perform various xenograft models that exhibit different features of PC, therefore creating models for different stages of disease (Rea *et al.*, 2016). Although these models have been used in the past, they are faced with significant limitations for the establishment of PC models. In order for PC cell lines to adapt to *in vitro* growth environment, these cells lose their ability to grow in a three-dimensional structure, hence losing their inter- and intra-tumour heterogeneity and unable to accurately reflect major features of human PC (Shi, Chen and Tan, 2019). Furthermore, it has been reported that these xenografts models cannot provide reliable data to support drug development, efficacy and prognosis. Many anticancer drugs have been shown to be potent in xenograft models, only a few of these drugs have been shown to have the same potency when used as a therapy in humans (Sharpless and DePinho, 2006).

The development of genome editing tools over the last three decades have allowed scientists to generate a number of PC mouse models (Parisotto and Metzger, 2013). These genetically modified mouse models can help define the molecular events of prostate tumorigenesis, and can be grouped into two types: those engineered to increase the expression of a specific promoter and those with target deletion of genes (Pienta *et al.*, 2008). These two types of GEM have enabled researchers to validate the biological importance of different molecular changes that occurs during PC tumorigenesis (Ittmann *et al.*, 2013). One of the most well-known GEM mouse model for PC is the transgenic adenocarcinoma of the mouse prostate (TRAMP) model generated and characterized in 1995-1997 (Valkenburg and Williams, 2011). TRAMP mice are known to display high grade prostatic intraepithelial neoplasia (PIN) or prostate cancer by 10-12 weeks of age due to the overexpression of SV-40 T-antigen (TAG) by rat probasin gene promoter (Gelman, 2016). Since its characterization, this model has been used to investigate the roles of specific pathway mediators, transcription factors, or metabolic pathways in PC progression (Gelman, 2016). With over 400

publications to date, the TRAMP model has been extensively used in PC research and drug discovery (Ittmann *et al.*, 2013).

1.4 Development of prostate cancer

Prostate cancer (PC) is the most commonly diagnosed malignancy and the second leading cause of cancer-related deaths in the Western male population (Rawla, 2019). The high incidence can be attributed to modern day increased life expectancy as well as the implementation of prostate specific antigen (PSA) testing (Hessels *et al.*, 2007). Many PC are diagnosed based on the elevated levels of PSA in the plasma (>4.0 ng/mL) (Rawla, 2019). However, in recent years, this test has been found to have problems with specificity and sensitivity. Although the screening of PC allows for early diagnosis and better management of disease, the use of the PSA testing has slowly become controversial (Stavridis *et al.*, 2010). The prostate gland is known to have a very good blood supply, therefore small amounts of PSA is constantly present in the bloodstream. Rather than only being expressed at the point of disease, levels of PSA reflects the whole gland instead of the presence of a tumour specifically (Reynard, Peters and Gillatt, 1995). When using the 4.0 ng/mL cut off, over 91% of men are positively diagnosed with PC, but this also leads to the increase in morbidity and the prescription of unnecessary procedures because their PSA may have been elevated due to benign conditions (David and Gopal, 2020). As the availability of the PSA testing has increased, this has also resulted in the increased in the detection of false positive PC as some men have naturally increased levels of PSA without cancer. This in turn leads to performing unnecessary biopsies as well as overtreatment. On the other hand, certain cancers can go undetected as they are either asymptomatic or do not show the typical elevated levels of PSA (Wilt, 2003; Rawla, 2019). There is currently a need to overcome these sensitivity and specificity issues in order to provide a more accurate diagnosis.

1.4.1 Steroid signalling in prostate cancer

1.4.1.1 Androgen biosynthesis

The two most important endogenous androgens are testosterone and dihydrotestosterone (DHT). Androgens are traditionally considered male sex

steroids responsible for the maintenance of male characteristics via the activation of the AR and its downstream signalling pathway (Freeman, Bloom and McGuire, 2001). Under normal physiological conditions, about 60% of circulating androgens are produced in the testicles. The remaining 40% derives from dehydroepiandrosterone (DHEA) synthesised in the zona reticularis of the adrenal glands (Pippione *et al.*, 2017).

The overall rate of steroidogenesis is controlled by peptide hormones, such as adrenocorticotropin hormone (ACTH), follicle stimulating hormone (FSH), and luteinizing hormone (LH). Binding of these peptide hormones to it's appropriate G-protein couple receptor (GPCR) leads to the activation of the cAMP dependent PKA signalling pathway. Stimulation of the cAMP-PKA cascade promotes the increased delivery of circulating cholesterol into the mitochondria of the Leydig cells or the adrenal gland (Hu *et al.*, 2010; Prough, Clark and Klinge, 2016). All steroid hormones are produced from cholesterol through a cascade of enzymes (Figure 1.2). In the mitochondria, cholesterol is converted to pregnenolone by P450scc, which is then further converted to DHEA by 17α-hydroxylase and 17,20 lyase. DHEA is then rapidly converted to testosterone by 3ß-hydroxysteroid dehydrogenasetype II or 17 ß -hydroxysteroid dehydrogenase III enzymes. Testosterone can be further processed into DHT by 5α-reductase (Miller, 2002; Singh *et al.*, 2005; Flück and Pandey, 2014; Miller and Auchus, 2019). The majority of circulating testosterone exists bound to carrier protein sex hormone binding globulin (SHBG) or albumin. (Heemers and Tindall, 2007).

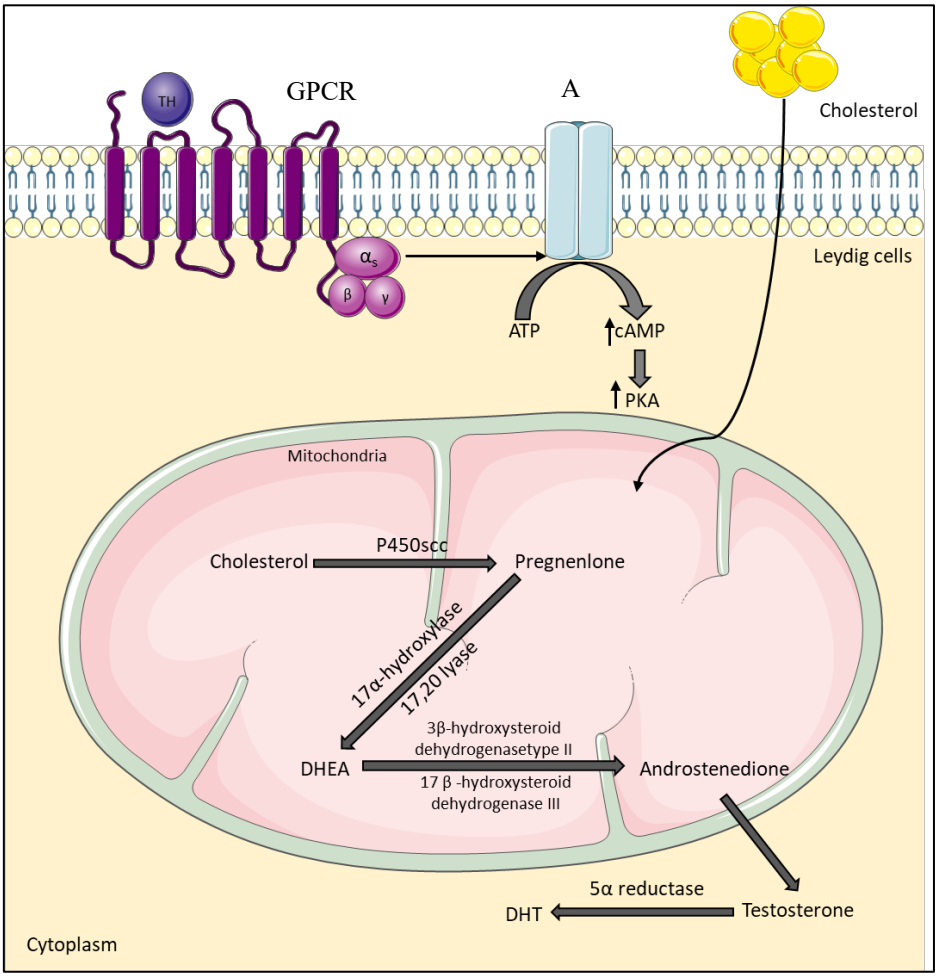

Figure 1.2: Androgen biosynthesis in Leydig cells. G-protein coupled receptor (GPCR) activation by binding of a tropic hormone (TH) leads to the activation of adenylyl cyclase (AC) leading to an increase level of PKA in the cytoplasm. Activation of the cAMP-PKA signalling pathway increases the delivery cholesterol into the mitochondria of the cell. Cholesterol is then sequentially enzymatically cleaved in order to produce testosterone.

1.4.1.2 Androgen receptor and signalling

The AR is a member of the steroid and nuclear receptor superfamily (Bennett *et al.*, 2010). The gene encoding this receptor can be found on the long arm of the X chromosome, more precisely at position Xq11-Xq12 (Tan *et al.*, 2015). Structurally, the AR compromises three main functional domains: The N-terminal transcriptional regulation domain (NTD), the DNA binding domain (DBD), and the ligand binding domain (LBD) (Figure 1.3). While the DBD remains highly conserved between the different members of the steroid hormone nuclear receptor family, the N-terminal region is highly variable (Davey and Grossmann, 2016). The LBD of the AR is only moderately conserved among the receptors, and contains activation function-2 (AF2) which is important for the ligand-dependent activation of the receptor (Culig *et al.*, 2003; Tan *et al.*, 2015). The activation function-1 (AF1) domain, located in the NTD, plays a pivotal role in AR function

and significant loss in AR's transcriptional activity can be seen when AF-1 is deleted (Culig *et al.*, 2003). The lysine rich hinge region between the DBD and LBD regions are important for the nuclear localization of the receptor. Deletion of this hinge region eliminates nuclear localization and transcriptional activity of the AR in the presence of a ligand (Culig *et al.*, 2003). All three domains are important for receptor function. The DBD region tethers the AR to a promoter and enhancer regions of AR regulated genes, or androgen responsive elements, by direct DNA binding to allow the activation functions of the NTD and LBD to stimulate transcription of these genes (Tan *et al.*, 2015, Green, Mostaghel and Nelson, 2012).

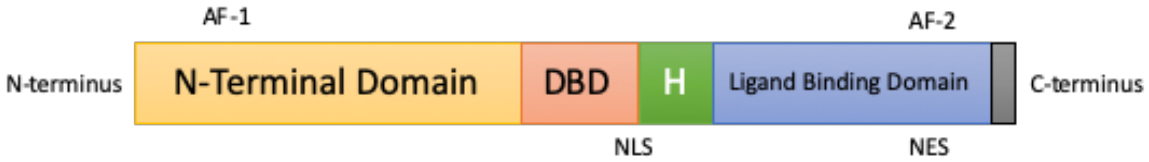

Figure 1.3 Functional domains of the AR. The N-terminal domain contains the activation function-1 domain (AF-1). The N-terminal domain is then followed by the DNA binding domain (DBD), the hinge region (H). The Ligand binding domain contains the activation function-2 domain (AF-2). Nuclear localization signal (NLS) and nuclear export signal (NES) are responsible for transporting the AR in and out of the nucleus.

In the absence of a ligand, the AR resides primarily in the cytoplasm in association with heat shock proteins (HSPs) as a monomer in an inactivate but highly responsive state. Nuclear import of the AR is crucial for its function. Upon ligand binding, the nuclear localization signal (NLS) is recognised in the cytoplasm by the importin-α/β complex allowing the receptor to move through the nuclear pore and into the nucleus (Cutress *et al.*, 2008). Alternatively, AR can be activated via phosphorylation at multiple sites along the protein. Phosphorylation at these different sites has been implicated in a number of different cellular responses, including AR transcriptional activity, regulation of AR expression, cell growth, and AR degradation (Daniels *et al.*, 2013). In response to androgen binding, Ser^{81} within the N-terminal transactivation domain is the most highly phosphorylated site within the AR (Russo *et al.*, 2018). AR can be phosphorylated by multiple kinases at this site, including cyclin-dependent kinase CDK1, CDK5, and CDK9, all of which are able to increase the transcriptional activity of AR as well as promoting its translocation into the nucleus (Daniels *et al.*, 2013).Translocation of the androgen/AR complex into the nucleus leads to the dimerization of the receptor, where it can then bind to

androgen response elements (ARE) target genes and modulate gene transcription (Davey and Grossmann, 2016). AR dimers recruit an array of factors, including co-activators and mediators of proteins whose enzymatic activities promote chromatic remodelling and transcriptional regulation of target genes, leading to cell differentiation, survival and proliferation (Figure 1.4) (Burnstein, 2005).

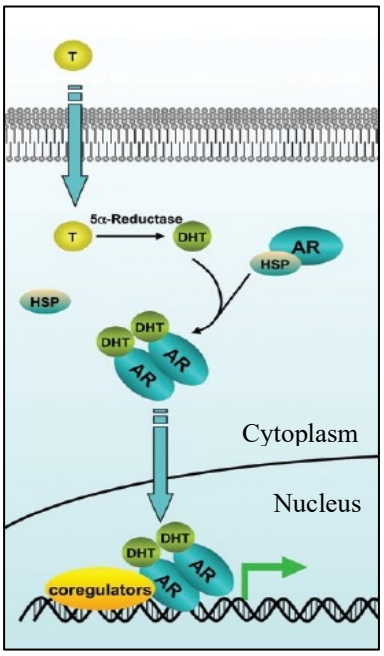

Figure 1.4 Classical androgen receptor signalling pathway. Binding of androgen or DHT, AR dimerizes and translocate to the nucleus where it can then bind to DNA. When bound to DNA, the AR forms a complex with co-activators, co-regulatory proteins, or ARE. Figure taken from Davey and Grossmann, 2016.

1.4.2 Initial development of prostate cancer

Although the prostate depends on androgens for normal prostate development, alone it does not promote the development of disease. Instead, PC development involves the accumulation of cancerous epithelial cells (Knudsen and Vasioukhin, 2010). The AR signalling pathway is vital for the normal functioning of the prostate. However, it also plays a pivotal role in prostate carcinogenesis and the progression to androgen-independent disease (Lonergan and Donald, 2011). In the normal prostate, the rate of cell death is 1-2% per day, which is balanced by a 1-2% rate of proliferation (Heinlein and Chang, 2002). Both healthy and malignant prostate growth depends on the ratio of cells proliferating to those dying. Androgens are the main regulator of this ratio by both stimulating proliferation and inhibiting apoptosis (Feldman and Feldman, 2001). However, this balance is disrupted in prostate cancer, with the rate of proliferation overtaking the rate of cell death (Kim *et al.*, 2017). The initiation of PC can be attributed to the activation of a distinct growth-promoting pathway. In a study

analysing 11 early-onset PC cases, an increase in the prevalence of structural rearrangements enriched in the AR binding sites was identified with 10 out of 11 cases having the androgen driven *Erythroblast Transformation Specific (ETS)* gene fusions (Russo and Balk, 2018). Most of these fusions were the *Transmembrane Serine Protease 2* (*TMPRSS2):ETS related gene (ERG)* fusions found in approximately 50% of PC. The presence of this rearrangement is a critical event in the development of disease (Hägglöf *et al.*, 2014), with the fusions only been identified only in clinically localised and hormone-refractory metastatic PC (Tomlins *et al.*, 2009).

TMPRSS2 is a serine protease that is highly expressed in the epithelium of the human prostate gland and depends on the binding to an ARE for its expression (Chen *et al.*, 2010). ERG is a member of the ETS family of transcription factor, with a role in the development and differentiation of a wide range of tissue and cell types (Adamo and Ladomery, 2016). This gene translocation occurs early during disease formation as it can be detected in precursor prostatic intraepithelial neoplasia lesions (PIN) (Cai *et al.*, 2009). In PC, ERG can recruit the AR to novel genomic loci as well as co-bind to AR binding sites across the chromatin. This interaction leads to an alteration in the transcriptional output induced by the activation of the AR signalling pathway (Kron *et al.*, 2017). The *TMPRSS2:ERG* gene fusion leads to an overexpression of a N-terminal truncated ERG protein that is still transcriptionally active (Zhou *et al.*, 2019). This leads to an increase in *ERG* mRNA expression in 62% of PC (J. Wang *et al.*, 2006), which may lead to the activation of pathways related to the initiation and progression of PC via the cGMP-PKG pathway (Zhou *et al.*, 2019).

Although AR activation most commonly stimulates growth through the *TMPRSS2:ERG* gene translocation (Sharifi, 2013), the ability of AR to activate and cross talk with other signalling pathways is known to contribute to disease initiation and progression (Kaarbø, Klokk and Saatcioglu, 2007). One such pathways is the phosphoinositide 3-kinase (PI3K)/Akt/ mammalian target of rapamycin (mTOR) pathway (Kaarbø *et al.*, 2010). Activation of PI3K leads to the generation of the secondary messenger phosphatidylinositol 3,5-triphosphate (PIP3). This in turn leads to the recruitment and activation of the Akt kinase, which is then able to translocate to the nucleus to promote cell growth and proliferation. Akt is negatively regulated by tumour suppressor phosphatase and

tensin homolog deleted on chromosome 10 (PTEN) (Lonergan and Donald, 2011). Activation of this pathways leads to PC progression due to its ability to integrate intra- and extracellular growth factors which are critical to cellular processes. This pathway is frequently overactive in advanced PC due to the loss of the tumour suppressor PTEN (D. E. Butler *et al.*, 2017). 30% of PC tumours are known to no longer express PTEN, which in turn leads to the constitutive activation of the PI3K/AKT/mTOR signalling pathway (Crumbaker, Khoja and Joshua, 2017). Interestingly, the AR and PI3K/AKT/mTOR signalling pathways are known to be activated in androgen sensitive (AS) cell line LNCaP. Combined inhibition of these two pathways using small molecular inhibitors results in an enhanced antitumoral activity in this cell line, indicating that these two pathways work synergistically in order to promote the progression of disease (Thomas *et al.*, 2013).

In addition to its transcriptional activity, AR is known to play a role in regulating the cell cycle machinery (Schiewer, Augello and Knudsen, 2012). While in the G1 phase, mammalian cells evaluate growth-promoting or growth inhibitory cues within their environment in order to progress through the mitotic cycle of enter quiescence. These cells depend on the cyclin-dependent kinases (Cdk) in order to regulate its transition through the mitotic cycle by promoting or inhibiting phosphorylation, binding to cyclins, and binding to CDK inhibitors (Knudsen, Arden and Cavenee, 1998). Studies have shown that androgen deprivation causes G0-G1 cell cycle arrest, while androgen stimulates cellular proliferation (Xu *et al.*, 2006). Androgens have been shown to increase Cdk activity and stimulate cells to enter the S-phase of the cell cycles, which in turn promotes cellular proliferation (Lu, Tsai and Tsai, 1997). Not only is AR and androgens able to stimulate disease via its transcriptional activity, but its interaction with multiple signalling pathways and its ability to contribute to their activation plays an important role in disease initiation and progression.

1.4.3 Progression into castration resistant prostate cancer

Androgen deprivation therapy (ADT) has been the primary standard of care in patients with locally advance PC. ADT generally leads to a decrease in PSA level and disease remissions in about 90 % of patients (Huang *et al.*, 2018). Unfortunately, after an average time of 2-3 years, the disease progresses despite

continuous hormone therapy. This PC is known as castrate-resistant PC (CRPC) (Karantanos, Corn and Thompson, 2013). CRPC is defined as disease progression following initial ADT and may present with an increased rise in serum PSA, progression of pre-existing disease, androgen insensitivity (AI), or the appearance of new metastases (Hotte and Saad, 2010). It has been shown that CRPC is characterised by the overexpression or hyperactivation of the AR (Nadiminty and Gao, 2012), despite being in an environment of serum testosterone below 50 ng/dL in the blood (Gomella, 2003). It is thought that the mechanisms involved in CRPC development include AR gene amplification and mutation, overexpression of co-activators, activation of growth factors, and cross-talk with other transcription factors and signalling pathways (Figure 1.5) (Nadiminty and Gao, 2012).

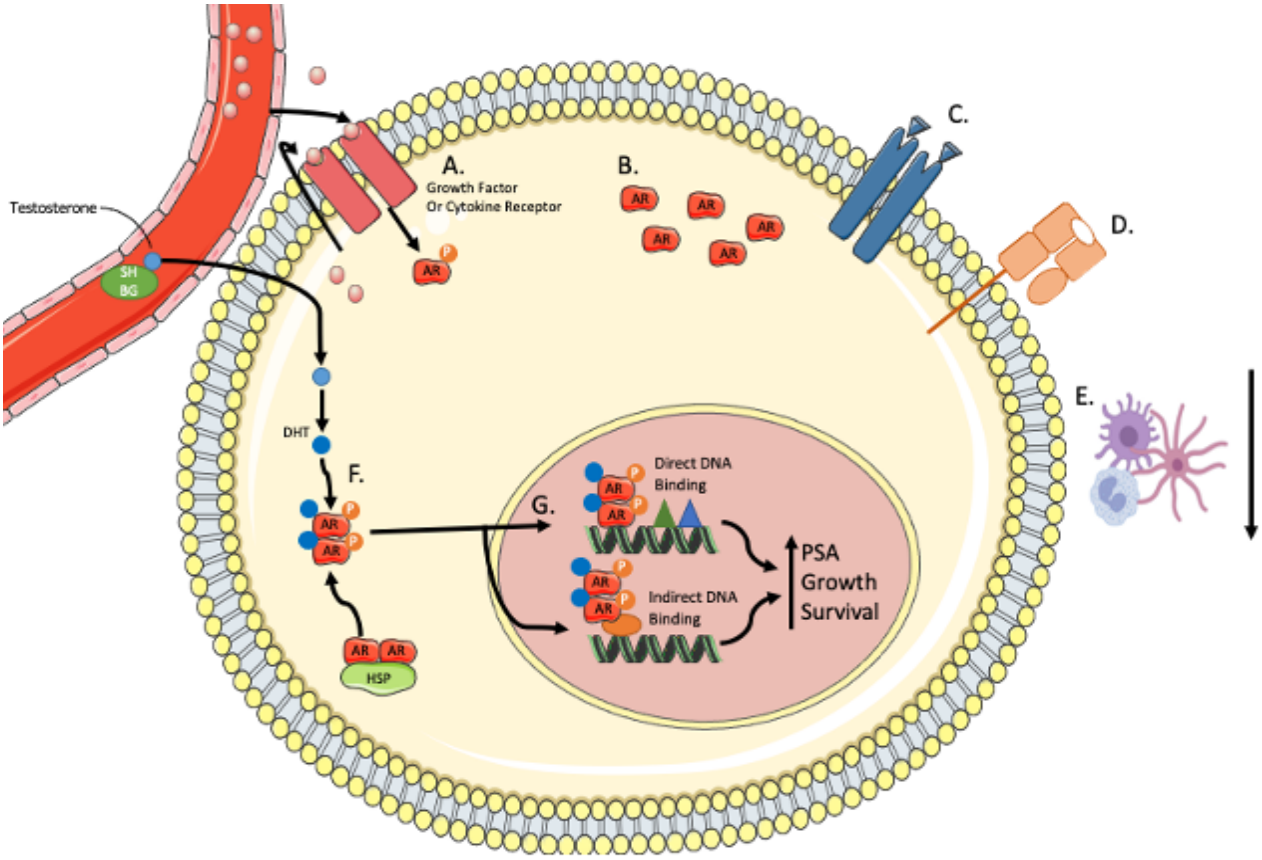

Figure 1.5 Known mechanism that leads to metastatic prostate cancer, including immune evasion. Although ADT is successful in most patients, they often progress to the more aggressive CRPC phenotype. CRPC is known to be androgen insensitive and unresponsive to AR inhibitors. Multiple mechanisms have been identified and illustrated above (A-G). These mechanisms are known to be resistant to ADT and associated with complex molecular alterations, all leading to the increase in PSA expression, increased growth and PC cell survival. **A.** Crosstalk with other activated receptors leads to the phosphorylation of the androgen receptor. **B.** Amplification of AR. **C.** Chronic IFN1 pathway activation. **D.** Loss of MHC Class I expression. E. Decreased chemotaxis of inflammatory immune cells. **F.** Autocrine hormone production and AR mutations. **G.** Altered expression or activity of co-activators and co-repressors. (Mills, 2014; Vitkin *et al.*, 2019).

1.4.3.1 Increased expression and amplification of AR

Increased AR expression is one of the most frequent changes in CRPC and is highly associated with resistance to anti-androgen. Using fluorescent in situ hybridization staining (FISH), Visakorpi et al. (1995) and Koivisto et al (1997) have seen an amplification in the *AR* gene in 30% and 28 % of recurrent tumours respectively (Visakorpi *et al.*, 1995; Koivisto *et al.*, 1997). Interestingly, Visakorpi et al. reports that this gene amplification was not observed in primary tumours (Visakorpi *et al.*, 1995) suggesting that *AR* amplification is an adaptive response to ADT (Jernberg, Bergh and Wikström, 2017). It has been suggested that AR gene amplification can lead to an increase in AR expression due to a gene dosing effect, which in turn can contribute to androgen resistance. The addition of even one gene copy of AR has been shown to increase AR expression, suggesting that even a small change gene dosage can dictate disease and therapy outcome (Edwards *et al.*, 2003). Furthermore, the amplification of the *AR* gene sensitizes PC cells to castration levels of androgens. Research lead by Fujimoto et al (2007) has shown that stimulation with DHT lead to a 4-fold increase in nuclear AR expression in late stage androgen insensitive (AI) cells when compared to early stage androgen sensitive (AS) cells. It is thought that the increase in AR protein can contribute to androgen hypersensitivity as well as disease progression (Fujimoto *et al.*, 2007). However, work by Edwards et al (2001), has suggested that AR gene amplification is not solely to blame for the development of antiandrogen-resistance PC. By studying paired tumours (early vs late-stage tumours) from 20 different patients, Edwards et al (2001) were able to investigate if AR gene amplification alone heavily contributes to CRPC progression. Of the 20 patients, only three patients were shown to have AR gene amplification after hormone relapse (Edwards *et al.*, 2001).

1.4.3.2 AR mutations

To date, 159 AR mutations have been identified in PC tissues, and most of these mutations are single-base substitutions (Eisermann *et al.*, 2013). Approximately 45% of these mutations occurs in the LBD, while 30% of mutations occurs in exon 1 (Gottlieb *et al.*, 2012). The most frequently detected AR mutation is T878A, which is a gain of function mutation that can be activated by both steroid hormones and first-generation antiandrogens (Jernberg, Bergh and Wikström,

2017). This mutation is also associated with resistance to abiraterone (Rathkopf *et al.*, 2017). A study by Romanel et al (2015) has shown that men who have this mutation in circulating tumour DNA (ctDNA) have a lower PSA response rate and shorter survival time following abiraterone treatment when compared with men with a wild-type AR gene (Romanel *et al.*, 2015).

1.4.3.3 AR splice variants

AR-variants have recently emerged as important players in PC progression as well as drug resistance. More than a dozen variants lacking the ligand binding domain have been identified from human PC cell lines and xenografts (Xu and Qiu, 2016). Increased expression of these variants has been associated with persistent AR activity after ADT (He *et al.*, 2018), as well as resistance to enzalutamide and abiraterone (Armstrong and Gao, 2019). AR-variant 7 (AR-V7) is the most widely studied of these variants, and its expression is known to be increased in patients that have progressed to CRPC. Expression of this variant has only been detected in response to primary ADT (Sharp *et al.*, 2019). It has been shown that in AR-V7 dependent CRPC, full-length AR binds to AR-V7 to repress transcription of growth-suppressive genes. Silencing of either full length AR or AR-V7 significantly decreases cell growth in CRPC cell models (Cato *et al.*, 2019). Work by Guo (2009) showed that not only does the expression of this splice variant increase between early and late stage disease, but AR-V7 expression is found to increase within the nuclear region in hormone-refractory tumours. Immunohistochemical staining of over 429 human tissue microarrays showed that ARV7 expression was significantly increased during PC progression. Interestingly, these stains also revealed that 44 % of AR-V7 in hormone resistant tumours samples was localised in the nucleus. In contrast, only 9% of AR-V7 was found in the nucleus when compared to their pair hormone-naïve tumours. AR-V7 expression significantly increases within the nuclear regions of hormone-resistant tumours, suggesting that the expression of this splice variant can drive PC progression (Guo *et al.*, 2009)

1.4.3.4 Alterations in cofactor recruitment

Due to its direct interaction with the receptor, AR cofactors have the ability to stimulate or repress the transcriptional activity of AR function (Heinlein and

Chang, 2002; Fujita and Nonomura, 2018). It has recently been shown that multiple AR-associated cofactors are able to modulate and reprogram AR binding events (Augello, Den and Knudsen, 2014). In recent years, researchers have observed diverse expression patterns of co-factors involved in human PC. Increased expression of some co-factors, such as SRC1, and decreased expression of others, such as ARA70 and ART27, are found in PC tissue when compared with benign tissue. Changes in concentration of AR cofactors can influence the selective expression of AR target genes and this in turn can determine the switch between proliferation and growth inhibition (Peng *et al.*, 2008).

1.4.3.5 Ligand-independent activation via cross talk with signal transduction pathways.

AR ligand independent activation is one of the key signalling mechanism under low androgen conditions (Lyons *et al.*, 2008). Increasing evidence has shown that PC cells have acquired the ability to survive and grow in low androgen environments by activating the AR pathway using growth factors, cytokines, and steroids. In the absence of androgens, growth factors such as epidermal growth factor (EGF), interleukin-6 (IL-6) or insulin-like growth factor I (IGF-I), can increase AR transcriptional activity despite not binding to normal ligand. This is mediated through protein kinases which are able to inhibit or activate AR transcription (Jenster, 2000). Increasing evidence has implicated cyclic adenosine monophosphate (cAMP) and the protein kinase A (PKA) pathway in the activation of AR. The activation of the cAMP signalling pathway will be further discussed in section 1.5.1. A study by Nazareth and Weigel (1996) has shown that PKA activation using forskolin, an adenylyl cyclase (AC) activator, lead to the activation of AR in the absence of androgens in AI PC3 cells, and this activation was blocked in the presence of a PKA inhibitor (Nazareth and Weigel, 1996).

In addition to the cAMP-PKA pathway, PI3K/Akt/mTOR pathway is known to contribute to disease progression by activating AR in absence of its ligand. This is most commonly mediated by the loss or mutation in PTEN, which in turn leads to an increased activation of Akt (Fang *et al.*, 2007). Work by McCall et al (2008) examined how deletion of *PTEN* gene and lower PTEN protein expression can contribute to PC progression in matched tumour samples. By using fluorescent in situ hybridisation and immunohistochemistry analysis, 23% of hormone sensitive

tumours were found to harbour *PTEN* gene deletions. This significantly increased to 52% when compared to their matched hormone refractory tumours (McCall *et al.*, 2008). PTEN is a key regulator of growth factor signalling and is able to regulate different cellular processes, including cell growth (Conley-LaComb *et al.*, 2013). Loss of PTEN expression leads to an activation in the PI3K/Akt/mTOR pathway, and is strongly associated with negative oncological outcomes (Jamaspishvili *et al.*, 2018). However, loss of PTEN expression also lead to an increase in AR activity as these two proteins have been shown to be direct interactors in LNCaP cells (El Sheikh *et al.*, 2008). The interaction between PTEN and AR has been shown to inhibit AR's ability to translocate into the nucleus, thus acting as a negative regulator of the AR pathway (Lin *et al.*, 2004). Additionally, loss of PTEN expression is known to increase Akt activity (D. E. Butler *et al.*, 2017), which in turn can increase AR phosphorylation *in vitro* and can increase AR activation (Edwards and Bartlett, 2005).

1.4.4 Detection and diagnosis of prostate cancer.

The main diagnostic tools for PC include the digital rectal examination (DRE), serum concentrations of PSA, and transrectal ultrasound (Gaudreau *et al.*, 2016). In 18% of patients, prostate cancer can be detected by DRE alone, highlighting the technique's importance in disease detection (Heidenreich *et al.*, 2014). Initial patient evaluation and treatment decisions are currently based on a risk stratification scheme that incorporates three important prognostic biomarkers at diagnosis: clinical stage, biopsy Gleason grade/score, and serum PSA (Gaudreau *et al.*, 2016).

1.4.4.1 PSA as a biomarker for PC

Although biomarkers, such as PSA, reflect the state of the whole gland, early screening for PC biomarkers may predict the likelihood of disease during a man's asymptomatic state of cancer progression. Diagnostic biomarkers can predict cancer in patients suspected of having disease, while prognostic biomarkers predict the course of disease progression. Many prostate cancer biomarkers have been identified, however only a few have been approved by the FDA, including the PSA protein. PSA is the most commonly used oncological biomarker and screening method to detect prostate cancer (Kohaar, Petrovics and Srivastava,

2019). PSA is a serine protease secreted exclusively by the prostate epithelial cells (Marshall and Kelch, 1986). PSA screening for PC has been associated with a substantial increase in the diagnosis of prostate cancer. In general, total serum PSA levels are less than 4ng/mL in healthy patients (Gao *et al.*, 2019). PC causes PSA to be released into the circulatory system, increasing the level in blood up to 10^5 fold. An increased PSA level of above 4 ng/mL prompts a recommendation that the man undergo prostate biopsy (Lilja, Ulmert and Vickers, 2008). The concentration of PSA is related to the size and the amount of glandular epithelium. However, other factors are known to increase normal PSA levels, such as race, body mass index, drugs, and age. (Pérez-Ibave, Burciaga-Flores and Elizondo-Riojas, 2018).

1.4.4.2 Disease staging and scoring

The tissue diagnosis of the adenocarcinoma is essential for establishing a positive diagnosis of prostate cancer (Humphrey, 2017). Samples are obtained via a prostate biopsy under ultrasound guidance and local anaesthesia (Heidenreich *et al.*, 2014). Currently, light microscopic examination by haematoxylin and eosin (H&E) staining of the tissue is most commonly used for patient diagnosis (Humphrey, 2017). The Gleason histopathologic grading is one of three determinants of prostate cancer staging and is an important indicator of the biologic behaviour. The classical Gleason system defines the tumour into one of five histological growth patterns. A Gleason grade of 1 indicates that the gland is well differentiated and is correlated with a favourable prognosis. While a grade of 5 indicates that the gland is least differentiated and correlate with poor prognosis (Chen and Zhou, 2016). The Gleason score is then the sum of the two most prevalent grades found within the gland, with values ranging between 2 and 10 (Gordetsky and Epstein, 2016). This method specifically looks at the extent of glandular differentiations and the pattern of growth of the prostatic stroma by using haematoxylin and eosin (H&E) staining (Humphrey, 2004). Since the initial study published by Gleason in 1966, there have been revisions in the guidelines of pathological reporting. Modification in the grading system in recent years has made it more complex for clinicians to grade the cancer (Gordetsky and Epstein, 2016). The new grading system has been proposed to increase grading accuracy and simplify the grading system into 5 grades, rather than the original 10. Under this new system. The lowest grade a patient can receive is 1

instead of 6, reducing the overtreatment of patients (Epstein *et al.*, 2016). Higher grades are associated with a greater likelihood of having metastasised disease and a worse outcome after treatment of localized disease (Figure 1.6) (Gaudreau *et al.*, 2016).

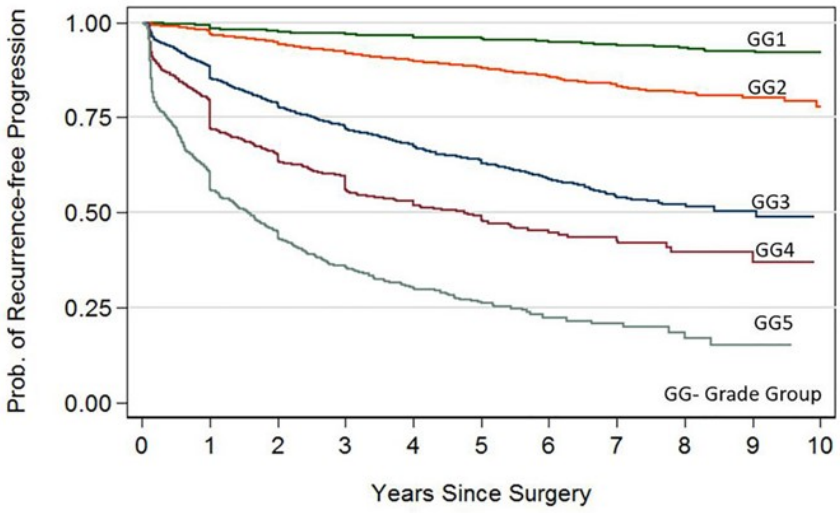

Figure 1.6 Five-year biochemical recurrence free progression probabilities in patients after radical prostatectomy. Patient in Gleason Grade group 5 have a 25% chance of being disease free 10 years after the removal of the prostate. On the other hand, patients in Gleason Grade 1 have a 90 % of being disease free within this same time frame (Figure taken from Sunassee, Al Sannaa and Ro, 2019).

1.4.5 Current courses of treatment

1.4.5.1 Active surveillance and watchful waiting

Active surveillance and watchful waiting are two non-invasive treatment options for patients with low-risk PC (Herden and Weissbach, 2018). However, they include two different strategies. Watchful waiting is used as a palliative option for patients who are asymptomatic but with reduced life expectancy and is currently considered the least aggressive course of treatment. It does not involve regular biopsies or frequent blood tests. Treatment is only provided when symptoms appear (Malinowski *et al.*, 2019). On the other hand, active surveillance is a curative option for patients with low risk of PC progression. In effect, the intention is to provide delayed treatment (Loeb *et al.*, 2017). This method of treatment mainly focuses on preventing overtreatment by selecting patients based on their low-risk features and strictly monitoring them overtime. This close follow up of the patients enables rapid re-classification of disease that would alter the course of treatment (Bul *et al.*, 2013; Kinsella *et al.*, 2018).

Patients undergo regular examinations with a yearly DRE, PSA check every six months, MRI and biopsy every one to three years (Malinowski *et al.*, 2019).

1.4.5.2 Androgen deprivation therapy (ADT)

ADT refers to treatments that act by reducing the effects of testosterone and other androgens and this can be achieved either surgically or chemically, but both methods aim to inhibit the progression of PC (Thomas and Neal, 2013). Surgical castration is the simplest and the most effective method to reduced levels of circulating testosterone and involves surgical removal of the testicles, reducing levels of androgens by over 90% within the first 24 hours, making this the most effective method to achieve a castrate state (Singer *et al.*, 2008). Androgen homeostasis in the normal adult male is maintained through the release of gonadotropin-releasing hormone (GnRH) by the hypothalamus (Gomella, 2003). GnRH is secreted in a pulsatile manner, which then induces the anterior pituitary gland to release LH (Gomella, 2003; Choi and Lee, 2011). ADT can achieve castration levels of androgens via the administration of GnRH agonist or antagonists. GnRH agonists are the most prescribed medication for ADT, with the two most commonly used being leuprolide and goserelin. GnRH agonists produce an intense stimulation of GnRH receptors, causing a rise in LH and FSH. This in turn results in a rapid release of testosterone, often referred to as a "surge", during the first two weeks of treatment (Thompson, 2001). The continuous stimulation leads to receptor desensitization which suppresses LH and FSH secretion, reducing testosterone to castrate levels (Boccon-Gibod, Van Der Meulen and Persson, 2011; Choi and Lee, 2011; Mason *et al.*, 2013). GnRH antagonists act by competitively binding to receptors in the pituitary gland, leading to reduced amounts of LH and FSH. Such compounds are able to decrease levels of testosterone immediately to castration levels, as well as avoiding the surge seen with the agonists (Kunath *et al.*, 2015; Crawford *et al.*, 2018).

1.4.5.3 Radiotherapy

Radiotherapy for prostate cancer can be separated into two types: external beam radiotherapy (EBRT) and brachytherapy (BT). BT is recommended to patients with low-intermediate stage PC, while EBRT can be used for any PC

stages (Heidenreich *et al.*, 2014).BT currently involves the permanent implantation of free or stranded iodine, called low-dose BT, as well as temporary placement of iridium, called high-dose BT. Low-dose BT has been shown to be one of the strategies that is recommended for the curative treatment as the implanted radioactive source is left within the prostate. (Stish *et al.*, 2018). In a follow up study of 757 men who underwent low-dose BT, 2.3% of patients developed distant metastasis following treatment. There was an overall survival rate of 97% in patients highlighting the curative effects of BT (Lazarev *et al.*, 2018). EBRT is a non-invasive treatment that delivers high-dose radiation to the region of interest (Kovacs and Pinkawa, 2019). The prescribed dose of radiation is delivered directly to the tumour to destroy the cancerous cells. The beams are arranged in a way that the tumour receives the maximum dose, sparing the normal tissue and surrounding organs (Podder, Fredman and Ellis, 2018). EBRT is recommended for patients with tumours that extend through the prostate capsule or that has invaded into the seminal vesicles (Kamran and D'Amico, 2018).

1.4.5.4 Enzalutamide, Abiraterone and Casodex in CRPC

Hormone therapies are currently considered the gold standard for PC treatment as they are safe and highly effective but their biggest downfall is the lack of sustained anti-tumour effects (Hara *et al.*, 2018). As previously mentioned, CRPC is an advanced form of PC that is resistant to lower levels of testosterone and has metastasised to other parts of the body. It has been shown that 80% of men with CRPC will progress to metastatic CRPC (mCRPC), with this progression being rapid in half of these patients (Albala, 2017). Abiraterone and enzalutamide are currently the first-line treatment in patients with mCRPC as both improve patient survival, but after a median of ~18 months resistance develops (Attard *et al.*, 2018). Abiraterone is an androgen biosynthesis inhibitor that irreversibly inhibits the enzymatic activity of cytochrome P45 17 (CYP17) (Rehman and Rosenberg, 2012). Administration of abiraterone supresses androgen production in the testes and adrenal glands, returning them to castrate levels (Altavilla *et al.*, 2012). Enzalutamide, also referred to as MDV3100, was the first second-generation anti-androgen to be characterised. This compound directly binds to AR and inhibits its androgen binding, AR translocation to the nucleus, and ARE mediated DNA-binding (Hussain *et al.*, 2018). In this situation, AR is no longer

able to activate the expression of its downstream genes or recruit any co-activators (Rice, Malhotra and Stoyanova, 2019). In addition to enzalutamide and abiraterone, casodex has also been used in the treatment of CRPC. Casodex, also known as bicalutamide, is a non-steroidal, first generation anti-androgen which has been approved for use in combination with LHRH analogue (Beebe-Dimmer *et al.*, 2018). Casodex binds competitively to the AR in the cell, which in turn causes it to alter its co-activator binding sites so that the receptor can no longer initiate gene transcription (Osguthorpe and Hagler, 2011; Waller and Sampson, 2018).

1.4.6 Novel PC therapies

Although ADT and other therapies are regarded as the first treatment of choice for PC, hormone resistant PC will eventually develop and will become CRPC. Although metastatic CRPC currently benefit from a wide range of treatment options, it remains incurable and the prognosis of these patients remain poor (He *et al.*, 2020). In the last few years, novel therapies have been approved in order to improve CRPC patient outcome. Most recently, polyadenosine diphosphate [ADP]-ribose polymerase (PARP) inhibitors have been approved for the treatment of CRPC (Powers *et al.*, 2020). Recent studies into CRPC have shown that mutations in DNA repair genes are associated with highly aggressive PC and CRPC. As such, these cancers are susceptible to PARP inhibitors. PARP are highly conserved enzymes that bind to DNA breaks and recruit DNA repair proteins to the damaged site (Virtanen *et al.*, 2019). Data from the phase 3 clinical trial PROfound has shown that PARP inhibitors are highly effective in the treatment of CRPC. In this trial, CRPC patients receiving PARP inhibitors had lower levels of PSA and an increase in overall survival following treatment. This inhibitor has been approved for the treatment of CRPC in May 2020 owing to its success in clinical trials (Powers *et al.*, 2020).

Furthermore, radium-223 is currently the only radiopharmaceutical treatment for metastatic CRPC.Radium-223 emits high energy alpha particles over a short range, results in a localised anti-tumour effect and the inhibition of tumour-induced osteoblastic activity (Heidenreich *et al.*, 2019). This radioactive isotope induces irreversible DNA double stranded breaks, leading to tumour and cell death. Treatment with radium-223 is known to increase the overall survival of

patients and a better biological response when compared to conventional CRPC treatments (Deshayes *et al.*, 2017).

As previously mentioned, cancer immunotherapy has made a huge impact on treatment of different cancers, and PC is not exempt from this. PC is often described as a cold tumour, with a immunosuppressive microenvironment. As such, current therapies are designed to enhance the presence of antigen-presenting cells and effector T-cells in the PC tumour environment (Fay and Graff, 2020). One of these strategies is by designing monoclonal antibodies raised against a tumour-associated antigen (TAA). This method marks the tumour cell for destruction via multiple pathways: activation of the complement system; antibody-dependent cytotoxic T-cell activation; or enhancing the uptake of phagocytes, followed by the presentation to an immature T-cell (Powers *et al.*, 2020). This method has been used to develop the Sipuleucel-T vaccine for the treatment of PC. When administered, Sipuleucel-T induces cytotoxic T-cells to recognise and kill prostate tumour cells due to the presence of the prostatic acid phosphatase antigen (Fay and Graff, 2020). In late-stage clinical trials, Sipuleucel-T significantly increased the survival by at least 4.1 months and increase the overall survival by 20 months when compared to placebo. Men receiving Sipuleucel-T experience a 22.5% reduction in risk of death following treatment (Anassi and Ndefo, 2011).

1.5 cAMP signalling

1.5.1 cAMP signalling pathway

Extracellular signalling cues, such as hormones, cannot enter the cell directly and rely on secondary messenger proteins that are produced inside cells following activation of cell surface receptors. cAMP was the first second messenger to be found and it remains the best characterised. cAMP is used by a range of Gs-coupled receptors to transduce extracellular signals into a compartmentalised signalling pathway in the target cell (Yan *et al.*, 2016; Rinaldi *et al.*, 2019). The levels of cAMP in any intracellular location are influenced by two key enzymes: adenylyl cyclase (AC) (the cAMP producer) and cyclic nucleotide phosphodiesterases (PDEs), the only family of enzymes capable

of degrading the cyclic-nucleotide. (Sassone-Corsi, 2012; Baillie, Tejeda and Kelly, 2019a) (Figure 1.7).

The classical model of activation of the cAMP pathway involves the heterotrimeric G-protein coupled receptor (GPCR). GPCRs are the largest of membrane proteins and mediates most cellular responses that involve an extracellular cue. These receptors are characterised by seven α-helical transmembrane domains separated by alternating intracellular and extracellular loop regions (Rosenbaum, Rasmussen and Kobilka, 2009). Heterotrimeric G proteins are made up of three subunits: Gα, Gß, Gγ. In the inactive state, Gα is bound to Gßγ dimer and guanosine diphosphate (GDP) (Tuteja, 2009). Binding of a ligand to the extracellular domain of the receptor leads to a conformational change of the receptor to accommodate the association of the G-protein complex (Latorraca, Venkatakrishnan and Dror, 2017). G-protein association triggers the guanylyl nucleotide exchange, from GDP to guanosine triphosphate (GTP), which leads to the dissociation of Gα from Gßγ as a free active subunit. GTP-bound Gα binds and activates AC, which can then in turn hydrolyse ATP to form cAMP (Ferre, 2015). The hydrolysis of GTP to GDP terminates the AC signalling and promotes the dissociation of Gα from AC and the reassembly of the free heterotrimer (Ferre, 2015). Four main cAMP effector proteins have been identified that transduce the cAMP signal: PKA, exchange protein directly activated by cAMP (EPAC), cyclic-nucleotide-gated ion (CNG) channels, and the Popeye domain containing protein family (POPDC) (Sassone-Corsi, 2012; Schindler and Brand, 2016) (Figure 1.7).

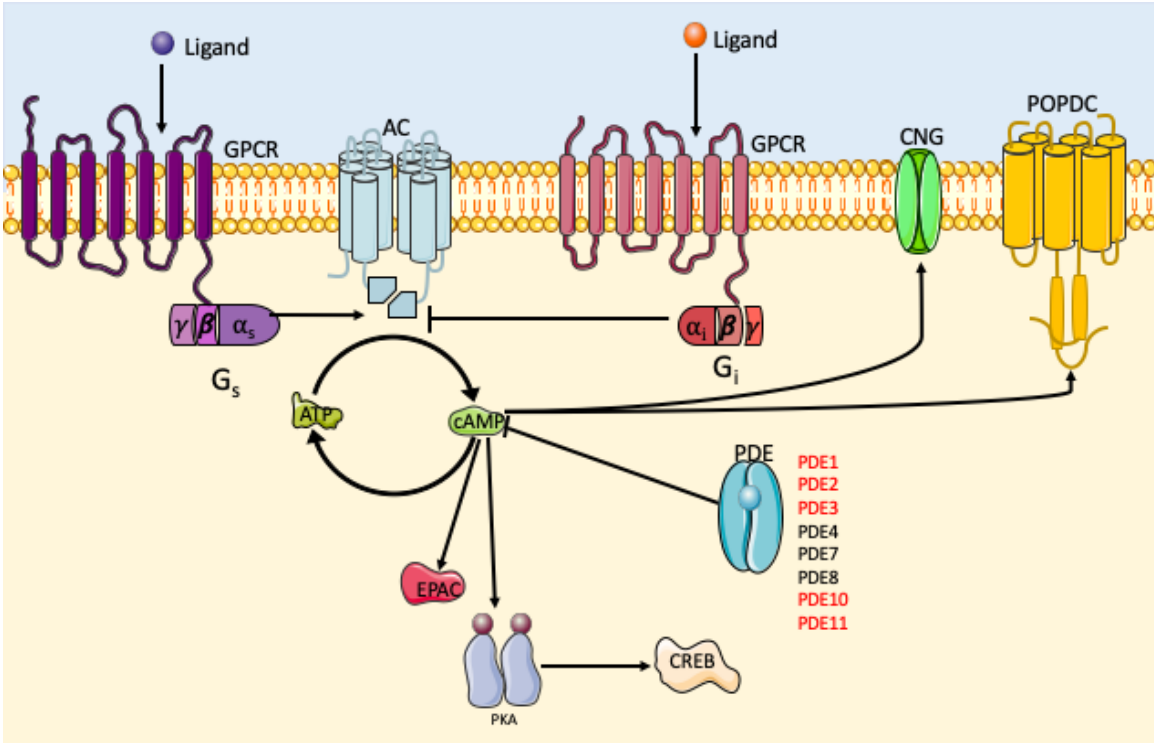

Figure 1.7 Cyclic nucleotide signalling pathways. Ligand binding to a G-protein coupled receptor (GPCR) leads to the activation of adenylyl cyclase (AC) by the $G\alpha_s$ subunit. AC is then able to synthesise the production of cAMP from ATP. cAMP can activate exchange protein activated by cAMP (EPAC), protein kinase A (PKA), popeye-domain containing protein (POPDC) and cyclic nucleotide gated channels (CNGs). Activation of proteins downstream of cAMP leads to the phosphorylation of multiple target, including the transcription factor cAMP response element binding protein (CREB). Phosphodiesterase (PDE) are currently known to be the only proteins known to hydrolyse cAMP to 5'AMP. PDEs in black only hydrolyse cAMP. On the other hand PDEs highlighted in red are known to also hydrolyse cGMP. (Baillie, Tejeda and Kelly, 2019).

1.5.2 Protein Kinase A

The 3', 5'-cyclic adenosine monophosphate (cAMP)-dependent protein kinase A (PKA) is considered essential for mediating a wide range of biological effects that are initiated by cAMP (Figure 1.7) (Chung *et al.*, 2009). The cAMP-PKA pathway is one of the major signalling pathways that is implicated in PC progression (Sarwar *et al.*, 2014). PKA is a hetero tetramer consisting of two catalytic subunits that bind to a pair of regulatory subunits and it is ubiquitously expressed and involved in multiple cellular processes. Four genes encode the regulatory (R) subunit (RIα, RIIα, Riß, RIIß), and three encodes the catalytic (C) subunit (Cα, Cß, Cγ) (Schächterle *et al.*, 2015). PKA can phosphorylate multiple targets in each individual cell following binding of two cAMP molecules to each R subunit that induce a conformational change that serves to release and activates the C subunit (Koschinski and Zaccolo, 2017). In order to maintain the normal functioning of PKA signalling, its activity is tightly controlled in space and time by scaffolding proteins known as A-kinase anchoring proteins (AKAPs) (Søberg *et*

al., 2017). Although PKA phosphorylation plays an important part in disease progression, changes in expression of PKA and its subunits is also known to be important in PC. Initial work by Cho et al (2000) demonstrated that PKA-I expression was increased in multiple cancers, including PC (Cho *et al.*, 2000). PKA-I is known to contribute to tumour growth and progression, as well as suppress the innate and adaptive arms of anti-tumour surveillance (Hussain *et al.*, 2015). Overexpression of PKA-I is often associated with poor disease outcome due to its ability to increase cell growth and neoplastic transformation (Khor *et al.*, 2008). Further details about PKA phosphorylation, and its role in PC, will be discussed in chapter 4.

1.5.3 Other cAMP effector proteins

EPAC proteins act as guanine nucleotide exchange factor (GEF) and activates the small GTP-binding proteins Rap1 and Rap2 (Tsalkova *et al.*, 2009). An important downstream effect of EPAC activation is the induction of integrin-mediated cell adhesion and E-cadherin mediated cell-junction formation (Rehmann, de Rooij and Bos, 2010). Cyclic-nucleotide-gated ion channels (CNG) are opened by the binding of cAMP (Kaupp and Seifert, 2002). These channels play an important role in the transduction olfactory signals in olfactory receptor neurones. Stimulation of odorant receptors leads to an increase in the intracellular levels of cAMP, which in turn activates CNG, leading to an influx of sodium and calcium ions (Brown *et al.*, 2006). There are currently three know isoforms of the membrane-bound POPDC proteins, POPDC1-3. Although their biochemical activity is poorly understood, some of their functions have been determined using genetically modified animal models (Amunjela and Tucker, 2016; Brand, 2018) (Figure 1.7). Interestingly, the loss of POPDC expression correlates with enhanced cellular proliferation, migration, invasion, metastasis, drug resistance, and poor patient prognosis in various human cancers (Amunjela and Tucker, 2016).

1.6 Phosphodiesterase

1.6.1 Overview of the PDE family

PDEs are currently the only known superfamily of enzymes that can hydrolyse cAMP to influence the spatial and temporal aspects of receptor-driven cAMP signalling and prevent the inappropriate activation of downstream signalling pathways under basal conditions (Fertig and Baillie, 2018). There are eleven known families of PDEs that exists in mammals, with multiple genes, alternative splicing and promoter diversity giving rise to many unique isoforms per family. Each isoform has different affinities for cAMP, cGMP or both and they are constrained within tight spatial localizations in order to sculpt the local cAMP or cGMP gradients formed by specific receptors (Formosa and Vassallo, 2014). All PDEs contain three functional domains: a conserved catalytic core, a regulatory N-terminus and a less well-defined C-terminus. The catalytic and C-terminal end of all PDEs share 18-46% sequence homology overall (Halpin, 2008). PDEs are categorised on their catalytic domain homology, however each isoform possesses a subfamily specific N-terminus containing differing lengths and complexity of regulatory domains. The role of PDEs is not only to control the total cellular content of cAMP but create nanodomains for compartmentalised cAMP signalling mechanisms that underpin receptor function that produced the cAMP in the first place. The precise subcellular location of a cornucopia of different PDEs within the cell allows a single cell to respond to multiple extracellular and intracellular signals. PDEs maintain the correct levels of cAMP in the correct place at the correct time and in doing so they regulate multiple physiological processes and their dysfunction is known to be a factor in many diseases (Baillie, Tejeda and Kelly, 2019a).

1.6.2 Structure of PDE4 isoforms

PDE4 was the first PDE to be characterised biochemically and can exclusively hydrolyse cAMP (Houslay and Adams, 2003). There are currently four genes (A, B, C, and D) that are able to generate approximately 25 different isoforms each containing a unique N-terminal targeting domain, and they are currently considered the largest of the 11 families of PDEs (Klussmann, 2016). The

regulatory region contains the upstream conserved regions 1 and 2 (UCR1 and UCR2), which is then followed by the catalytic domain (Figure 1.8).

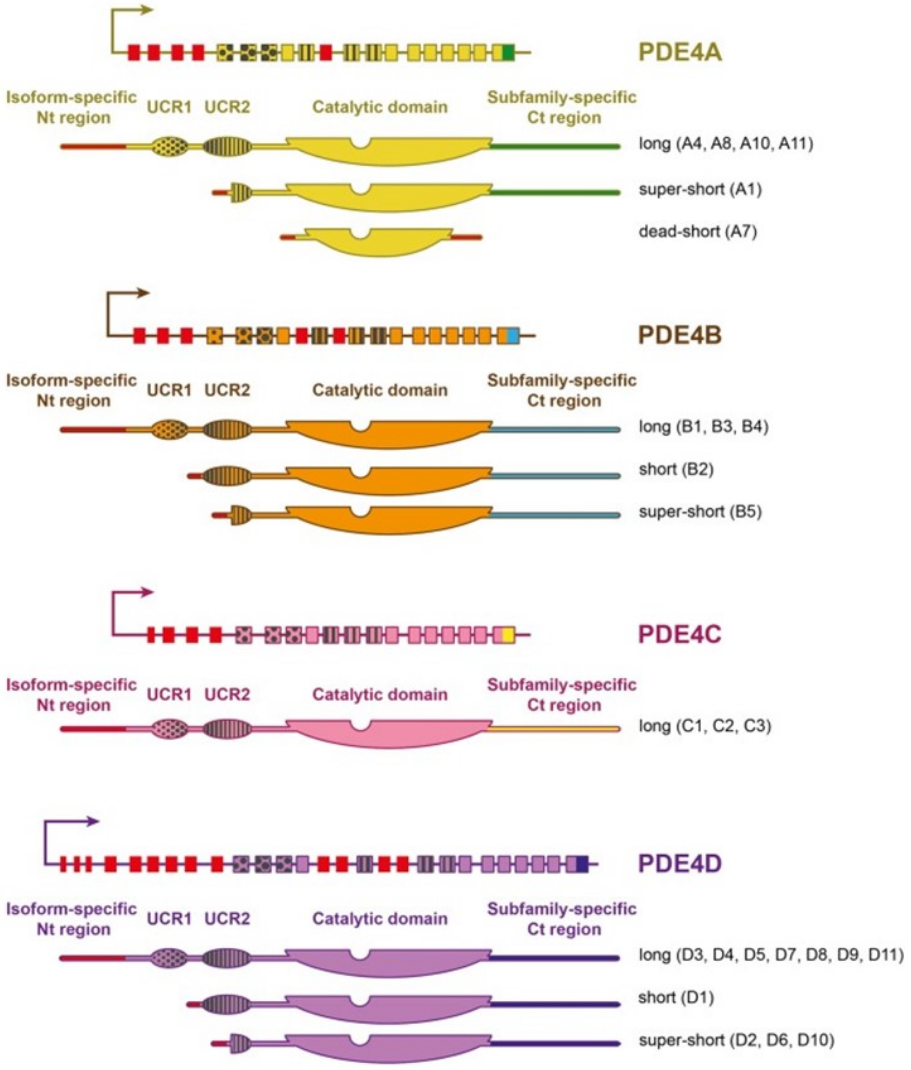

Figure 1.8 Schematic representation of PDE4A, B, C, and D. Each isoform distinguishes themselves from its unique N-terminal region. PDE4 isoforms are categorised based on their regulatory UCR1 and UCR2 region. All PDE4 isoforms share a highly conserved catalytic domain and a C-terminal region. (Figure taken from Tibbo, Tejeda and Baillie, 2019).

The UCR1/2 region is connected to the catalytic domain by the linker region 1 and 2 (LR1 and 2) respectively (Fertig and Baillie, 2018a). The unique N-terminal of each PDEs often mediates protein-protein or protein-lipid interactions in order to target each enzyme to the appropriate subcellular compartment or signalling complex. Each individual PDE4 isoform controls one or more distinct pools of cAMP and has unique physiological functions that do not overlap with another PDE4 isoform (Xie *et al.*, 2014). Interestingly, the expression of PDE4 isoforms has been shown to increase following prolonged, raised intracellular levels of cAMP. The long-term elevation in cAMP levels leads to the increase in

mRNA and protein expression of multiple PDE4 isoforms, particularly PDE4D1 and PDE4D2 (MacKenzie *et al.*, 2002).

PDE4s can be further divided into three categories: long, short and super short. Long isoforms contain both UCR1 and UCR2 regions, whereas short isoforms only express the UCR2 region and super short isoforms have a truncated UCR2 region (Houslay and Adams, 2003). It has also been demonstrated that PDE4s can form dimers via the UCR1 region. In general, long isoforms exist as dimers, whereas short isoforms are only able to behave as monomers as they lack components which facilitate interaction of the monomers. Specifically, the UCR1 region has been shown to mediate intermolecular interactions that allow the dimerization of long isoforms and deletions of this region leads to the ablation of this interaction and the formation of monomeric proteins. Furthermore, the isolation the UCR1 regions results in its oligomerization (Xie *et al.*, 2014). It has been shown that C-terminal end of the UCR1 region of a long-isoforms is able to bind to the N-terminal end of UCR2 and that this interaction can be inhibited by the PKA phosphorylation of a serine within the UCR1 domain (Beard *et al.*, 2000).

1.6.3 PDE4 activation and regulation

PDE4 isoforms are important in the cross talk between cAMP and other signalling pathways. Therefore, tight control of their catalytic activity is necessary in order to maintain normal cell homeostasis. In addition to aiding the dimerization of PDE4 long isoforms, the UCR1/2 region has been shown to be important in the regulation of its catalytic activity. Using structural analysis, it has been shown that the UCR2 region of one of the subunit of the dimers crosses over to the catalytic region of the other dimer (Cedervall *et al.*, 2015). This conformational change regulates the autoinhibition of PDE4 activity. The evidence shows that the crossing over of the UCR1/2 region regulates the catalytic activity (Francis, Blount and Corbin, 2011) in a trans-capping modality whereby one member of the dimer has its catalytic pocket occluded by the other's UCR2 .
Phosphorylation of the UCR1 by PKA disrupts the UCR2's ability to block the catalytic domain, activating the enzyme. Increased levels of intracellular cAMP are known to increase the cellular activity of long PDE4 isoforms in this manner (Figure 1.9) (MacKenzie *et al.*, 2002).

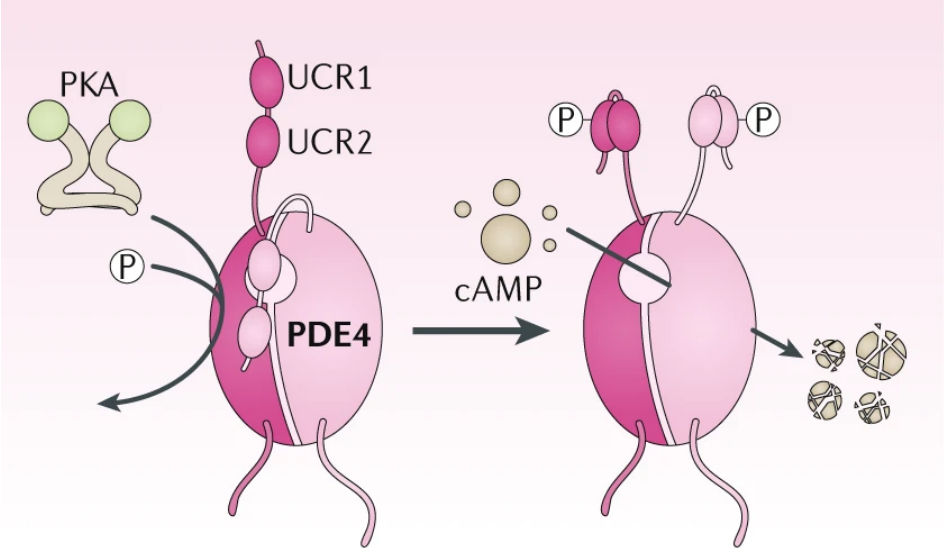

Figure 1.9 Phosphorylation of PDE4s by PKA regulates its activation. Phosphorylation of long PDE4 isoforms leads to the phosphorylation of UCR1 region. This in turn leads to the binding of UCR1 to bind to its own UCR2 domain instead of the catalytic domain. Thin in turn leads to the activation of the catalytic activity of PDEs (figure taken from Baillie, Tejeda and Kelly, 2019).

PDE4 activity can be further regulated by the phosphorylation via the ERK MAP kinase pathway. This pathway is a key route by which various growth factors and hormones exert their effects on cell growth and survival. All PDE4 isoforms, apart from PDE4A, contain a single ERK phosphorylation site within its catalytic domain (Houslay and Adams, 2003). In cells expressing long PDE4 isoforms, phosphorylation by ERK leads to the inhibition of its enzymatic activity leading to an increase in cellular levels of cAMP. This in turn allows for the activation of PKA and the phosphorylation of UCR1, leading to the ablation of the inhibitory effects of ERK phosphorylation. This provides a regulatory system, with the effects of ERK phosphorylation only being transient and rapidly overturned (Baillie *et al.*, 2000).

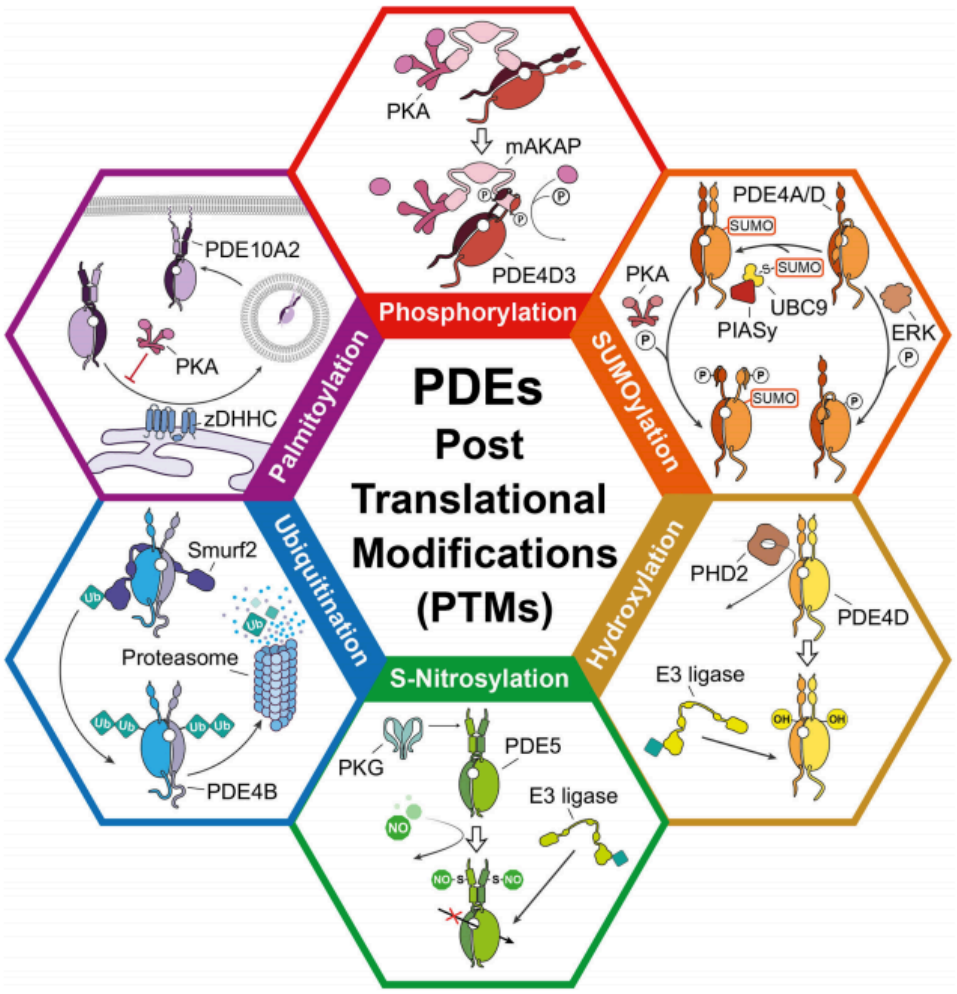

Figure 1.10 Overview of PDE post-translational modifications. The intracellular concentration of cyclic nucleotides is highly dependent on the addition of different functional groups to PDEs. Phosphorylation of PDEs is the most common mechanism by PDE activity is regulated. Some PDE isoforms, such as PDE10A2, can be palmitoylated, enabling its translocation to the membrane. Ubiquitination, s-nitrosylation, and hydroxylation of PDE can all lead to the enzymes' degradation by increasing their detection by an E3 ligase. SUMOylation of a PDE isoform can lead to an increase in its activity. Figure taken from Baillie, Tejeda and Kelly, 2019.

1.6.4 PDE4D involvement in prostate cancer

In the last 10 years, there has been increasing evidence indicating that PDE4D has a role in the progression in PC. First identified by Rahrmann et al (2009), the expression of PDE4D isoforms was found to be overexpressed in human PC patient samples and cell lines. Changes in *PDE4D* mRNA isoform expression was also observed in patient samples and this was verified when experimentation showed that knockdown of *PDE4D* lead to reduced growth and migration of PC xenografts *in vivo*. This study was the first indication that *PDE4D* promotes the proliferation of PC (Rahrmann *et al.*, 2009). Since then, expression levels of various PDE4D isoforms have been determined. Using quantitative polymerase chain reaction (qPCR) technology, the mRNA expression levels of *PDE4D* was evaluated in 19 different PC cells lines and xenografts and led to the

identification that the overall levels of *PDE4D* mRNA was decreased during the transition between the AS to AI state (Henderson *et al.*, 2014). Further investigation revealed that a significant proportion of this decrease was due to the decrease in PDE4D7 expression (Figure 1.11). This was observed at both mRNA and protein level. Decreased expression of PDE4D7 in AI samples lead to the reduced ability of PC cells to hydrolyse cAMP. In addition, it was noted that selective knockdown of PDE4D7 using small interfering RNA (siRNA) in an AS cell line (VCaP) resulted in increases in cellular proliferation. On the other hand, re-expression of PDE4D7 in an AI cell line (PC3) by transfection impeded cellular proliferation, indicating that PDE4D7 mediated cAMP signalling processes within the AI cell results in the inhibition of proliferation. This same trend was observed when increases in cell cAMP were mimicked when PC3 cells were stimulated with the AC activator forskolin (Henderson *et al.*, 2014).

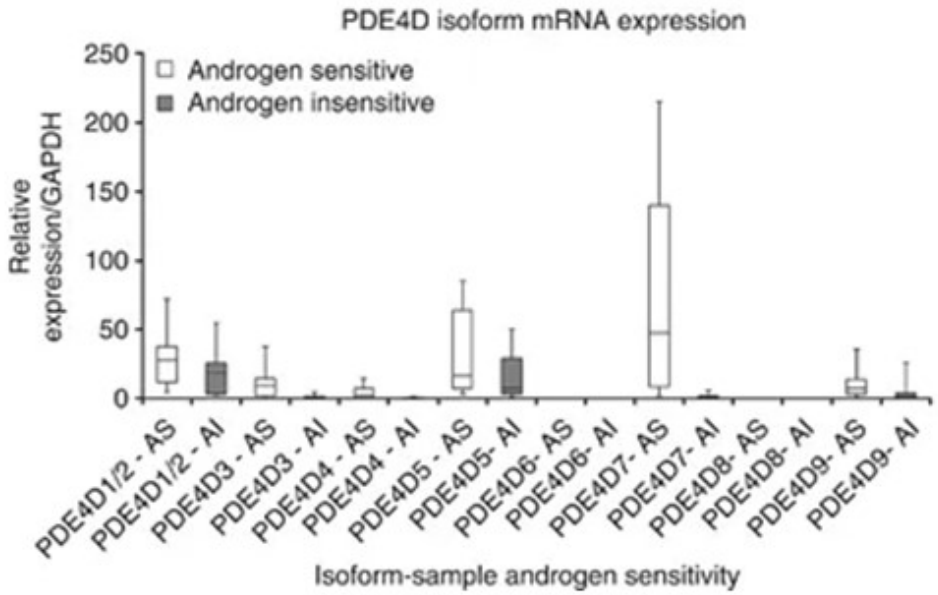

Figure 1.11 PDE4D1-9 expression in PC cell lines and xenografts. Expression of various PDE4D isoforms was assessed using Real Time qPCR. PDE4D7 expression was shown to have the highest expression in PDE4D transcripts in PC cells and is significantly downregulated in AI samples. (Henderson *et al.*, 2014).

The need for more accurate biomarkers to reflect molecular pathologies lead to the further characterisation of PDE4D7 in PC. In order to understand whether *in vitro* data can be translated to patient samples, over 1045 patient samples were screened for PDE4D7 expression. The *TMPRSS2-ERG* gene rearrangement status was also examined. PDE4D7 expression has been shown to positively correlate with disease progression and expression of this isoform significantly decreased

between primary PC tumours and CRPC samples. Interestingly, the expression of PDE4D7 was highest in primary PC samples indicating PDE4D7 may have a role with initial tumorigenesis. PDE4D7 was significantly highly expressed in tumour samples containing the *TMPRSS2-ERG* gene fusions when compared to *TMPRSS2-ERG* negative samples (Böttcher *et al.*, 2015).

It has been proposed that the changes in PDE4D7 expression can be used as a novel prognostic marker for PC. This would then allow clinicians to provide patients with a "PDE4D7 score" that may reflect their stage of disease progression. Henderson et al (2019) propose that by determining the levels of PDE4D7 mRNA transcript, they could potentially predict post-surgical disease outcome (Henderson *et al.*, 2019). For example, the risks of post-surgical progression would significantly increase in patients with a low PDE4D7 score. On the other hand, patients with a very high score are much less at risk of disease progression. In such a manner, the "PDE4D7 score" has the potential to be a more accurate and effective prognostic tool to clinicians (Böttcher *et al.*, 2016; Henderson *et al.*, 2019). Recent work by van Strijp et al (2018) further validated the prognostic power of PDE4D7 as a new biomarker for PC. The correlation between PDE4D7 scores were studied in pre-surgical and post-surgical samples. mRNA from patient and biopsy samples were extracted, and a Cox regression was applied to combine the clinical score with PDE4D7. Once again, results showed that PDE4D7 expression was highly associated with PSA recurrence after surgery and the expression of PDE4D7 was shown to provide risk information for pre-treatment risk stratification. Combinations of clinical scores with PDE4D7 status significantly improved the clinical risk stratification before surgery (van Strijp *et al.*, 2018). This combination allows a more accurate definition of the disease as well as suggesting the most appropriate course of treatment (Figure 1.12).

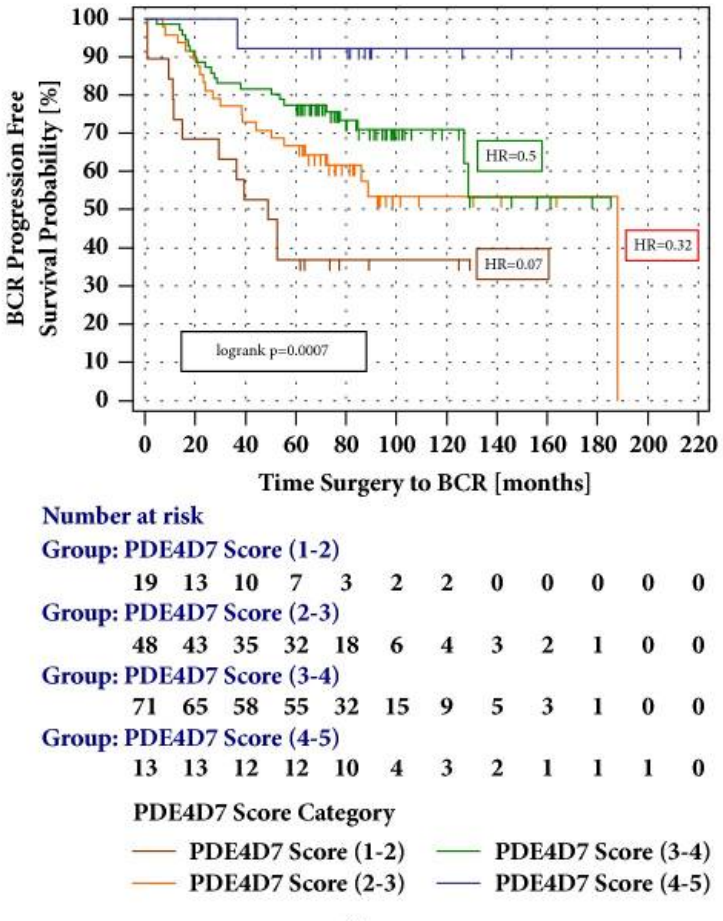

Figure 1.12 Kaplan-Meier survival analysis of the biochemical recurrence free survival (BCR) in the patient diagnostic biopsy. A cohort of patient biopsies were given a PDE4D7 score, and this was plotted against BCR progression and survival probability. Patients with a lower PDE4D7 score (brown) were less more to show disease progression. However, patients with a higher score (blue) were less likely to show signs of disease reoccurrence. Figure taken from van Strijp et al., 2018.

1.7 DExH-Box Helicase 9 (DHX9) and cancer

1.7.1 Structure and function of DHX9

DHX9, also referred to as RNA helicase A (RHA) or nuclear DNA helicase II, is a nucleoside triphosphate (NTP)-dependent helicase that has been shown to unwind both DNA and RNA, as well as aberrant polynucleotide structures (Lee and Pelletier, 2016). DHX9 is a protein that is approximately 140 kDa in size and it contains eight domains (Fidaleo, De Paola and Paronetto, 2016). The N-terminal region of DHX9 is characterised by two copies of double stranded RNA binding domain (dsRBD), then followed by the minimal transactivation domain (MTAD). The dsRBD region has the ability to bind to the post-transcriptional control elements (PCEs) in the 5' untranslated region (UTRs) of specific mRNAs to modulate their translation (Fidaleo, De Paola and Paronetto, 2016). The core helicase domain consists of 8 motifs that are subdivided into two Rec-A like

domains, with motifs 1-3 residing in the first domain while motifs 4-6 reside in domain 2 (Lee and Pelletier, 2016). The helicase region contains an ATP binding site with the consensus sequence GCGKT (A site) and FILDD (B site) in the first motif of the helicase domain (Zhang and Grosse, 1997). The C-terminal domain contains the helicase-associated domain 2 (HA2) followed by the oligonucleotide/oligosaccharide-binding fold (OB-fold) overlapping the nuclear localization/export signal (NLS/NES). Also of note is the arginine and glycine (RG) rich domain at the very end of the C-terminal end of the protein is able to bind to single-stranded nucleic acids (Lee and Pelletier, 2016) (Figure 1.12)

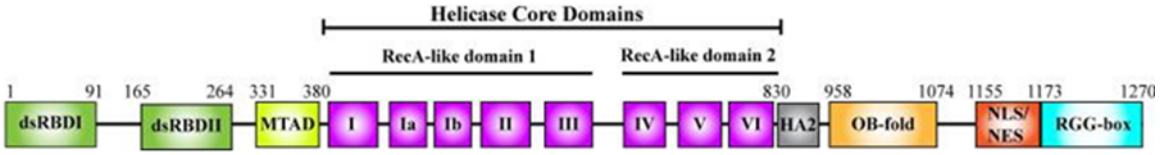

Figure 1.13 Schematic representation of functional domains of DHX9. DHX9 is a 140kDa protein formed of eight distinct domains. The N-terminal region is composed of the dsRBD and MTAD regions. The helicase core domain contains the conserved ATP-dependent helicase domain. Finally, the C-terminal domain contains the HA2, OB-fold, NLS/NES, and RGG-box (Figure taken from Lee and Pelletier, 2016).

DHX9 is a protein that is known to have diverse functions in the cell. The function of DHX9 includes regulating DNA replication, transcription, translation, microRNA biogenesis, RNA processing and transport, and maintenance of genomic stability (Lee and Pelletier, 2016). DHX9 is part of the DExD/H-box superfamily of helicases that form a large superfamily of proteins which are conserved from bacteria, viruses and humans (Tanner and Linder, 2001). DHX9, like other members of the family, has the ability to bind to both DNA and RNA via its dsRBD regions (Figure 1.14). DHX9 unwinds double stranded DNA and RNA, as well as aberrant structures such as DNA/RNA hybrids, R-loops, intramolecular triplex DNA, and G-quadruplexes (Figure 1.14) (Fidaleo, De Paola and Paronetto, 2016). Although DHX9 is able to bind to both DNA and RNA, the dsRBD has a higher affinity for double stranded RNA (dsRNA) and a weaker affinity for single stranded DNA (ssDNA) (Zhang and Grosse, 2004). DHX9 moves in a 3’ to 5’ direction and can use ATP for its unwinding activity. In order for this enzyme to work efficiently, DHX9 binds to a 3’ single-stranded tail that serves as an anchor for enzyme binding (Lee and Pelletier, 2016).

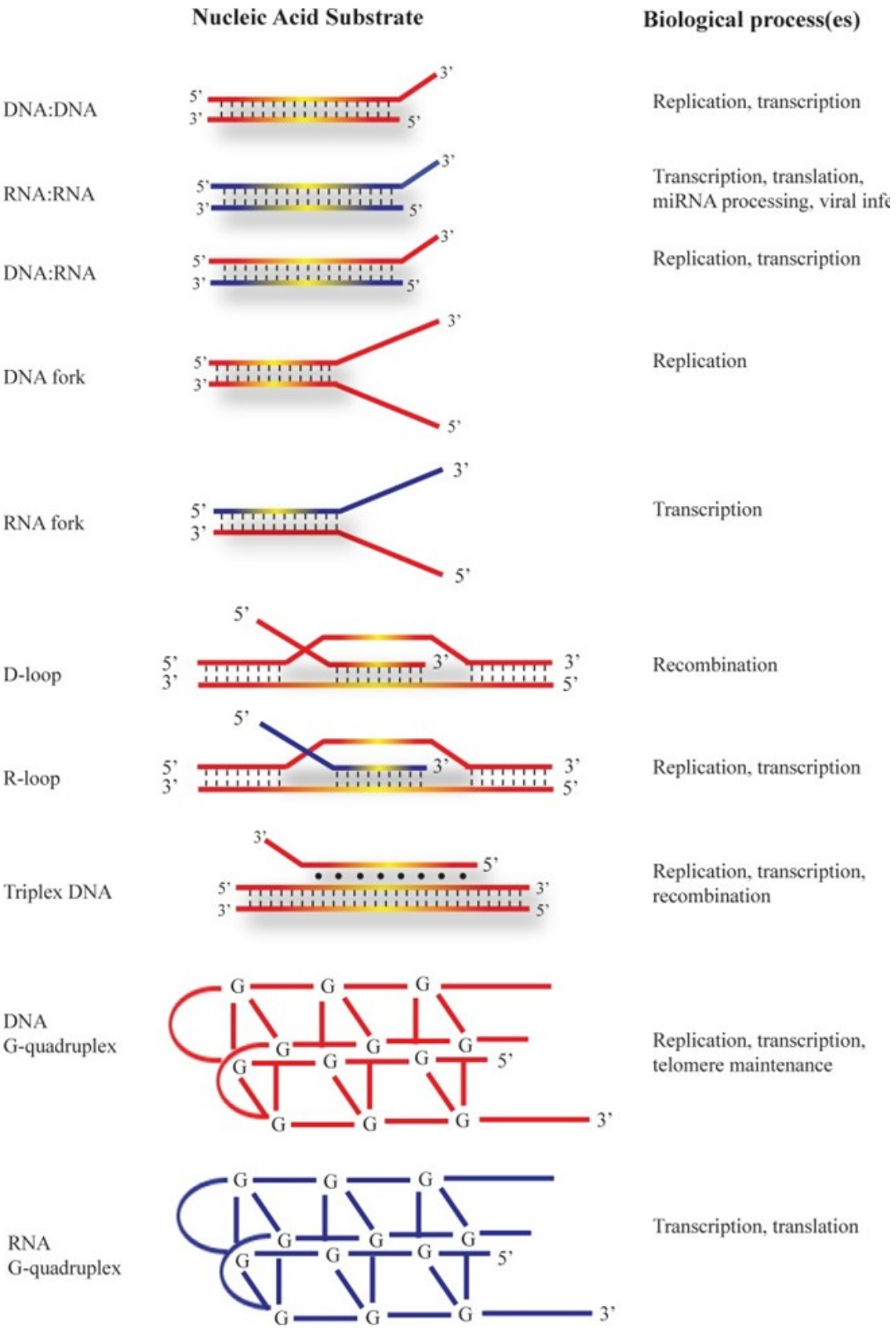

Figure 1.14 DHX9 nucleic acid substrates. DNA is coloured in red, and RNA strands in blue. DHX9 binds to the 3' single stranded tail that can be found on multiple substrates (Lee and Pelletier, 2016).

1.7.2 DHX9 in cancer

The expression of multiple DNA helicases, including DHX9, are upregulated in cancer cells/tissues and is required for cancer cell proliferation or resistance to DNA damage in response to DNA damage acquired during chemotherapy (Figure 1.15). This reflects the need to respond to increased replicative lesions that arise in highly proliferative states (Brosh, 2013). Multiple missense mutations in human helicase genes have been identified and linked strongly with cancer, highlighting the importance of this protein in maintaining genomic stability (Suhasini and Brosh Jr, 2013). Dysregulation of this functionally diverse superfamily can have disastrous effects on normal cellular homeostasis and contribute to cancer development and progression (Cai *et al.*, 2017).

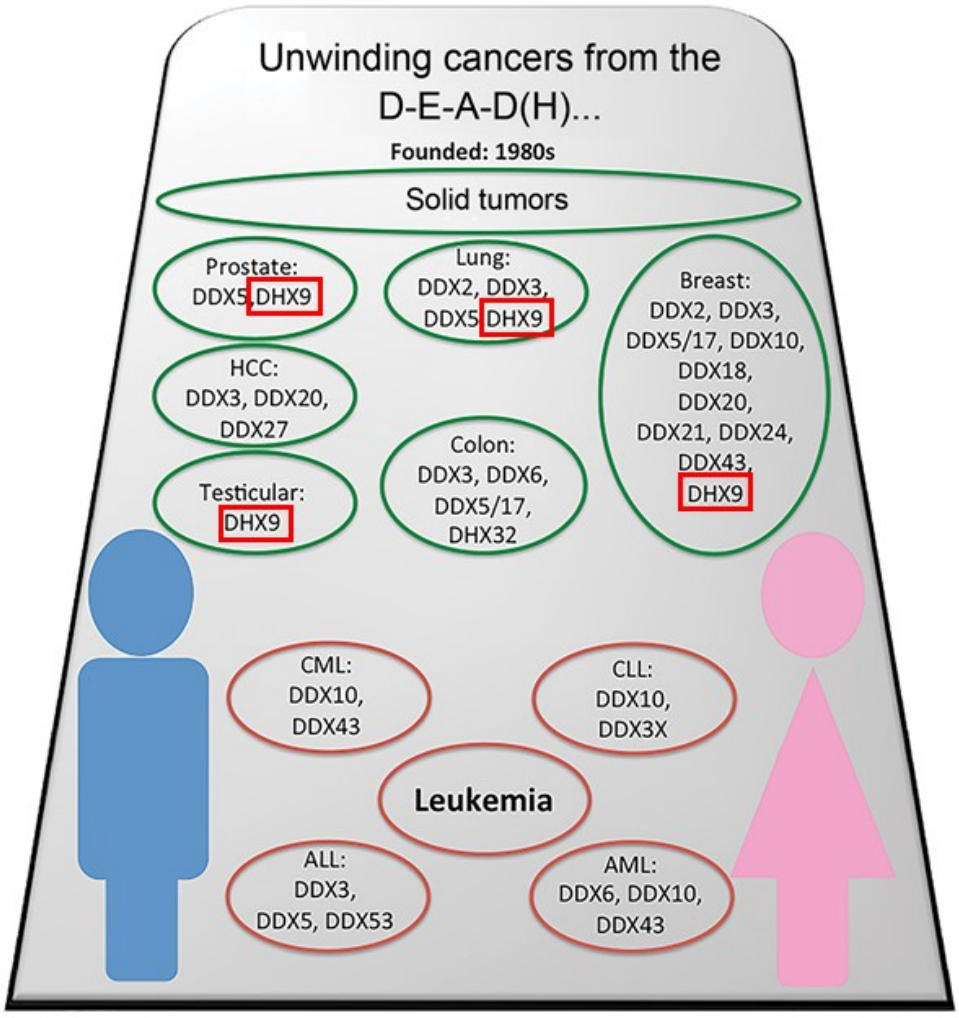

Figure 1.15 DExD/H helicases in adult cancers. DExD/H helicases have been reported to be involved in multiple solid and blood cancers. DHX9 has is known to be involved in prostate, lung, breast and testicular cancers. Figure taken from Cai *et al.*, 2017.

One cancer where the expression of DHX9 has been shown to be increased is in lung cancer. Using RT-PCR, DHX9 mRNA expression is increased in tumour samples when compared to normal lung tissue, however, there is no correlation between DHX9 expression and disease stage and survival (Wei *et al.*, 2004). As well as being overexpressed, DHX9 has been shown to inhibit the effects of enoxacin in lung cancer cell lines. Enoxacin has been used as an anti-tumoral agent due to its ability to induce microRNA biogenesis (Sousa *et al.*, 2013).

In recent years, DHX9 has slowly become an interesting new target to slow the progression of different cancers. It has been reported that the inhibition of DHX9 expression reduces the fitness of different cancer cell types. Cells lines derived from multiple myeloma, osteosarcoma, breast, lung, and cervical cancer were transfected with shRNA targeting DHX9 and suppression of DHX9 in all cell lines lead to an increase in the rate of cellular apoptosis and growth arrest. Interestingly, when this same experiment was repeated in murine lymphoma models, the prolonged suppression of DHX9 did not result in negative off-target effects being recorded and as body weight, blood biochemistry, and histology were similar to that of control mice. The suppressed expression of DHX9 was tolerated *in vivo*, suggesting that DHX9 can be a new chemotherapeutic target with tolerable side effects (Lee *et al.*, 2016). Using FISH, Southern blotting and PCR analysis, the DHX9 gene was shown to locate to chromosome 1q25. This is known to be a major susceptibility locus for hereditary PC supporting the suggestion that potential mutation at this site can lead to dysfunctional regulation of transcription as well as increase cellular proliferation in the prostate (Lee *et al.*, 1999). This observation is highly relevant to the direction of travel within my thesis and how will this impact the field.

1.8 PDE4D7 and DHX9 – Potential interactors in prostate cancer

Recent work in the Baillie lab has identified DHX9 as a potential interacting partner for PDE4D7 in PC (unpublished work funded by Prostate Cancer UK). In recent years, DHX9 has emerged as an important protein in multiple cancers by either acting as an oncogene or as a tumour suppressor (Yan *et al.*, 2019) and it has a large number of interacting partners, involving it in multiple biological processes (Lee and Pelletier, 2016). The function and molecular mechanisms surrounding the PDE4D7-DHX9 signalosome have not been characterised. To date, DHX9 and PDE4D7 has only been suggested to be novel interactors by the Baillie, and this can only be speculated as both proteins are expressed in the prostate (Figure 1.16).

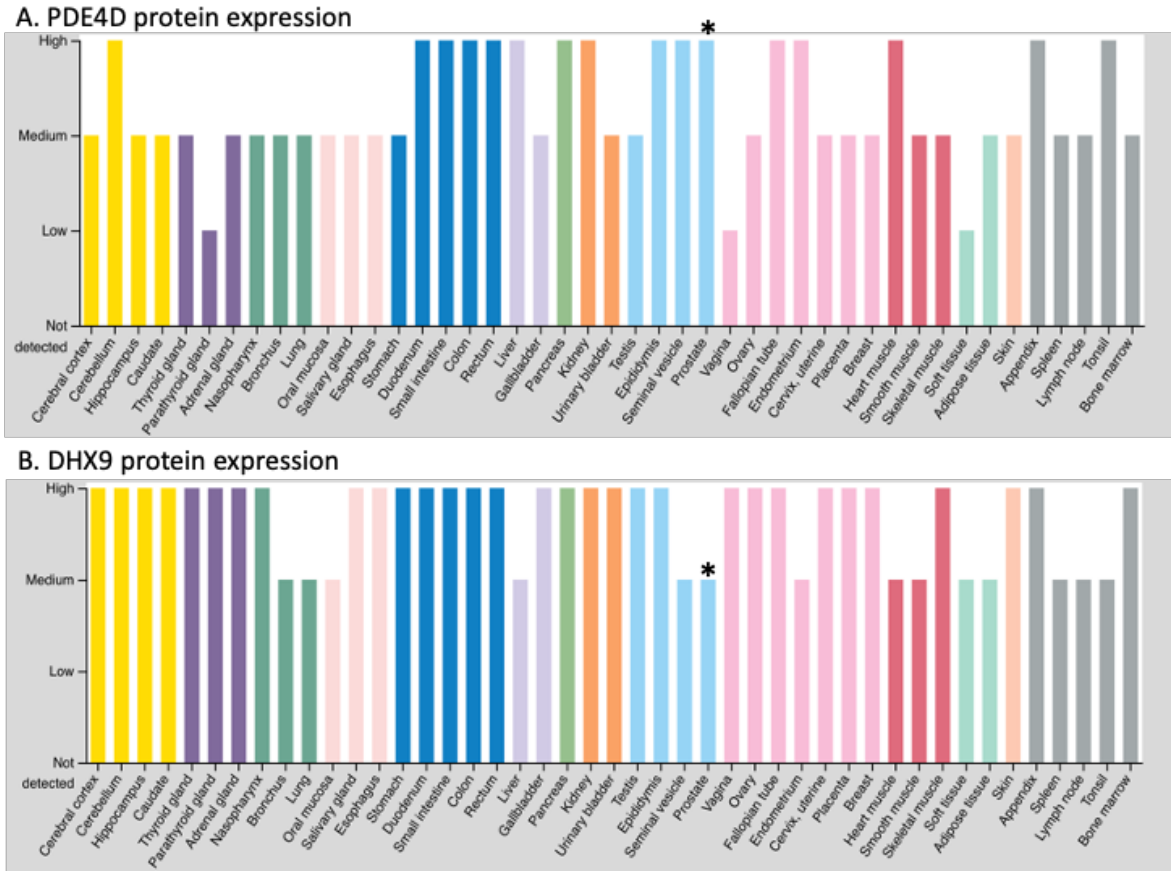

Figure 1.16 Expression of DHX9 and PDE4D in different tissues. Expression of DHX9 (B.) and PDE4D7 (A.) was investigated in multiple tissues sections, then analysed. Both proteins are expressed in the prostate, highlighted with an asterisk. Data obtained from The Human Protein Atlas (http://www.proteinatlas.org).

Although PDE4D is highly expressed in the prostate, DHX9 is moderately expressed in the prostate. However, these two proteins are expressed in different compartments. Data from the Human Protein Atlas has shown that

DHX9 is highly expressed in the nucleus, whereas PDE4D is expressed in the plasma membrane and the cytosol (Uhlen *et al.*, 2017). However, recent work by multiple groups have shown that DHX9 is able to shuttle in and out of the nucleus thanks to a NLS/NES signal in its C-terminal region (Lee and Pelletier, 2016). Interestingly, PDE4D is able to mediate reactions within the nucleus (Robinson *et al.*, 2020), indicating that these two proteins can exist in the same cellular compartment. In addition to looking at the expression of these two proteins in healthy tissues, the expression of PDE4D and DHX9 was expression was investigated in diseased prostate tissue (Figure 1.17). Interestingly, these two proteins have opposite expression patterns in prostate cancer. Higher expression of DHX9 (figure 1.17 B) is associated with low survivability, while higher expression of PDE4D7 is associated with high survivability (figure 1.17 A).

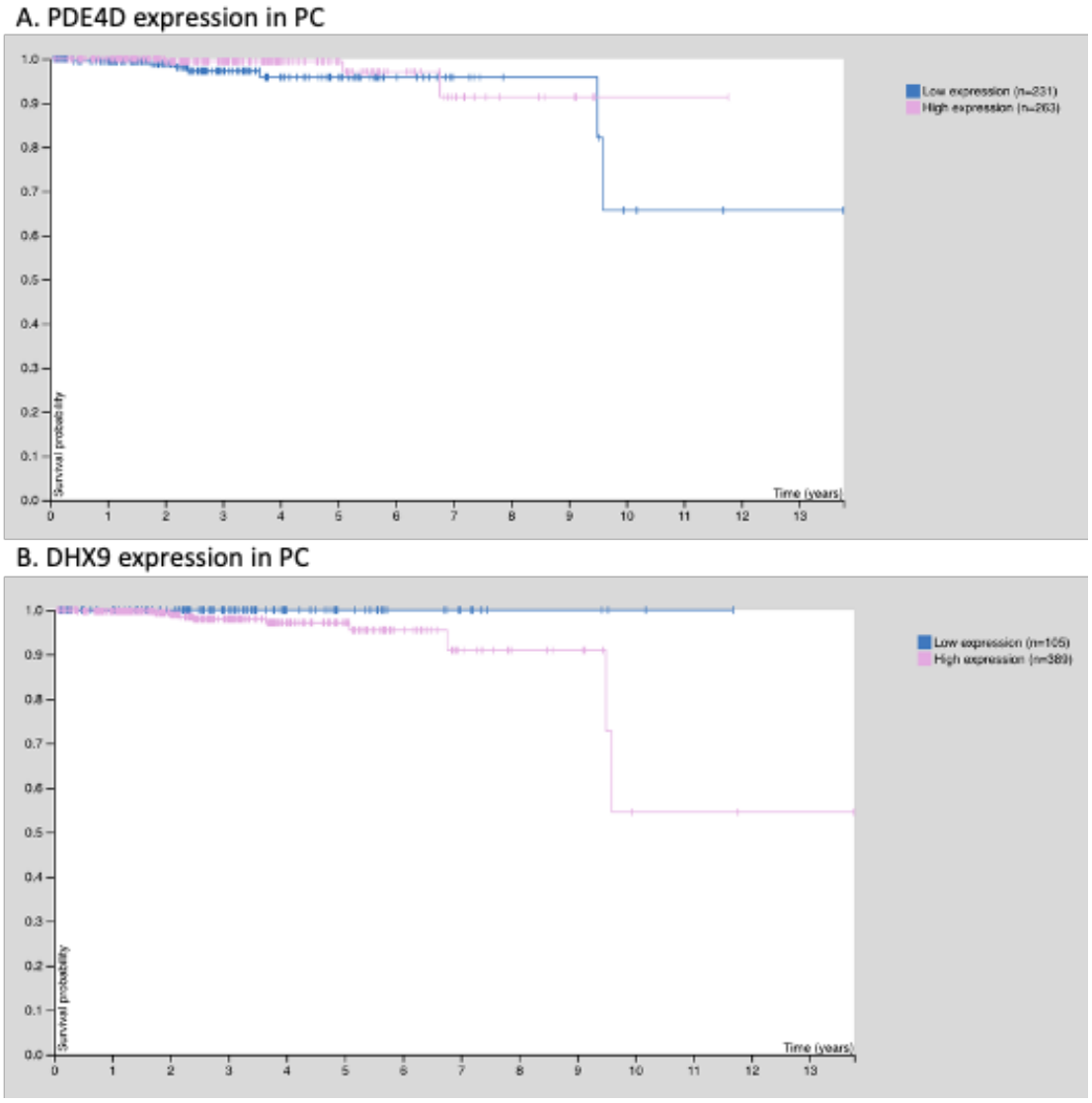

Figure 1.17 PDE4D and DHX9 expression in PC. The expression of PDE4D7 (A) and DHX9 (B) was investigated in multiple PC tissues. Protein expression was related to survival probability. Data taken from The Human Protein Atlas (Uhlen et al., 2017)

Data collected from the Human Protein Atlas, as well as from the Baillie lab, highly suggests that these two proteins are important in PC pathogenesis and progression. While the expression of PDE4D7, more specifically PDE4D7, decreases as the disease progresses, DHX9 expression increases, suggesting the expression and function of these two proteins are linked to one another.

1.9 Thesis Aims

The literature reviewed above has highlighted the importance of PDE4D7 in the development and progression of PC and has indicated that DHX9 is also involved in cancer, including PC. In this light, the fact that PDE4D7 and DHX9 form a signalling complex in PC cells suggests that they may coordinate cancer related signalling mechanisms. If true, the DHX9-PDE4D7 signalling axis could represent a novel target for therapeutic intervention in PC. My thesis seeks to verify the existence of the DHX9-PDE4D7 complex and to use novel biochemical tools and assays to gain some understanding of the molecular mechanisms that underpin the influence of the complex on PC cell growth. The thesis is divided into three sections with the following aims:

AIM 1: To confirm the interaction between PDE4D7 and DHX9. Biochemical techniques were used to show the direct interaction between DHX9-PDE4D7 and data was supported by complementary imaging techniques that visualised co-localisation of the proteins in a cellular context. Peptide array technology was used to map the DHX9-PDE4D7 protein-protein interaction domains and this information used to develop cell penetrating disruptor peptides that acted to specifically disassemble the complex. These novel bio-tools were used in “functional” assays as part of AIM 3.

AIM 2: To determine whether DHX9 is a substrate for PKA phosphorylation. As many PDE4 containing protein complexes contain PKA substrates, I was keen to find out if DHX9 could be modified in this way. Using peptide array technology, a putative PKA phosphorylation site was identified on the helicase. Using sequence information, I developed novel custom phospho-DHX9 to the site. Such a tool could be used to gauge the influence of PDE4D7 on putative PKA phosphorylation of DHX9. DHX9 phosphorylation was studied *in vitro* using biochemical and imaging techniques.

AIM 3: To characterise the role of DHX9 in PC cells. By using Real Time Cell Analyzer (RTCA) xCELLigence technology, the effects of DHX9 silencing via siRNA knockdown or treatment with a DHX9 inhibitor was studied. The functional implication of the disruption of the PDE4D7-DHX9 complex (using DHX9-PDE4D7 peptide from AIM1) was examined by measuring the levels of R-loops and monitoring PC cell growth. Finally, changes in downstream PC signalling pathways influenced by DHX9 were evaluated using Reverse Phase Protein Array (RPPA) following treatment of PC cell lines with DHX9-specific siRNA .

Chapter 2 Material and Methods

2.1 Molecular Biology

2.1.1 Constructs

Table 2.1 List of plasmids used for this thesis

Construct	Antibiotic Resistance	Source
pcDNA3.1 PDE4D7-VSV	Ampicilin (Sigma, A9393)	I. Gall
pCMV3 DHX9-FLAG	Kanamycin (Thermo Fisher, 11815032)	Sino Biological
pGEX-6P-1 DHX9-GST	Ampicilin (Sigma, A9393)	Dr J. Capitanio and Prof R. Wozniak, University of Alberta, Canada
pGEX-6P-1 GST-DHX9 1-380	Ampicilin (Sigma, A9393)	
pGEX-6P-1 GST-DHX9 381-820	Ampicilin (Sigma, A9393)	
pGEX-6P-1 GST-DHX9 821-1270	Ampicilin	
pGEX-5X-1 4D UCR1-GST	Ampicilin (Sigma, A9393)	Dr G. Bolger, University of Alabama, USA
pGEX-4X-1 GST	Ampicilin (Sigma, A9393)	Dr Y.Y Sin, University of Glasgow, UK

2.1.2 Transformation of plasmid DNA into competent cells

DH5α (Agilent, 200231) and BL21(DE3) Codon Plus (Agilent, 230245) were stored at -80°C and thawed on ice prior to use. 1-10 ng of plasmid DNA (**Error! R eference source not found.**) was added to 50 μL competent cells, mixed gently by pipetting, and incubated on ice for 30 minutes. After incubation, the cells were heat shocked for 45 seconds at 42°C and placed on ice for a further 2 minutes. 450 μL of Luria broth (LB) (10g/L tryptone, 10g/L NaCl, 5 g/L yeast extract) was added to the transformant, then grown for an hour at 37°C, 300 RPM. 50 - 150 μL of the transformation mixture was then spread onto a LB Agar plate (10g/L tryptone, 10g/L NaCl, 5 g/L yeast extract, 20 g/L agar) containing the appropriate antibiotic and incubated overnight at 37°C.

2.1.3 Isolation and quantification of plasmid DNA

Single colonies from the transformation plate were picked and grown overnight in 5 mL of LB containing 50 μg/mL of kanamycin at 37°C, 220 RPM. Isolation of 2 mL of the overnight culture was conducted using the QIAprep Miniprep kit (Qiagen, 27106) according to manufacturer's instructions. For an overnight 250 mL bacterial culture, plasmid DNA was purified using PureLink HiPure Plasmid Maxiprep kit (Invitrogen, K210007) according to manufacturer's instruction. The purified DNA was resuspended in ultra-pure nuclease free H_2O and stored at -20°C.

2.1.4 Quantification

A NanoDrop 3300 spectrophotometer (Thermo Fisher Scientific) was used to determine the concentration and purity of the plasmid DNA. The absorbance of the sample was measured at 260 nm and 280 nm. Absorbance at 260 nm was used to quantify the concentration of dsDNA in the sample, whereas the $A_{260/280nm}$ ratio was used to determine the purity of the sample.

2.1.5 Storage of plasmid DNA

For plasmid storage, 1 mL of the overnight culture grown in 2.1.3 was mixed with 1 mL of 50% glycerol / 50% LB in a sterile cryovial. The glycerol stock was snap frozen on dry ice and stored at -80°C until needed. For future DNA preparations, a sterile pipette tip was used to scrape cells from the frozen vial an inoculate 250 mL of LB with the appropriate antibiotic. The culture was incubated overnight at 37°C, 220 RPM. Plasmid DNA was purified as described in 2.1.3.

2.1.6 Analysis of plasmid DNA

In order to check the correct identity of purified plasmid DNA, 50 ng of plasmid DNA was incubated with 1 unit of restriction enzyme. Plasmid DNA was digested using the following reaction composition:

Enzyme 1: 1 μL

Enzyme 2: 1 μL

10 x reaction buffer: 5 μL

Plasmid DNA: 50 ng

Nuclease free water: up to 50 μL

6 x Purple Loading Dye: 10 μL

The restriction enzymes used to cut each plasmid is included in table Table 2.2 Restriction enzymes used for each plasmid

Table 2.2 Restriction enzymes used for each plasmid

Plasmids	Restriction enzymes	Fraction sizes
pGEX-6-P-1 DHX9	BglII + BamHI	5 364bp + 3 424bp
pGEX-6-P-1 DHX9 1-380 aa	BamHI + HindIII	5 334bp + 784bp
pGEX-6-P-1 DHX9 381 - 820 aa	BamHI + NotI	4 955bp + 1 163bp
pGEX-6-P-1 DHX9 821 - 1270 aa	BglII + BamHI	5 364bp + 967bp

The digestion was allowed to incubate for one hour at 37°C. The reaction was stopped by adding 10 μL of 6 x Purple Loading Dye. Agarose gel electrophoresis was used to analyse 20 μL of the restriction enzyme digest. 1% agarose (w/v) was dissolved in Tris-acetate EDTA (TAE) buffer (40mM Tris, 20mM Acetate and 1mM EDTA). The solution was allowed to cool slightly, and SybrSafe (Invitrogen, S33102) was added to visualise the DNA fragments under UV light. The gel was cast in the Bio-Rad SubCell GT Agarose gel system with a comb inserted to create wells and allowed to cool. Once set, the comb was removed, and the gel placed in gel tank containing TAE buffer. A 1kb DNA ladder (NEB) was used as a marker. The gel was run for an hour at 100 V, or until the dye front migrated two thirds of the gel. The gel was then removed from the tank and imaged using the Gel Doc XR+ system (Bio-Rad). If the digest suggested that the correct plasmid was purified, 100 ng plasmid DNA, in a final volume of 20 μL, was sent to GATC (Eurofins) for sequencing.

2.2 Mammalian Cell Culture

2.2.1 Culture of human cell lines

All cell culture procedures were performed in class II hoods using aseptic technique with sterile plastics and instruments. All cell culture reagents were purchased from Sigma. Culture flasks were purchased from Corning. The cells

were observed using a phase contrast inverted microscope in order to ensure that the cells were healthy and free of any contaminants. Cells were maintained at 37°C with 5% CO_2 and 95% air. DU145, VCaP, and HEK293 cells were maintained in Dulbecco's Modified Eagle's Medium (DMEM) (SAFC, D5671) supplemented with 10% foetal bovine serum, 100 units/mL penicillin and streptomycin, and 2mM L-glutamine. HEK293 media was further supplemented with 1 x non-essential amino acids (Invitrogen, 11140050). VCaP media was further supplemented with 1 mM sodium pyruvate. LNCaP cells were maintained in RPMI-1640 (SAFC, R8758) supplemented with 10 % FBS and 100 units/mL of penicillin and streptomycin. All cells were sub-cultured when 80% confluent. Cells were passaged when 80% confluent. All culture medium, phosphate buffered saline (PBS), and trypsin was pre-warmed to 37°C. Conditioned VCaP media was set aside for future use. However, for all other cell lines, culture medium was aspirated from flasks. Cells were washed with 5 mL PBS. Cells were removed from the culture flasks with the addition of 5 mL of 0.25% trypsin-EDTA solution. The flask was placed back in the 37°C incubator for five minutes or until the monolayer has detached from the flask. An equal volume of growth medium was added to the flask to neutralise the trypsin, and the cell were collected by centrifugation at 700 RPM for three minutes at room temperature. The cell pellet was resuspended in fresh growth medium, or conditioned medium for VCaPs, and seeded as required.

2.2.2 Cryopreservation of cells

In order to freeze cells for future use, pelleted cells were resuspended in 1 mL freezing medium containing complete growth medium supplemented with 10% sterile DMSO. Cells were transferred to a sterile 1.8 mL cryovial and stored in a freezing container with 100 % isopropanol at -80°C for 24 hours. Frozen cells were transferred to liquid nitrogen for long term storage the following day. In order to revive cells, cryovials containing the cells was thawed by incubated in a water bath at 37°C. Cells were added to a 75 cm^2 culture flask containing 10 mL of prewarmed media and placed in the 37°C 5% CO_2 incubator. After 24 hours, the cells were washed with PBS and fresh medium was added in order to remove DMSO.

2.2.3 Transient transfection of plasmid DNA

Plasmid DNA was transiently transfected into HEK293 cells. Cells were passaged 24 hours prior to transfection and seeded into the appropriate culture flask in order to ensure cells were at 50-70% confluency on the day of transfection. Transfections were performed using Lipofectamine LTX (Thermo Scientific, 15338100) and OptiMEM reduced serum medium (Thermo Scientific, 11058021) as per manufacturer's instructions. Plasmid DNA and transfection reagent concentrations were either scaled up or down for the culture plate in use. Cells were incubated with transfection medium for 24-48 hours to ensure plasmid expression. Mock transfections were performed as control without plasmid DNA.

2.2.4 siRNA mediated knockout

Small interfering RNA (siRNA) gene knockdown was used in order to assess the function of DHX9 in PC cells, as well as to test the novel phosphor-DHX9 antibody. ON-TARGETplus SMART POOL siRNA against human DHX9, PDE4D7, SFPQ, GAPDH, and non-targeting were purchased from Dharmacon. Cells were plated until they reached 50-70% confluency in the culture plate. The following day, the cells were transfected with siRNA to a final concentration of 25 nM using either DharmaFECT 1 for DU145 and HEK293 cells or DharmaFECT 3 for LNCaP cells according to manufacturer's instructions. Percentage knockdown was assessed by western blotting after 48 hours incubation at 37°C with 5% CO_2.

Table 2.3 siRNA and reagents used in the thesis

siRNA	Catalogue number
siNon-Targeting	D-001810-10-05
Human GAPDH	D-001830-10
Human DHX9	L-009950-00-0005
Human PDE4D7	Custom Made against following sequence: Sense strand: 5' AUACCUGUGAUUUGCUUUC 3' Antisense strand: 5' GAAAGCAAAUCACAGGUAU 3'
Human SFPQ	J-006455-09-0005
Dharmafect 1	T-2001-03
Dharmafect 3	T-2003-03
5 x siRNA Buffer	B-002000-UB-100
RNA/DNA Free water	B-003000-WB-100

2.2.5 Treatment of cells

2.2.5.1 Forskolin, IBMX, and rolipram

Cells were seeded in either 6 well plates or 10 cm cell culture dishes. Treatments were carried out when cells reached 80% confluent. Cells were treated with 25 μM forskolin (Sigma, F6886), 100 μM IBMX (Sigma, I5879) or 10 μM rolipram (Sigma, R6520) for the indicated times at 37°C with 5% CO_2. All drugs were reconstituted in DMSO, aliquoted into 10 µl aliquots and stored at -20°C until required.

2.2.5.2 Disruptor peptide treatment

Disruptor peptides were reconstituted in DMSO, aliquoted into 10 µl aliquots and stored at -20°C until required. All peptides were synthesised by Genescript. Cells were plated in the appropriate culture flask until they reached 80 % confluency. They were then either treated with 10 μM of scrambled peptide, 10 μM of UCR1-disruptor peptide, or DMSO for two hours at 37°C with 5% CO_2. The cells were washed and analysed by immunoprecipitation (IP) with western blotting or immunocytochemistry (ICC) with confocal microscopy.

2.3 Preparation of whole cell lysate

2.3.1 Whole Cell Lysate

Protein extracts from were produced from cells in culture. Culture media was removed, and cells were washed once in PBS. The cells were then harvested in 3T3 lysis buffer (25mM HEPEs, 10% v/v glycerol, 50 mM NACl, 1% v/v Triton X-100, 50 mM NaF, 30 mM NaPPi, 5 mM EDTA, pH 7.4) supplemented with cOmplete, EDTA-Free Protease inhibitor cocktail and PhosStop Phosphotase inhibitor cocktail (Roche, 5056489001, 5892970001). When 80% confluent, culture plates were scraped and lysates were transferred into 1.5 mL Eppendorf tubes where they were then incubated for an hour on an end-on-end rotation at 4°C. Samples were centrifuged at 14 000 x G for 10 minutes at 4°C and the supernatants were transferred to a fresh tube and stored at -20°C for short term storage. Samples were stored at -80°C for long term.

2.3.2 Protein concentration assay

A Bradford dye-binding method was used to determine the total protein concentration in cell lysates and purified recombinant protein. One-part Bradford dye (Bio-Rad, 5000006) was mixed with four parts of dH_2O. Protein standards ranging from 0-5 µg/µL of Bovine Serum Albumin (BSA) was prepared, and experimental samples were diluted accordingly. All samples were loaded onto a 96 well plate in triplicate, followed by 200 µL of Bradford Dye. The absorption was measure at 595 nm using the Spectra Max Plus spectrophotometer. Protein concentrations corrected for the dilution factor was determined based on the standard curve.

2.4 Subcellular fractionation

All centrifugation steps were performed at 4°C. VCaP cells were plated into 10 cm^2 dishes and grown until 80% confluent. Cells were washed twice in phosphate buffered saline (PBS) then scraped in 500 µL of fractionation buffer (20 mM HEPES, 10 mM KCl, 2mM $MgCl_2$, 1 mM EDTA, 1 mM EGTA) supplemented with 1 mM DTT and cOmplete EDTA free protease inhibitor. Scraped cells were transferred to 1.5 mL Eppendorf tubes and incubated on ice for 15 minutes. Cells were then homogenised by passing the suspension through a 25-gauge needle 10 times, then further incubated on ice for 20 minutes. 100 µL of the suspension was transferred into a fresh Eppendorf and used as the whole cell lysate (WCL). The remaining suspension was centrifuged at 720 x G for 5 minutes to pellet the nuclei from the sample. The supernatant was transferred into a fresh Eppendorf tube in order to obtain the cytoplasmic, mitochondrial, and membrane fractions.

The nuclear sample was resuspended in 200 µL of nuclear preparation buffer (NPB) (10 mM NaCl, 10 mM Tris-HCl pH 7.5, 2 mM $MgCl_2$, 0.5% NP-40). The nuclear pellet was lysed by passing the suspension through a 25-gauge needle 10 times then incubated on ice for 15 minutes. The suspension was sonicated 3 times for 15 seconds, then centrifuged for 5 minutes at 720 x G. The supernatant was transferred into a fresh tube and kept as the nuclear fraction (NF).

The supernatant from the first spin was further centrifuged at 10 000 x G for 5 minutes. The pellet from the spin was further processed as mentioned above.

The supernatant was then transferred into 1 mL UltraCentrifuge tubes (Beckman Coulter, 343778) and centrifuged for one hour at 100 000 x G in an Optima TLX Ultracentrifuge. The supernatant was transferred into a fresh Eppendorf tube and used as the cytoplasmic fraction (CF). The pellet was washed in 400 µL of fractionation buffer and resuspended by passing through a 25-gauge needle 10 times. Samples were then centrifuged again at 100 000 x G for 45 minutes. The pellet was resuspended in 400 µL of fractionation buffer and used as the membrane fraction (MF). Samples were stored at -20˚C until required. Fractionation was checked by SDS-PAGE gel with western blotting.

2.4.1 SDS-PAGE gel electrophoresis

Sodium dodecyl sulfate–polyacrylamide gel electrophoresis (SDS-PAGE) was used in order to separate samples based on protein molecular weight. Following the Bradford assay, equal concentrations of protein samples were boiled in 5 x SDS loading buffer (10% SDS, 300 mM Tris-HCl pH 7.2, 0.05% bromothymol blue, 10% ß-mercaptoethanol) to denature the proteins. Samples were loaded onto precast NuPage 4-12% SDS-PAGE gels (Invitrogen, NP0321BOX, NP0322BOX) in MOPs (Invitrogen, NP0001) according to manufacturer's instructions. A protein ladder (Bio-Rad, 1610393) was loaded alongside protein samples and the gel was run at 200 V for 50 minutes.

2.4.2 Western Immunoblotting

SDS-PAGE gels were transferred onto nitrocellulose membrane using the Invitrogen Mini Blot module. Transfer sponges, filter paper, and nitrocellulose membranes (ThermoFisher Scientific, 88018) were soaked in transfer buffer (5% v/v Invitrogen transfer buffer Invitrogen NP00061, 20 % v/v methanol). The transfer sandwich was assembled in the Mini blot module and subjected to a constant 25 V for an hour and a half in transfer buffer. Nitrocellulose membranes were stained with Ponceau S (0.1% w/v Ponceau S, 5% v/v acetic acid) in order to confirm protein transfer, after which the membrane was washed in TBST until the stain was removed. Membranes were either blocked in 5% (w/v) non-fat milk (Marvel) or 5% (w/v) BSA) in TBST for one hour at room temperature after which they were incubated overnight with the appropriate primary antibody in 1% (w/v) milk or 1% BSA (w/v) in TBST (Table 2.4).

Table 2.4 Primary antibodies used for western blotting

Primary Antibody	Company and Catalogue Number	Host	Dilution Factor
B-Actin	Sigma, A5441	Mouse	1:5000
Cofilin pSer3	Cell Signalling, 3313S	Rabbit	1:1000
DHX9	Abcam, ab26271	Rabbit	1:1000
E-Cadherin	Cell Signalling, 3195	Rabbit	1:1000
FLAG	Thermo, PA1-984B	Rabbit	1:1000
GAPDH	Abcam, ab8245	Mouse	1:5000
GST	Santa Cruz, sc-138	Mouse	1:1000
NDH II (DHX9)	Santa Cruz, sc-137232	Mouse	1:1000
P70 S6 Kinase pThr 389	Cell Signalling, 9205S	Rabbit	1:1000
PAN4D	In House	Goat	1:5000
PDE4D7	In House	Sheep	1:1000
Phospho AKT Substrate	Cell Signalling, 9614S	Rabbit	1:1000
Phospho PKA substrate	Cell Signalling, 9624S	Rabbit	1:1000
Phospho-DHX9	In House	Rabbit	1:200
PKA Rii Ser96	Merck, ABT58	Rabbit	1:1000
S6 Ribosomal Protein Ser 235 236	Cell Signalling, 2211S	Rabbit	1:1000
S6 Ribosomal Protein Ser 240 244	Cell Signalling, 5364S	Rabbit	1:1000
VSV	Abcam, ab1874	Rabbit	1:1000

Membranes were washed three times in TBST the next day, after which it was incubated in the appropriate secondary antibody for one hour at room temperature (Table 2.5). Following a final three washes in TBST, membranes were imaged using either ECL substrate with X-ray film development or using the Odyssey Licor scanner.

Table 2.5 Western Blot secondary antibody

Antibody	Company and Catalogue number	Dilution
IRDye® 800CW Donkey anti-Rabbit IgG Secondary Antibody	Licor, 926-32213	1:5000
IRDye® 680RD Donkey anti-Mouse IgG (H + L)	Licor, 925-68072	1:5000
IRDye® 680RD Donkey anti-Goat IgG (H + L)	Licor, 925-68074	1:5000
Anti-Mouse	Licor	1:5000
Goat Anti Rabbit HRP	Jackson ImmunoResearch, 111-035-144	1:2000
Rabbit Anti Mouse HRP	Jackson ImmunoResearch, 315-035-003	1:2000
Donkey Anti Sheep HRP	Invitrogen, A16041	1:2000

2.5 GST Protein Purification

2.5.1 Determining IPTG concentration

This protocol was developed by Amy J. Tibbo and adapted for DHX9 expression plasmids (Table 2.1). In order to determine the optimum concentration of isopropyl ß-d-1-thiogalactopyranoside (IPTG), 5 mL of LB supplemented with 100 µg/mL of ampicillin was inoculated with the DHX9-GST constructs overnight at 37°C, 220 RPM. 10 mL of fresh LB supplemented with 100 µg/mL was inoculated with 200 µL of the overnight culture until the OD_{600} reached between 0.6-0.8. The OD_{600} of 1 mL of culture was recorded in order to calculate the volume in

which 1 mL of cell culture needed to be normalised to. 1 mL of culture was centrifuged for 10 minutes at 13 000 x G, and the pellet kept in the -20˚C and kept as the pre-induced sample. The remainder of the culture was induced for protein expression with either 1, 0.5, 0.2 or 0.1 mM of IPTG. Cultures were left to incubate overnight at 16˚C 220 RPM. At the end of the induction period the next day, the OD_{600} was measured of 1 mL of culture. 1 mL of the culture was centrifuged for 10 minutes at 13 000 x G and the pellet was kept as the post-induction sample. The remainder of the culture was appropriately discarded.

The pre- and post-induction cell pellets were resuspended in 60 µL of GST binding buffer (25 mM Tris-HCl pH 8.0, 150 mM NaCl, 0.1 mM EDTA) supplemented with 25 units of Benzonase (Sigma, E1014-5KU). Each sample was then made up to a final volume of 150 x OD_{600} with water. 5 µL of each sample was transferred into a fresh Eppendorf tube. 10 µL of water was added to each sample, and these were kept as either the total pre-induction or the total post-induction sample. The remainder of the post-induction sample was further centrifuged for 5 minutes at 13 000 x G. The supernatant was transferred into a new Eppendorf tube and used as the post-induction soluble fraction. The pellet was resuspended in the original final volume, and 5 µL was transferred into a fresh Eppendorf tube. 10µL of water was added, and the sample was used as the post-induction pellet fraction. 3 µL of 5 x SDS sample buffer was added to each tube, then boiled for 5 minutes at 85˚C. Samples were loaded onto a SDS-PAGE gel and stained using Coomasie blue in order to determine optimum IPTG concentrations.

2.5.2 Purification of GST tagged proteins

BL21 *E.Coli* cells containing an N-terminal GST-tagged plasmid of the UCR1 domain, GST tag only, or N-terminal GST-tagged DHX9 constructs were inoculated in 10 mL of LB supplemented with 100 µg/mL of ampicillin. Cells were incubated overnight at 37˚C, 220 RPM. The overnight was then added to 500 mL of fresh LB supplemented with 100 µg/mL of ampicillin. OD_{600} nm was measured every 30 minutes in order to assess cell growth. When OD_{600} reached between 0.6-0.8, the protein expression was induced with 0.2 µM of IPTG. The GST-UCR1 and GST tag constructs were incubated at 37˚C, 220 RPM, for 3-5 hours. DHX9 constructs were incubated overnight at 16˚C, 220 RPM. Cultures

were then pelleted at 4˚C by centrifugation at 6 000 x g for 10 minutes. Pellets can be stored at -80˚C until required.

Pellets were resuspended in GST-binding buffer (25 mM Tris-HCl pH 8.0, 150 mM NaCl, 0.1 mM EDTA) supplemented with 0.5 % Triton X-100 and protease inhibitor tablets. Suspensions were frozen at -80˚C for 30 minutes then thawed on ice and subjected to sonication (40-60 kHz) for seven 30 second cycles with 30 second pause for cooling. Following sufficient lysis, cell debris was removed by centrifugation at 13 000 RPM for 15 minutes at 4˚C. The supernatant was then collected and incubated with pre-equilibrated glutathione beads (GE Healthcare, GE17-0756-01) for 1 hour at 4˚C with gentle rotation. The protein bound beads were then transferred to a gravity flow column (BioRad, 7321010) and washed three times with GST-binding buffer. Elution buffer (50 mM Tris-HCl pH 8.0, 10 mM reduced glutathione) was then used to collect successive fractions of recombinant purified protein. Purity of the sample was assessed by SDS-PAGE, Coomassie staining, and immunoblotting as described in section 2.5. The purest fractions were subjected to ultrafiltration using Vivaspin with a 20 kDa or 50 kDa molecular weight cut off (Sartorius, VS15RXETO, VS0631) containing dialysis buffer (5% glycerol (v/v), 50 mM Tris-HCl pH 8.0, 100 mM NaCl) for buffer exchange and sample concentration. Protein concentration was determined by Bradford assay as described in 2.3.2, and samples were aliquoted and stored at -80˚C until required.

2.6 Protein Chemistry

2.6.1 Peptide array synthesis

Peptide arrays were synthesised by automatic SPOT synthesis using the Auto Spot Robot (Intavis Instruments) and 9-fluorenylmethoxycarbonyl chloride (FMOC) chemistry (Figure 2.1). Solutions containing the amino acids and coupling reagents are spotted onto specific locations on a membrane. Spots are absorbed and form a circular spot to then acts as a reaction vessel. Full length DHX9 and PDE4D7 was spotted as overlapping 25-mer peptides, shifted by 5 amino acids. Specific protein domains were further spotted in order to determine crucial amino acids for protein-protein interactions (PPIs). Peptide array membranes

can be overlaid with purified protein, overexpressing cell lysate, or antibodies to verify PPIs and antigen epitopes.

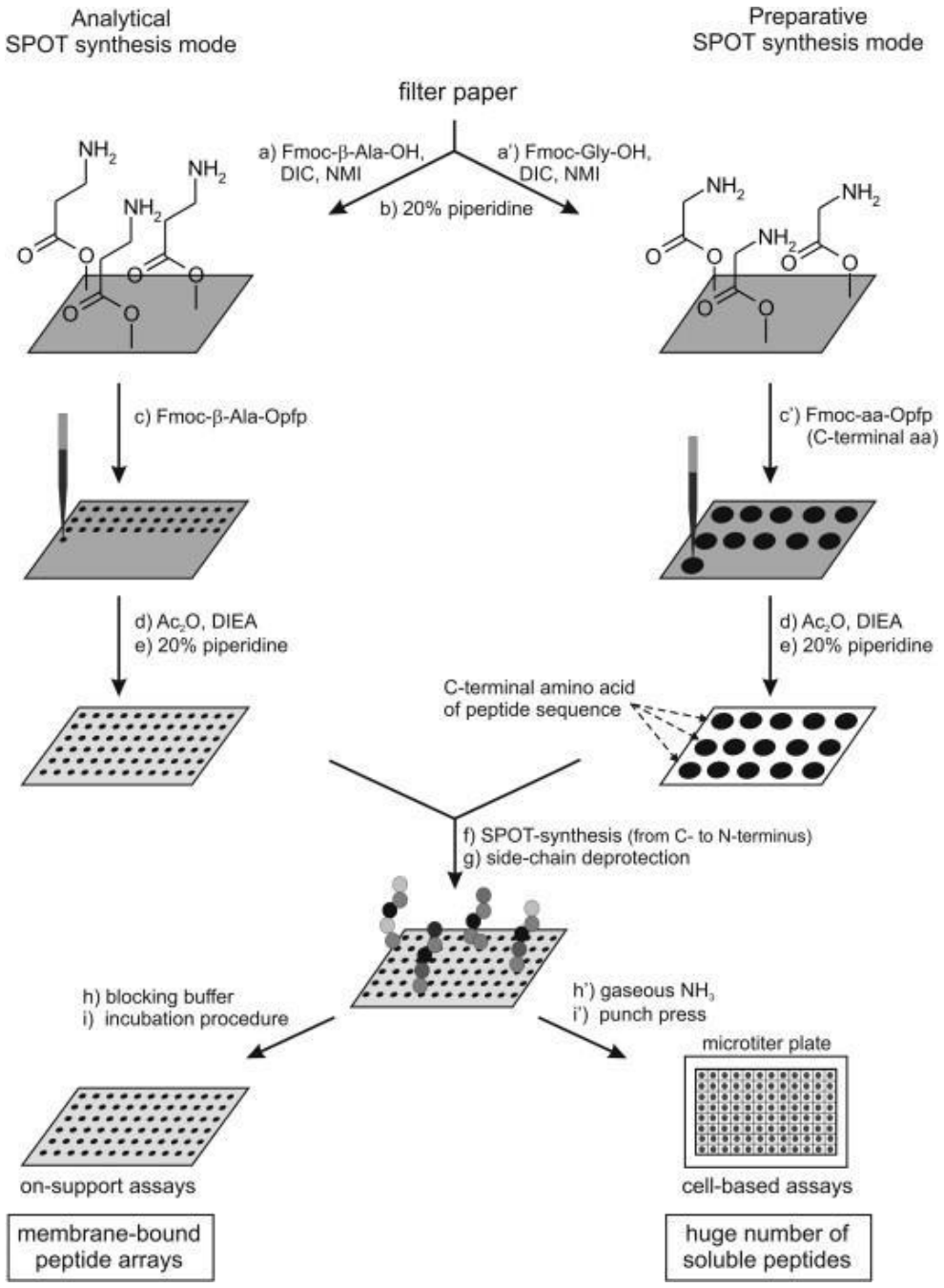

Figure 2.1 Principles of SPOT synthesis. Peptide array SPOT synthesis allows for the immobilization of peptide onto supports such as cellulose membranes (left panel). Peptides can be spotted as 5-mer shifts in order to spot the full-length protein, or specific regions can be spotted in order to investigate post-translational modifications or crucial amino acids for protein-protein interaction. Figure taken from Volkmer, Tapia and Landgraf, 2012.

2.6.2 In vitro PKA phosphorylation of DHX9 peptide arrays

DHX9 peptide arrays were blocked in 5% BSA containing 0.5 mM DTT and 1 mM ATP in TBST for one hour at RT with gentle shaking. Peptide arrays were then incubated in phosphor-buffer (20 mM Tris-HCl; pH 7.5, 10 mM MgCl2, 0.5 mM

CaCl2, 1 mM DTT, 0.2 mg/ml BSA, 1 mM ATP) with or without 100 units of active bovine PKA catalytic subunit for 1 hours at 30˚C with gentle shaking. Following the phosphorylation, the arrays were washed three times in TBST and incubated PKA phospho-substrate antibody that detects the conserved RXXpS/T consensus sequence. Following three TBST washes, the array was incubated in the appropriate HRP secondary antibody and subjected to ECL western blotting substrate with X-ray film development.

2.6.3 Peptide array validation of novel phospho-DHX9 antibody

The epitope for the novel phospho-DHX9 membranes were spotted onto membranes with truncations, alanine substitutions, and 5-mer shifts. Membranes were activated and blocked as described in 2.6.2, after which the array was incubated overnight in phospho-DHX9 antibody at 4˚C with gentle agitation. The membrane was washed three times in TBST, then incubated with rabbit HRP secondary antibody for one hour at RT. After three final washes in TBST, the membrane was subjected to Immobilon Western blotting substrate (Merck, WBLUC0100) for X-ray film development.

2.7 Protein-Protein Interaction studies

2.7.1 Immunoprecipitation (IP)

IPs were performed using 500 µg of cell lysate, adjusted to a final volume of 500 µL with 3T3 lysis buffer, which were pre-cleared for one hour at 4˚C with pre-washed protein G Sepharose beads. Beads were briefly centrifuge and the supernatant was transferred into a fresh 1.5 mL Eppendorf with 1 µg/µL of the appropriate antibody, or IgG control, and protein G Sepharose beads (Table 2.6). The IP left overnight at 4˚C on an end-end rotator with the appropriate antibody and the beads.

Table 2.6 Antibodies used for IPs

Antibody	Company and Catalogue Number	Host
DHX9	Abcam, ab26271	Rabbit
PDE4D7	In House	Sheep
VSV	Abcam, ab1874	Rabbit
FLAG	Sigma, F3165	Mouse
phosphoPKA Substrate	Cell Signalling, 9624S	Rabbit
Mouse IgG	Millipore, NI03	Mouse
Rabbit IgG	Millipore, NI01	Rabbit
Sheep IgG	Thermo Fisher, 31243	Sheep

The samples were centrifuged four times at 500 x G for 3 minutes the next day with a TBS wash between spin. IP samples were then eluted off the beads by boiling for 5 minutes at 95˚C in 2 x SDS loading buffer. Samples were analysed for interacting partners and post-translational modification by SDS-PAGE with western blotting using the antibodies in Table 2.4Table 2.5.

2.7.2 Peptide array validation for PDE4D7-DHX9 binding

Peptide array membranes were incubated in 100 % ethanol for 5 minutes in order to activate the spots, after which they were washed three times in 1 x TBST. The membranes were then blocked in 5% non-fat milk in TBST for 1 hour at RT with gentle shaking. Arrays were then incubated with either purified protein or overexpressing cell lysate in 1% milk overnight at 4˚C with gentle shaking. The arrays were washed three times the following day in incubated with the appropriate antibody in 1% milk for three hours at RT, washed then incubated with the appropriate HRP secondary antibody for one hour at RT (Table 2.4Table 2.5). The arrays were washed a final three times in TBST before subjected to enhance chemiluminescence (ECL) western blotting substrate for X-ray film development. Dark spots that were detected is indicative of a positive interaction with the array (Figure 2.2).

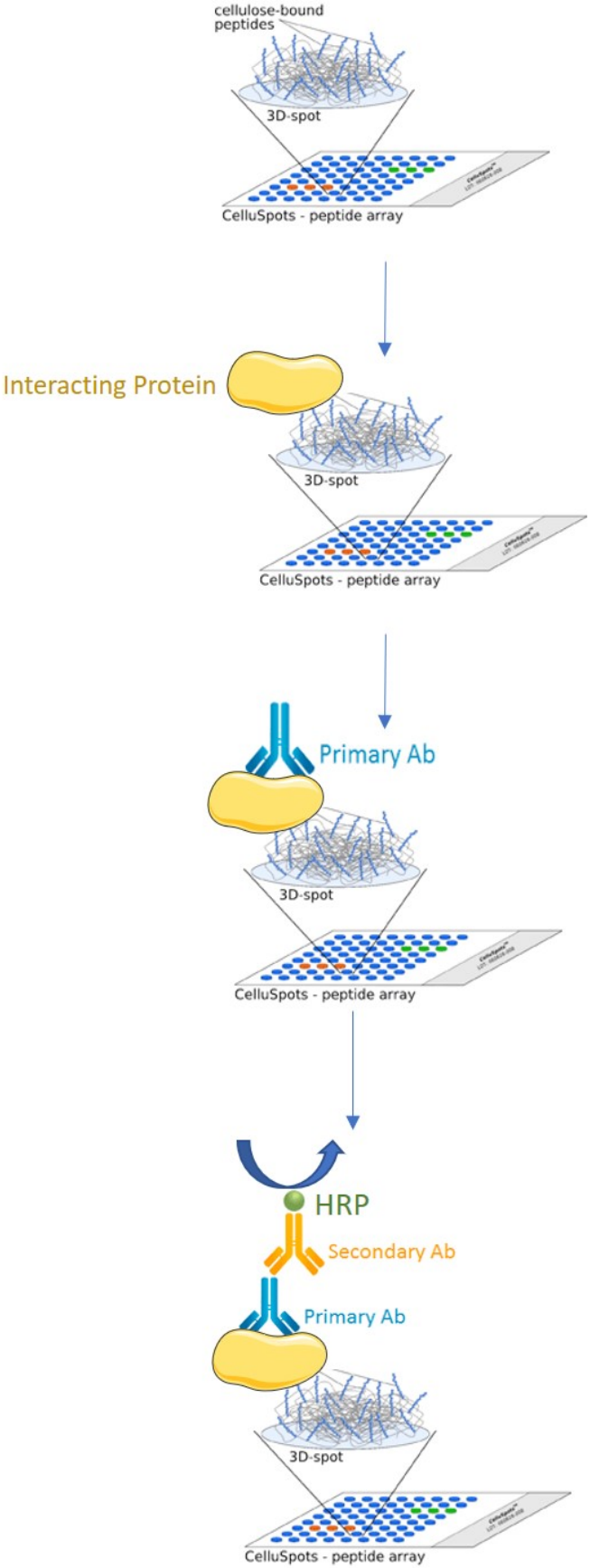

Figure 2.2 Peptide array workflow. Peptide array spotted for the protein of interest with overlaid with its interacting protein overnight at 4˚C. The array is then washed the following days and incubated with primary antibody that recognises the overlaid protein for three hours at RT, then washed. The membranes are then finally incubated in the appropriate secondary antibody and binding sequences are determined using HRP with ECL development.

2.8 Microscopy techniques

2.8.1 Immunocytochemical (ICC) staining

HEK293 cells were seeded onto sterile glass coverslips in either a 12 or 24 well plates and transfected as previously mentioned. PC cells were seeded in either 12 or 24 well plate until it reached 80% confluency. Cells were fixed onto coverslips in 4% (v/v) paraformaldehyde in PBS for one hour at RT. The cells were washed three times in PBS. If only staining for one protein, the membrane was counter stained using Wheat Germ Agglutinin (WGA) (Thermo Scientific, W11261) in the dark for 20 minutes at RT. Cells were washed three times then blocked in blocking buffer (PBS, 0.5% BSA, 0.25% Triton-X100) for one hour. Primary antibodies were then incubated overnight at 4˚C diluted in blocking buffer in a humidity chamber at the appropriate concentration (Table 2.7). Coverslips were wash three times in PBS the following day, then incubated for two hours in a humidity chamber with Alexa-Fluor secondary antibody in the dark at RT. Cells were washed a further three times in PBS, before mounting face down onto glass slides with either DAPI or Sytox Orange nuclear stain (Thermo, P36935, P36987). Slides were left to dry overnight in the dark and imaged using a Zeiss Pascal laser scanning microscope (LSM) 510 Meta and an Axiovert 100 microscope with oil immersion objective. Images were acquired on the Zeiss LSM examiner and mean fluorescence intensity (MFI) was obtained on ImageJ.

Table 2.7 Antibodies and stains for ICC

Primary Antibody	Company and Catalogue Number	Host	Dilution Factor or Concentration
DHX9	Abcam, ab26271	Rabbit	1:500
NDH II (DHX9)	Santa Cruz, sc-137232	Mouse	1:1000
PDE4D7	In House	Sheep	1:500
Phospho PKA Substrate	Cell Signalling, 9624S	Rabbit	1:1000
Phospho-DHX9	In House	Rabbit	1:100
VSV	Abcam, ab1874	Rabbit	1:500
Nucleolin	Cell Signalling, 14574S	Rabbit	1:1000
Anti-DNA-RNA Hybrid Antibody, clone S9.6	Merck, MABE1095	Mouse	1:100
Alexa Fluor anti Rabbit 488	Thermo, A32790	Donkey	1:500
Alexa Fluor anti Mouse 546	Thermo, A10036	Donkey	1:500
Alexa Fluor anti Sheep 488	Thermo, A-11055	Donkey	1:500
Alexa Fluor anti Rabbit 546	Thermo, A10040	Donkey	1:500
Wheat Germ Agglutinin Alexa Fluor 488	Thermo, W11261	N/A	1.0 mg / mL

2.8.2 Proximity ligation assay (PLA)

All PLA reagents were purchased from Sigma. PLA enzymes and buffers were provided as a kit (Sigma, DUO92105, DUO92101). HEK293 cells were seeded onto sterile glass coverslips in a 24 well plate and transfected as previously mentioned. AS PC cells were seeded in a 24 well plat until it reached 80% confluency. Cells were fixed and stained for the membrane and blocked as described in section 2.8.1. Primary antibodies were then incubated overnight at

4˚C as previously describe (Table 2.7). After washing the coverslips three times in PBS, cells were blocked for 30 minutes at RT in blocking buffer. Secondary PLA probes, that are combined with oligonucleotides, was pre-incubated for 20 minutes on an end-to-end rotor at RT. Coverslips were then incubated with secondary probes in a humidity chamber for one hour at 37˚C. Coverslips were washed three times in Wash Buffer A (Sigma), then incubated for 30 minutes with ligase enzyme at 37˚C. Oligonucleotides on the secondary probes would only be able to hybridize if proteins or PTM were less than 40 nm of each other. Coverslips were then washed a further three times in wash buffer A, then incubated for 100 minutes with polymerase enzyme at 37˚C. After a final two washes in wash buffer B, coverslips were mounted face down onto glass slides with Sytox Orange nuclear stain. Images were taken the next day to allow the mounting media to dry. Interacting proteins or PTMs can only be visualised as small punctuate dots under the microscope (Figure 2.3).

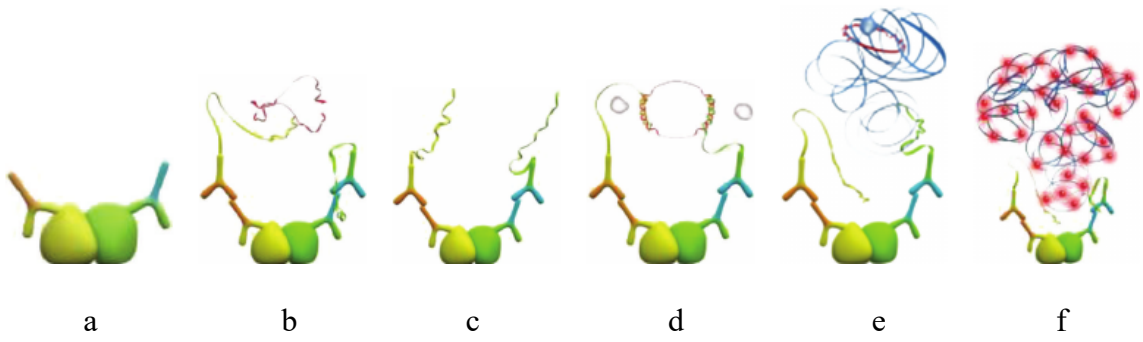

Figure 2.3 Principal of DuoLink proximity ligation assay. a. Binding of primary antibodies to target proteins. b. Binding of PLA secondary antibodies containing complementary DNA strands. c. Oligos will only bind if proteins are less than 40 nm from each other. d. Ligation of the oligos forms a circular template. e. Rolling circle amplification. f. Amplification results in the replication of the oligos, which is labelled with fluorophore indicating a positive reaction. Signal can be imaged using a confocal microscope. Figure taken from Bobrich *et al.*, 2013.

2.8.3 DHX9 Functional Assay – R-Loop assay

This protocol was developed by Dr.Prasun Chakraborty from the University of Dundee and adapted for LNCaP cells. LNCaP were seeded onto a sterile cover glasses in a 24 well plate and left to grow until 80% confluent. Cells were then transfected with siRNA targeting Splicing Factor Proline and Glutamine Rich (SFPQ), GAPDH, or non-targeting control as mentioned in 2.2.4. The cells were washed with PBS, then fixed for 20 with 100 % methanol at -20˚C. The methanol was then removed and replaced with 100 % acetone for one minute. The coverslips were washed three times in PBS, then blocked with blocking buffer for

one hour. Coverslips were incubated with primary antibody against nucleolin and DNA-RNA hybrids overnight. After a further three washes PBS, coverslips were incubated in the appropriate secondary antibody for two hours at room temperature. Cells were washed a further three times in PBS, before mounting face down onto glass slides. Slides were left to dry overnight in the dark and imaged using a Zeiss Pascal laser scanning microscope (LSM) 510 Meta and an Axiovert 100 microscope with oil immersion objective. Images were acquired on the Zeiss LSM examiner and mean fluorescence intensity (MFI) was obtained on Image J.

2.9 Real Time Cell Analysis (RTCA) measurement of cell proliferation (xCELLigence)

The xCELLigence is a non-invasive electrical impedance instrument that is able to quantify cell proliferation. Cell growth can be monitored based on the change in the resistance of current flowing through the gold-electrode plate. Changes in electrical impedance is recorded by the RTCA instrument and interpreted by the software. Changes in impedance is represented as cell index (CI), where a CI of 0 indicates there are no cells present. Increase in CI indicates that the cells are proliferating (Figure 2.4).

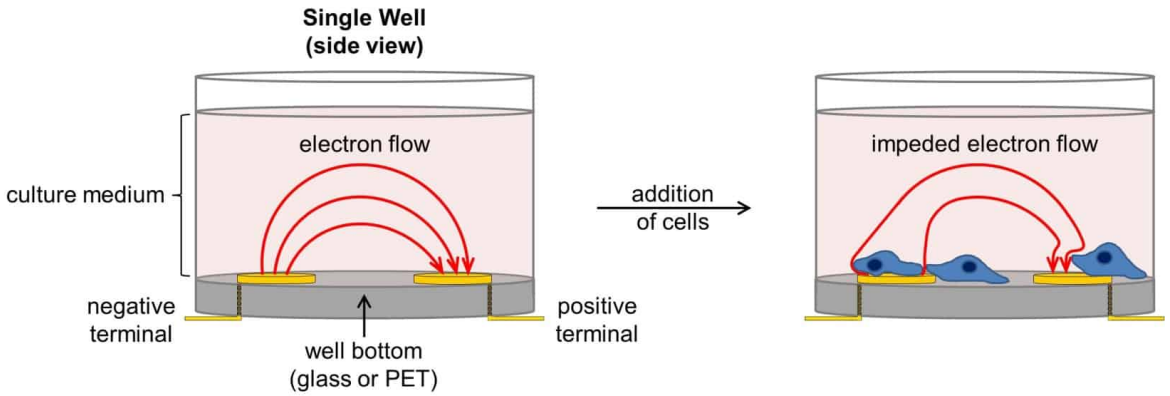

Figure 2.4 Overview of xCELLigence technology. In the absence of cells, the electrical current is allowed to freely flow through the culture medium. It can complete the circuit between the electrode. In the presence of adhering and proliferating cells, the electrical current is impeded. This system provides a sensitive readout of cell number, cell morphology, and attachment quality. Figure taken from ACEA Biosciences.

The xCELLigence system comprises a gold-plated 96 well plate, often referred to as E-Plate, a docking unit placed inside the incubator, and an impedance measurement unit kept at room temperature. The measurement unit is

connected to a computer with the software running in order to collect the data. The collected CI data is plotted as a growth curve and analysed using the RTCA software.

2.9.1 RTCA plate set up

96 cell E-plates (ACEA Biosciences, 300600910) were used to monitor cell growth. These plates are specifically designed as they contain interdigitated electrodes used to monitor cell growth. A cell number titration was initially carried out in order to obtain the optimum cell number to produce a growth curve. Prior to the addition of the cells, 10 sweeps every minute was performed with just media in order to obtain the background reading. A cell number titration for VCaP and LNCaP was then carried out into order to obtain the optimum cell number and cell line required to produce a growth curve. The appropriate cell number was seeded into each well. The plate was left in the hood for thirty minutes to allow the cells to settle to the bottom. The plate was then returned to the docking stations and the electrical impedance was measured every 15 minutes for 5 days. 5 000 cells per well of LNCaP cells was found to be the optimum cell density and cell line. The E-plate was set up as previously mentioned. However, after recording the impedance for 24 hours, cells were treated with either siRNA (Table 2.3), YK-4-279 (Tocris, 4067), or disruptor peptides (custom made by Genescript) at the required concentration. Impedance was measured every 15 minutes for a further four days. YK-4-279 was reconstituted to a stock concentration of 10 mM in DMSO and stored at 4˚C until required. The cell growth data was analysed using the RTCA software. Changes in maximum cell index or slope were extrapolated from the growth curves and analysed using GraphPad Prism 8.

2.10 Reverse Phase Protein Assay (RPPA)

All RPPA assay were performed at the HTPU MicroArray services at the MRC institute of Genetics and Molecular Medicine, University of Edinburgh. DU145 cells were plated into a 10 cm dish and transfected with either non-targeting or DHX9 specific siRNA as previously described. Cells were washed twice in ice-cold PBS then lysed in1 x lysis buffer (1% Triton X-100, 50 mM HEPES (pH 7.4), 150 mM NaCl, 1.5 mM MgCl2, 1 mM EGTA, 100 mM NaF, 10 mM Na4P2O7, 1 mM Na3VO4,

10% glycerol, freshly added protease and phosphatase inhibitors). The cells were then scraped and collected into a fresh 1.5 mL Eppeondorf tube and centrifuged at 14 000 x G for 10 minutes at 4˚C. The supernatant was collected, and the protein concentration was determined using a standard Bradford assay. The samples were normalised to 2 mg/mL in sample buffer and boiled at 95˚C for 5 minutes. Samples were stored at -80˚C until required. Samples for RPPA analysis was then sent to the University of Edinburgh for analysis.

The samples for RPPA analysis were transferred into a 96-well plate and serially diluted in order to serially dilute the samples to 1.5mg/ml, 0.75 mg/ml, 0.375 mg/mL, and 0.1875 mg/mL. Dilutions were prepared in PBS containing 10% glycerol. RPPA samples were then printed in arrays of 12 x 12 spots at a 500µm spot-to-spot distance using the Aushon 1740 Arrayer platform with two rounds of sample deposition. Sample dilution series were spotted in triplicate on each array, with 16 arrays per slide, on a single pad SuperNova Nitrocellulose slides (GraceBioLabs). The slides were incubated with the sample for at least one hour in order to ensure sample capture on the nitrocellulose membrane.

RPPA slides were washed four time for 15 minutes in deionised water with gentle agitation, the incubated with Antigen Retrieval Reagent for 15 minutes. The membrane was then washed another two times with deionized water then washed twice in PBS with tween for 15 minutes. RPPA slides were then incubated for 10 minutes in SuperBlock blocking buffer (ThermoScientific, 37536), washed once in PBS-Tween, then incubated for one hour with primary antibody (Table 2.8) diluted 1:250 in SuperBlock. The slides were then washed twice in TBST for five minutes each time, then blocked for 10 minutes as previously mentioned. Slides were then incubated with secondary antibody diluted 1:2500 in Superblock for 30 minutes. After a final wash in TBST and deionised water, the slides were left to dry for 10 minutes at RT and imaged using an Innopsys 710 slide scanner. Array images were analysed using Mapix software, with the spot diameter set to 270 µm. The net signal for each spot was determined by subtracting the background signal from the sample spot.

Table 2.8 Primary antibodies used for RPPA analysis

Antibody	Type	Pathway, Function
CamKII P Thr286	rabbit	Calcium Signaling
HSP27 (HSPB1) P Ser78	rabbit	Chaperones, MAPK Signaling, Stress pathway
MEK1/2 P Ser217/221	rabbit	MAPK Signaling
MNK1 (MKNK) P Thr197,Thr202	rabbit	MAPK Signaling, Translational Control
MSK1 P Ser376	rabbit	MAPK Signaling
PKA RII P Ser96	rabbit	cAMP Signaling
Rap1	rabbit	Integrin Signaling, cAMP Signaling
IGF-1R beta P Tyr1162,Tyr1163	rabbit	Metabolism, Receptors, Tyrosine Kinases
Stat5 P Tyr694	rabbit	Cytokine Signaling, Jak/Stat Signaling
Akt P Thr308	rabbit	Akt Signaling, Metabolism
S6 Ribosomal protein P Ser235,Ser236	rabbit	Lipid Signaling, Metabolism, Translational Control
p44/42 MAPK (ERK1/2)	rabbit	MAPK Signaling
p44/42 MAPK (ERK1/2) P Thr202/Thr185,Tyr204/Tyr187	rabbit	MAPK Signaling
Akt	rabbit	Akt Signaling, Metabolism
Akt P Ser473	rabbit	Akt Signaling, Metabolism
beta-actin	rabbit	Housekeeping, Cytoskeleton
NFkB p65 Ser536	rabbit	inflammatory and immune responses
Chk1 P Ser345	rabbit	Cell Cycle Control
Chk2 P Thr68	rabbit	Cell Cycle Control
E-Cadherin	rabbit	Adhesion
4E-BP1 P Ser65	rabbit	Metabolism, Translational Control, mTOR signalling
4E-BP1 P Thr37,Thr46	rabbit	Metabolism, Translational Control, mTOR signalling
p70 S6 Kinase P Thr389	rabbit	Lipid Signaling, Metabolism, Translational Control
p70 S6 Kinase P Thr421,Ser424	rabbit	Lipid Signaling, Metabloism, Translational Control
GSK-3-alpha/beta P Ser21/Ser9	rabbit	Akt Signaling, Metabolism, Wnt Signaling, Hedgehog Signaling
Stat6 P Tyr641	rabbit	Cytokine Signaling, Jak/Stat Signaling
p38 MAPK PThr180,Tyr182	rabbit	MAPK Signaling, Stress pathway
mTOR P Ser2448	rabbit	mTOR Signaling, Translational Control, Metabolism

mTOR	rabbit	mTOR Signaling, Translational Control, Metabolism
PLC-gamma1 P Tyr783	rabbit	Calcium, cAMP, Lipid Signaling
p90 S6 kinase (Rsk1-3) P Thr359,Ser363	rabbit	MAPK Signaling
p70 S6 Kinase	rabbit	Lipid Signaling, Metabolism, Translational Control
c-Myc P Thr58,Ser62	rabbit	MAPK Signaling, Transcription Factors
S6 Ribosomal protein p Ser240,Ser244	rabbit	Lipid Signaling, Metabolism, Translational Control
S6 Ribosomal Protein	rabbit	Lipid Signaling, Metabolism, Translational Control
Rb P Ser807,Ser811	rabbit	Apoptosis, Cell Cycle Control
AMPK alpha	rabbit	Metabolism
AMPK alpha P Thr172	rabbit	Metabolism
Caspase 3	rabbit	Apoptosis
Caspase 3 cleaved	rabbit	Apoptosis
CREB	rabbit	Calcium, cAMP, Lipid Signaling, PKC Signaling
GSK-3-beta P Ser9	rabbit	Akt Signaling, Metabolism, Wnt Signaling, Hedgehog Signaling
GSK-3-beta	rabbit	Akt Signaling, Metabolism, Wnt Signaling, Hedgehog Signaling
Tau Phospho/non Phos ser 305	rabbit	Neuroscience
Profilin (C56B8)	rabbit	actin binding proteins, cell motility
4E-BP1	rabbit	Metabolism, Translational Control, mTOR signalling
mTOR (7C10)	rabbit	mTOR Signaling, Translational Control, Metabolism
Integrin Beta 1 [EP1041Y]	rabbit	scaffold protein
Eph1A [EPR1786]	rabbit	metastasis and invasion
EphB3 [EPR8280]	rabbit	brain development
EphB2 [EPR10072(B)]	rabbit	regulating growth and development of multiple tissues and organs, interacts with FAK
Cofilin P Ser3 (C77G2)	rabbit	cytokinesis, endocytosis, embryonic development, stress response, and tissue regeneration
Cortactin (H222)	rabbit	coordinate actin reorganization during cell movement

Integrin alpha 4	rabbit	scaffold protein
Integrin beta3	rabbit	scaffold protein
Integrin beta4	rabbit	scaffold protein
Akt substrate P (RXXS/T) (110B7E)	rabbit	Akt Signaling, Lipid Signaling, Metabolism
PKA substrate P (RRXS/T) (100G7E)	rabbit	cAMP Signaling
mTOR P Ser2481	rabbit	mTOR Signaling, Translational Control, Metabolism
CamKII alpha (22B1) P Thr286	mouseI gG1	Neuroscience, Calcium, cAMP, Lipid Signaling, PKC Signaling

2.11 Fluorescence Polarization (FP) Assays

This protocol was developed by Dr Yuan Yan Sin and adapted for PDE4D7-DHX9 binding assays. All FP measurements were performed on Mithras LB 940 plate reader (Berthold technologies) in a black 384 nonbinding well plate. Polarisation was measured at λexc = 485 nm and λem = 535 nm at room temperature. The sequence to which PDE4D7 binds to DHX9 was determined was determined by scanning peptide array. A 25-mer peptide was generated based on the DHX9 peptide array (E^{576}DCIQMTHFVPPPKDKKKKDKDDDG^{600}), with an N-terminal 5-FAM tag. The peptide was synthesised by GenScript and dissolved in DMSO to a stock concentration of 10 mM.

2.11.1 Determining minimum peptide concentration

In order to determine the stable range of the DHX9 peptide, an assay was performed where the polarisation of a decreasing concentration of peptide was measure. A 1 µM peptide stock was prepared in FP buffer (PBS, 1 mM DTT and 0.25% Tween-20), then serially diluted by 2 fourteen times. 10 µL of the diluted peptide was transferred in duplicate into the 384 dark walled plate then read on the Mithras LB 940 plate reader. All polarisation results were expressed in millipolarisation (mP). mP was then plotted on a Log scale and the minimum peptide concentration was determined.

2.11.2 Direct binding assay

62.5 nM of the 5-Fam DHX9 peptide, in FP buffer, was added into the 384-assay plate. Purified protein was serially diluted in dialysis buffer in a 96 well plate, then transferred to the 384 well assay plate. The plate was incubated for a maximum five hours at room temperature, with a reading taken at 0.5, 1, 3 and 5 hours of incubation. mP values were plotted in GraphPad Prism 8 and a sigmoidal curve was produced.

2.12 Statistical analysis

All data generated are representative of three independent experiments, unless stated otherwise. Values are presented as the mean ± the standard error of the mean (SEM). Statistical significance was determined using an ordinary one-way analysis of variance (ANOVA) with a Dunnet's multiple comparison test or a T-test if only comparing two variables. A $p>0.05$ value was considered not significant, a p of < 0.05 was considered significant (*), $p<0.01$ was considered highly significant (**), $p<0.001$ considered extremely significant (***), and $p<0.0001$ as considered most significant (****). All statistical analysis and data plotting were performed on GraphPad Prism 8.

Chapter 3 PDE4D7-DHX9 interaction in Prostate Cancer

3.1 Introduction

PDE4 enzymes degrade cAMP and are important in controlling the compartmentalized signalling of cAMP through their targeting to specific downstream protein complexes (Omar *et al.*, 2019). In recent years, increasing evidence has shown the PDE4D7 expression is "protective" in PC, with high expression at early stages of PC predicting a better disease outcome (van Strijp *et al.*, 2018). However, the molecular mechanisms behind these protective effects remains uncharacterised. One potential mechanism that could help explain how PDE4D7 is able to protect PC patients is the targeting of the enzyme to protein complexes that influence cell signalling during PC progression. Protein-protein interactions (PPIs) represent a highly promising, but challenging, class of targets for therapeutic intervention. In cancer, PPIs form signalling networks that can promote tumorigenesis, tumour progression, and metastasis (Ivanov, Khuri and Fu, 2013). Understanding these networks has gradually changed our view on cell biology by offering new ways of understanding the internal organization of a cell. With the rise of omics analysis, increasing information about PPIs in PC has emerged, providing important biological information for uncovering molecular mechanisms of PC progression (Chen *et al.*, 2016). If successful, drugs that either interrupt or enhance PPI could replace ADT or AR inhibitors in the treatment of PC.

There is currently a need to develop new therapies to overcome resistance to ADT and AR inhibitors. In PC, recruitment of co-regulators to the AR could potentially offer an opportunity to develop new therapeutic agents that could be used during early and late stages of disease. Key structural surfaces involved in PPIs have been identified with co-regulators with the aim of developing novel binding inhibitors (Biron and Bédard, 2016). Cell-penetrating peptides (CPP) have quickly emerged as alternatives to classic drugs with the ability to directly disrupt target PPIs. CPPs are short peptides with the ability to cross biological membranes in an energy-dependent and -independent manner. Since initial discovery, natural and synthetic CPPs have been developed for applications ranging from imaging to gene editing and therapeutic delivery. CPP-based

therapies are considered highly efficacious due to their rapid delivery and low toxicity compared to most drugs (Habault and Poyet, 2019). Therapeutic CPPs are a promising new approach for the development of anti-cancer agents (Marqus, Pirogova and Piva, 2017).

Previous work by the Baillie lab has revealed that DHX9 is a novel PDE4D7 interactor (unpublished work). Increasing evidence has shown that DHX9 is important in the progression of multiple cancers, including breast and colon cancer (Fidaleo, De Paola and Paronetto, 2016; Lee and Pelletier, 2016). The potential PDE4D7-DHX9 interaction could indicate that these two proteins are part of a signalosome that could coordinate PC-related mechanisms. Development of small molecule inhibitors from CPPs has great potential in cancer biology, with specific peptides currently being developed against the Ras-Raf-MEK-ERK pathway (Marqus, Pirogova and Piva, 2017). For example, work by Blair et al. (2019) has shown promising data supporting the use of CPPs in the treatment of cell models for melanoma by targeting the PDE8A-CRAF complex . PDE8A can bind c-Raf inhibiting PKA phosphorylation, leading to CRAF activation. Using a rational substitution approach, a peptide designed against the protein-binding domains between PDE8A and CRAF was developed and shown to significantly increase levels of protective c-Raf phosphorylation both *in vitro* and in mouse melanoma models. This in turn resulted in significantly decreased cell growth and decreased ERK signalling (Blair *et al.*, 2019). Due to the high success of targeting PDE8A-c-Raf interaction in melanoma, the hope would be that disruption of the interaction between PDE4D7-DHX9 could have similar results for PC.

3.2 Chapter Aims

PDE4D7 is known to be protective in PC, with decreased expression of this protein known to drive disease progression leading to poor patient prognosis. However, the mechanism underlying how its decreased expression leads to increased cell growth is still unknown (Henderson *et al.*, 2014). The interaction between PDE4D7-DHX9 could potentially be a novel PPI target that could have a role in the progression of disease. Hence, the aims of this chapters are as follows:

Aim 1: Show that interaction between PDE4D7 and DHX9 can be verified in my hands. By using a range of biochemical techniques, such as immunoprecipitation and proximity ligation assay, this will show the direct and robust interaction between these two proteins.

Aim 2: Map the PDE4D7-DHX9 PPI domains using peptide array technology. This information can then be used to develop CPPs that act specifically to disassemble the PDE4D7-DHX9 complex

Aim 3: Determine PDE4D7-DHX9 binding affinity using fluorescence-polarization technology. This platform could then be configured into a small molecule screening assay to discover compounds with the ability to enhance or disrupt the PDE4D7-DHX9 interaction.

3.3 Results

3.3.1 DHX9 and PDE4D7 expression in PC cell lines

Although previous work by the Baillie lab has shown that PDE4D7 was highly expressed in AS (Henderson *et al.*, 2014; Böttcher *et al.*, 2015) , the expression levels of DHX9 in different stages of PC are still unknown. The expression levels of DHX9 and PDE4D7 was therefore determined in DU145, LNCaP and VCaP cell lines. DU145 was once considered one of the most highly used cell line PC research. This cell line was first isolated from a brain metastasis. It is hormone independent and no longer expresses AR at both the mRNA and protein level (Table 3.1) (Cunningham and You, 2015). Although both LNCaP and VCaP are both AS cell lines, they differ in AR expression. The LNCaP cell line was first derived from a needle aspiration biopsy of a lymph node metastatic lesion. Although it does express the AR, it contains the T877A mutations which alters its response to steroids (Table 3.1). VCaP were first derived from a vertebral metastatic lesion and expresses WT AR. Furthermore, this cell line expresses the TMPRSS2:ERG gene translocation, making it an ideal cell line to study the early stages of PC (Table 3.1) (Sobel and Sadar, 2005). DU145, LNCaP and VCaP cell lysates were therefore run on an SDS-PAGE gel and protein expression of DHX9 was assessed by western blotting (Figure 3.1).

Table 3.1 PC cell line characteristics

	DU145	LNCaP	VCaP
Androgen Sensitive	No	Yes	Yes
PSA expression	No	RNA + protein	RNA + Protein
AR Expression	No	RNA + protein T877A AR mutation	RNA + Protein WT AR
Derived from	Brain	Lymph	Vertebrate

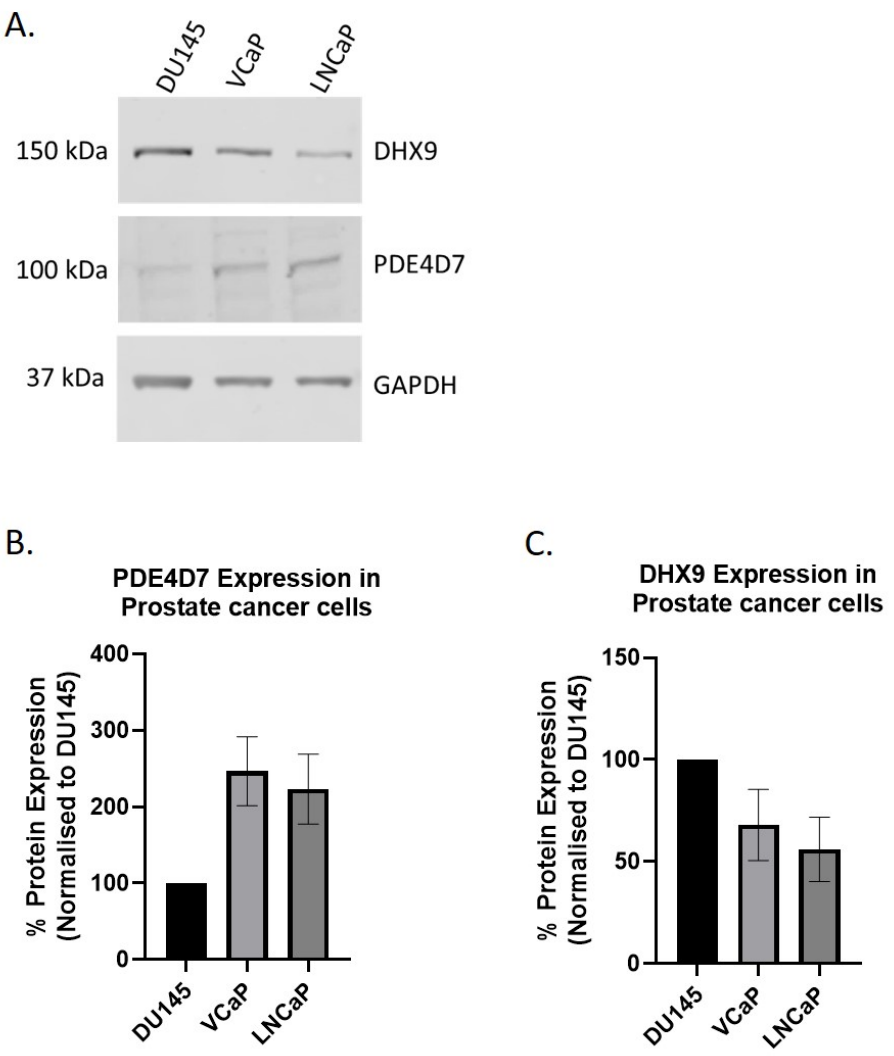

Figure 3.1 PDE4D7 and DHX9 expression in PC cell lines. A. PDE4D7 and DHX9 expression was assessed by SDS-PAGE with western blotting. B. PDE4D7 expression in all cell lines were determined densitometrically. C. DHX9 expression in all cell lines were determined densitometrically. Data is presented as the mean ± SEM of three independent experiments and analysed using a one-way Anova. Data is not significant.

Western blot analysis showed that DHX9 expression is highest in DU145 cell line (Figure 3.1 C). In recent years DU145, along with PC3, have become the most widely used cell models of late stage PC as they no longer express the AR (Cunningham and You, 2015). On the other hand, LNCaP and VCAP cells are currently used as models for early stage disease due to their expression of a functional AR. VCaP cells also express the *TMPRSS2:ERG* fusion protein, making it a very useful tool to study PC (Sampson *et al.*, 2013). Previous work has shown that PDE4D7 expression is highest in AS cell lines, whereas AI cell lines no longer express high levels of this protein (R. Böttcher *et al.*, 2015). My data confirms what has previously been reported (Figure 3.1 B), and in addition, I show that as the expression of PDE4D7 decreases, the expression of DHX9 increases. Due to the expression of both proteins of interest in the cell lysate, these three cell

lines were used throughout this thesis to study the interaction of PDE4D7 and DHX9 in prostate cancer.

3.3.2 PDE4D7 mainly localizes to the cytoplasm, while DHX9 is expressed in the nucleus and cytoplasm

So far, we have observed a negative correlation between the expression of PDE4D7 and DHX9 in cell lines. As the disease progresses into a more metastatic state, the expression of PDE4D7 decreases as the expression of DHX9 increases. Although previous work by Henderson et al (2015) demonstrated that PDE4D7 expression was found at the plasma membrane (Henderson *et al.*, 2014), I wanted to see if PDE4D7 could be expressed in other cellular compartments where DHX9 could also be present. Additionally, DHX9 is mainly expressed in the nucleus, however it has the ability to shuttle in and out of this compartment using the nuclear localisation (NLS) and nuclear export signal (NES) found within the C-terminal region of DHX9 (Lee and Pelletier, 2016; Ng *et al.*, 2018). I therefore decided to perform a cellular fractionation in order to separate subcellular compartments for analysis. VCaP were chosen for these experiments as they had the highest expression of both PDE4D7 and DHX9 (Figure 3.1). Using a series of centrifugation steps at different speeds, VCaP cells were separated into the nuclear, mitochondrial, cytoplasmic, and membrane fractions by sequentially centrifuging the cell lysate at different speeds. Each fraction was then run on an SDS-PAGE gel and protein expression was assessed by western blotting. The percentage of protein expressed in each fraction was normalised to the whole cell lysate (Figure 3.2).

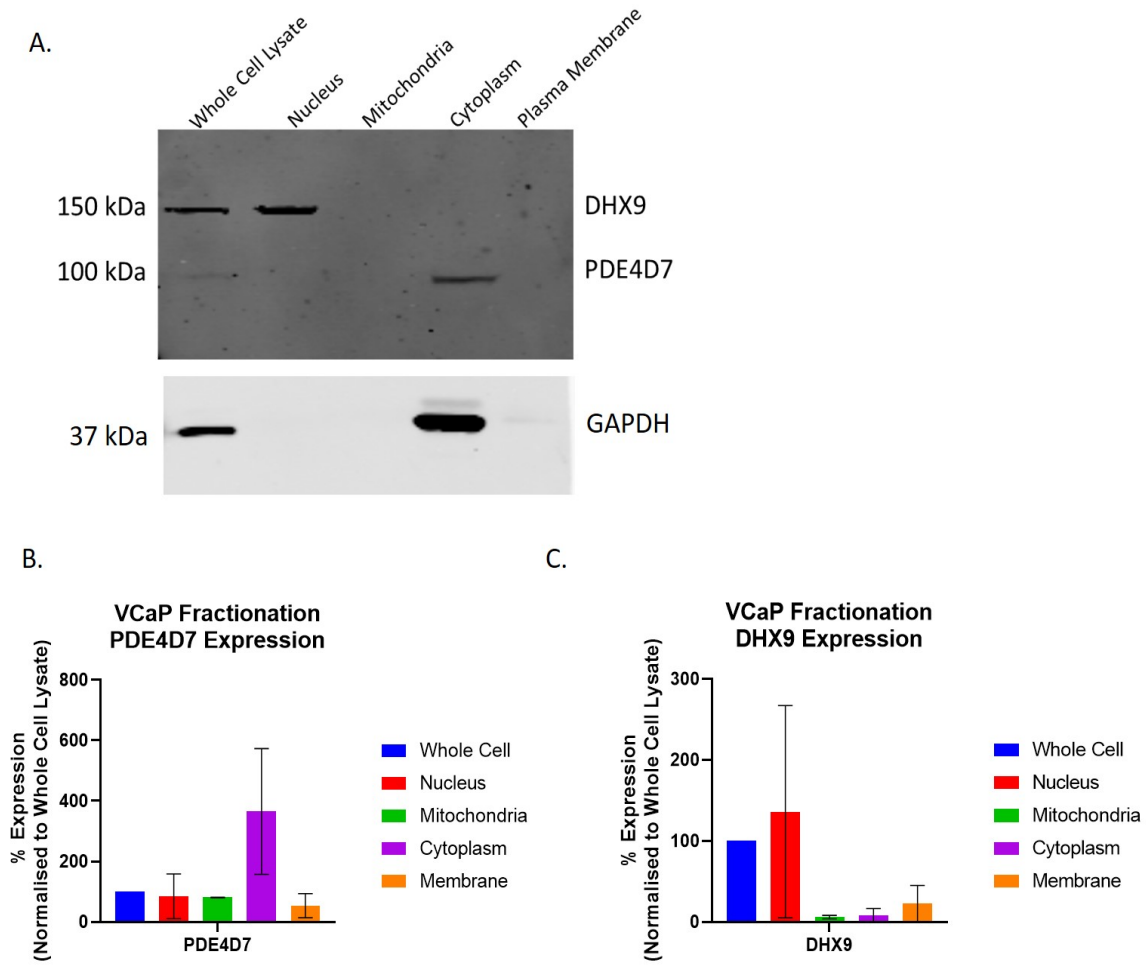

Figure 3.2 VCaP fractionation. A. VCaP cells from a confluent 10 cm dish were lysed, then separated into nuclear, mitochondrial, cytoplasmic, and membrane fractions by sequential centrifugation. Each fraction was run on an SDS-PAGE gel for protein expression analysis with western blotting. GAPDH was used as a control to ensure that each fraction was separated correctly. B and C. PDE4D7 and DHX9 expression from each . Data is presented at the mean ± SEM of two independent experiments.

By running the different cellular fractions on an SDS-PAGE gel with western blotting, I was able to determine where each of these proteins were mainly expressed when probed with the appropriate antibody. By blotting for GAPDH, I was able to confirm that each fraction was separated from one another by sequential centrifugation (Figure 3.2 A bottom membrane) as the protein was only present in the cytoplasmic fraction. The cellular fractionation showed that PDE4D7 was almost completely expressed in the cytoplasm (Figure 3.2 A and B), whereas DHX9 expression was predominantly expressed in the nucleus (Figure 3.2 A and C). Although PDE4D7 expression was previously reported to be at the plasma membrane by Henderson et al (2015), no detectable amounts of PDE4D7 could be seen in the membrane fraction. Although I did not blot for a positive control for the nuclear fraction, DHX9 is known to be highly expressed in the nucleus in order to play an active role in gene transcription (Ng *et al.*, 2018).

The fractionation presented here further supports the fact that DHX9 is almost exclusively expressed in the nucleus (Figure 3.2 A), while PDE4D7 is only expressed in the cytoplasmic region (Figure 3.2 B).

However, this fractionation does raise the questions as to where the interaction between PDE4D7 and DHX9 could take place. The data shown here suggests that these two proteins exist in two separate compartments. Subcellular fractionations are known to enrich proteins in their cellular compartment. This technique is most commonly used in proteomic analysis to study a protein when expressed in its original organelle (Lee, Tan and Chung, 2010). Furthermore, data from the Human Protein Atlas (Figure 3.3) support the data presented here. The data presented in the database suggests that DHX9 is only expressed in the nucleus, while PDE4D7 is expressed in the cytoplasm (Berglund *et al.*, 2008).

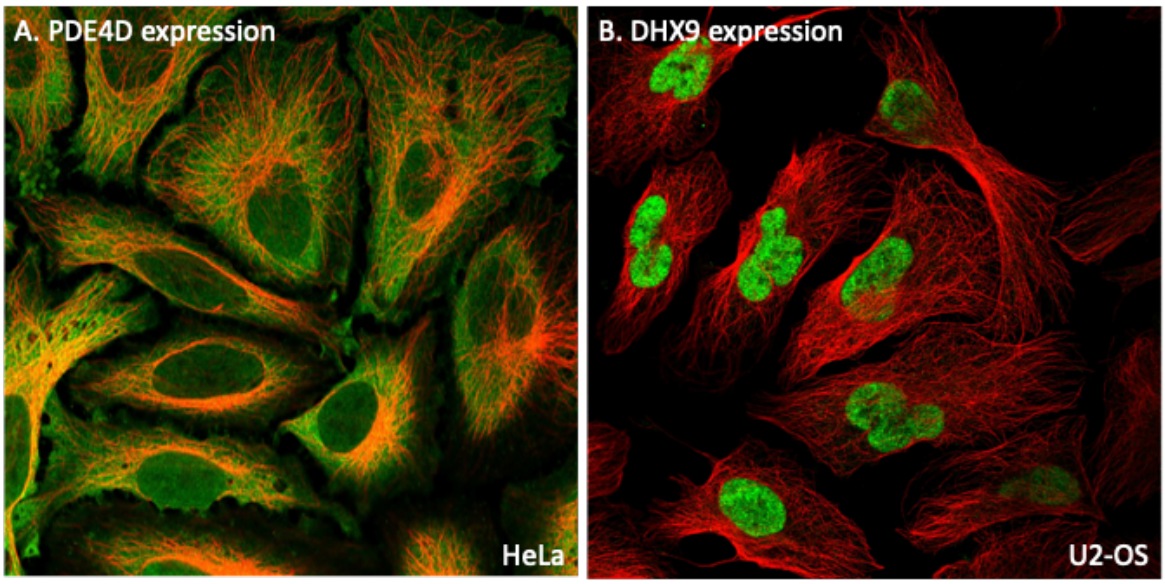

Figure 3.3 PDE4D and DHX9 expression *in vitro*. PDE4D (A) and DHX9 (B) was investigated in HeLa and U2-OS cells. The protein of interest is stained in green in both images, while microtubules are stained in red (Berglund et al., 2008). Image were obtained from the Human Protein Atlas (https://www.proteinatlas.org/).

Although DHX9 was not detected in the cytoplasmic fraction, DHX9 is known to shuttle in and out of the nucleus to the cytoplasm using its nuclear export signal (NES) and nuclear localization signal (NLS) both found within DHX9's C-terminal domain (Lee and Pelletier, 2016). NLS signals direct the import of the proteins form the cytoplasm into the nucleus, whereas NES directs the export of protein from the nucleus to the cytoplasm (Xu *et al.*, 2012). DHX9 therefore can shuttle in and out of the nucleus, and this is mediated by the NES/NLS signal. I therefore

decided to use immunocytochemistry with confocal microscopy to further investigate where the two proteins are expressed naturally in the cell. DU145, LNCaP and VCaP were all stained for PDE4D7 (green), DHX9 (red), and the nucleus (blue). Images were taken using a Zeiss LSM confocal microscope where I was able to visualise where each protein was expressed. I then used these images to quantify the levels of colocalization between the signal from PDE4D7 and DHX9 using the Pearson's coefficient (Figure 3.4). The Pearson's coefficient between the staining for PDE4D7 and DHX9 was measured using the colocalization tool on Image J. Colocalization can often be considered subjective and only judged by the merging of colours. Pearson's coefficient is a statistic tool to quantify the colocalization between two probes, with a value near 0 indicating that the probes are unrelated to one another, whereas a value closer to 1 indicates that the two probes are overlapping (Dunn, Kamocka and McDonald, 2011).

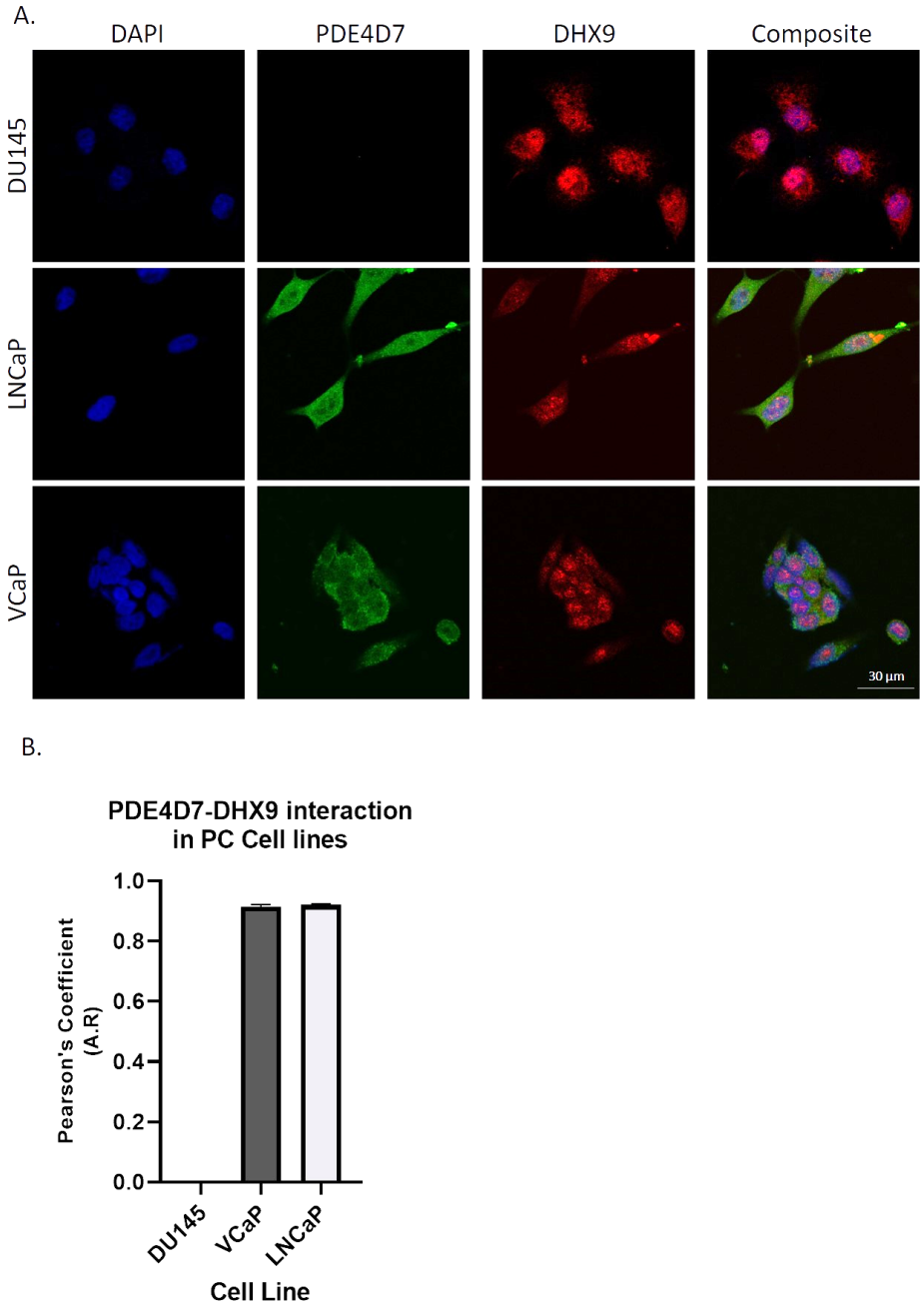

Figure 3.4 PDE4D7 and DHX9 staining in PC cells. A. DU145, LNCaP, and VCaP cells were stained for PDE4D7 and DHX9 expression using immunocytochemistry with confocal microscopy. Images were taken under a x 40 water immersion lens on the Zeiss LSM microscope. B. The Pearson's coefficient between PDE4D7 and DHX9 staining across the whole cells was determined using the Colocalization plug in on Image J. Data is presented as the mean ± SEM of 15 cells from each cell line.

Immunocytochemical staining of DU145 (Figure 3.4 A top row) further confirmed that there is very little PDE4D7 expressed in this cell line. However, DHX9 could be seen in both the nuclear and cytoplasmic regions of the cell (Figure 3.4 A top row). DU145 served as a negative control for quantifying the levels of colocalization between PDE4D7 and DHX9. The lack of PDE4D7 signal in DU145 resulted in a Pearson coefficient of 0 (Figure 3.4 B). On the other hand. LNCaP and VCaP both expressed PD4D7 within the cytoplasmic region, and small

amounts of PDE4D7 could be seen in the nucleus. The opposite observation could be made for DHX9, where the majority of the protein could be seen in the nucleus, and small amounts of it could be seen in the cytoplasm (Figure 3.4 A middle and bottom panel). The Pearson coefficient of the whole cell between PDE4D7 and DHX9 was 0.910 in VCaPs and 0.920 in LNCaPs, indicating that these two proteins are likely to be co-localizing *in vitro* (Figure 3.4 B). However, these images contradict the subcellular fractionation. The subcellular fractionation, as well as the data collected from the Human Protein Atlas, suggests that DHX9 is only expressed in the nucleus, while PDE4D7 is only expressed on the cytoplasm. However, subcellular fractionations are known to enrich proteins in their respective organelles (Lee, Tan and Chung, 2010), meaning DHX9 that may be expressed in the cytoplasm may not be detected using this method. Using confocal microscopy, we show here the DHX9 cam be expressed in the cytoplasm due to the presence of an NLS/NES sequence in its C-terminal (Lee and Pelletier, 2016). Collectively, the data in this chapter so far has shown that DHX9 is mainly expressed in the nucleus, but small traces of this protein can be detected in the cytoplasm by confocal microscopy.

As PDE4D7 and DHX9 were predominantly in different cellular locations I then set up an experiment to determine whether the colocalization between these two proteins could be increased when subjected to leptomycin B treatment. Leptomycin B (LMB) was originally identified as a metabolite of Streptomyces and has recently been used as a potent anti-tumour agent against murine tumours. LMB was shown to inhibit the function of chromosomal region maintenance/exportin 1 (CRM1) which is critical for the import/export of RNA and proteins that contains NES and NLS signals. Proteins that are expected to shuttle between the nucleus and the cytoplasm become trapped in the nucleus after LMB treatment, which in turn leads to their accumulation in this region (Kudo *et al.*, 1998; Jang *et al.*, 2003). DHX9 is known to be insensitive to LMB treatment and does not lead to any changes in DHX9's cellular location following treatment (Lee and Pelletier, 2016), however PDE4D7 has never before been subjected to LMB treatment. Here, LNCaP cells were treated for either 0, 3 or 8 hours with 20 nM of LMB, then stained for PDE4D7 and DHX9. The 8 hour time point was chosen as the longest treatment time as previous work has shown that this was the shortest time point used to inhibit nuclear export (Wolff, Sanglier

and Wang, 1997). The cells were visualised as previously mentioned, and the Pearson's coefficient between the PDE4D7 and DHX9 staining was measured (Figure 3.5).

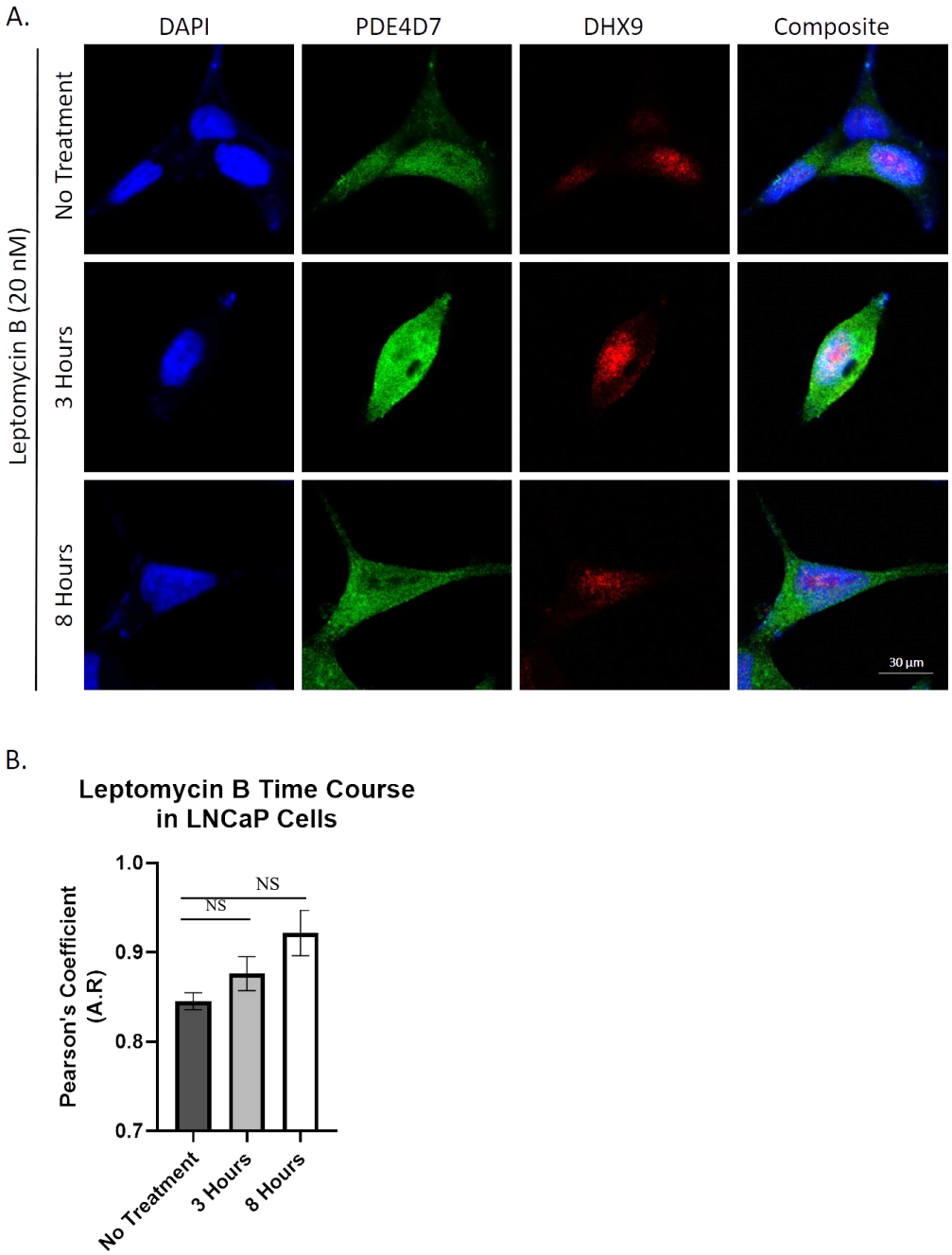

Figure 3.5 Leptomycin B time course in LNCaP. A. LNCaP cells were treated for 0, 3 or 8 hours with 20 nM of leptomycin, then stained for PDE4D7 (green), DHX9 (red) and the nucleus (blue). Images were taken using a Zeiss confocal microscope under a x 40 water immersion lens. B. Pearson's coefficient between the PDE4D7-DHX9 staining was determined using the Colocalization tool on ImageJ. Data is presented as the mean ± SEM of N > 15 individual cells from each condition. The data was analysed using a One-way Anova. Data was not significant.

Treatment of LNCaP with LMB resulted in a visible increase of PDE4D7 within the nuclear region as the cells were subjected to longer exposure to LMB (Figure 3.5 A). This also correlated to an increased in the Pearson's coefficient between

PDE4D7 and DHX9 across the whole cell, although this was not shown to be a statistically significant increase when analysed using a One-way Anova (Figure 3.5 B). To date, only the short PDE4D1 isoforms has been reported to be expressed in the nucleus, whereas other PDE4D isoforms are restricted to the cytoplasm. Sequence analysis revealed that the unique N-terminal region of PDE4D1 contains an NLS sequence allowing it shuttle in and out of the nucleus (Chandrasekaran *et al.*, 2008). Using the NLS Mapper (http://nls-mapper.iab.keio.ac.jp/cgi-bin/NLS_Mapper_form.cgi), the PDE4D7 amino acid sequence was analysed in order to identify potential NLS (Kosugi *et al.*, 2009) (Figure 3.6). The NLS predictor identified a 33 amino acid sequence (D^{187}RAPSKRSPMCNQPSINKATITEEAYQKLASET^{220}) within the linker and UCR2 region of PDE4D7 that is a potential NLS sequence (Beard *et al.*, 2000). In addition to identifying NLS sequences, this predictor is also able to predict the protein's cellular location. A score between 7 and 10 indicates that the protein is only expressed in the nucleus. A score between 3 and 6 indicates that the protein can be expressed in both the nucleus and the cytoplasm. A score below 3 indicates the protein is expressed only in the cytoplasm (Kosugi *et al.*, 2009). The NLS mapper revealed that PDE4D7 has a score of 5.3 indicating that the protein can be expressed in both the nucleus and the cytoplasm.

Predicted NLSs in query sequence

```
MKRNTCDLLSRSKSASEETLHSSNEEEDPFRGMEPYLVRRLSCRNIQLPP 50
LAFRQLEQADLKSESENIQRPTSLPLKILPLIAITSAESSGFDVDNGTSA 100
GRSPLDPMTSPGSGLILQANFVHSQRRESFLYRSDSDYDLSPKSMSRNSS 150
IASDIHGDDLIVTPFAQVLASLRTVRNNFAALTNLQDRAPSKRSPMCNQP 200
SINKATITEEAYQKLASETLEELDWCLDQLETLQTRHSVSEMASNKFKRM 250
LNRELTHLSEMSRSGNQVSEFISNTFLDKQHEVEIPSPTQKEKEKKKRPM 300
SQISGVKKLMHSSSLTNSSIPRFGVKTEQEDVLAKELEDVNKWGLHVFRI 350
AELSGNRPLTVIMHTIFQERDLLKTFKIPVDTLITYLMTLEDHYHADVAY 400
HNNIHAADVVQSTHVLLSTPALEAVFTDLEILAAIFASAIHDVDHPGVSN 450
QFLINTNSELALMYNDSSVLENHHLAVGFKLLQEENCDIFQNLTKKQRQS 500
LRKMVIDIVLATDMSKHMNLLADLKTMVETKKVTSSGVLLLDNYSDRIQV 550
LQNMVHCADLSNPTKPLQLYRQWTDRIMEEFFRQGDRERERGMEISPMCD 600
KHNASVEKSQVGFIDYIVHPLWETWADLVHPDAQDILDTLEDNREWYQST 650
IPQSPSPAPDDPEEGRQGQTEKFQFELTLEEDGESDTEKDSGSQVEEDTS 700
CSDSKTLCTQDSESTEIPLDEQVEEEAVGEEEESQPEACVIDDRSPDT   748
```

Predicted bipartite NLS

Pos.	Sequence	Score
187	DRAPSKRSPMCNQPSINKATITEEAYQKLASET	5.3

Figure 3.6 NLS prediction in PDE4D7. A potential NLS sequence within the linker and UCR2 region was identified using the software (Kosugi *et al.*, 2009).

Using confocal microscopy and bioinformatic analysis, my data suggests that the interaction between PDE4D7 and DHX9 could potentially take place in both the nucleus or the cytoplasm of LNCaP and VCaP.

3.3.3 Confirming PDE4D7-DHX9 interaction using pulldown and proximity ligation assays

So far, I have shown that PDE4D7 and DHX9 proteins express well in PC cell lines and that there is a small amount of cross-over in their cellular location. In order to provide further evidence that these two proteins are novel interactors in PC, I transfected HEK293 cells with plasmids containing VSV-tagged PDE4D7 and FLAG-tagged DHX9 and performed immunoprecipitation assays on the resulting cell lysates. This was used as a "proof of concept" step in order to verify that these two proteins could interact with one another. VSV-tagged PDE4D7 and Flag-tagged DHX9 plasmids were transiently transfected into HEK293 for 24 hours, then lysed using 3T3 lysis buffer. The cell lysates were then incubated with Protein G beads with either anti-VSV or anti-FLAG antibody for three hours. The beads were thoroughly washed in order to remove any unbound protein, and the remaining protein was boiled off the beads in SDS-PAGE sample buffer. The eluate was separated on an SDS-PAGE gel and immunoblotted for VSV or FLAG (Figure 3.7).

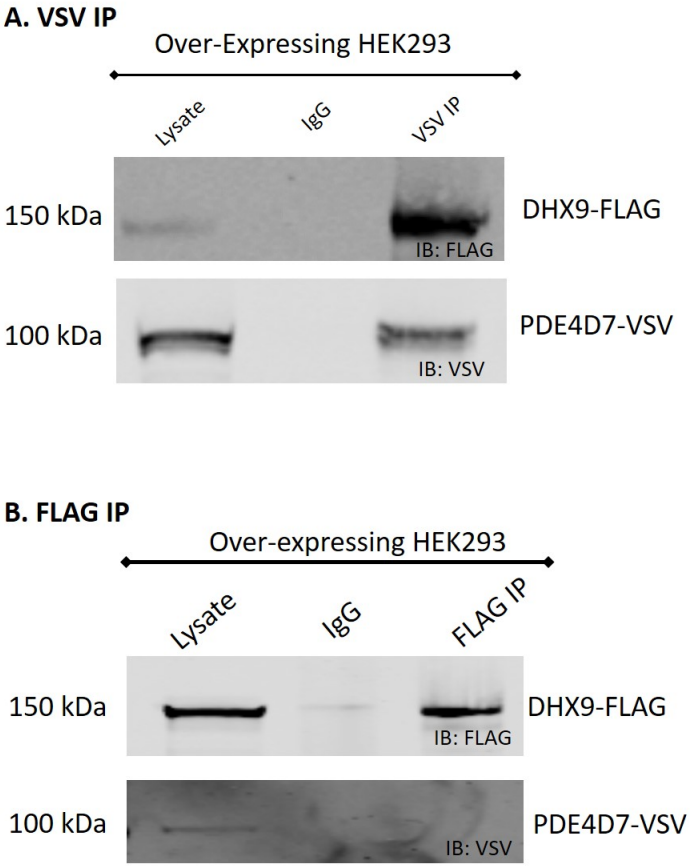

Figure 3.7 **PDE4D7-VSV and DHX9-FLAG IPs in overexpressing HEK293 Lysates.** A. VSV-tagged PDE4D7 was pulled down from HEK293 cells and probed for Flag-tagged DHX9 and VSV-tagged PDE4D7 B. Flag-tagged DHX9 was pulled down from HEK293 cells and probed for Flag-tagged DHX9 and VSV-tagged PDE4D7Data is representative of N=3 independent experiments.

Both IPs were successful with respect to pulling down proteins using their respective tags (Figure 3.7) and a positive co-IP was clearly observed in the cells that were pulled down for PDE4D7-VSV (Figure 3.7 A) and blotted for the FLAG tag of DHX9. Conversely, a pull down for DHX9-FLAG did not result in the co-IP for PDE4D7-VSV (Figure 3.7 A). This effect could possibly be due to the native structure of DHX9, as the natural 3D structure of DHX9 could prevent the protein from binding both the antibody and PDE4D7 concomitantly. Despite this, I was able to show that PDE4D7 and DHX9 are interacting when overexpressed in HEK293 cells. I then repeated this IP in VCaP and DU145 in order to ensure that this interaction could take place endogenously. Endogenously-expressed PDE4D7 and DHX9 were pulled down in VCaP or DU145 cells using target-specific antibodies (Figure 3.8). The cell lysate was incubated with either PDE4D7 isoform-specific or DHX9 antibody overnight with protein G beads. The supernatant was then separated on an SDS-PAGE gel and the PPI was investigated using western blotting (Figure 3.8).

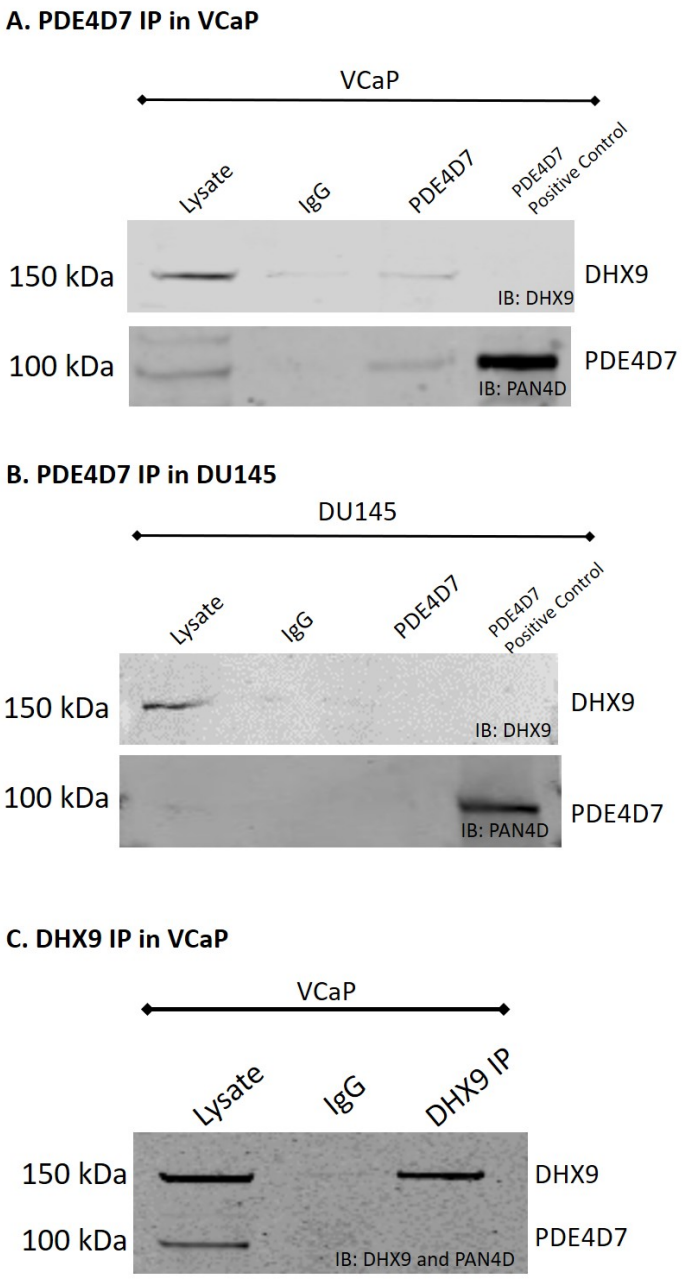

Figure 3.8 IP assay in PC cells to confirm PDE4D7-DHX9 binding. A+B. PDE4D7 was pulled down using an isoform specific antibody in VCaP (A) and DU145 (B). Membranes were probed for PDE4D7 and DHX9. C. DHX9 was pulled down in VCaP lysate using a target specific antibody. The membrane was probed for PDE4D7 and DHX9. Data is representative of N=3 independent experiments.

As in the HEK293 experiment with transfected proteins (Figure 3.7), pulldown of endogenous PDE4D7 lead to a successful co-IP of endogenous DHX9 in VCaP cells (Figure 3.8 A). However, as expected, this co-IP was not observed in DU145 cells where no PDE4D7 expression could be seen (Figure 3.8 B). Furthermore, like in the HEK293 cells, pulldown for DHX9 in VCaP cells did not lead to a positive pulldown for PDE4D7 (Figure 3.8 C). Again, it is possible that the DHX9 antibody epitope and the PDE4D7 docking domain are close on the 3D structure preventing

IP. Nevertheless, I show here that DHX9 and PDE4D7 interact with each other endogenously in PC cell lines.

Next, to further verify existence of the interaction, I performed proximity ligation assay (PLA) in the same cell lines. PLA uses oligonucleotide-modified antibodies, also called PLA probes, to visualise target proteins. Upon binding of the PLA probes, the conjugated oligonucleotides pair to generate circular DNA, and replication of this DNA signals that the target proteins are interacting at this site. DNA signals can be visualised using a fluorescent microscope as these PLA probes are often hybridized with a fluorophore. A positive reaction will only be seen if the two target proteins are less than 40 nm from each other (Klaesson *et al.*, 2018). Overexpressing HEK293 cells, as well as LNCaP and VCaP, were stained for PDE4D7 and DHX9 then subjected to PLA staining (red). The cells were also stained for the membrane (green) and the nucleus (blue) in order to visualise where putative DHX9 and PDE4D7 PPI may happen (Figure 3.9 and Figure 3.10).

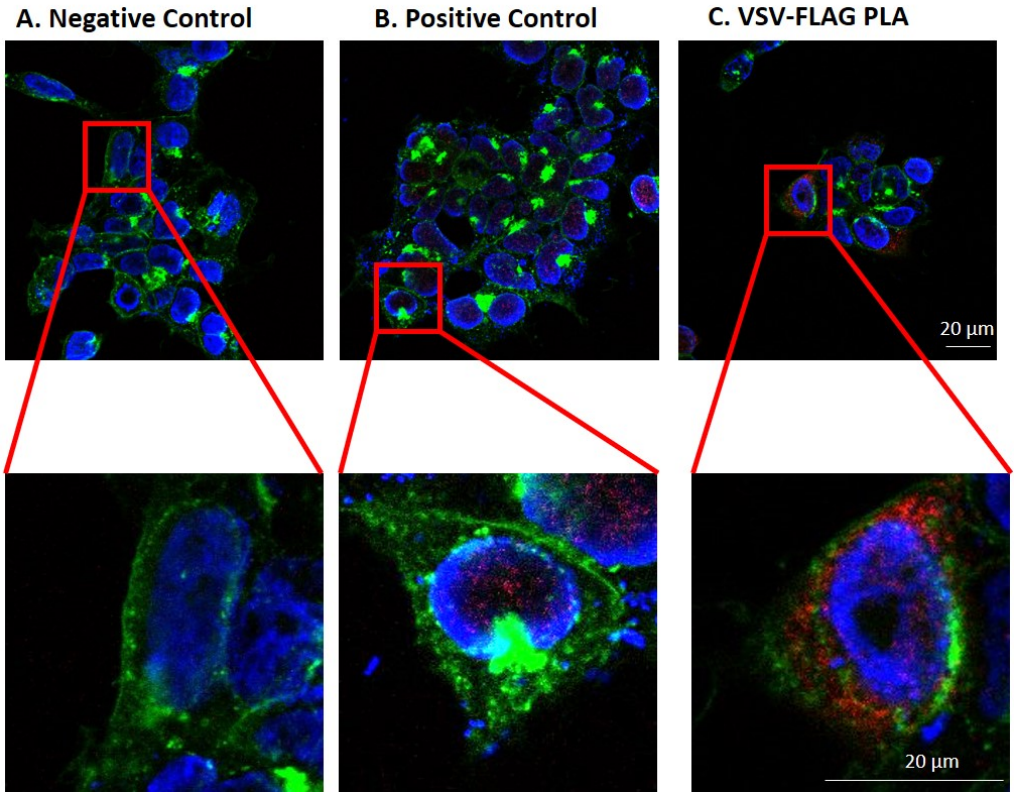

Figure 3.9 **PLA between PDE4D7-VSV and DHX9-FLAG in overexpressing HEK293 cells.** Wheat Germ Agglutinin (green) was used to stain the membrane of these cells, while SYTOX orange was used to stain the nucleus (blue). PLA signal are shown in red. Images are representative of eight different cell images. A. Negative control for PLA, where no primary antibody was present. B. Positive control for PLA, where the cells were probed for anti-mouse and anti-rabbit DHX9. C. PLA between VSV-tagged PDE4D7 and Flag-tagged DHX9.

As expected, no PLA signal was visible in the negative control as no primary antibody was present (Figure 3.9 A). PLA signal could be seen in the positive control, which was probed for DHX9 using a rabbit and mouse primary antibodies (Figure 3.9 B) indicating that the PLA probes can successfully bind to each other and generate a fluorescent signal. Interestingly, PLA signals was also visible in the sample probed for VSV tagged PDE4D7 and Flag tagged DHX9 (Figure 3.9 C), indicating that PDE4D7-DHX9 are within 40 nm of each other and are potentially interacting with one another. The PLA spots were observed across the whole cell, which is often the case in HEK293 cells transfected with plasmid constructs. In order to pinpoint where this interaction occurred, the PLA was performed in LNCaP and VCaP to probe for endogenous PDE4D7-DHX9 complexes (Figure 3.10 C and F).

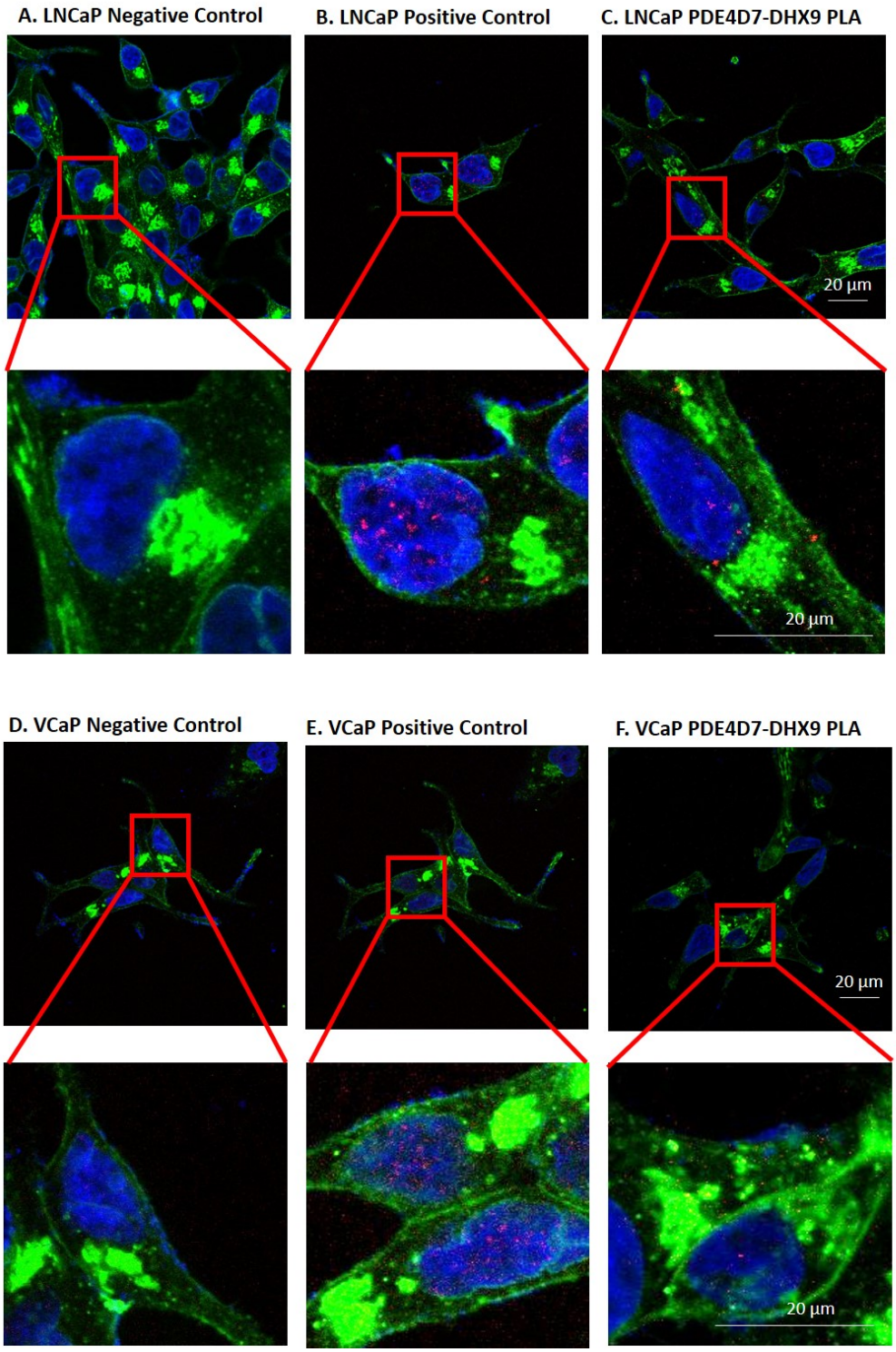

Figure 3.10 PLA between PDE4D7 and DHX9 in LNCaP and VCaP cells. Wheat Germ Agglutinin (green) was used to stain the membrane of these cells, while SYTOX orange was used to stain the nucleus (blue). PLA signal are shown in red. Images are representative of eight different cell images. Cells were stained with different antibodies. A+D. Negative control for PLA where the cells were not probed for primary antibody. B+E. Positive control for PLA where the cells were probed for anti-rabbit and anti-mouse DHX9 primary antibody. C+F. PLA between PDE4D7 and DHX9.

As in the HEK293 cells, a PLA signal was observed in the positive control (Figure 3.10 A and D), indicating that the probes are able to bind to each other and generate a fluorescent signal. This signal was absent in the negative control

where no primary antibody was present (Figure 3.10 B and E). Visible spots could be observed in the cells probed for PDE4D7 and DHX9 (Figure 3.10 C and F) indicating that these two protein are able to interact with each other in an intact cell. Upon closer inspection, PDE4D7 and DHX9 complexes could be observed in the cytoplasm and the nucleus (Figure 3.10 C and F). Hence I have been able to provide further evidence that these two proteins are interacting and that this interaction takes place within the cytoplasmic and nuclear regions.

3.3.4 Mapping PDE4D7-DHX9 binding domains

Although I have been able to show that PDE4D7-DHX9 exist in a complex, it is unknown whether the binding between these two proteins is direct and if so, the binding domains remain undetermined. I therefore used peptide array technology to demonstrate direct interactions and map the binding domains between the two interactors. A large proportion of PPIs are mediated by compact interaction motifs within different regions of the protein. These regions are recognised and/or post-translationally modified by a structured domain of an interacting partner (Tompa *et al.*, 2014). These regions, most commonly known as peptide motifs, can be categorised into two groups: binding motifs which mediate the interaction between two proteins, and posttranslational modification sites recognised by modifying enzymes (Tompa *et al.*, 2014). These protein binding motifs are short segments found within either the terminal end or within a loop of an interacting protein. Interestingly, numerous oncogenic proteins either contain a motif, or recognise these binding motifs, for which inhibiting these is a potential drug target (Corbi-Verge and Kim, 2016). These binding motifs not only help PPIs, but they also coordinate protein function, localization, and degradation (Tompa *et al.*, 2014). Modulating PPIs with small drug-like molecules targeting these motifs holds great promise in drug discovery (Shen *et al.*, 2019). Traditionally, mapping of binding motifs were discovered using tandem affinity purifications or yeast-two hybrids experiments, However, in recent years, high throughput screening assays and computational studies, such as direct peptide library and protein chip-based assays, have been used to identify novel binding motifs that mediate PPIs Tompa *et al.*, 2014)

In recent years, peptide array technology has been used to map novel PPI binding motifs. Peptide array technology was first developed by Ronald Frank in

the early 1990s and since then, it has become a powerful tool to investigate PPI as well as post translational modifications (PTMs) (Volkmer, Tapia and Landgraf, 2012). Using an array approach, specific domains or sequential sequences of full-length proteins can be immobilised on cellulose for further investigation. Here, full length DHX9 or PDE4D7 amino acid sequences were spotted onto CelluSpot™ glass slides as 25-mer spots, with each spot shifting by 5 amino acids (Figure 3.11).

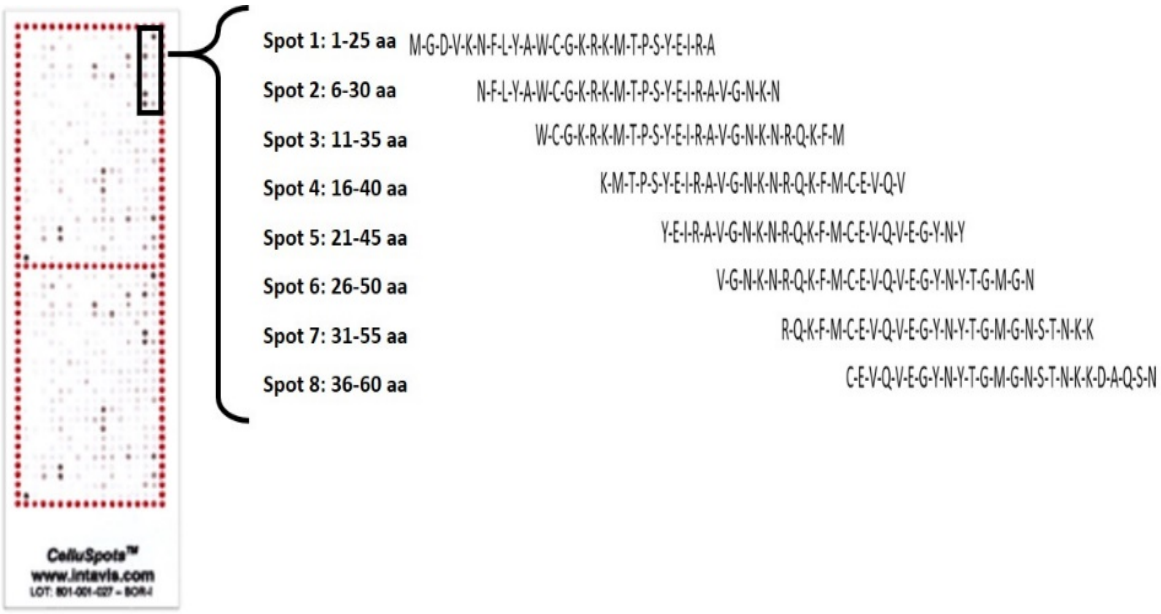

Figure 3.11 Peptide Array design layout. Full length protein in 25-amino acid peptides is spotted onto a glass slide with a cellulose membrane where each spot is shifted by 5 amino acids.

PDE4D7 full length slides were incubated with HEK293 lysate overexpressing DHX9-FLAG, then probed for the FLAG tag in order to identify which 25-mer peptides from PDE4D7 could be bound by DHX9-FLAG. The slides were then probed with the appropriate secondary antibodies, then imaged using chemiluminescence detection (Figure 3.12).

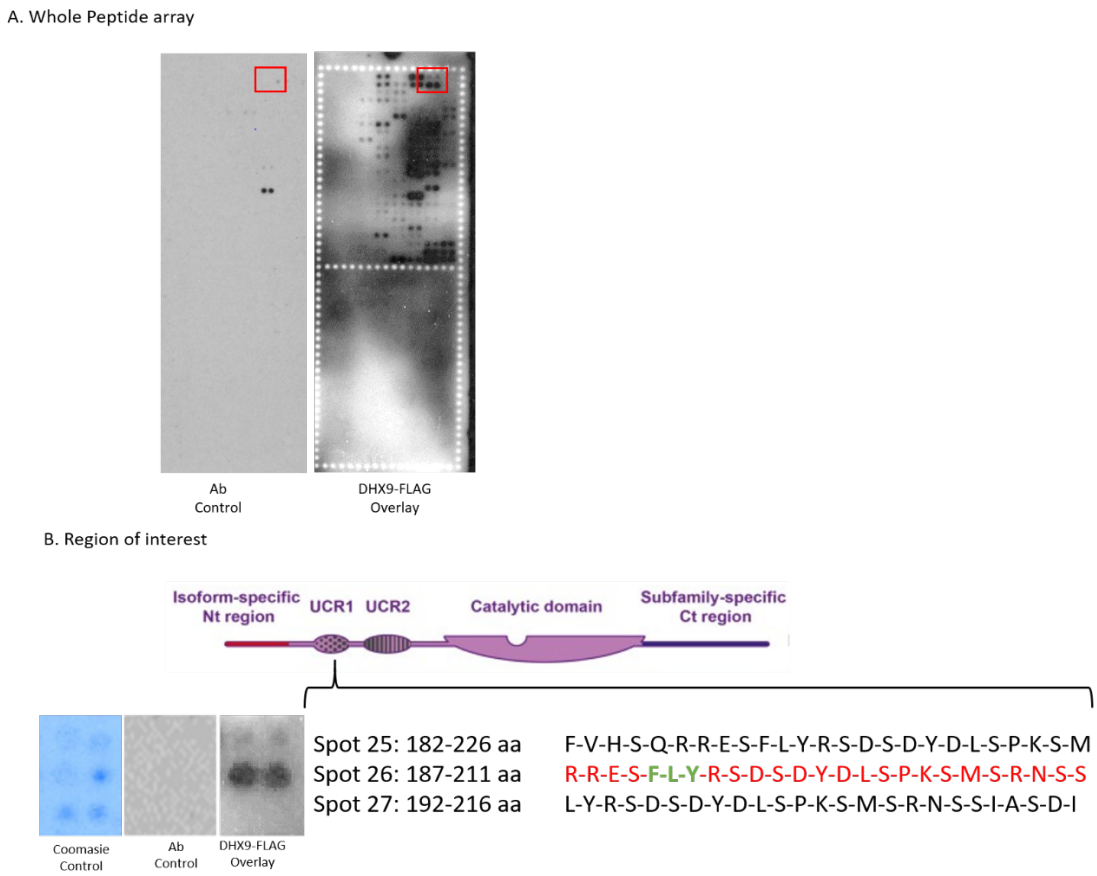

Figure 3.12 PDE4D7 peptide array overlaid with HEK293 overexpressing DHX9-FLAG lysate. A. Whole peptide array images. Regions of interest are highlighted in the red box. B. Full length PDE4D7 peptide array was incubated with DHX9-FLAG cell lysate, then probed for the binding sites using a FLAG tag antibody. Image adapted from Tibbo, Tejeda and Baillie, 2019.

Peptide array technology revealed that DHX9 binds to a PDE4D7 25mer within the UCR1 region (Figure 3.12). Within this binding site is the FLY motif, highlighted in green in Figure 3.12, has recently been shown to be an important multi-docking site for protein interactors of PDE4 isoforms (Houslay *et al.*, 2017). Although the UCR1 is highly conserved between all long PDE4 isoforms there are some small areas of divergence and the binding site sequence identified above (Figure 3.12) is unique to PDE4D isoforms due to the presence of a single serine at residue 205 (Figure 3.13).

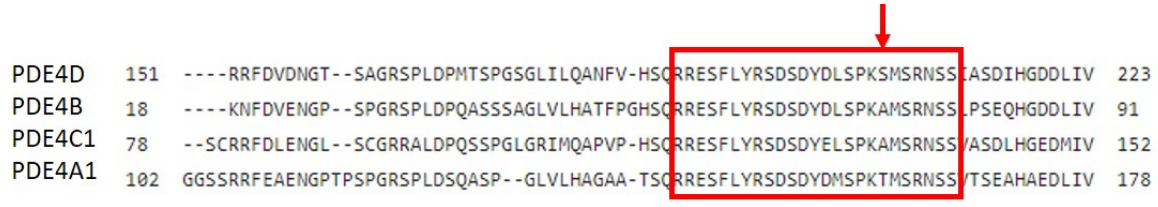

Figure 3.13 PDE4 Sequence alignment. PDE4 isoforms were BLASTed against each other in order align the newly identified DHX9 binding site. This site is unique to long PDE4 isoforms due to the presence of a single serine at position 205 (highlighted by a red arrow). (Altschul et al., 1997).

In order to identify any crucial amino acids for DHX9 binding, a walking alanine substitution scan on the sequence was performed. Furthermore, single and triple substitution of the FLY docking site (to alanine) was also performed in order to determine whether the loss of one or all these amino acids is detrimental to DHX9 binding (Figure 3.14).

A. Walking Alanine Scan

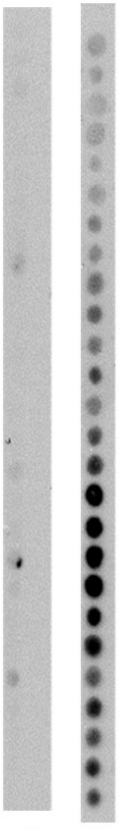

		187 aa 211 aa
Spot	1	R-R-E-S-F-L-Y-R-S-D-S-D-Y-D-L-S-P-K-S-M-S-R-N-S-S
Spot	2	A-R-E-S-F-L-Y-R-S-D-S-D-Y-D-L-S-P-K-S-M-S-R-N-S-S
Spot	3	R-A-E-S-F-L-Y-R-S-D-S-D-Y-D-L-S-P-K-S-M-S-R-N-S-S
Spot	4	R-R-A-S-F-L-Y-R-S-D-S-D-Y-D-L-S-P-K-S-M-S-R-N-S-S
Spot	5	R-R-E-A-F-L-Y-R-S-D-S-D-Y-D-L-S-P-K-S-M-S-R-N-S-S
Spot	6	R-R-E-S-A-L-Y-R-S-D-S-D-Y-D-L-S-P-K-S-M-S-R-N-S-S
Spot	7	R-R-E-S-F-A-Y-R-S-D-S-D-Y-D-L-S-P-K-S-M-S-R-N-S-S
Spot	8	R-R-E-S-F-L-A-R-S-D-S-D-Y-D-L-S-P-K-S-M-S-R-N-S-S
Spot	9	R-R-E-S-F-L-Y-A-S-D-S-D-Y-D-L-S-P-K-S-M-S-R-N-S-S
Spot	10	R-R-E-S-F-L-Y-R-A-D-S-D-Y-D-L-S-P-K-S-M-S-R-N-S-S
Spot	11	R-R-E-S-F-L-Y-R-S-A-S-D-Y-D-L-S-P-K-S-M-S-R-N-S-S
Spot	12	R-R-E-S-F-L-Y-R-S-D-A-D-Y-D-L-S-P-K-S-M-S-R-N-S-S
Spot	13	R-R-E-S-F-L-Y-R-S-D-S-A-Y-D-L-S-P-K-S-M-S-R-N-S-S
Spot	14	R-R-E-S-F-L-Y-R-S-D-S-D-A-D-L-S-P-K-S-M-S-R-N-S-S
Spot	15	R-R-E-S-F-L-Y-R-S-D-S-D-Y-A-L-S-P-K-S-M-S-R-N-S-S
Spot	16	R-R-E-S-F-L-Y-R-S-D-S-D-Y-D-A-S-P-K-S-M-S-R-N-S-S
Spot	17	R-R-E-S-F-L-Y-R-S-D-S-D-Y-D-L-A-P-K-S-M-S-R-N-S-S
Spot	18	R-R-E-S-F-L-Y-R-S-D-S-D-Y-D-L-S-A-K-S-M-S-R-N-S-S
Spot	19	R-R-E-S-F-L-Y-R-S-D-S-D-Y-D-L-S-P-A-S-M-S-R-N-S-S
Spot	20	R-R-E-S-F-L-Y-R-S-D-S-D-Y-D-L-S-P-K-A-M-S-R-N-S-S
Spot	21	R-R-E-S-F-L-Y-R-S-D-S-D-Y-D-L-S-P-K-S-A-S-R-N-S-S
Spot	22	R-R-E-S-F-L-Y-R-S-D-S-D-Y-D-L-S-P-K-S-M-A-R-N-S-S
Spot	23	R-R-E-S-F-L-Y-R-S-D-S-D-Y-D-L-S-P-K-S-M-S-A-N-S-S
Spot	24	R-R-E-S-F-L-Y-R-S-D-S-D-Y-D-L-S-P-K-S-M-S-R-A-S-S
Spot	25	R-R-E-S-F-L-Y-R-S-D-S-D-Y-D-L-S-P-K-S-M-S-R-N-A-S
Spot	26	R-R-E-S-F-L-Y-R-S-D-S-D-Y-D-L-S-P-K-S-M-S-R-N-S-A

B. Alanine Substitution of FLY domain

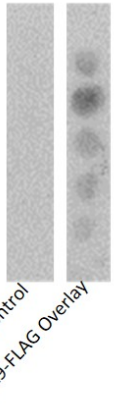

		187 aa 211 aa
Spot	1	R-R-E-S-F-L-Y-R-S-D-S-D-Y-D-L-S-P-K-S-M-S-R-N-S-S
Spot	2	R-R-E-S-A-L-Y-R-S-D-S-D-Y-D-L-S-P-K-S-M-S-R-N-S-S
Spot	3	R-R-E-S-F-A-Y-R-S-D-S-D-Y-D-L-S-P-K-S-M-S-R-N-S-S
Spot	4	R-R-E-S-F-L-A-R-S-D-S-D-Y-D-L-S-P-K-S-M-S-R-N-S-S
Spot	5	R-R-E-S-A-A-A-R-S-D-S-D-Y-D-L-S-P-K-S-M-S-R-N-S-S

Figure 3.14 Walking alanine and triple substitution of DHX9 binding site. A. Walking alanine scan of the DHX9 binding site. B. Single and triple substitution of the FLY docking site.

Alanine substitution of Ser^{190} at spot 5 (Figure 3.13 A) appears to decrease the binding between PDE4D7 and DHX9 when compared to the control spot (spot 1). However, single amino substitutions between spots 12 and 21 increases the interaction probably due to change in the overall charge of the peptide sequence (Figure 3.14 A). Interestingly, single substitutions of the amino acids between spots 14 and 23 increases the binding of DHX9-FLAG to the peptide array (Figure 3.14 A). As with other binders of the FLY motif (Houslay *et al.*, 2017) , triple substitution of the FLY with alanine decreases the interaction between PDE4D7 and DHX9, however this interaction is not completely ablated (Figure 3.14 B). We can then assume that this region may be needed for the interaction between the two proteins as reported for the interaction between PDE4A5 and mitogen-activated protein kinase-activated protein kinase 2 (MK2) (Houslay *et al.*, 2017).

I was then interested in repeating this peptide array experiment with purified recombinant DHX9. A group led by Professor Richard Wozniak at the University of Alberta had recently been able to purify a full length functional, as well as truncated, DHX9 GST recombinant protein (Capitanio, Montpetit and Wozniak, 2017). The truncated proteins consisted of a 67.8 kDa N-terminal region protein, a 75 kDa helicase core domain protein, and a 75.8 kDa C-terminal protein (Figure 3.14 A). The full-length protein has an expected molecular weight of 166 kDa. I transformed each GST-tagged DHX9 plasmids into *E.coli* BL21-Codon Plus (DE3) cells (Figure 3.15 A). Protein expression was induced with the addition of 0.2 mM of IPTG and the cells were left overnight at 16˚C with shaking. The cells were pelleted and lysed the next day and the proteins purified as detailed in the methods. Protein expression was determined by running the samples on an SDS-PAGE gel with western blotting, where the membrane was probed for GST (Figure 3.15 B,C and D).

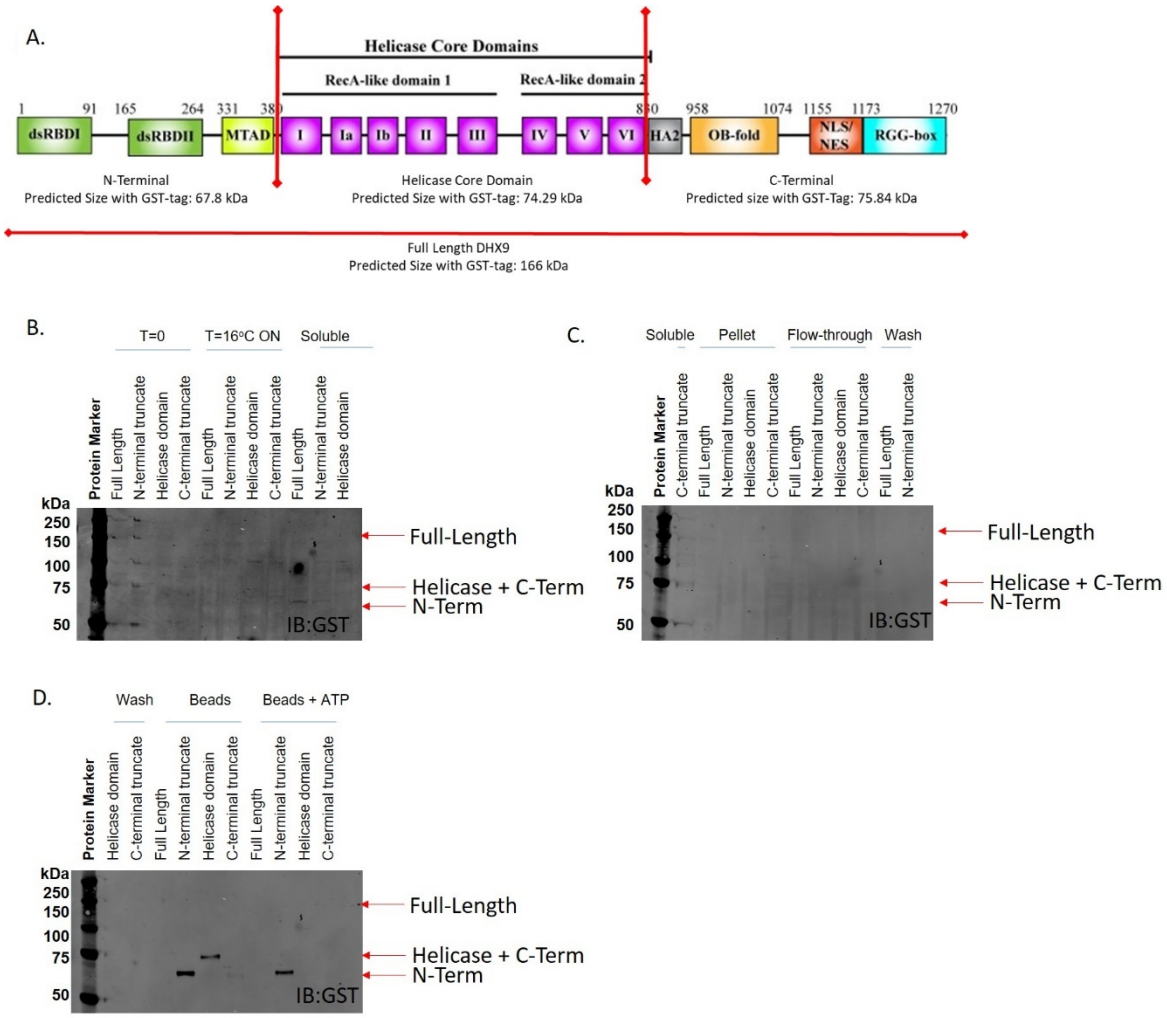

Figure 3.15 **Purification of recombinant DHX9 purified protein.** A. Schematic diagram showing the full-length and truncated DHX9 recombinant proteins used in these experiments. DHX9 plasmids were a kind gift from Prof Richard Wozniack at the University of Alberta. B-D. E.coli cells transformed with these plasmids were induced overnight with 0.2 mM of IPTG at 16˚C. Quality control samples were taken at each step of the purification and run on an SDS-PAGE gel. Protein expression was assessed by western blotting. All membranes were probed for GST. This work was carried out by Dr Yuan Yan Sin.

Although we were able to express the N-terminal and Helicase domain of DHX9 (Figure 3.15 D, lane 4 and 5), we were unable to elute the protein from the GST tagged beads (Figure 3.15 D, lane 8). Bizarrely, the bands representing the N-terminal and helicase domain of DHX9 was not detected in the other gels, potentially indicating that the expression is at very low levels and can only be detected when bound to GST beads (Figure 3.15 B and C). We were therefore unable to verify our peptide arrays using the purified DHX9 protein. Alternative methods were used to elute the protein, such as the addition of NaCl to increase the ionic strength, however this remained unsuccessful (data not shown here). I was therefore unable to verify that the purified DHX9 protein could bind the same peptide sequence as the DHX9-FLAG lysate. However, using HEK293 DHX9-FLAG lysate I was able to show that DHX9 binds to the UCR1 region of PDE4D7

(Figure 3.12); I therefore purified this region of PDE4D to investigate where PDE4D7 binds to DHX9 using full length DHX9 peptide arrays. Unfortunately, I did not have access to an appropriate construct to purify the full length PDE4D7 protein for these experiments. I chose to purify this region as it is highly conserved within PDE4D isoform (Houslay, 2010). PDE4D-UCR1 was cloned by a previous member of the Baillie lab into the pGEX-5X-1 expression vector then transformed into BL21 *E.Coli* competent cells. The GST tag alone was also purified in order to ensure that any possible positively interacting spots were due to protein binding, and not due to the tag itself. Each construct was induced with 0.2 mM of IPTG for 5 hours at 37˚C, then pelleted and lysed in order to obtain the protein (Figure 3.16 A and B). Proteins eluted from GST beads was then dialysed in order to remove any remaining salts and detergents, and proteins were stored at -80˚C until required (Figure 3.16 C and D). Quality control samples, eluted, and dialysed proteins were then all run on an SDS-PAGE in order to check for protein expression by western blotting (Figure 3.16).

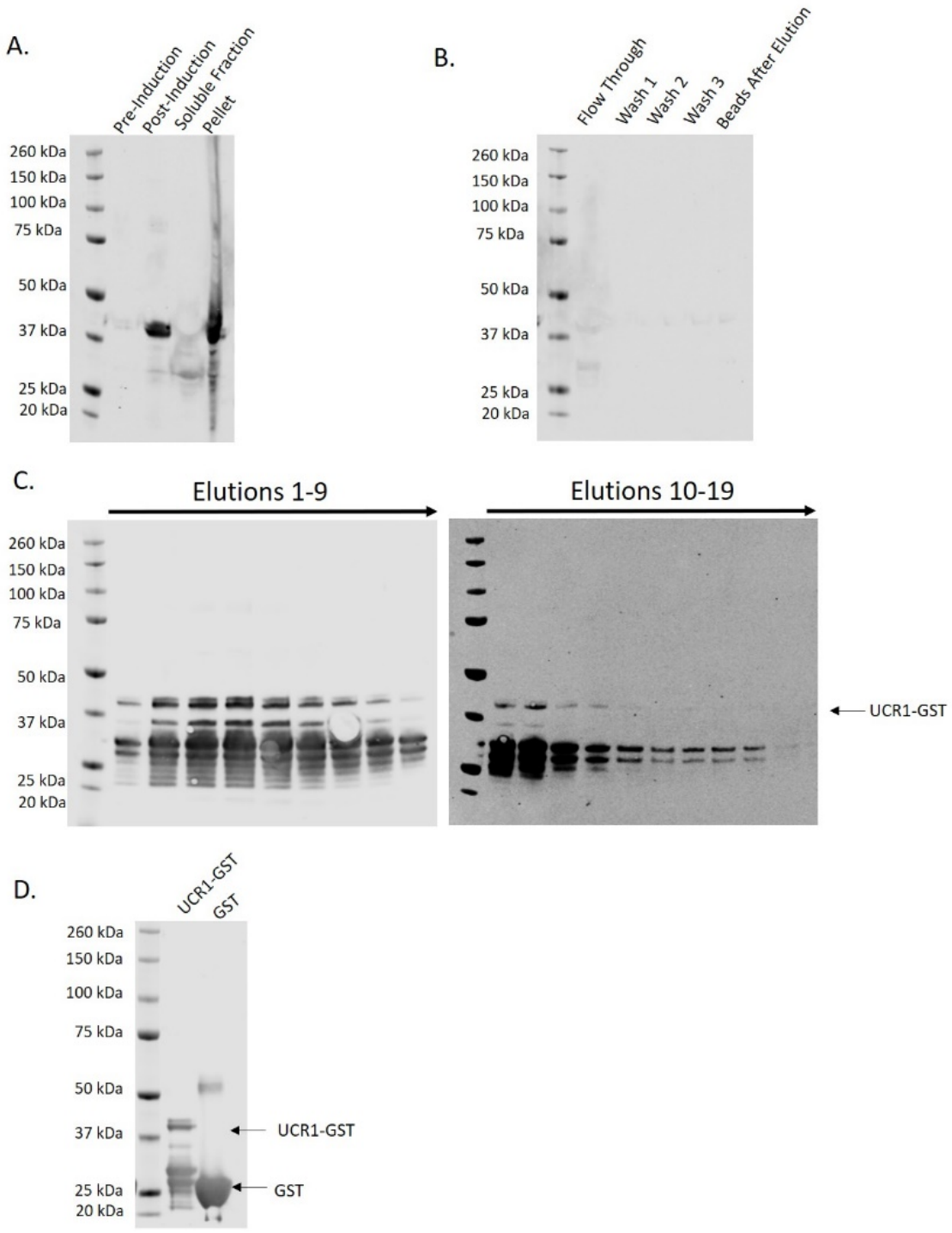

Figure 3.16 PDE4D UCR1-GST purification from BL21 *E.Coli*. The following samples were all run on an SDS-PAGE gel and UCR1-GST expression was assessed by western blotting using a GST antibody. A. Pre, post-inductions, soluble and insoluble fractions. B. Flow through, washes and beads from the purification column. C. Elutions 1-9 in D. UCR1-GST and GST purified protein after dialysis.

By running all the elution samples on an SDS-PAGE gel and probing for GST by western blotting, I was able to show that I successfully purified recombinant PDE4D-UCR1 GST, as shown by a band at 39 kDa (Figure 3.16 C and D). Purified PDE4D proteins are highly prone to protein degradation, even in the presence of protease inhibitor, as shown by the presence of multiple smaller bands (Figure

3.16 C). In order to obtain the purest recombinant protein, I decided to only dialyse elutions 9-13 as these samples contained the least amount of degradation (Figure 3.16 C). The dialysed protein (Figure 3.16 D) was then used in order to map PDE4D7 binding on immobilised DHX9 peptides via peptide array. The recombinant purified proteins were overlaid onto full length DHX9 peptide array slides, then probed using a GST antibody. Purified recombinant GST alone was used as a control in order to ensure that the spot detected were due to protein binding, and not the tag binding to the peptide sequence (Figure 3.17 B).

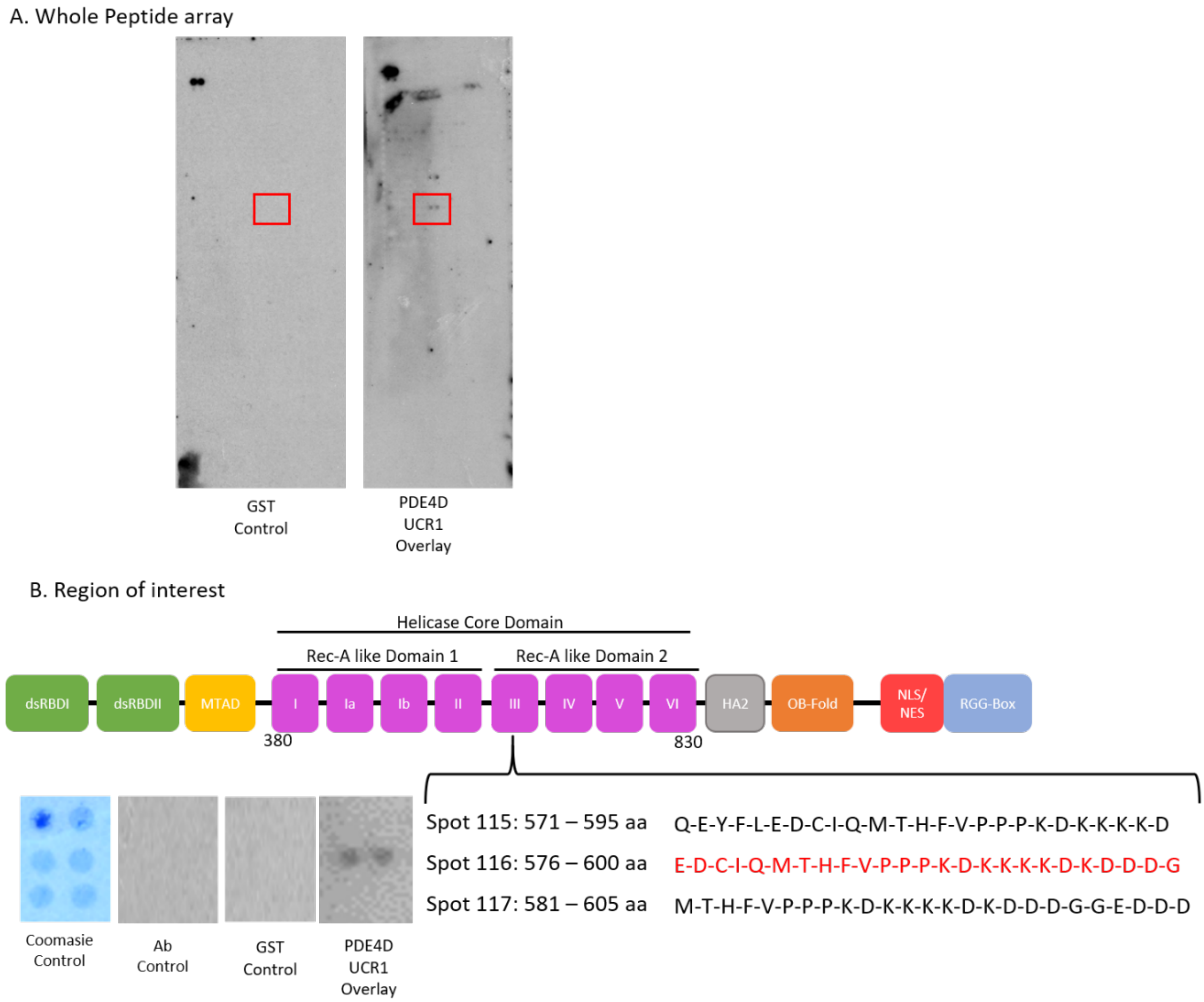

Figure 3.17 Mapping PDE4D7 binding on DHX9. A. Whole peptide array. Regions of interest are highlighted in the red boxes. B. Full length DHX9 peptide array, spotted as duplicates on the slide, was overlaid with either GST or PDE4D UCR1-GST, then probed using a GST antibody. PDE4D UCR1 was shown to bind to DHX9 within its helicase core domain.

The data from the peptide array suggests that PDE4D7 binds within the helicase core domain of DHX9. This could mean that the binding of PDE4D7 could have a role in regulating the helicase activity of DHX9 by potentially regulating its phosphorylation. This helicase core domain is highly conserved between species, and its structure has been partially solved using X-Ray crystallography (Schütz *et*

al., 2010). However, the sequence used for this structure unfortunately does not include the PDE4D7 binding sequence therefore we were unable to model the potential binding site. Interestingly, this binding region also contains multiple prolines, lysines and aspartic acids (Figure 3.17 B). In order to identify which amino acids were crucial for PDE4D7 binding, peptide array membranes were synthesised with a walking alanine scan, as well as substitutions of specific amino acids (Figure 3.18).

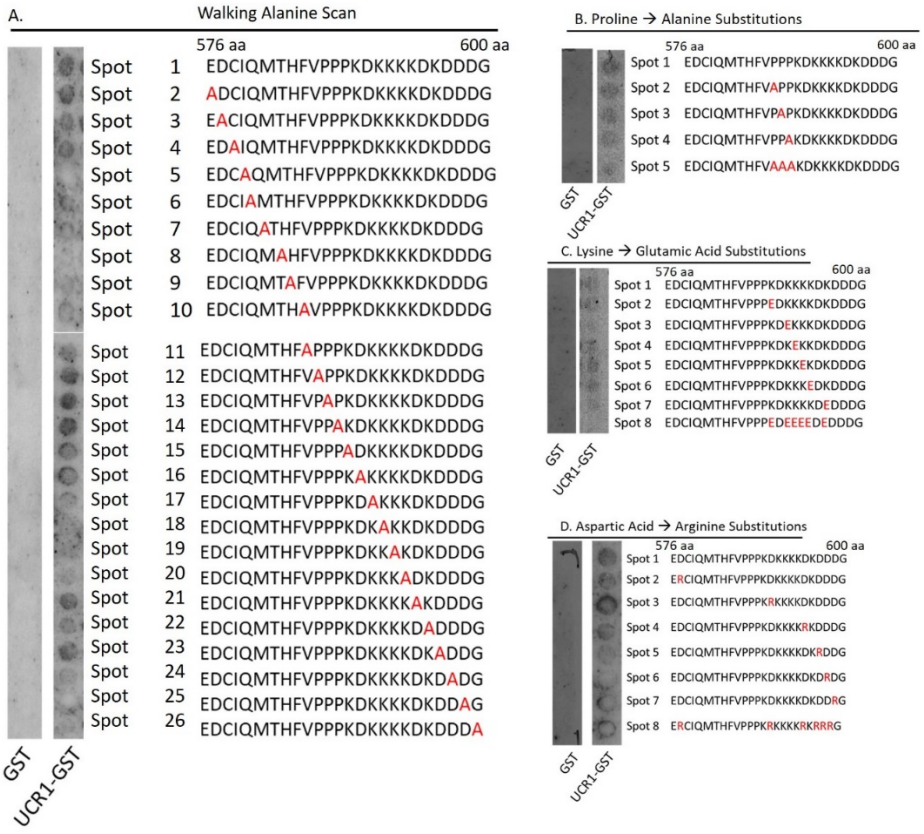

Figure 3.18 Amino Acid Substitutions of the PDE4D7 binding site on DHX9. The peptide array membranes were incubated with either GST or PDE4D-UCR1 GST. They were then probed with GST primary antibody. Binding sites were detected after probing the membrane with an anti-mouse HRP secondary. A. Walking alanine scan of the PDE4D7 binding sequence. B. Single and multiple substitution of the proline to an alanine. C. Single and multiple substitution of the lysine to a glutamic acid. D. Single and multiple substitution of aspartic acid to an arginine.

The walking alanine scan suggests that the I^{579} (spot 5) and H^{583} (Spot 9) are important for PDE4D7 binding (Figure 3.18 A). Interestingly, substitution of the lysines between spots 18-20 (Figure 3.18 A) lead to a decrease in PDE4D-UCR1 binding. Furthermore, when these lysines were substituted with a negatively charged glutamic acid led to inhibition of PDE4D7 binding onto the membrane indicating that these residues are important for protein binding at spot 8 (Figure 3.18 C). Substitution of the prolines and the aspartic acids had no deleterious effects on binding (Figure 3.18 B and D). Studies have shown that lysine residues

of proteins play an important role in protein-protein and protein-DNA binding. The amino group of the residue itself often binds to the hydrogen bonds and catalyses the interaction with a ligand that may be important for protein function and substrate specificity (Sun *et al.*, 2013). Lysine-rich regions are also known to be important in multiple post translational modifications, such as SUMOylation (Lamoliatte *et al.*, 2014). I was then interested to see if the deletion, rather than substitution, of any of these lysines led to a decrease in PDE4D7 binding. Peptide array membranes with either N-, C-, or simultaneous N- and C-terminal truncations of the DHX9 binding sequence were constructed (Figure 3.19) and overlaid with either GST, as a control, or recombinant PDE4D-UCR1 GST.

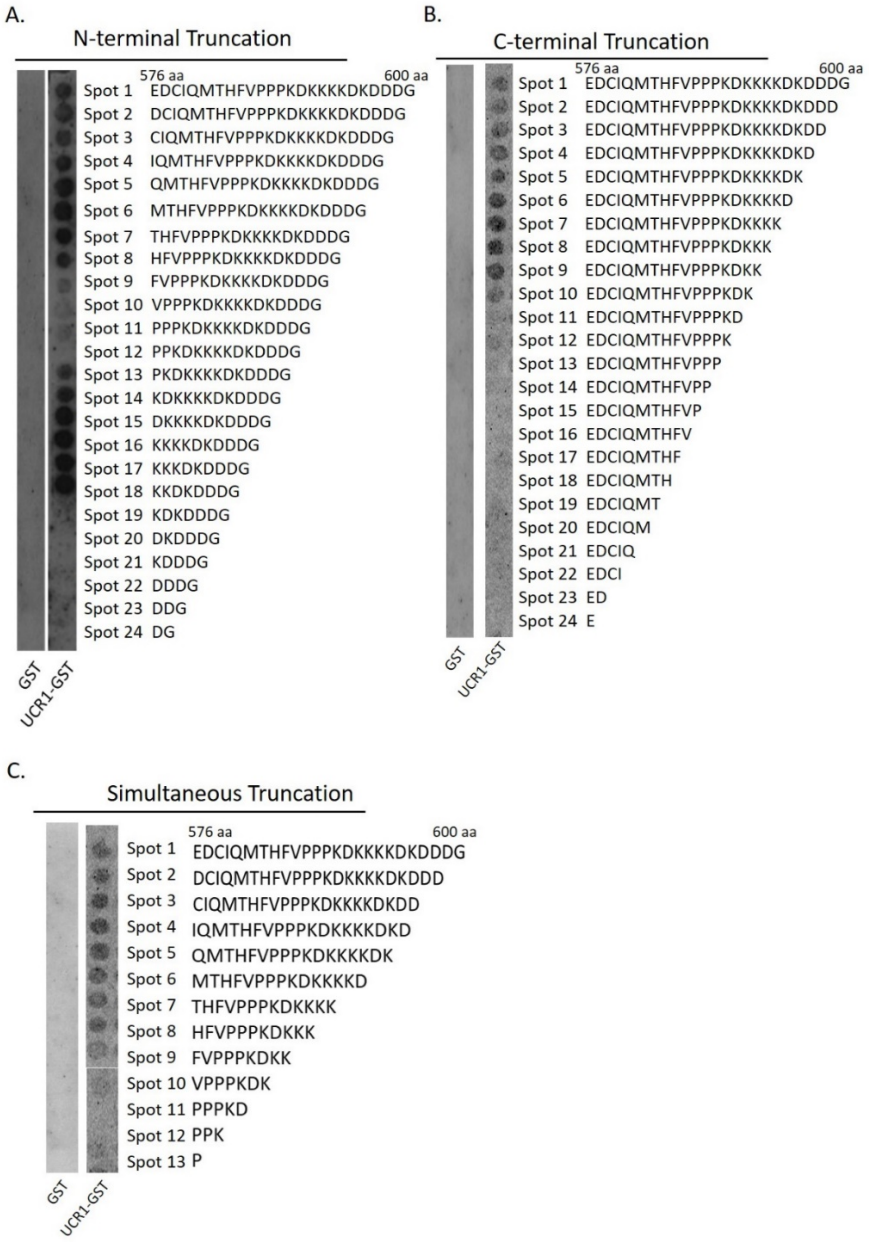

Figure 3.19 **PDE4D7 binding site truncations** A. N-terminal truncations. B. C-terminal truncations C. Simultaneous N and C terminal truncations

Loss of F^{584} to P^{587} by N-terminal sequence truncation appeared to reduce the interaction between PDE4D7 and DHX (Figure 3.19 A spot 9-12). Single alanine substitution of F^{584} in Figure 3.17A (spot 10) also led to a loss in interaction. It has been shown that in soluble proteins, hydrophobic amino acids such as phenylalanine play a significant role in rapid protein folding as well as stabilizing protein scaffolds (Makwana and Mahalakshmi, 2015). Loss or substitution of this F^{584} in DHX9 could potentially cause the interaction to destabilise, leading to a decrease in protein-protein interaction. Truncations that resulted in the loss of the lysine at position 593 lead to a complete loss of PDE4D7 binding, indicating that this is a crucial residue for binding (Figure 3.19 A spot 19 and B Spot 10). This was also observed in the simultaneous N- and C-terminal truncations (Figure 3.19 C spot 11). In order to further investigate if this lysine is crucial binding, site-directed mutagenesis of this lysine (K^{592}) could be undertaken in our DHX9-FLAG plasmids. The PDE4D7 IPs could be repeated, and if there is a decrease in co-IP this could further confirm that this lysine is important for the interaction between PDE4D7 and DHX9. Unfortunately, due to time constraints, I was unable to design and create these mutants.

3.3.5 Development of cell penetrating peptides to disrupt PDE4D7-DHX9 interaction

In recent years, peptide therapeutics have played an important role in medical practices. Currently, there are over 60 peptide drugs approved in the United Stated and other major countries, and an increasing amount of clinical trials include the use of therapeutic peptides (Lau and Dunn, 2018). These therapeutic peptides have a maximum of 40 residues and are not limited to the 20 genetically encoded amino acid (Davenport *et al.*, 2020). These peptides have a high affinity and specificity to their target tissue or cell. They are typically identified using phage display experiments. In recent years, therapeutic peptides have grown in interest due to the fact that they can easily be synthesised, are smaller in size, and have a lower toxicity. These peptides can often be conjugated with carriers or therapeutic agents, improving its pharmacokinetics (Mousavizadeh *et al.*, 2017; Davenport *et al.*, 2020). Classically, these peptides are delivered as injectable. However, alternative methods of administration forms are gaining interests, such as oral, intranasal, and transdermal delivery routes (Fosgerau and Hoffmann, 2015).The main

diseases currently driving the use of peptide drugs are metabolic diseases, such as type 2 diabetes, and oncology. However, with the development of alternative delivery methods, such as topical administration, the hope is to enable the greater use of peptide therapeutics in other disease areas (Fosgerau and Hoffmann, 2015).

Although we have been able to map putative binding sites between the two proteins using peptide arrays, these needed to be further verified *in vitro* using the overexpressing HEK293 and VCaP cell lines. One way of doing this would be to use peptide disruptors that could disassociate the PDE4D7-DHX9 complex. Hence, I used information gathered from the peptide arrays (Figure 3.12 and Figure 3.17), to devise cell-permeable peptide encompassing residues R^{187}-S^{212} of PDE4D7. This peptide was synthesised and named "UCR1 disruptor peptide" (Figure 3.20 A). At the same time, a complementary approach using a peptide containing residues E^{576}-G^{606} from DHX9 was also used. This peptide was named "DHX9 disruptor peptide" (Figure 3.20 B). Both peptides were made by GenScript, to a purity of 98% and dissolved in sterile DMSO to a stock concentration of 10 mM for future use. Although these peptides were synthesised using the information gained in the peptide arrays, they may not be specific to this interaction alone. The UCR1 domain is shared between all long PDE4D isoforms (Houslay and Adams, 2003), while the helicase domain is shared between all DExD/H helicases (Lee and Pelletier, 2016). This could potentially mean that these peptides have the potential to disrupt other protein-protein interactions that could take place in these domains.

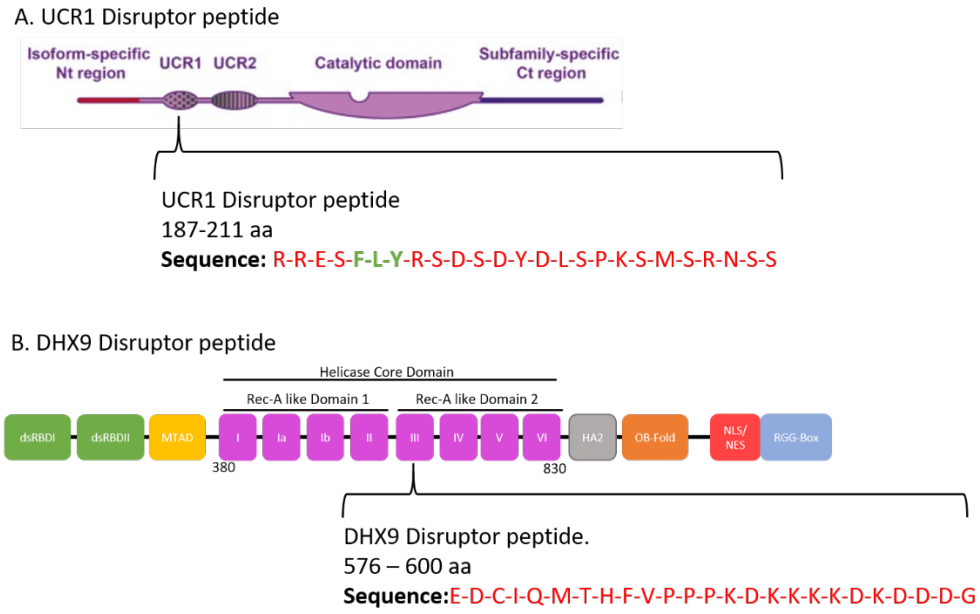

Figure 3.20 Designing peptide to disrupt the PDE4D7-DHX9 interaction. A. The UCR1 disruptor sequence in based on the DHX9 binding domain on PDE4D7. B. The DHX9 disruptor peptide is based on the PDE4D7 binding domain of DHX9.

A control peptide which consisted of a 25-mer peptide that was different from both disruptor peptides (PEVPLSYRRKLPGEFKKVRIKELM) was also synthesised and named “scrambled peptide”. This scrambled peptide was made by a previous member of the Baillie lab and was shown to not have any effects on their protein-protein interaction of interest (data not shown here). This scrambled peptide sequence was checked against the UCR1 and DHX9 disruptor peptide sequence in order to ensure that there were no similarities between peptides. Furthermore, this scrambled peptide was used by a previous member of the lab and was not shown to disrupt any PPIs or interest. All peptides contained an N-terminal stearic acid allowing it to cross the cell membrane. The ability of these peptides to displace the PDE4D7-DHX9 interaction was first assessed by IP. By repeating the IPs shown in Figure 3.7 and Figure 3.8 in the presence of our newly synthesised disruptor peptides, I would be able to further confirm that I had successfully mapped the binding sites in PDE4D7 and DHX9. PDE4D7 was pulled down from lysates extracted from overexpressing VSV-tagged PDE4D7 in HEK293 and VCaP cells using a VSV and PDE4D7 isoform-specific antibody respectively. The IPs were then thoroughly washed, and the amount of DHX9 that was co-IPed with PDE4D7 was assessed by SDS-PAGE gel electrophoresis with western blotting (Figure 3.21 and Figure 3.22).

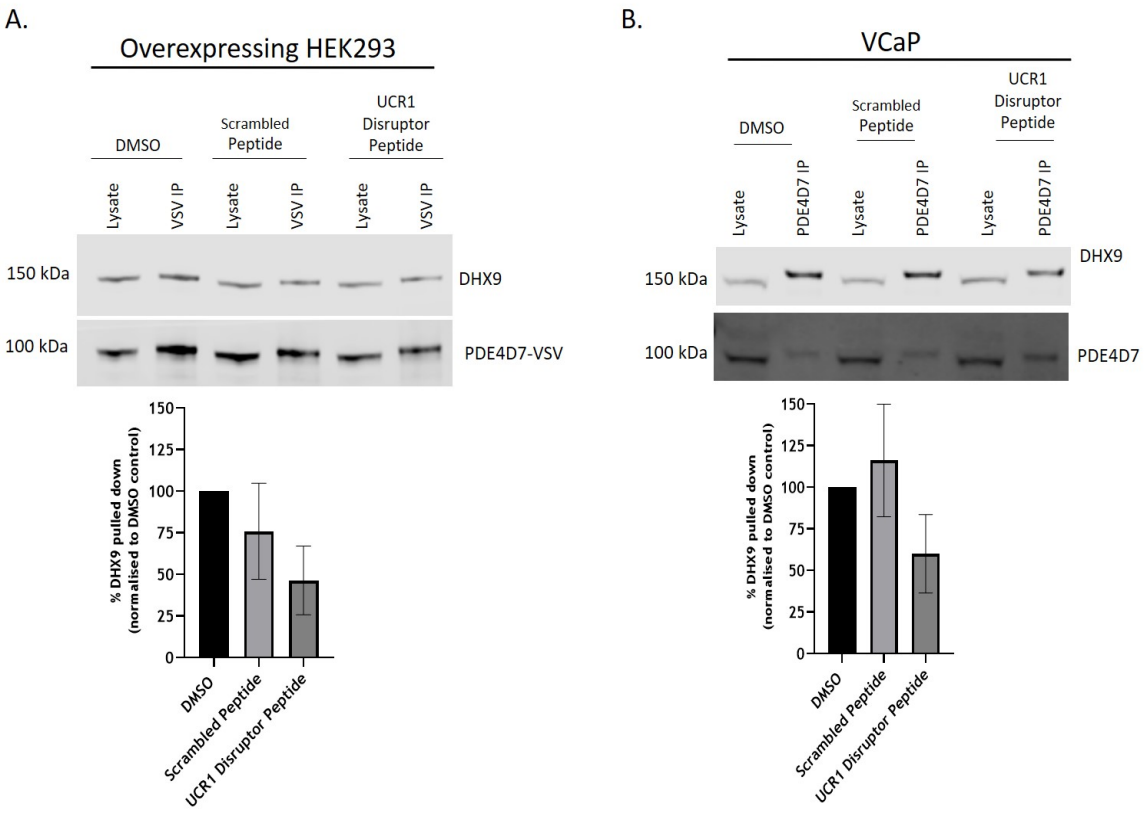

Figure 3.21 Disruption of PDE4D7-DHX9 interaction in HEK293 and VCaP using the UCR1 disruptor peptide. A. HEK293 were transfected with a plasmid encoding PDE4D7-VSV and treated with 10 μM of either disruptor peptide, scrambled peptide or DMSO vehicle control for 2 hours. Lysates were immunoprecipitated for PDE4D7-VSV and probed for VSV and DHX9. The amount of DHX9 pulled down was normalised to PDE4D7-VSV IP, then normalised to DMSO vehicle control. B. VCaP cells were treated with 10 μM of either disruptor peptide, scrambled peptide or DMSO vehicle control for 2 hours. Lysates were immunoprecipitated for PDE4D7 and probed for Pan4D and DHX9. The amount of DHX9 pulled down was normalised to PDE4D7 IP, then normalised to DMSO vehicle control. The data is presented as mean ± SEM of three independent experiments. Statistical significance was determined using a One-Way Anova.

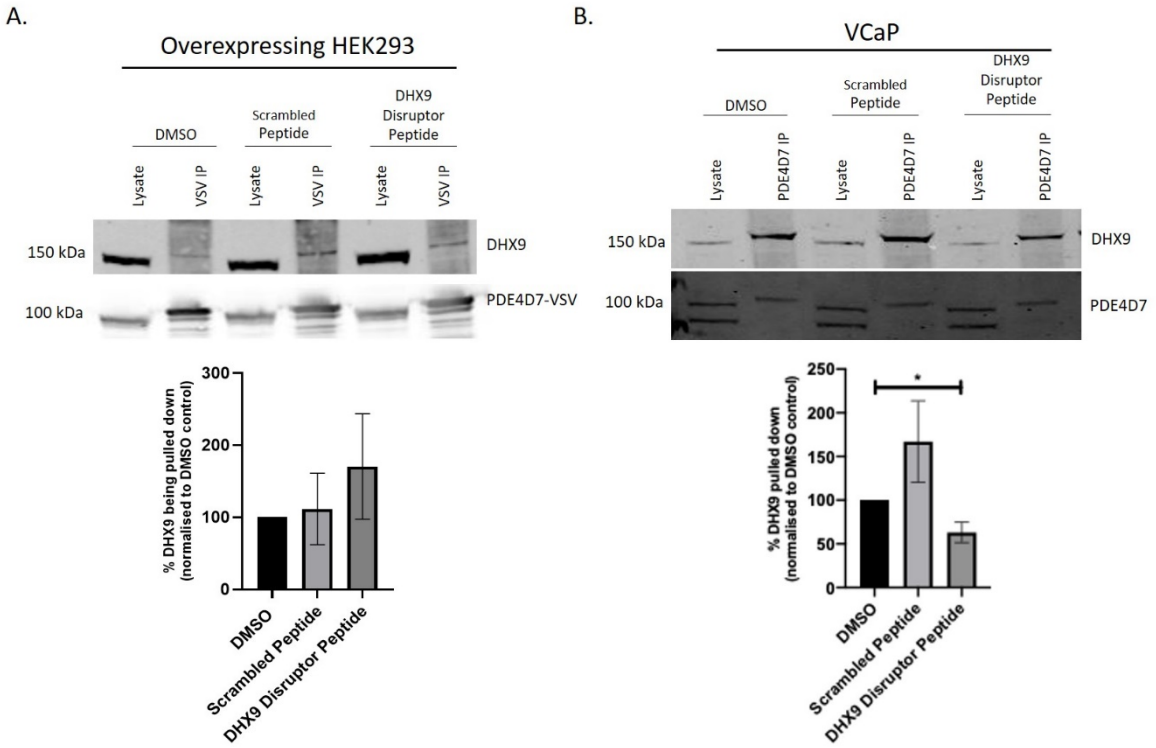

Figure 3.22 Disruption of PDE4D7-DHX9 interaction in HEK293 and VCaP following DHX9 disruptor peptide treatment. A. HEK293 were transfected with PDE4D7-VSV and treated with 10 μM of DHX9 disruptor peptide, scrambled peptide or DMSO vehicle control for 2 hours. Lysates were immunoprecipitated for PDE4D7-VSV and probed for VSV and DHX9. The amount of DHX9 pulled down was normalised to PDE4D7-VSV IP, then normalised to DMSO vehicle control. B. VCaP cells were treated with 10 μM of either disruptor, scrambled peptide or DMSO vehicle control for 2 hours. Lysates were immunoprecipitated for PDE4D7 and probed for Pan4D and DHX9. The amount of DHX9 pulled down was normalised to PDE4D7 IP, then normalised to DMSO vehicle control. The data is presented as mean ± SEM of three independent experiments. Statistical significance was determined using a One-Way Anova, where p*=0.0355.

Although not significant in statistical terms, treatment of PDE4D7-VSV-overexpressing HEK293 and VCaP with the UCR1 disruptor peptide decreased the interaction between both ectopic PDE4D7-VSV (HEK293, Figure 3.21 A lane 6 compared to lane 2) and endogenous PDE4D7 (VCaP, Figure 3.21 B lane 6 compared to lane 2) and DXH9 when compared to the DMSO vehicle control. Treatment with the DHX9 disruptor peptide had little effect in overexpressing HEK293 (Figure 3.22 A), but significantly reduced the interaction of endogenous PDE4D7-DHX9 in VCaP cells (Figure 3.22 B lane 6 compared to lane 2). As often is the case, exogenously expressed proteins do not reflect what is occurring endogenously. Overexpressing a protein in cell line is often used in order to understand a function of a protein, as well as identify any interacting proteins. However, this does potentially force an interaction to take place (Prelich, 2012), thus not truly reflecting what is happening when endogenous levels of proteins are expressed. Overexpression of PDE4D7 and DHX9 in HEK293 cells allowed for

the protein to remain bound to one another, despite being treated with the disrupted peptide.

The newly synthesised UCR1 disruptor peptide was able to disrupt the interaction between PDE4D7 and DHX9 by out-competing DHX9 for binding site within the UCR1 domain. I then decided to repeat the PLA experiments investigating the interaction between PDE4D7 and DHX9 in the presence of the UCR1 disruptor peptide or the scrambled peptide. VCaP cells were treated for two hours with DMSO, 10 μM UCR1 disruptor peptide, or 10 μM scrambled peptide. The PLA was then performed and imaged, and the red fluorescent spots representing each PLA signal was quantified using Image J (Figure 3.23). Since the FLY region has been shown to be a multi-docking site for PDE4 isoforms, I decided to first further validate this binding domain. Unfortunately, due to time constraints, I was unable to further test the DHX9 disruptor peptide by PLA assay with confocal microscopy.

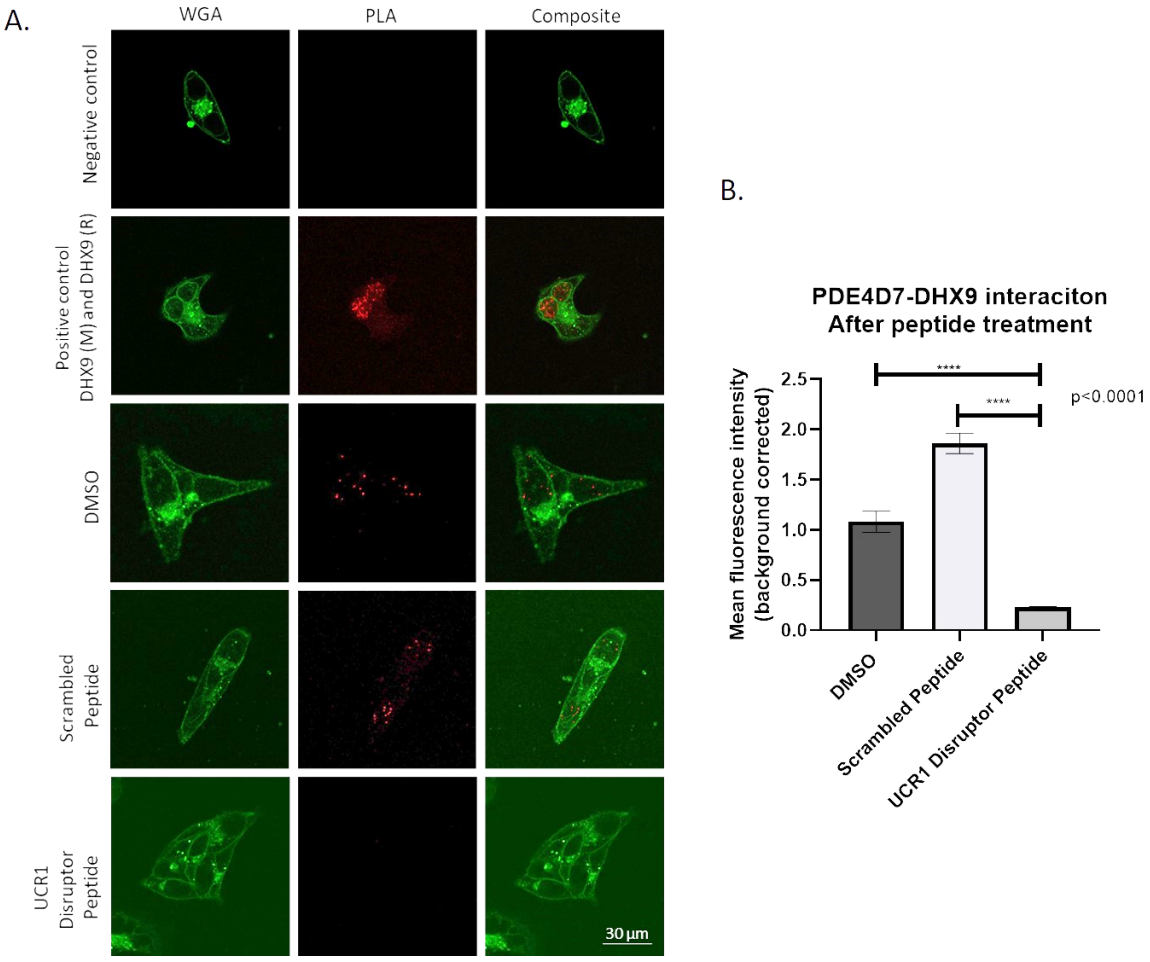

Figure 3.23 Disruption of the PDE4D7-DHX9 interaction by the UCR1 disruptor peptide. A. VCaP cells were treated with 10 µM of disruptor peptide, scrambled peptide or DMSO vehicle control for 2 hours, then probed by PLA for PDE4D7 and DHX9. Cell membrane was stained using wheat germ agglutinin (green), and PLA was detected using a x 40 oil immersion lens. B. Mean fluorescence intensity of at least 20 cells from each condition was measured. Statistical significance was determined using a One-Way Anova where p>0.0001. Data is presented as the mean ± SEM of n>20 cells.

Treatment of VCaP cells with the UCR1 disruptor peptide significantly decreased the interaction between PDE4D7 and DHX9 (Figure 3.23 A, last row). I then quantified the PLA signal from the cells treated with DMSO, scrambled peptide or UCR1 disruptor peptide (Figure 3.23, middle column). These values were plotted against each other, and a One-Way Anova was performed (Figure 3.23 B). This analysis revealed that the interaction between PDE4D7 and DHX9 was significantly decreased when compared to the DMSO and scrambled peptide controls (Figure 3.23 B). The data presented so far confirms that DHX9 binds within the UCR1 domain of PDE4D7, and this interaction can be ablated with the use of our newly synthesised disruptor peptide.

3.3.6 Determining PDE4D7-DHX9 binding affinity using fluorescence polarization

The data presented thus far in this chapter has confirmed that PDE4D7 and DHX9 are novel interactors in PC cell lines. By using peptide array technology, I was able to map where these interactions took place. PDE4D7 binding to DHX9 within its helicase domain, while DHX9 binds within the UCR1 region of PDE4D7. By using the peptide array information, novel cell penetrating peptides were developed in order to confirm these binding sites. Treatment of VCaP and HEK293 cells with these peptides lead to a decrease in PDE4D7 and DHX9 interaction when compared to the vehicle control (Figure 3.21Figure 3.22Figure 3.23). Knowing that the interaction of PDE4D7 and DHX9 took place within the UCR1 domain, I was then interested in determining the binding affinity between these two proteins. Currently, fluorescence polarization (FP) is the most commonly used technique to study molecular interactions including PPIs (Lea and Simeonov, 2011). FP provides a nondisruptive way of measuring the association of a fluorescent ligand with a larger molecule, such as a purified recombinant protein (Rossi and Taylor, 2011). When a fluorophore is covalently bonded to small ligand, such as a peptide in solution, it is excited by the polarized light causing the emitted light to be largely depolarized. This is due to the rapid reorientations, or tumbling, of the fluorophore giving a low polarization value (Figure 3.24 A). However, if the labelled ligand is bound to a high molecular weight protein (> 10 kDa), the fluorophore reorients itself and this results in a slower molecular rotation. The binding of the larger molecule leads to a decrease in ligand rotation, which in turn leads to an increase in FP signal (Moerke, 2009) (Figure 3.24 B). By plotting these FP values, we are then able to then produce a sigmoidal curve from which we can obtain the dissociation constant of a PPI. By interpolating this information from the sigmoidal curve, we are able to quantify the strength of the interaction between two partners (Rossi and Taylor, 2011).

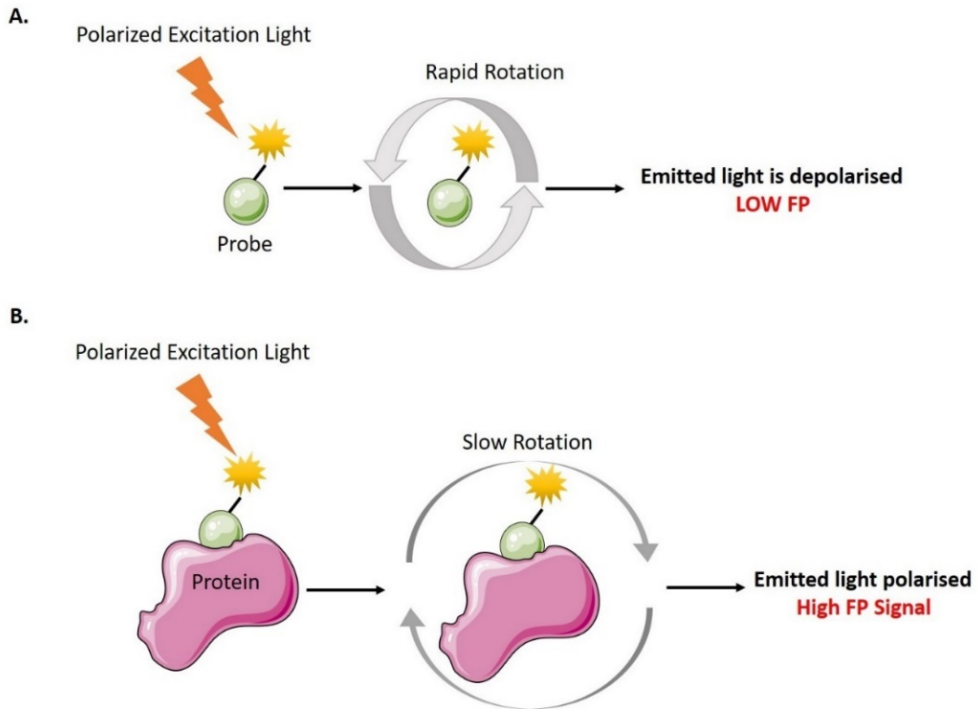

Figure 3.24 Ligand binding analysis by fluorescence polarization. A. In the absence of a high molecular weight protein, the rapidly rotations ligand gives low FP signal. B. The association of the ligand with a large molecule slows does the motion of the fluorophore, leading to an increase in the FP signal. Image adapted from Arkin *et al.*, 2004.

In this series of experiments, the interaction between UCR1-GST, or GST control, and a fluorescently tagged DHX9 peptide (5-FAM DHX9) was studied using FP. The DHX9 peptide sequence was the same sequence as the disruptor peptide as this contains the binding domain for PDE4D7. The UCR1-GST and the GST protein that was previously purified was used for this assay (Figure 3.16 D). Furthermore, full length PDE4D5-GST was also used in this assay in order to investigate if the full-length protein conformation is needed for the interaction. Like PDE4D7, PDE4D5 is a long isoform and shares the same UCR1 region (Tibbo, Tejeda and Baillie, 2019). These two proteins are identical in their sequences, apart from their unique N-terminal regions, and both contain the unique Ser^{196} previously identified as only being expressed in PDE4D isoforms (Figure 3.13). PDE4D5-GST, expressed in the pGEX-6P-1 expression vector, was previously purified by Connor Blair (Baillie Lab) from BL21 *E.Coli* bacterial cells. Protein expression was induced 0.1 mM IPTG at 16˚C overnight. Cells were collected the next day and subjected to lysis. Cells lysates were then sonicated, and the supernatant incubated in Glutathione Sepharose beads. Recombinant purified protein was then eluted from the beads (Figure 3.25 A).

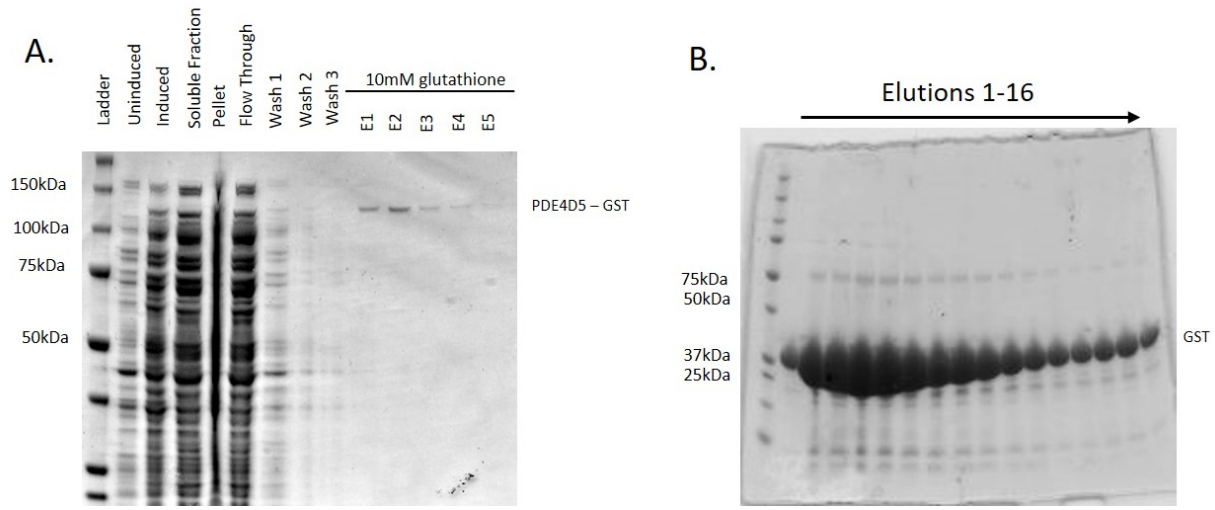

Figure 3.25 PDE4D5-GST and GST protein purification. PDE4D5-GST and GST were purified from *E.*Coli. A. Expression and purity of the recombinant protein was assessed via SDS-PAGE gel stained with Coomassie Blue. Presence of a 140 kDa protein confirmed that PDE4D5-GST was successfully purified. This protein purification was performed by Connor Blair. B. Expression and purity of recombinant GST protein was assessed via SDS-PAGE with Coomasie Blue staining. Presence of a 25 kDa protein confirmed that GST was successfully purified.

By running the eluted proteins on an SDS-PAGE gel, then staining with coomasie blue, I was able to show that both PDE4D5-GST (Figure 3.25 A)and GST alone (Figure 3.25 B) were both purified to the highest quality. Although the UCR1-GST sample previously purified showed slight protein degradation (Figure 3.16 D), this sample was still taken forward for FP binding assays. Using the information from the peptide array (Figure 3.17 Spot 116), a 25-mer peptide was generated from the PDE4D7 binding site in DHX9. Residues E^{576}-G^{606} based on the PDE4D7 binding sequence on DHX9 was synthesised with an N-terminal 5-FAM fluorescent tag. This peptide was generated by Genscript and dissolved in DMSO to a stock concentration of 10 mM. Although we have been able to purify the proteins of interest, a pilot assay with just the newly synthesised peptide needs to be performed. This allows us to determine the minimum amount of peptide needed for future FP binding assays (Figure 3.26).

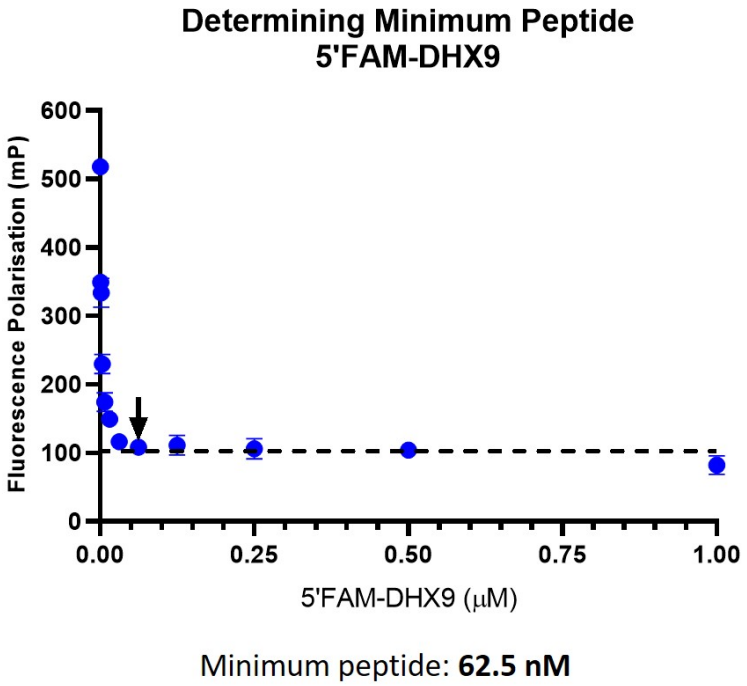

Figure 3.26 Determining minimum DHX9 peptide concentration for FP assay. Fluorescently tagged DHX9 peptide was serially diluted, and the FP value was plotted against the concentration of peptide present.

By using the linear portion of the graph (indicated by dotted lines in Figure 3.26), we were able to determine the lowest amount of peptide needed for future FP assays. The lowest peptide concentration was chosen in order to minimise the amount of DMSO present in the FP assay. DMSO concentration above 4% of the final volume can potentially destabilize PPI (Chan *et al.*, 2017). The minimum peptide needed for future binding assays was found to be 62.5 nM. Using this information, the direct binding assay was performed using the previously obtained purified recombinant protein. All proteins were serially diluted 1:2, from a starting concentration of 10 µM. 62.5 nM of the 5'FAM-DHX9 peptide was then added and the reaction was left to incubate at room temperature. The FP value was recorded after 0.5, 1, 3 and 5 hours, and the values obtained were plotted against the $\log_{10}$ of the protein concentration present (Figure 3.27).

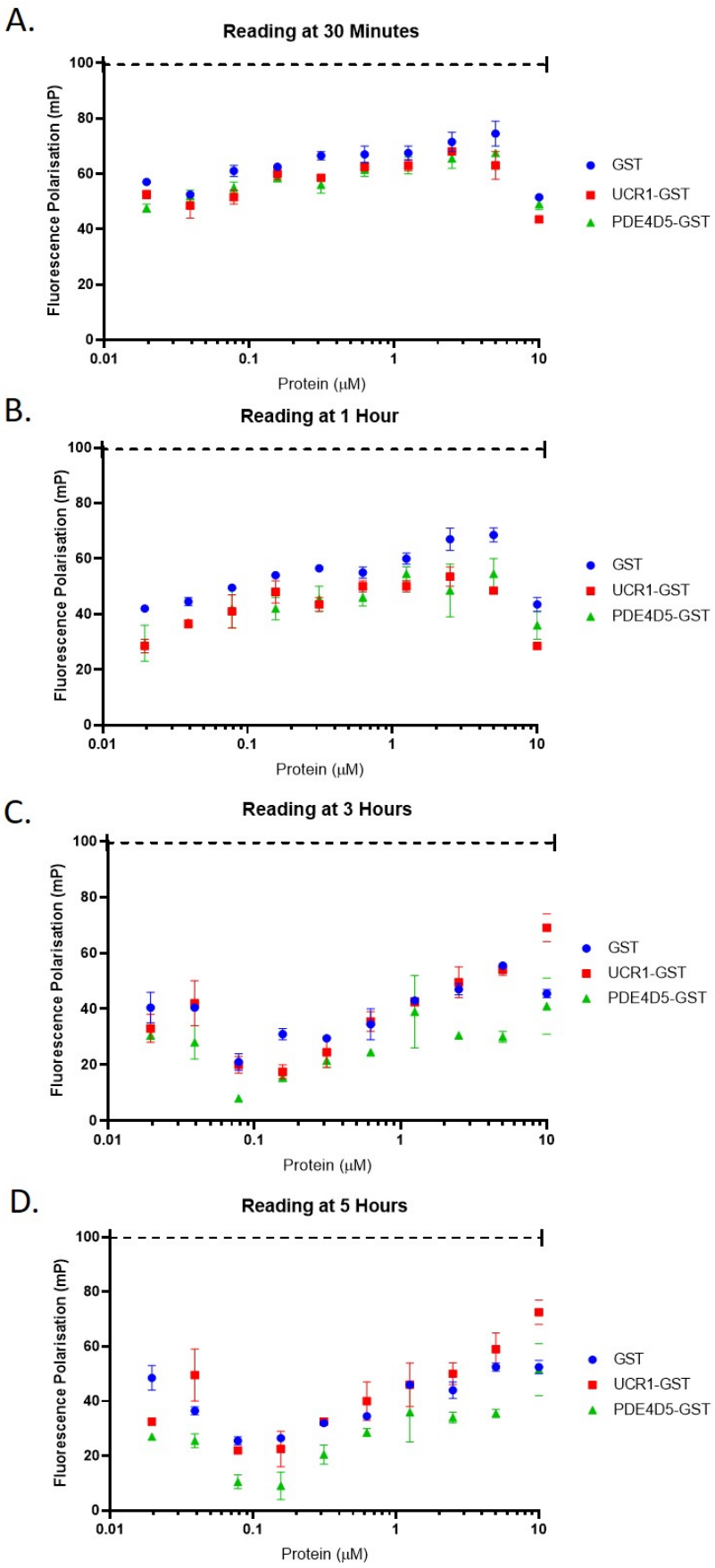

Figure 3.27 PDE4D UCR1-GST and PDE4D5-GST binding assay to DHX9 peptide. Serial dilutions of purified PDE4D UCR1-GST protein, full-length PDE4D5 protein or GST alone (10 μM to 0.02 μM) were incubated with 62.5 nM of 5-FAM DHX9 peptide. FP values were measured at the indicated times and plotted against the $\log_{10}$ values of protein concentration. This is representative of two independent protein purifications.

Upon ligand-protein binding, the FP value would normally result in a reading above 100 mP (indicated as a dotted line in Figure 3.27) (Speranzini, Fish and Mattevi, 2014, and personal conversation with Dr Yuan Sin). Highest mP values could be seen after 30 minutes of incubation (Figure 3.27 A), however no difference could be seen between any of the protein samples. Furthermore, the presence of the UCR1 domain, either in the truncated or full-length protein, did not result in the increase in mP values indicating the our DHX9 peptide was not binding to the protein. Increased incubation at room temperature led to a decrease in the mP values, suggesting that the protein was slowly degrading at room temperature (Figure 3.27 B,C and D). Due to continuous decrease in the FP values after the first 30 minutes reading, it can be suggested that if the interaction were to take place, it may have taken place prior to the first reading. This could mean that the interaction between PDE4D7 and DHX9 is rapid and transient. Ideally, the UCR1 peptide sequence should have been synthesised and binding assays be performed using purified recombinant DHX9. However, as we were unable to purify recombinant DHX9 protein, this approach was not possible. UCR1 and PDE4D5 GST tagged protein was used for these binding assays as they were highly abundant in the lab at the time. Unfortunately, I was unable to repeat these experiments and optimise conditions in order to obtain any binding affinity information due to time constraints.

3.4 Discussion

3.4.1 DHX9 is a novel interactor of PDE4D7 in PC cell lines

In recent years, PC has become one of the most common type of cancers diagnosed in men over the age of 50 across Europe and the USA. Although risk factors have been identified, these are not fully understood. There is currently a need to identify and understand PC-associated cell signalling processes and how these link to pathogenesis. In order to fully understand the signalling machinery that leads to disease progression, identification of new protein-protein interactions is needed in order to understand molecular regulatory networks (Chen *et al.*, 2016). Importance of these interactions can be assessed using network analysis which can predict how mutations within the genome can affect each interaction, as well as any other downstream pathways (Ruffalo and Bar-Joseph, 2019). Detection of key regulators and regulatory pathways is important in order to discover new genes in cancer (Mangangcha *et al.*, 2019).

Here, I was able to confirm that PDE4D7 and DHX9 are novel interactors *in vitro*. This interaction was first identified by Dr Ashleigh Byrne in a PDE4D7 IP coupled with mass spectrometry (MS) (Byrne, 2014), which is a tool that can be used to identify novel interacting proteins (Smits and Vermeulen, 2016). By using biochemical techniques, we were able to provide further evidence that these two proteins are interacting *in vitro* (Figure 3.7 and Figure 3.8), and this interaction could be disrupted in the presence of the newly synthesized CPP (Figure 3.21, Figure 3.22, and Figure 3.23). Interestingly, DHX9 was found to bind a sequence containing the newly discovered FLY multi docking site (Houslay *et al.*, 2017) for PDE4 interacting proteins, whereas PDE4D7 binds within the helicase domain of DHX9 (Figure 3.12 and Figure 3.17). As previously mentioned, DHX9 belongs to the DExD/H box superfamily of proteins that are highly conserved across all species. RNA helicases are enzymes that are able to unwind dsRNA and DNA in an energy-dependent fashion through the hydrolysis of ATP (Tanner and Linder, 2001b). Members of this family are defined by the presence of seven or eight evolutionarily conserved motifs that are involved in the binding of ATP within the helicase domain (de la Cruz, Kressler and Linder, 1999). While individual DExD/H helicase family members have been extensively studied, identifying novel cofactors and protein interactors for them is crucial in order to

fully understand the function and regulation of these helicases (Silverman, Edwalds-Gilbert and Lin, 2003).

Recent work has identified DHX9 and Nup98 to be novel interactors. Nup98 is a member of the highly conserved nuclear pore complex (NPC) family of proteins. Nup98 lies near or at the nuclear membrane and forms scaffolds that act as binding surfaces for other members of the NPC family. This in turn helps to facilitate the movement of nuclear transport factors, and their cargo, across the nuclear membrane. Nup98, is also involved in the export of mRNA as well as the shuttling of proteins from the nucleus via its numerous interacting partners (Franks and Hetzer, 2013). DHX9 was recently identified as a novel interactor of Nup98. Using a bead halo assay, they were able to show that Nup98 was able to bind to the N-terminal region of DHX9, containing the RNA binding motif, and the C-terminal region, containing the RGG box. The interaction of Nup98 and DHX9 within this region appeared to be facilitated by the presence of RNA as this interaction was sensitive to the endoribonuclease RNAse A. Interestingly, the binding of NUP98 within these regions of DHX9 stimulated the ATPase activity of DHX9. In the presence of RNA, the addition of recombinant NUP98 induced a dose-dependent increase in the ATPase activity of DHX9 (Capitanio, Montpetit and Wozniak, 2017). This data indicates that Nup98 acts as a positive regulator of DHX9 helicase activity. PDE4D7, and other members of the PDE4 family, are able to control the total cellular content of cyclic nucleotides and are able to create nanodomains of cyclic nucleotide signalling. (Baillie, Tejeda and Kelly, 2019a; Houslay *et al.*, 2019). As previously discussed, the PDE8A-cRAF interaction was shown to activate downstream signalling pathways, which could in turn lead to the progression of melanoma (Blair *et al.*, 2019). I suggest here that the interaction between PDE4D7 and DHX9 could potentially influence DHX9 helicase activity that could have a knock-on effect on disease progression. This interaction could potentially regulate the expression of downstream proteins, which in turn could alter the rate at which the disease could progress. The effects of PDE4D7 and DHX9 interaction on cell growth and helicase activity will be further investigated in chapter 5.

Interestingly, DHX9 is also able to form a complex formation with cAMP Response Element-Binding Protein (CREB) binding protein (CBP) and RNA polymerase II (Nakajima, Uchida, Stephen F. Anderson, *et al.*, 1997). CREB is one of the best

characterised phosphorylation-dependent transcription factors, and several kinases have been shown to promote its phosphorylation at its transactivation site. Once phosphorylated, CREB interacts with its coactivator protein, CBP or p300, at CREB responsive-genes (Wen, Sakamoto and Miller, 2010). CBP/p300 is thought to serve as a bridge between diverse gene-specific transcription factors and components of the basal transcriptional machinery (Karamouzis, Konstantinopoulos and Papavassiliou, 2007). Using transient transfections, DHX9 was found to cooperate with CBP in mediating target gene activation via CREB, and mutation of its helicase domain was found to reduce the expression of proteins containing CREB-dependent transcription factors (Nakajima, Uchida, Stephen F. Anderson, *et al.*, 1997). Examination of the promoter regions of PDE4D7 identified multiple CREB binding sites upstream of the starting methionine, suggesting that the cAMP/ PKA pathway may regulate the transcriptional expression of PDE4D7 (Wang *et al.*, 2003). I tentatively suggest here that DHX9 could potentially play a role in the transcriptional expression of PDE4D7. DHX9 could form a complex with RNA polymerase II and CBP (Aratani *et al.*, 2001) at one of the CREB binding sites in the PDE4D7 gene, potentially altering its expression at different stages of disease. It has been suggested DHX9 can reduce expression of certain proteins. Binding of DHX9 to the transcriptional activator of tonicity-responsive enhancer (TonE) binding protein (TonEBP) results in the decreased activity of TonEBP, leading to a decrease in its transcriptional activity (Colla *et al.*, 2006). Furthermore, the *C.elegans* DHX9 homologue RHA-1 is required for silencing transcription. Transcriptional silencing due to RHA-1 activity lead to a decrease in lysine methylation of histone H3, which in turn lead to defects in meiosis and a sterile phenotype. RHA-1 has since been suggested to be an important protein in maintaining appropriate transcriptional activity in order to control germline proliferation and development in *C.elegans* (Walstrom *et al.*, 2005). My data has shown that the expression of DHX9 increases from early to late stage models of disease, whereas PDE4D7 expression decreases (Figure 3.1). It can be suggested that the increased expression of DHX9 in the late stages of disease acts as a repressor of PDE4D7 expression by recruiting other transcription factors, which in turn could contribute to disease progression. Further work is needed to verify this hypothesis.

3.4.2 DHX9 binds within the UCR1 domain of PDE4D7

PDEs represent a large family of enzymes that hydrolyse cAMP and cGMP and at least 25 PDE genes have been identified and cloned. By using multiple promoters and alternative mRNA splicing, a single PDE gene can generate variant products in a tissue-specific manner (Ong *et al.*, 2009). PDE4 enzymes exclusively hydrolyse cAMP and it is the predominant cAMP degrading enzyme in a number of specific cell types. PDE4 plays a crucial role in cell signalling and it has been a target for clinical drug development for various diseases, with actions ranging from anti-inflammation to memory enhancement (Zhang *et al.*, 2005). Functional PDE4 isoforms can be divided into four major categories: long, short, super short, and dead short (Figure 1.8). The expression of various UCR1/2 combinations allows each specific PDE4 isoform to regulate distinct pools of cAMP by their cellular location and ability to be phosphorylated by a variety of kinases, including PKA (Omar *et al.*, 2019). The PDE4D family is characterised by the expression of seven long isoforms (D3, D4, D5, D7, D8, D9, D11), one short isoform (D1), and three super short isoforms (D2, D6, D10) (Tibbo, Tejeda and Baillie, 2019). Of the long PDE4D isoforms, PDE4D3, D5, D7, D9 are expressed in PC, and the mRNA expression of PDE4D3 and PDE4D7 is differentially affected between AS and AI models (Henderson *et al.*, 2014).

Long PDE4D isoforms all contain a UCR1 domain and, along with UCR2, provide the molecular machinery that confers key regulatory functions on the PDE4D catalytic unit (Houslay and Adams, 2003). The presence or absence of these UCR domains determines critical functional differences between long and short isoforms. The UCR1 region of all PDE4 isoforms harbours a PKA consensus site which in turn activates the cellular activity of PDE4 when modified (Xie *et al.*, 2014). The data presented in this chapter has shown that the UCR1 region of PDE4D7 can also act as a binding site for interaction partners. DHX9 was seen to bind within the UCR1 domain by peptide array (Figure 3.12), and this interaction was significantly reduced in IPs and PLA when cells were treated with disruptor peptide that was designed based on the binding sequence (Figure 3.21 and Figure 3.23). This binding sequence is unique to PDE4D isoforms by the presence of a single serine at residue 196 (Figure 3.13) and shared between other long PDE4D isoforms. This could indicate that DHX9 has the potential to bind to other long PDE4D isoforms that are present in the prostate. However, as PDE4D7 is the

most highly expressed isoform in PC (Henderson *et al.*, 2014), we can assume that the majority of the DHX9 would be bound to PDE4D7. It is unknown if the single serine change at residue 196 is enough to make this binding site PDE4D-specific, though this could easily be resolved by further peptide array experiments.

Interestingly, the UCR1 binding sequence for DHX9 contained the newly identified FLY multi-docking sequence. PDE4 enzymes having binding domains that allow interactions with various kinases, and domains that allow binding to other scaffolding proteins. These allow for the spatial degradation of cAMP in order to provide compartmentalised signalling, which in turn can then regulate the cross talk with other signalling processes (Houslay, 2010). The FLY docking site was first identified as a binding site for MK2 on PDE4A5 (Houslay *et al.*, 2017). The stress-activated p38 mitogen activated protein kinase (p38MAPK) pathway regulates a range of cellular processes, including apoptosis and cell invasion. The downstream substrate of this pathway, mitogen-activated protein kinase-activated protein kinase 2 (MK2), is involved in the post-translational regulation of cytokines (Soni, Anand and Padwad, 2019). Interestingly, PDE4A5 can be phosphorylated by MK2 on Ser 147 within the UCR1 domain. Phosphorylation of this serine was shown to attenuate the activation of PDE4A5 by PKA phosphorylation at Serine 140 (MacKenzie *et al.*, 2002b, 2011). Mutation of the FLY sequence within the UCR1 domain was shown to completely inhibit the interaction with MK2. Furthermore, loss of MK2-PDE4A5 interaction led to a reduction in the phosphorylation of Serine 147 in PDE4A5. The interaction between PDE4A5-MK2 via the docking site is needed to facilitate the efficient activation of PDE4A5 at Ser 147 (Houslay *et al.*, 2017). Although the phosphorylation of PDE4D isoforms by MK2 has not been extensively studied, we can assume that DHX9 and MK2 could potentially be competing for this binding domain. Binding with MK2 could act as a negative regulator of PDE4D7 activity by attenuating PKA phosphorylation of the UCR1 domain, whereas DHX9 could potentially act as a positive regulator by outcompeting for this binding site. The loss of regulation of PDE4D activity can have a profound effect on compartmentalised cAMP signalling, and could contribute to disease progression (Böttcher *et al.*, 2016).

3.4.3 Using cell permeable peptides as therapeutic agents in PC

In recent years, ADT has been the mainstay treatment for PC, and a marked increase in its use can be observed (Liu *et al.*, 2019). In most men, ADT leads to the relief of PC-related symptoms, regression of metastases, and a fall in serum PSA levels. If managed correctly, the median survival for men with metastasis is 30-49 months with the potential to extend it to 10 years if managed correctly. However, with time, the disease no longer responds to hormone treatment and the patient eventually develops the CRPC lethal phenotype (Varenhorst *et al.*, 2016). Furthermore, long-term use of ADT has been reported to reduce quality of life and increase the risk of adverse events, such as cardiovascular events, fractures, metabolic syndrome, and memory loss (Casey, Corcoran and Goldenberg, 2012; Kim *et al.*, 2018). There is currently a need to find new therapeutic targets for the treatment of PC in order to potentially alleviate the negative outcomes of long-term ADT use. Therapeutic peptides are potentially a novel approach to treat many diseases, including cancer (Marqus, Pirogova and Piva, 2017). Furthermore, protein-protein interactions in cancer has slowly become a new target in multiple cancers as they allow clinicians to target cancer cells expressing protein complexes that are known to progress the disease (Ruffalo and Bar-Joseph, 2019).

Using the information obtained from our peptide arrays, we were able to synthesise two cell penetrating peptides. The UCR1 disruptor peptide was based on the DHX9 binding sequence in PDE4D7, while the DHX9 peptide was based on the PDE4D7 binding sequence in DHX9 (Figure 3.12 and Figure 3.17). These peptides were synthesised with an N-terminal stearic acid making them cell permeable. Using biochemical techniques, the interaction between PDE4D7 and DHX9 was significantly reduced when the cells were treated with the UCR1 disruptor peptide (Figure 3.21 and Figure 3.23). In recent years, peptides have become promising therapeutic agents in the treatment of cancer. When compared to other biological treatment options, such as monoclonal antibodies, peptide therapeutics possess many advantages such as their small size, ease of synthesis and their tumour penetrating ability (Thundimadathil, 2012). The *TMPRSS2:ERG* gene fusion product remains an attractive therapeutic target as it is known to be an oncogenic driver in both early and late stage of PC (Brenner *et al.*, 2011). By screening a phage display peptide library, Wang *et al.* (2017) were

able identify peptides that were able to interact specifically with wild-type ERG. Specifically, they discovered 12 unique ERG inhibitory peptides (EIPs) that were able to bind to the protein itself. These EIPs were able to block the interaction of ERG with both DNA and interaction partners, which attenuated ERG-mediated transcription, PPIs, cell invasion and proliferation *in vitro* (Wang *et al.*, 2017). In my view, the newly designed UCR1 disruptor peptide has the potential to impact the progression of PC in a similar manner to EIPs. The disruption of the PDE4D7-DHX9 interaction could potentially decrease the transcriptional activity of DHX9, as the EIPs did on ERG-mediated transcription. This would then lead to decreased mRNA translation, potentially resulting in PC cell death. Methods such as individual-nucleotide resolution UV crosslinking and immunoprecipitation (iCLIP) can be used to map mRNA DHX9 binding sites in different cell lines to determine how DHX9 mRNA binding can be affected by the disruption of PDE4D7-DHX9 complex (Huppertz *et al.*, 2014; Murat *et al.*, 2018).

Alternatively, cell penetrating peptides could potentially be used to transport therapeutic cargos into cells (Hoffmann *et al.*, 2018). Discovery of novel peptides has traditionally been performed by screening large libraries of peptides, produced either synthetically or biologically. These large libraries include phage, ribosomal, and mRNA displays and have become the standard for peptide discovery (Henninot, Collins and Nuss, 2018). Peptides can be used directly as cytotoxic agents by targeting protein complexes or receptors, or they can be modified to act as a carrier of cytotoxic agents and radioisotopes to specifically target cancer cells. These types of therapies have been extensively studied in PC (Boohaker *et al.*, 2012). As well as the UCR1 peptide, we also synthesised a disruptor peptide that was able to compete with PDE4D7 for the DHX9 binding site (Figure 3.17 and Figure 3.22). Although this peptide did not lead to a significant decrease in PDE4D7-DHX9 interaction in both cell models, this peptide could potentially be reutilised as a homing peptide to specifically target cancer cells that are expressing both PDE4D7 and DHX9. Homing peptides are capable of selectively delivering many kinds of molecules and hold great promise for the development of less toxic therapies in several diseases (Wada *et al.*, 2019). Normal and diseased organs can be treated with a specific macromolecular tag, or homing peptide, that can be used to specifically target only the diseased cells (Laakkonen and Vuorinen, 2010).

Such an approach has already been shown to be successful in mouse models of PC. D(KLAKLAK)$_2$ is an amphipathic D-amino acid peptide that binds selectively to bacterial cell membrane. This peptide is known to initiate apoptosis in eukaryotic cells by disrupting mitochondrial membranes (Ma *et al.*, 2012). In recent years, D(KLAKLAK)$_2$ has been conjugated with multiple homing peptides to target specific cancer, in turn causing cell death (Agemy *et al.*, 2011). By conjugating the prostate homing peptide with D(KLAKLAK)$_2$ and delivering it systemically through an IV, they were able to cause tissue destruction in the prostate, but not in other organs in PC mouse models (Ma *et al.*, 2012) This chimeric peptide also delayed the development of cancers in PC-prone transgenic mice (Arap *et al.*, 2002). Our newly synthesised DHX9 peptide could potentially be reutilised as homing peptide that could transport anti-cancer agents to the prostate directly. If delivered systemically, this would be an alternative to ADT and could reduce PC recurrence. However, due to the expression of DHX9 in multiple organ systems, further phage display studies would need to be carried out in order to ensure that this peptide will only target the prostate itself. Additionally, we would also need to ensure that this peptide would not interfere with other members of the DExD/H helicase proteins.

3.4.4 Fluorescence polarization as a new screening tool to identify binding enhancers or disruptors

Since its discovery in the 1920s, FP has become one of the most widely used methods in clinical and biomedical sciences for assessing protein-protein interactions (Croney, 2003). FP is a powerful tool for characterizing the interaction between two proteins, or between a protein and DNA fragments, in order to provide details on the strength of these interactions (Lundblad, Laurance and Goodman, 1996). FP assay allows the user to closely monitor the association and dissociation of a fluorescent ligand with its interacting protein without the need to separate the bound ligand from the unbound ligand (Rinken, Lavogina and Kopanchuk, 2018). This allows ligand binding to be quantified without perturbing the binding equilibrium, making it a suitable way to measure low affinity interactions. Once the assay is optimized, the FP assay can be used to provide high throughput screening in order to find small molecule drugs that can either enhance or disrupt an interaction. FP assays are non-destructive, allowing repetitive measurements of the same sample under different conditions

(Rossi and Taylor, 2011). In this chapter, I tried to establish a simple binding assay between the purified recombinant UCR1 protein and a fluorescently tagged DHX9 peptide. I was able to show that the minimum peptide required for the assay was 62.5 nM (Figure 3.26). However, once the peptide was incubated with the purified recombinant protein, no binding information could be obtained as all FP measurements were similar to the GST tag negative control (Figure 3.27). Furthermore, as we increased the incubation time between the protein and the fluorescent peptide, the FP value continually decreased (Figure 3.27 B, C and D). Highest FP values could be observed after 30 minutes of incubation (Figure 3.27 A), suggesting that the interaction between the UCR1 region and DHX9 is rapid and transient. However, lack of FP change in the samples of interest can also be due to the purity of the sample. Although we were able to purify the UCR1 domain, the dialysed protein still contained multiple smaller bands indicating that the protein itself was highly degraded (Figure 3.16). Although we were able to use these protein samples in our peptide array experiments, this sample may not have been suitable for FP. The presence of precipitated matter in the assay solution can cause light scattering interference with FP measurements (Moerke, 2009). It could be possible that the high presence of degraded UCR1 protein was interfering with the accurate detection of FP.

Once a successful binding assay can be established, the assay can be adapted in order to identify small molecular drugs that are able to modulate the interaction. Although therapeutic peptides have emerged as a novel tool in the treatment of PC, it would be of interest to find small molecule drugs that can complement or replace the existing peptide therapy. Small molecules that inhibit the interaction between the protein and the fluorescent peptide, and are able to displace the peptide from the its binding site, can be observed as a decrease in FP value (Lea and Simeonov, 2011). Alternatively, if maintenance of the interaction between two proteins is needed to inhibit progression of a disease, small molecules that are able to stabilize and enhance the interaction can be identified (Simonetta *et al.*, 2019). Such an approach has been used in order to increase the interaction between the oncogenic transcription factor ß-catenin and its E3 ligase ß-TRCP (Simonetta *et al.*, 2019). ß-catenin is a multifunctional protein that is central to many physiological processes but high expression of this protein contributes to various diseases such as cancer. It acts

both as a transcriptional regulator and an adaptor protein for intercellular adhesion. Continuous activation of its signalling pathway gives rise to the accumulation of ß-catenin in the nucleus, which in turn promotes the transcription of many oncogenes such as *c-Myc* and *Cyclin-D1*. ß-catenin contributes to the carcinogenesis and progression of several cancers, such as colorectal cancer (Shang, Hua and Hu, 2017). Oncogenic activation of ß-catenin occurs by escaping ubiquitin-mediated proteasomal degradation. Proteasomal degradation of ß-catenin is mediated by the ß-TrCP subfamily of F-box proteins, which regulate the turnover of many proteins by acting as a E3 ubiquitin-protein ligase that target its substrates for protein degradation. However, mutations within ß-catenin can impair the ability of ß-TrCP to effectively bind, leading to ß-catenin stabilization and oncogenic activity (Ougolkov *et al.*, 2004). Simonetta *et al.* (2019) therefore used FP to find prospective small molecule drugs that work by restoring the binding between ß-TrCP and mutant ß-catenin. They were able to identify a compound that was able to potently increase the interaction between ß-TrCP and mutant ß-catenin, and induced ß-catenin degradation *in vitro*. This small molecule was able to insert into the PPI binding site, and increase the interaction between substrate and ligand (Simonetta *et al.*, 2019). Although I was unable to determine if the interaction between PDE4D7 and DHX9 increases the speed at which PC progresses, FP assays such as the one described above could help find novel small molecule drugs that could be used to enhance or disrupt the interaction. When established, the optimized FP conditions can be used in high throughput screening assays (HTSs) to evaluate more than 20 000 compounds from a library (Alquicer *et al.*, 2012) in order to identify novel small molecules for the treatment of PC. This in turn could potentially modulate down-stream signalling pathways that could alter the progression of disease.

3.4.5 Chapter summary

The data presented in this chapter has confirmed the interaction between PDE4D7 and DHX9. These two proteins can interact with each other in overexpressing VSV-tagged PDE4D7 and Flag-tagged DHX9 HEK293 and endogenously in VCaP cells. Although these two proteins are expressed in two different cellular compartments, PDE4D7 has the potential to shuttle into the nucleus through an NLS sequence that has been identified within the linker and UCR2 domain of PDE4D7. Treatment with LMB increased the presence of PDE4D7

within the nuclear region, which in in turn increased the interaction between PDE4D7 and DHX9 in LNCaP cells. The interaction between PDE4D7 and DHX9 was confirmed by IPs and PLA imaging and using peptide array we were able to map where this interaction takes place in each protein. DHX9 was found to bind within the UCR1 region of PDE4D7 and this binding sequence was found to contain the FLY docking site of PDE4 isoforms. Although this domain is shared between all long PDE isoforms, this binding sequence was found to be unique to PDE4D due to the presence of a serine at residue 196. PDE4D7 was found to bind within the helicase domain of DHX9, indicating that this interaction could potentially have a role in regulating the helicase activity of DHX9. By using cell permeable peptides, I was able to confirm that DHX9 binds within the UCR1 domain, but the binding site of PDE4D7 within DHX9 still needs further confirmation. Using purified recombinant UCR1 and PDE4D5, FP binding assays were performed in order to determine the dissociation constant. Unfortunately, due to the purity of UCR1 I was unable to determine this constant. However, if this binding assay was established, this assay would permit us to find new small molecules that could enhance or disrupt the interaction between PDE4D7 and DHX9.

Chapter 4 DHX9 Phosphorylation by Protein Kinase A

4.1 Introduction

The cAMP-PKA signalling pathway is known to have an important role in a range of physiological processes, including cell growth, secondary metabolism, and cell differentiation (Zhu *et al.*, 2017). cAMP controls a wide range of cellular processes that are triggered by a variety of extracellular signals, such as hormones or neurotransmitters. Many signalling pathways are initiated by the binding of a ligand to a G_S-coupled GPCR at the plasma membrane, which in turn leads to the activation of AC converting ATP into cAMP (Figure 1.7) (Koschinski and Zaccolo, 2017). GPCRs are the largest family of plasma membrane receptors, mediating the effects of multiple ligands. Due to their involvement in fundamental biological processes and their accessibility, GPCRs are targets for major drug classes, including beta-blockers (Calebiro, Nikolaev and Lohse, 2010). The major effector for cAMP in cells is PKA, which has the ability to phosphorylate multiple targets in each individual cell (Koschinski and Zaccolo, 2017). PKA is a serine/threonine kinase which is composed of a dimer of two regulatory subunits (R) that each bind to a catalytic subunit (C) when inactive. Four types of R subunits (RIα, RIß, RIIα, and RIIß) and three types of C subunits (Cα, Cß, Cγ) have been identified in humans. All PKA holoenzymes are named based on their R subunit isoform, referred to as PKA-I and PKA-II. PKA-I contain homodimers of RIα and Riß, whereas PKA-II contain homodimers of RIIα or RIIß subunits (Yang and Yang, 2016; Smith and Scott, 2018). Each R subunit contains two cAMP binding sites, and binding of cAMP leads to a conformational change that results in release of the active C subunit (Figure 4.1) (Yang and Yang, 2016). Furthermore, each R subunit contains an N-terminal docking and dimerization domain (D/D domain) that not only facilitates formation of the heterotetramer, but also tether is to an A-kinase anchoring protein (AKAP) (Nygren and Scott, 2015). Once activated by cAMP, the C subunit can phosphorylate nearby substrates, before being sequestered by an AKAP bound to an R subunit, forming small signalling complexes in the cell (Autenrieth *et al.*, 2016). AKAPs tether PKA and other signalling proteins, such as PDEs, to defined cellular sites, providing compartmentalized cAMP signalling. AKAPs can coordinate multiprotein complexes, allowing for compartmentalized signalling (Christian *et al.*, 2011).

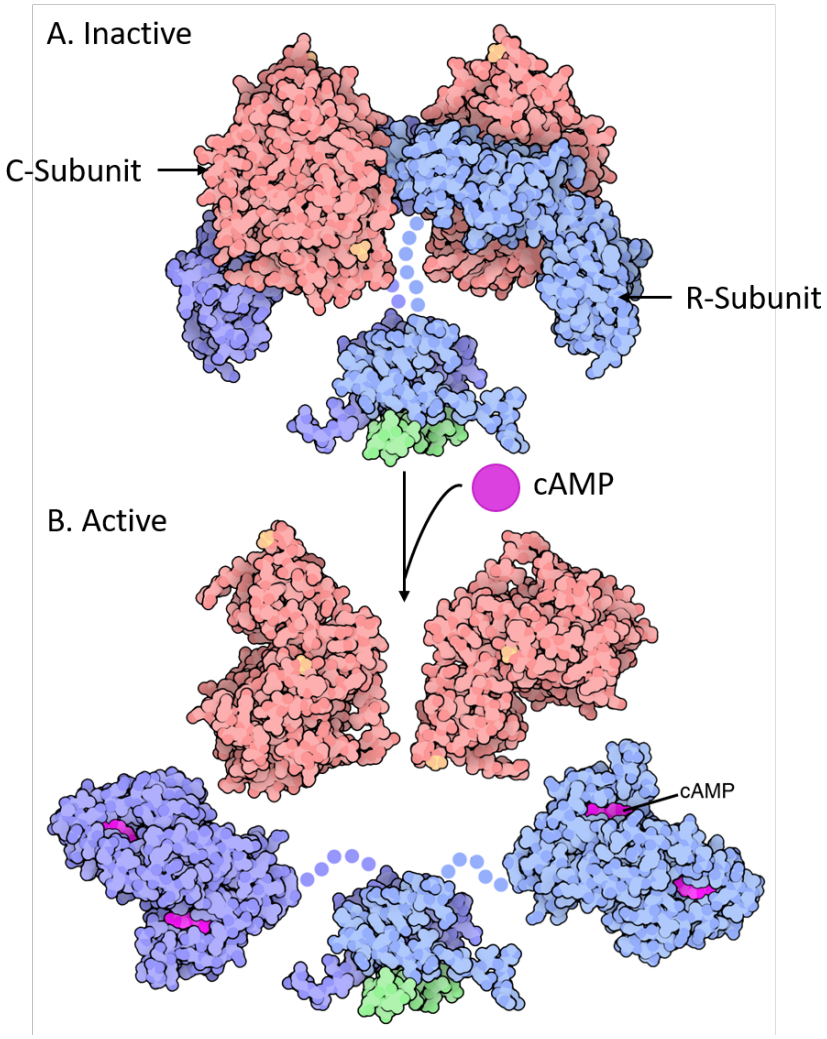

Figure 4.1 Structure of inactive and active PKA. A. Inactive PKA is as a dimer of two regulatory subunits (R) that each bind to a catalytic subunit (C). B. When bound to cAMP, the C-subunit is released from the R-subunit, allowing it to phosphorylate near-by proteins. Figure taken from Zhang *et al.*, 2012.

Although ADT is seen as a highly successful therapy, PC tumours often become hormone refractory (androgen insensitive) and can grow despite low levels of androgens. One possible way that these tumours can grow in such conditions is through cross talk with other signalling pathways, such as the cAMP-PKA pathway (G. Wang *et al.*, 2006). The activity of many transcription factors, including AR, is regulated by their phosphorylation status. In the case of steroid receptors, increased phosphorylation of the receptor itself leads to an increase in its transcriptional activity. The AR is phosphorylated by PKA, which in turn can modulate AR activity and downstream gene expression (Nazareth and Weigel, 1996). The AR is a phosphoprotein with at least 16 residues that can be phosphorylated by multiple kinases (Figure 4.2). These residues are sequentially phosphorylated upon the treatment of PC cells with androgens, antiandrogens,

or reagents that activate downstream signalling pathways. This results in alteration in the transcriptional activity of AR, its cellular localization, and its stability (van der Steen, Tindall and Huang, 2013). Interestingly, phosphorylation of different serines or threonines in AR can predict disease outcome. For example, phosphorylation of Ser^{515} by Cdk1 may predict biochemical relapse in PC patients. Work by Willder et al (2013) suggested that phosphorylation at AR at Ser^{515} may be the driving force in PC disease progression. However, their work also showed that high expression of Ser^{515} lead to a shorter time to biochemical relapse and a reduction in disease specific survival in hormone naïve PC patients (Willder *et al.*, 2013). Furthermore, phosphorylation of AR at Ser^{81} by PKC was also shown to be associate with poor disease outcome. Increase expression of pAR Ser^{81} has been shown to be associated with decrease disease-specific survival (Patek *et al.*, 2017).

A

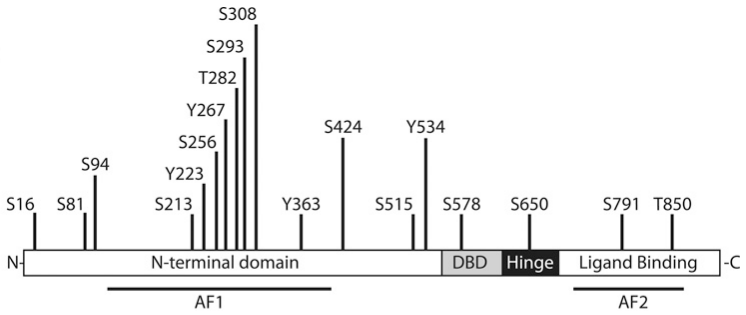

B

Phospho-site	Function				Kinases
	Transcription	Stability	Localization	Growth	
S81	+	+	+	+	CDK1, CDK5, CDK9
S213	+	+	+	+	Akt, PIM-1(L, S)
Y223	+				Fer
Y267	+			+	Ack
T282	+			+	Aurora-A
S293	+			+	Aurora-A
S308	+			+	$CDK11^{p58}$
Y363	+				Ack
S515	+	+			CDK7, MAPK
Y534	+	+		+	Src, Etk
S578	+				PKC, PAK6
S650	+		+		JNK, p38
T850	+			+	PIM-1 L

Figure 4.2 AR can be phosphorylated at multiple sites and by multiple kinases. A. Schematic representation of AR phosphorylation within different regions of the protein. B. Overview of AR phosphorylation, their kinases, and functional effects. (Figure taken from Koryakina, Ta and Gioeli, 2014).

Elevated levels of cAMP/PKA in LNCaP cells following treatment with the PDE4 inhibitor rolipram induces an increase in expression of AR and PSA proteins in the absence of androgens. Lower expression of PDE4 isoforms and increased levels of cAMP/PKA at later stages of disease favours the constitutive activation of the AR pathway, which in turn could contribute to disease progression (Sarwar *et al.*, 2014; van Strijp *et al.*, 2018).

Changes in protein phosphorylation represent a major way transcription factors can regulate their activity. Exposure of cells to different extracellular stimuli leads to the phosphorylation of downstream transcription factors by different kinases, such as PKA, which can change the cell's behaviour due to altered gene expression (Whitmarsh and Davis, 2000). Although DHX9 is not considered as a transcription factor itself, most of DHX9's functions have been found because of its interaction with multiple transcription factors, such as CREB and RNA polymerase II (Fuller-Pace, 2006). Through its ability to unwind secondary RNA structures, DHX9 is able to mediate the initiation of transcription (Murat *et al.*, 2018). To date, DHX9 is only known to be phosphorylated by DNA-dependent protein kinase (DNA-PK) in the presence of RNA, as well as by phosphatidylinositol 3-kinase-related kinases (PI3KKs) (Zhang *et al.*, 2004; Lin *et al.*, 2020). The phosphorylation of DHX9 was increased when mediated by RNA binding (Zhang *et al.*, 2004). Inhibition of PI3KK-mediated phosphorylation of DHX9 was shown to decrease the ability of colorectal cancer cells to develop chemoresistance. This was the first study where phosphorylation of DHX9 was linked with the development of chemoresistance (Lin *et al.*, 2020).

4.2 Chapter aims

Increasing evidence has shown that the cAMP-PKA pathway is involved in PC by modulating the activity of AR. However, nothing is known about whether DHX9 can be phosphorylated by PKA and if this phosphorylation could be modulated by PDE4D7 activity in the vicinity of DHX9. The aims of this chapter are as follows:

AIM 1: Determine if DHX9 can be phosphorylated by PKA. By using a range of biochemical techniques, the ability of DHX9 to be PKA phosphorylated will be investigated *in vitro*.

AIM 2: Map putative DHX9 PKA phosphorylation site using peptide array technology and develop a phospho-DHX9 antibody. This antibody can be used to confirm DHX9 phosphorylation.

AIM 3: Investigate if interaction between PDE4D7 and DHX9 has a role in regulating the phosphorylation of DHX9. Using the UCR1 disruptor peptide described in other chapters of this thesis, I have investigated if the disruption of this interaction can alter the levels of DHX9 phosphorylation.

4.3 Results

4.3.1 DHX9 can be phosphorylated by PKA at multiple serines.

To date, DHX9 is only known to be phosphorylated by DNA-PK and PI3KKs. However, due to the role the cAMP/PKA has in PC and disease progression, I was interested to know if DHX9 can also be phosphorylated by PKA. Using the NetPhos 3.1 server, I was able to predict whether DHX9 could potentially be phosphorylated by PKA. This server was first developed by Blom *et al.* (1999) in order to identify serine, threonine or tyrosine residues that can be phosphorylated by multiple protein kinases (Blom, Gammeltoft and Brunak, 1999). Here, the full-length sequence for DHX9 (accession number Q08211) was submitted. The server can identify putative PKA phosphorylation sites that contain the consensus sequence $RX_{1-2}S/T$, where X_{1-2} means one or two amino acid residues follows the first arginine. The server identified 5 serines that can potentially be phosphorylated by PKA. A prediction score above 0.500 indicates that these are most likely to be phosphorylated *in vitro* (Table 4.1).

Table 4.1 DHX9 can be phosphorylated at multiple serines by PKA

Residue Number	Sequence	Score
449	PRRISAVSV	0.870
477	VRFESILPR	0.552
485	RPHASIMFC	0.600
506	IRGISHVIV	0.723
1142	ISRPSAAGI	0.505

Of the 5 serine residues identified, residues 449, 477, 485, and 506 are all found within the helicase core domain of DHX9. Interestingly, PDE4D7 binds DHX9 from residues 576-600 (Figure 3.16), indicating that PKA-mediated phosphorylation of DHX9 may be partly regulated by the interaction with PDE4D7. The last serine residue potentially phosphorylated by PKA (1142) is situated between the OB-fold and NLS/NES sequence of DHX9 (Figure 1.13).

4.3.2 Serine 449 is readily phosphorylated in DHX9

One of the advantages of peptide array technology is the ability to identify novel post-translational modifications (PTMs) using PTM-specific antibodies. Knowing that DHX9 could potentially be phosphorylated at 5 different serine residues, the DHX9 peptide arrays that, were prepared at the same time as the arrays used in chapter 3, were used to identify which of these residues could readily be phosphorylated *in vitro* using a PKA phosphorylation assay. To do so, the peptide arrays were incubated with the PKA catalytic subunit and ATP for 30 minutes at 37˚C. The peptide arrays were then incubated with Phospho-(Ser/Thr) PKA Substrate Antibody (CST, 9621L) overnight at 4˚C. Phospho-(Ser/Thr) PKA Substrate Antibody is able to detect peptides or proteins with a phosphorylated PKA consensus site (RXXpS/pT). The DHX9 was incubated with the appropriate secondary antibody, and the spots detected using chemiluminescence (Figure 4.3).

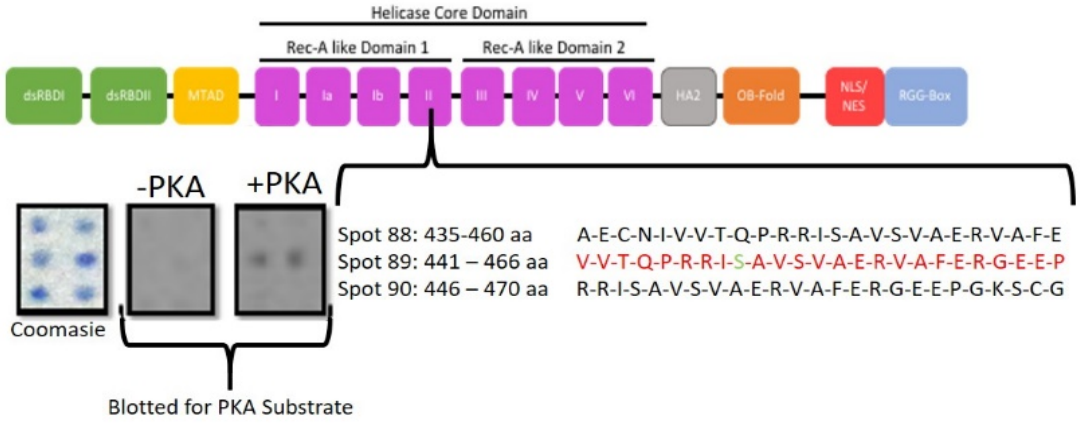

Figure 4.3 Serine 449 is phosphorylated by PKA *in vitro*. Full length DHX9 peptide array was incubated with purified recombinant PKA catalytic subunit and ATP. Phosphorylated serine or threonine were detected using a Phospho-(Ser/Thr) PKA Substrate Antibody. This experiment was performed by Jane Findlay.

Of the 5 residues that was predicted to be phosphorylated by PKA (Table 4.1), only the serine at residue 449 was detected by peptide array analysis at spot 89 (Figure 4.33). Although the PKA consensus sequence was available on spots 88 and 90, these did not result in a positive detection by the PKA antibody (Figure 4.33). As previously mentioned, and illustrated in Figure 4.1, the serine that is readily phosphorylated by PKA was found within the helicase core domain of DHX9. Interestingly, this site was recently identified as an important phosphoprotein by mass spectrometry (MS)-based phosphoproteomics (Zhou *et*

al., 2013). In order to provide further evidence that this serine is readily phosphorylated by PKA, the sequence at spot 89 was truncated at either the N- or C-terminus. Furthermore, the PKA consensus site was substituted with either an alanine, aspartic acid or a phospho-serine in order to ensure that changes to this sequence also leads to a change in detection. These peptide array membranes were incubated with PKA catalytic subunit and PKA antibody as previously described. (Figure 4.4 and Figure 4.5)

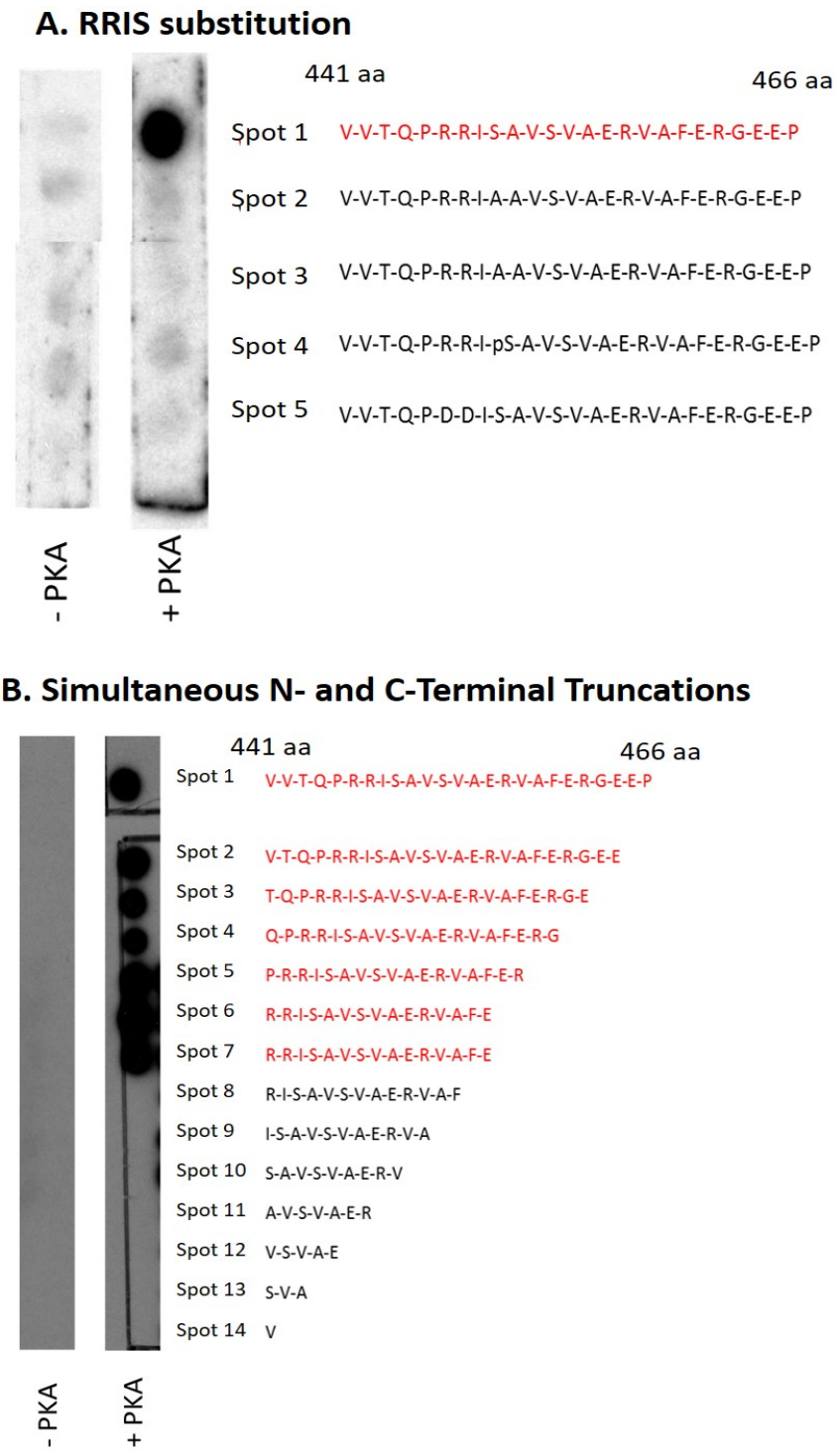

Figure 4.4 **Substitution and truncation of the newly identified PKA site of DHX9. Peptide array membranes were spotted for the newly identified DHX9 PKA site.** One set of membranes were incubated with bovine catalytic PKA subunit in order to phosphorylate the Serine 449. A. Substitution of serine 449 with an alanine and arginine 446 and 447 with aspartatic acid leads to a loss of DHX9 phosphorylation. B. Simultaneous N- and C- terminal truncation

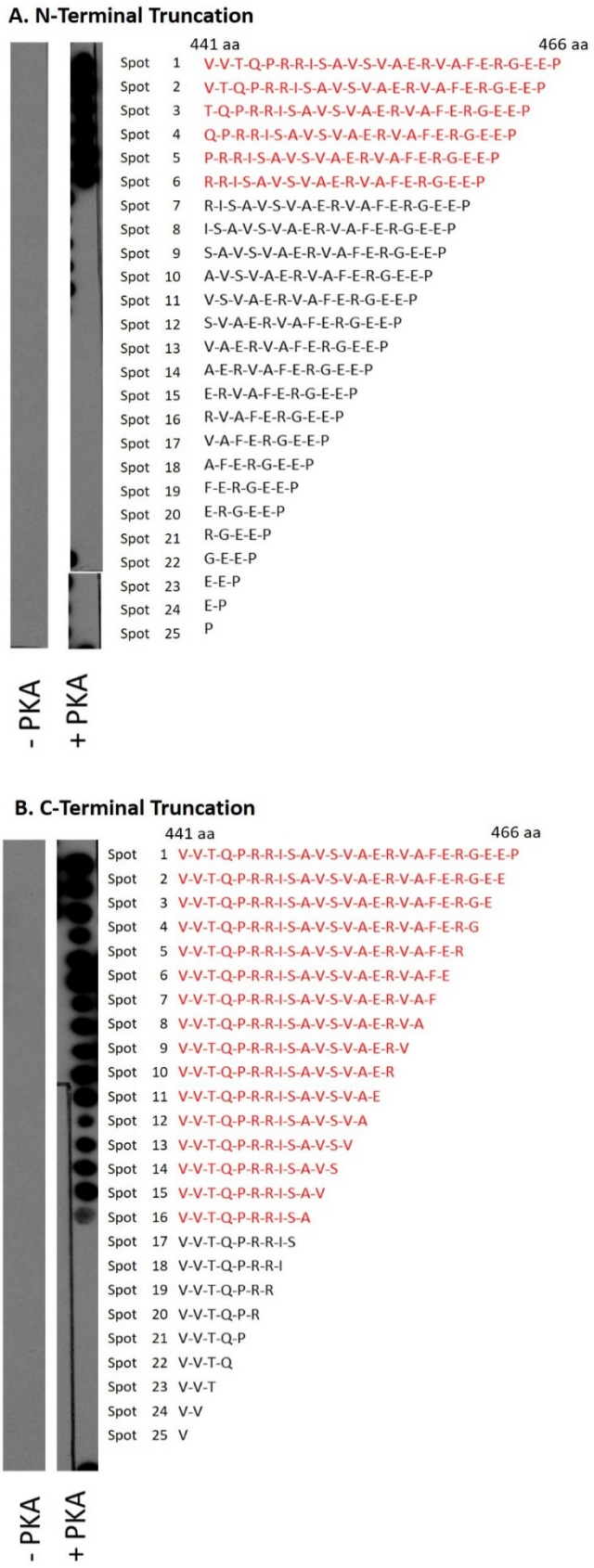

Figure 4.5 N- and C-Terminal truncation in order to identify minimum sequence for DHX9 phosphorylation. Peptide array membranes were spotted for the newly identified DHX9 PKA site. One set of membranes were incubated with bovine catalytic PKA subunit in order to phosphorylate the Serine 449. A. N-Terminal truncation. B. C-terminal truncation

Loss of the RRIS PKA sequence, either by substituting the serine with an alanine (Figure 4.4 A spot 2 and 3) or the arginine with aspartic acid (Figure 4.4 A spot 5), inhibited the ability of this sequence to be phosphorylated by the PKA catalytic subunit. Recent advances in peptide array technology permits the direct spotting of phosphorylated amino acids (Parikh *et al.*, 2009). By doing so, I was able to design a spot that already contains a phosphorylated serine in the PKA consensus sequence (Figure 4.4 A spot 4). Although this phospho-serine was detected, it was detected at a much lower level than spot 1, where the serine was only phosphorylated after incubation with bovine PKA C-subunit (Figure 4.4 A spot 1 and 4). Although this serine was predicted to have the highest score in the NetPhospho analysis, the sequence specifically spotted with this phospho-serine could barely detect it. This could potentially be due to the fact that this particular spot was not correctly deposited on the membrane. By creating N- and C-terminal truncations of this, I was able to determine the minimum amino acids required to phosphorylate DHX9. These peptides arrays provided further evidence that DHX9 can be phosphorylated by PKA at serine 449. Interestingly, loss of arginine 446 and the alanine at residue 450 by sequence truncation also leads to a loss of DHX9, highlighting the importance of these amino acids in the phosphorylation of serine 449 (Figure 4.5 A and B). Using the information gathered in Figure 4.4 and Figure 4.5, the minimum sequence for DHX9 phosphorylation was found to be T^{443}QPRRI**S**AVS^{452}. This information was then used later in the chapter in order to generate a custom DHX9 phospho-specific antibody.

4.3.3 DHX9 can be phosphorylated by PKA *in vitro*

My data so far has shown that the serine at residue 449 of DHX9 is readily phosphorylated by PKA on peptide arrays. Although detection of PTMs on peptide arrays is a useful tool, this may not always mimic what is happening *in vitro*. The DHX9 peptide arrays were incubated with purified PKA catalytic domain, therefore we may have forced this phosphorylation to occur by creating the optimum conditions. In order to ensure that DHX9 can be phosphorylated in a cellular context, HEK293 cells were transfected with Flag-tagged DHX9 plasmid for 24 hours. They were then treated for 5 minutes with 25μM of forskolin and 100 μM of 3-isobutyl-1-methylxanthine (IBMX) in order to increase the levels of intracellular cAMP. IBMX is a nonspecific PDE inhibitor that is known to elevate

the levels of intracellular cAMP (Schroeder *et al.*, 2012). Forskolin is a rapid and reversible activator of AC, which in turn contributes to an increase of intracellular levels of cAMP (Alasbahi and Melzig, 2012). After forskolin and IBMX treatment, the cells were lysed and the protein concentration was determined using a standard Bradford assay. Before subjecting these lysates to IP, 30 µg of the non-treated and treated lysates from all experiments were run on an SDS-PAGE gel and blotted for phosphorylated PKA substrate and GAPDH. This was done in order to ensure that all cells treated with forskolin and IBMX did lead to an increase in the detection of total PKA phosphorylated proteins (Figure 4.6).

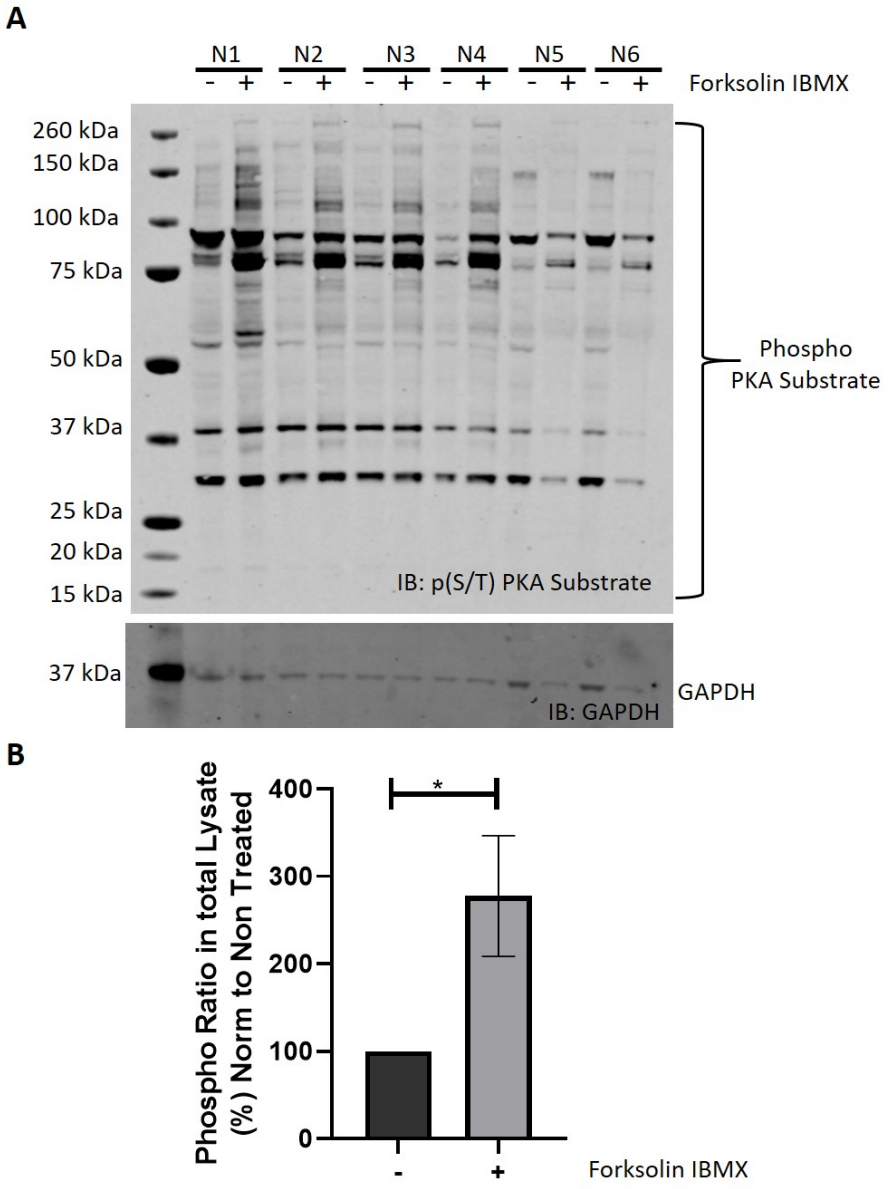

Figure 4.6 Treatment of HEK293 cells transfected with Flag-tagged DHX9 with forskolin and IBMX. A. Lysates from 6 independent experiments were run on an SDS-PAGE gel and blotted for phospho-PKA substrate and GAPDH. B. Total PKA phosphorylation from each sample was measured densitometrically and normalised to the GAPDH loading control. The data is presented as the mean ± SEM of 6 independent experiments. Statistical significance was determined using a Student's T-Test, where p*= 0.0277.

Treatment with forskolin and IBMX led to a visible increase in PKA phosphorylation when compared to the non-treated controls (Figure 4.6 A). When the signal from each lysate was quantified, forskolin-IBMX treatment led to a significant increase in the total amount of proteins that could be phosphorylated by PKA (Figure 4.6 B). Knowing that the treatment with forskolin-IBMX led to an increase in PKA phosphorylation, these lysates were then further used for an IP. The lysates were incubated for 3 hours at 4˚C with protein G beads that were conjugated with FLAG antibody to pull down ectopic DHX9. The beads were thoroughly washed, and the protein was eluted off the beads by boiling. IP samples were run on an SDS-PAGE gel and blotted for FLAG and phospho PKA substrate (Figure 4.7).

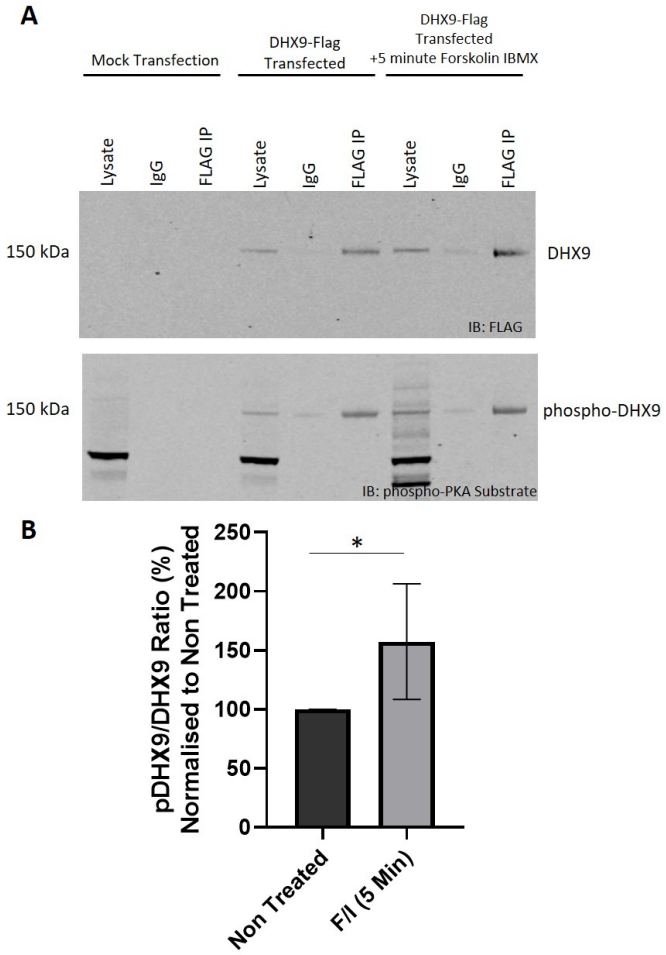

Figure 4.7 Flag-tagged DHX9 IP following forskolin-IBMX treatment in HEK293. A. Flag-tagged DHX9 was pulled down in HEK293 transfected cells following treatment with 25 μM forskolin and 100 μM IBMX. Western blot membranes were probed for Flag (top) and phospho PKA substrate (bottom). B. The ratio between Flag-tagged DHX9 in the PKA substrate and FLAG blot was measured. Data is presented as the mean ± SEM of six independent experiments. Statistical significance was determined using a T-Test where p*=0.049.

Flag-tagged DHX9 was successfully pulled down from the HEK293 transfected cells (Figure 4.7 A top membrane). Furthermore, a band representing DHX9 was recognised by the PKA substrate from this pulldown (Figure 4.7 A bottom membrane). The ratio between phosphorylated and total DHX9 was then measured from the six independent experiments. Treatment with forskolin-IBMX lead to a 50% increase in the detection and pulldown of phosphorylate DHX9, and this was shown to be significant when statistically analysed (Figure 4.7 B). The data presented above demonstrate that DHX9 is readily phosphorylated by PKA when over-expressed in HEK293 cells. This same experiment was then repeated in VCaP cells in order to see if endogenously expressed DHX9 can be phosphorylated by PKA. VCaP cells from a 10 cm dish were treated with 25 µM of forskolin and 100 µM IBMX for five minutes. The cells were then lysed and protein concentration of was determined using a standard Bradford assay. These lysates were then incubated with protein G beads and DHX9 specific antibody overnight at 4˚C. IP samples were then washed and analysed by SDS-PAGE gel and western blotting. Membranes were probed for DHX9 and PKA substrate (Figure 4.8)

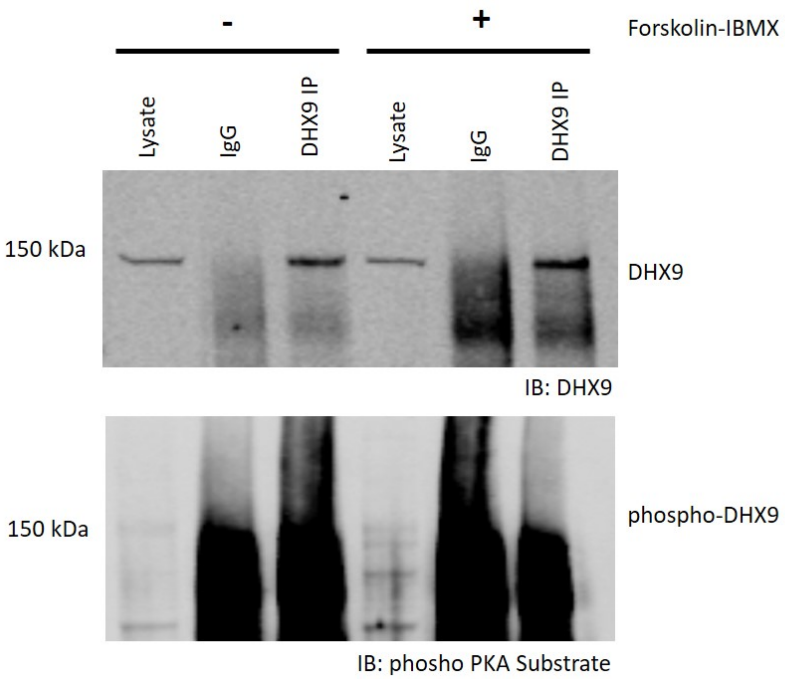

Figure 4.8 DHX9 IP following forskolin-IBMX treatment in VCaP. VCaP cells were treated with 25 µM forskolin and 100 µM IBMX, after which endogenously expressed DHX9 was IPed. Western blot membranes were probed for DHX9 (top) and phospho-PKA substrate (bottom). Representative of N=3.

Although endogenously expressed DHX9 was pulled down in the VCaP lysates (Figure 4.8 top membrane), I could not clearly identify if it was readily phosphorylated in these cells due to smear that appeared in the IP (Figure 4.8 bottom membrane). I therefore decided to use PLA to identify if DHX9 can be phosphorylated *in vitro*. LNCaP cells were chosen for this experiment as their morphology was better suited for confocal microscopy. LNCaP cells were plated in a 24 well plate with glass coverslips for 24 hours. They were then treated with 25 µM of forskolin for five minutes then fixed and stained for phospho-PKA substrate and DHX9. The cells were then subjected to PLA secondary antibody treatment and visualised using the Zeiss LSM confocal microscope (Figure 4.9).

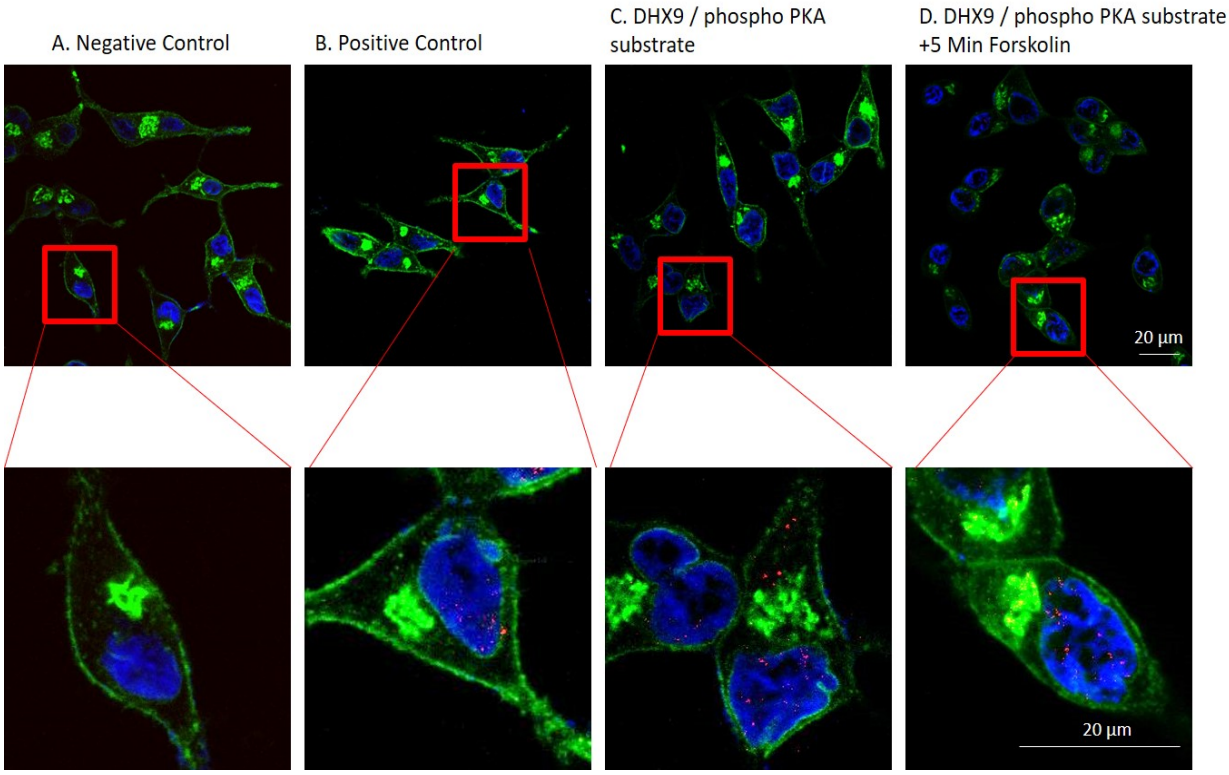

Figure 4.9 **PLA between DHX9 and phospho-PKA substrate in LNCaP cells.** LNCaP were plated onto coverslips and probed for either DHX9 alone for the positive control (B), or DHX9 and PKA phospho-substrate with or without 250 µM forskolin (C+D). No primary antibody was included for the negative control (A). All cells were stained for the membrane (green) and the nucleus (blue) in order to appropriately identify each cell. PLA signal is visible in the red channel.

As expected, the positive control resulted in the detection of spots when visualised under the microscope (Figure 4.9 B), whereas no spots were detected in the negative control (Figure 4.9 A). This indicated that any spots detected can only be attributed to the interaction between secondary antibodies bound to our primary antibody. Furthermore, PLA spots could be detected in samples stained with DHX9 and phospho-PKA substrate antibody (Figure 4.9 C and D) indicating

that DHX9 can readily be phosphorylated by PKA in LNCaP cells. The PLA signal from the cells from each conditions were then quantified using Image J in order to determine if treatment with forskolin led to any changes in detection (Figure 4.10).

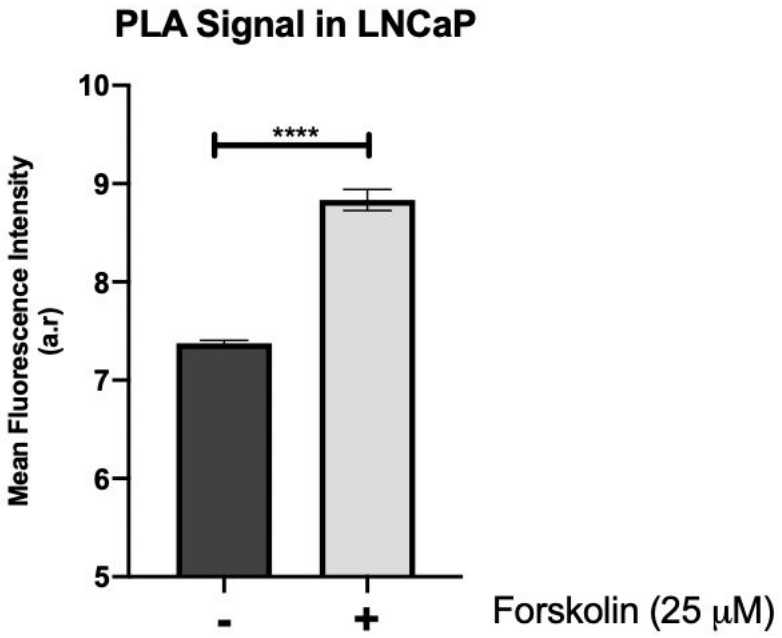

Figure 4.10 Quantification of PLA in LNCaP. PLA signal from the non-treated control and forskolin treated cells were quantified. Data is presented as the mean ± SEM of at least 20 cells from each condition. Statistical significance was determined using a T-Test, where p****<0.0001.

Interestingly, treatment with forskolin led to a significant increase in PLA signal when compared to the other condition (Figure 4.9 D and Figure 4.10) The data so far has shown that DHX9 is readily phosphorylated by PKA in exogenous and endogenous settings. Further experiments, such as site-directed mutagenesis of S^{449}, would have added more support to this chapter. By creating a phospho-null mutant, I could have investigated if the loss of S^{449} ablates the phosphorylation of DHX9 by PKA.

4.3.4 Testing of novel phospho-DHX9 antibody

My data so far has shown that DHX9 is readily phosphorylated by PKA in exogenous and endogenous settings. DHX9 has been shown to be phosphorylated at S^{449}, and the phosphorylation of this serine can be increased by forskolin-IBMX treatment. Using the information gathered in Figure 4.4, a custom phospho-antibody (Ab) against DHX9 was commissioned. The amino acid sequence T^{443}QPRRI**pS**AVS^{452} was used to create a peptide antigen that was injected into a rabbit to raise the antibody. The rabbit was immunized six times at two weeks

intervals and a blood samples were taken after each immunization. After the final round of immunisation, the rabbit serum was collected from which the phospho-antibody was purified using an affinity column. The purified antibody was first tested on peptide arrays in order to ensure that the antibody was able to recognise the epitope against which it was raised. Encouragingly, the DHX9 phospho-Ab recognised phosphorylated epitopes, and these were attenuated following treatment with a blocking peptide (T^{443}QPRRI**S**AVS^{452}) (Figure 4.111).

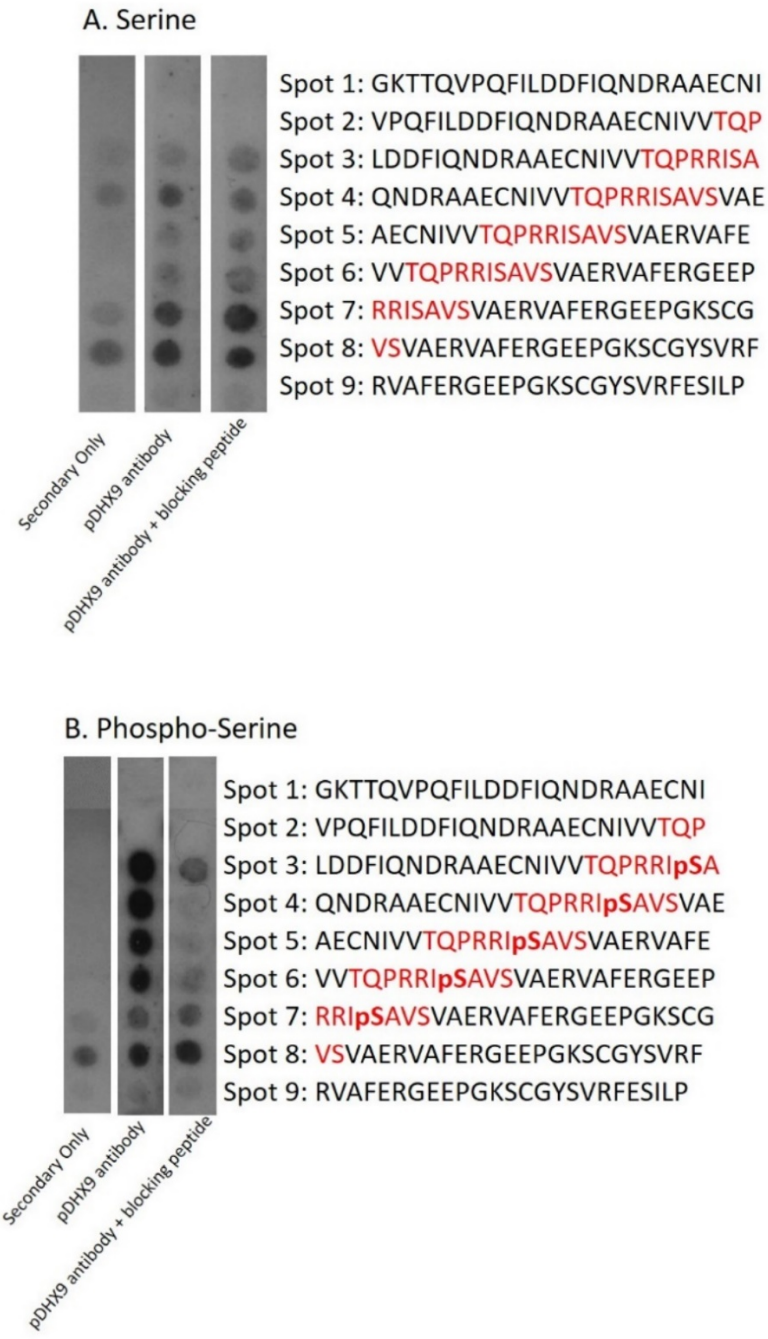

Figure 4.11 Testing of novel pDHX9 antibody using peptide array technology. Peptide array technology was used to verify that the novel pDHX9 antibody was able to bind to its epitope. A. Non-phosphorylated sequence. B. Phosphorylated sequence.

The strongest signal could be seen between spots 4-6 where the full antigen was present (Figure 4.11 B array 2). Interestingly, the presence of the blocking peptide in the third peptide array ablated the detecting of the antigen (Figure 4.11 B array 3). Spot 8, where only the last two amino acid of the antibody epitope was observed to show a positive signal, in all three arrays including the two negative controls. This may be due to unspecific binding from the secondary antibody (Figure 4.11 all three arrays). Although the antibody was able to detect the non-phosphorylated epitope (Figure 4.11 A), the signal was visibly weaker when compared to the arrays with the phosphorylated serine. In order to provide further evidence that the newly purified antibody was able to detect phospho-S^{449}, the *in vitro* PKA assay previously performed should have been repeated. This would have confirmed that the antibody does in fact recognise its epitope and would have also further validated the results from the initial PKA assay. Furthermore, this antibody should have been tested against other members of the DExD/H helicase family by peptide array in order to ensure that the antibody is able to only detect DHX9, and no other isoforms. This is due to the high homology within the helicase core domain amongst the DExD/H helicase family. Spotting of other DExD/H helicase proteins on peptide arrays, such as DHX15 which has recently been shown to be involved in CRPC (Xu *et al.*, 2019), would have allowed us to test the specificity of this antibody. Unfortunately, due to time constraints and technical issues with the peptide array spotter, I was unable to perform this experiment.

Although I was unable to test the specificity of the antibody by peptide array, the newly synthesised antibody was tested for western blotting detection of phospho-DHX9. HEK293 cells were transfected with Flag-tagged DHX9, and the next day the cells were treated for 0, 3, 10, 15 or 30 minutes with 25 μM forskolin and 100 μM IBMX. 30 μg of cell lysate were then run on an SDS-PAGE gel and both total and phosphorylated DHX9 was detected by western blotting (Figure 4.12 A). The ratio between phosphorylated and total protein was determined in order to see if the treatment with forskolin and IBMX lead to an increase in the detection of phospho-DHX9. (Figure 4.12 B).

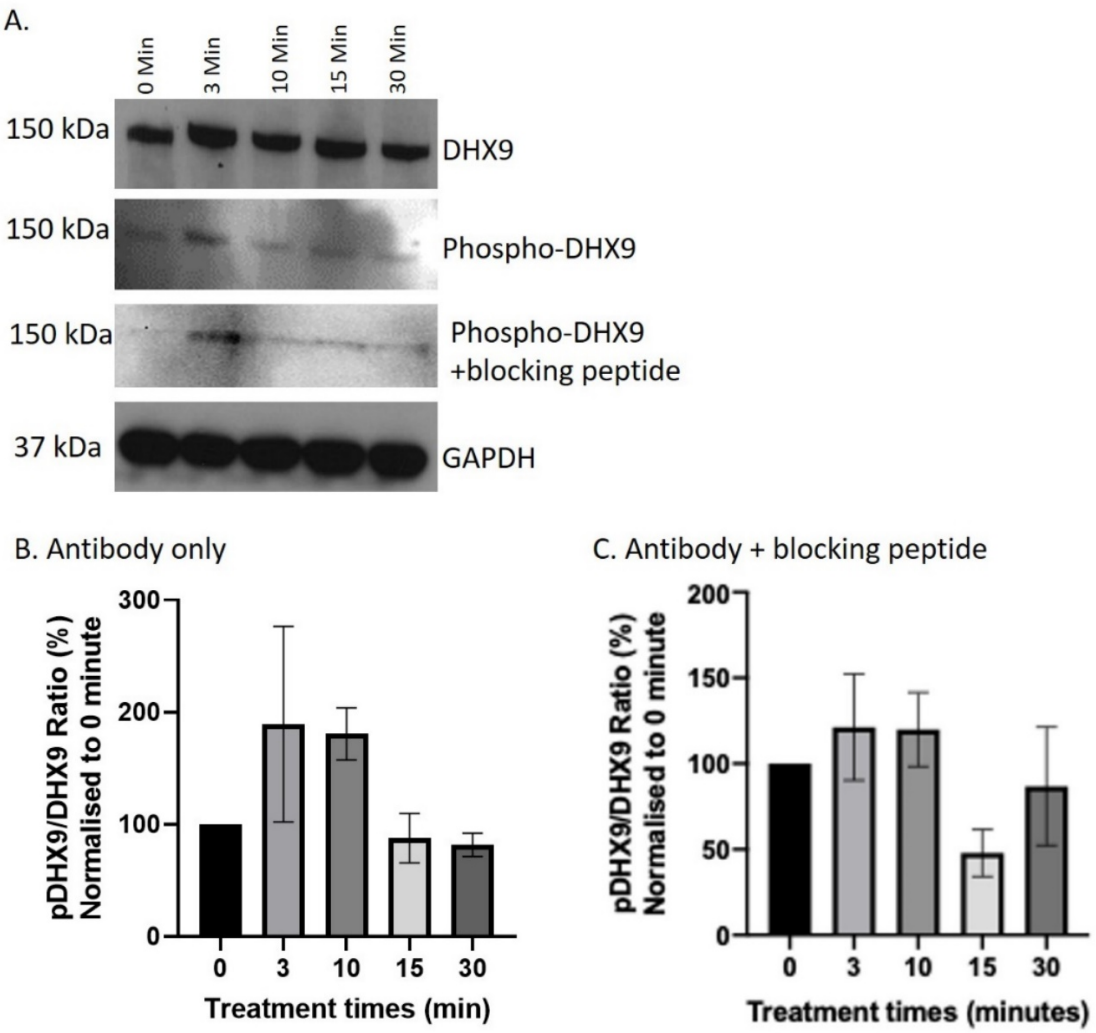

Figure 4.12 **Forskolin and IBMX in Flag-tagged DHX9 transfected HEK293 cells.** A. HEK293 cells transfected with Flag-tagged DHX9 were treated with 25 μM forskolin and 100 μM IBMX for the indicated times. Lysates were run on an SDS-PAGE gel and proteins were detected using western blotting. Membranes were probed for total DHX9, phospho-DHX9, and GAPDH. B. The ratio between phospho-DHX9 and total DHX9 was measured and normalised to the non-treated (0) control. C. B. The ratio between phospho-DHX9 and total DHX9 was measured and normalised to the non-treated (0) control after being incubated with the phospho-Ab and the blocking peptide. Data is presented as the mean ± SEM of three independent experiments. No statistical significance was found when analysed using a One-Way Anova.

Our newly synthesised antibody was able to detect phosphorylated DHX9 by western blotting (Figure 4.12 A membrane 2 and 3). Interestingly, treatment with forskolin-IBMX for 3- and 10-minutes led to the highest levels of phosphorylated DHX9 detected. Although this data is not significant due to the high variability between experiments, this western blot shows that the purified phospho-DHX9 antibody is able to recognise the protein (Figure 4.12 A, blot 2). When incubated with the phospho-Ab and a blocking peptide, I am still able to detect phosphorylated DHX9 after 3- and 10-minutes of treatment (Figure 4.12 A, blot 3). However, when analysed, these bands were detected at a much lower level (Figure 4.12 C), indicating that like in the peptide array in Figure 4.11,

incubating the membrane with the blocking peptides reduces the detection of phosphorylated DHX9. Interestingly, treatment for longer than 15 minutes lead to a rapid decrease in DHX9 phosphorylation, like that of the non-treated control (Figure 4.122 B). Knowing that the antibody can successfully detect phosphorylated DHX9 by western blotting, I then decided to test its ability to detect phospho-DHX9 by confocal microscopy. HEK293 were transfected with a Flag-tagged DHX9 plasmid, the treated with 25 μM forskolin and 100 μM IBMX for 0, 3 or 10 minutes. These times were chosen as the western blots showed that these times points lead to the highest detection of phospho-DHX9 (Figure 4.12 B). The cells were then fixed and stained for phospho-DHX9 using our newly commissioned antibody (Figure 4.13).

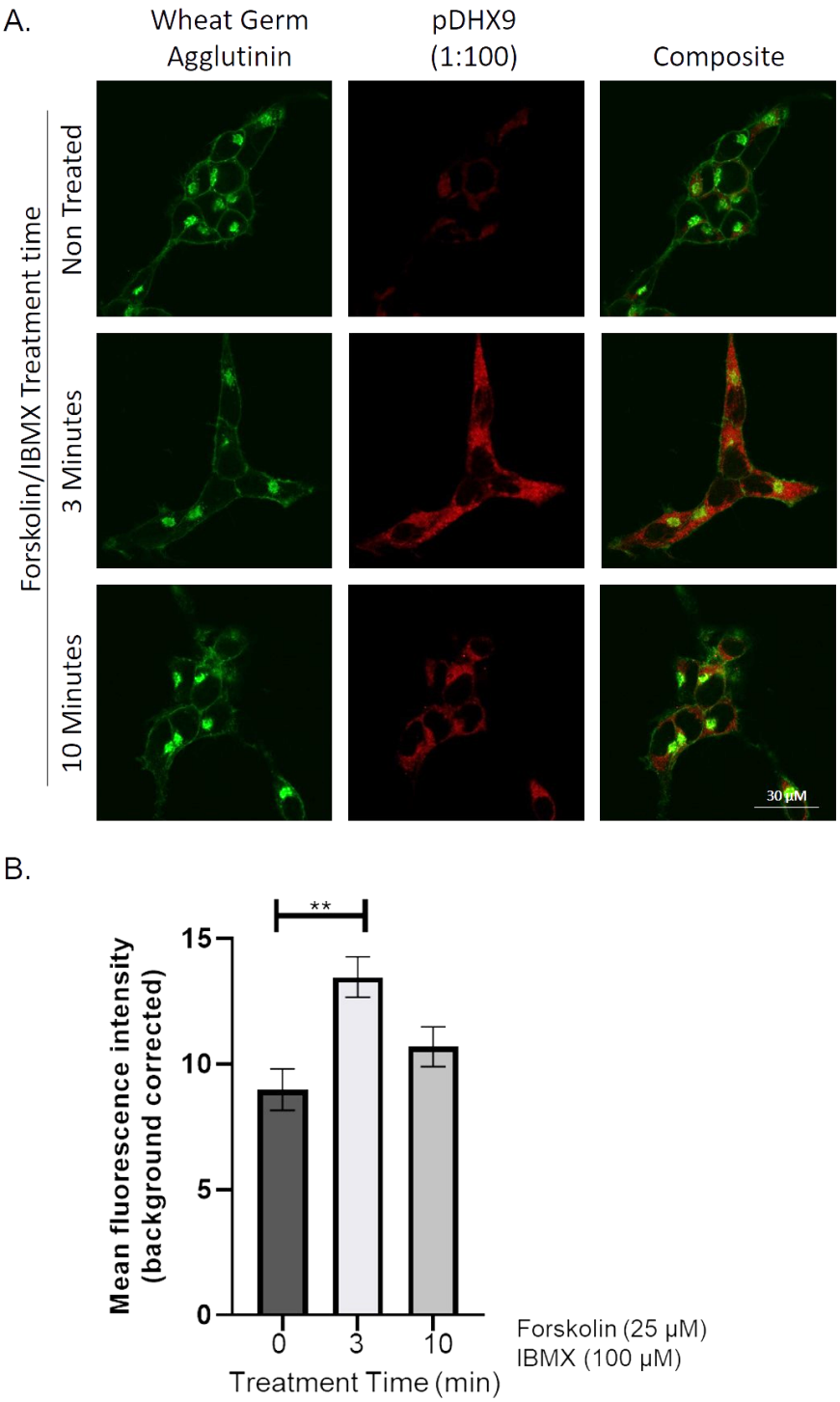

Figure 4.13 Testing of Novel phospho-DHX9 antibody by confocal microscopy. A. HEK293 overexpressing Flag-tagged DHX9 were treated for either 0, 3, or 10 minutes with 25 µM forskolin and 100 µM IBMX, then stained for the membrane using wheat germ agglutinin (green) and phospho-DHX9 (red). B. The mean fluorescence intensity of each condition was measured in at least n>30 cells. The data is presented as the mean ± SEM. Statistical significance was measures using a One-Way Anova, where p**=0.0041.

The newly synthesised phospho-DHX9 antibody was able to detect the protein by ICC with confocal microscopy. Under basal conditions, some phospho-DHX9 staining can be visible. However. treatment with forskolin-IBMX for 3- or 10-minutes led to a visible increase in phospho-DHX9 staining (Figure 4.13 A). When

the mean fluorescence intensity (MFI) was measured, treatment for 3-minutes with forskolin-IBMX led to a significant increase in the detection of phospho-DHX9. Treatment for 10-minutes also led to an increase in the detection of phospho-DHX9, however this was shown not to be a statistically significant increase (Figure 4.13 B). Interestingly, phosphorylated DHX9 could only be detected in the cytoplasmic region, which is also where the highest concentration of cAMP and PKA can be found (Koschinski and Zaccolo, 2017). In order to confirm that this is truly the case, a subcellular fractionation following forskolin-IBMX treatment could be performed. We would expect to only detect a band in the cytoplasmic fraction, compared to the nuclear fraction, following treatment with forskolin-IBMX.

My data so far has shown that the newly synthesised antibody is able to detect phospho-DHX9 in HEK293 overexpressing Flag-tagged DHX9. However, I was interested to know if this antibody can detect endogenously expressed phospho-DHX9. Therefore, the ICC experiment was repeated in DU145 cells. Previous work has shown that out of the three PC cell lines used in this thesis, DU145 has the highest expression of DHX9 (Figure 3.1 C). Furthermore, DU145 expresses the lowest amount of PDE4D7 (Figure 3.1 B), leading to a potential accumulation of cAMP and PKA in the cell. This could mean that DHX9 exists in a hyperphosphorylated state in DU145 cells. DU145 cells were seeded onto glass coverslips in a 24 well plate, then treated with 25 μM forskolin and 100 μM IBMX for 0, 3, or 10 minutes. The cells were then stained for the membrane using wheat germ agglutinin, and for phospho-DHX9 using the custom antibody. The cells were then fixed onto a glass slide then visualised using the Zeiss LSM confocal microscope (Figure 4.14).

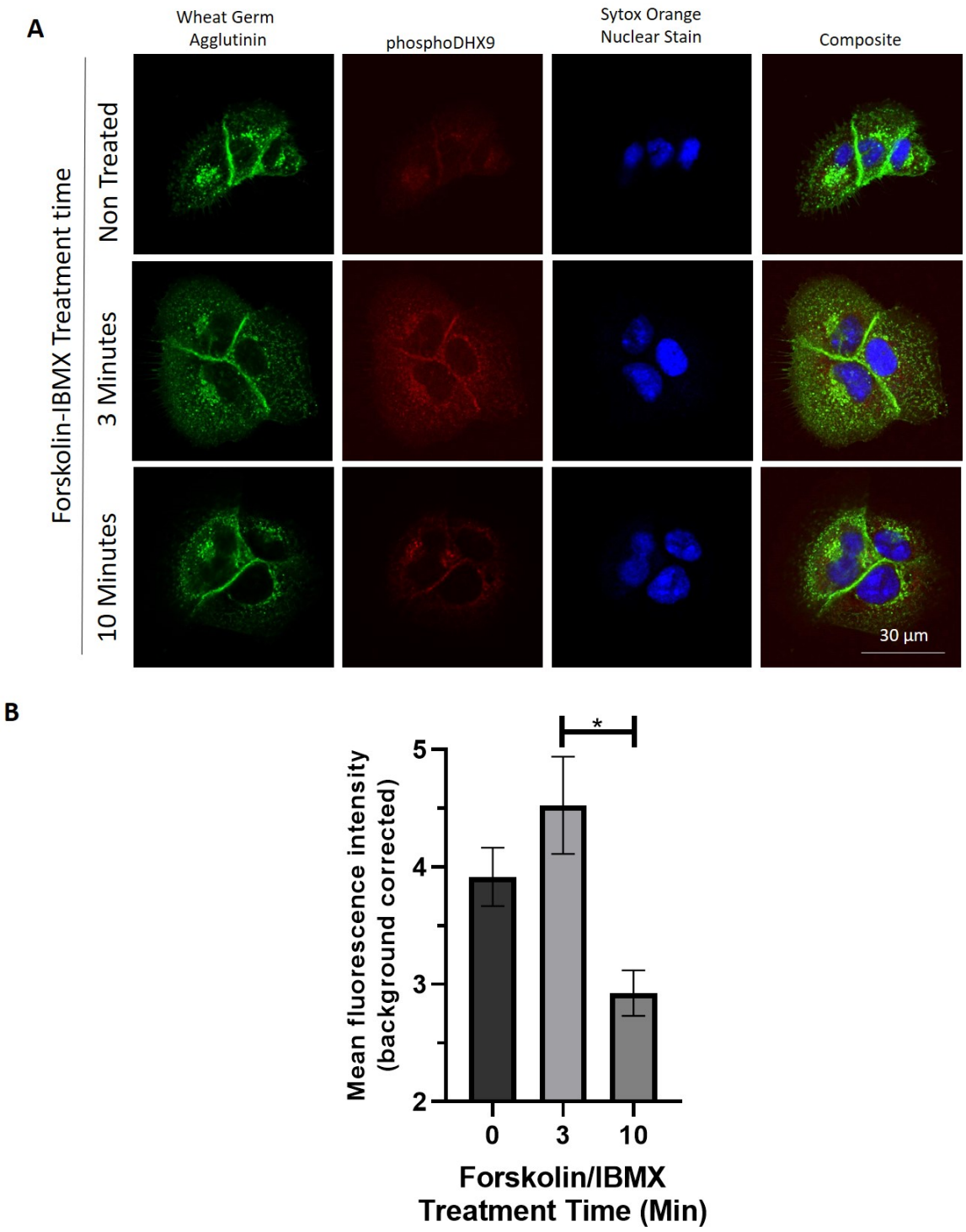

Figure 4.14 Testing of the new phospho-DHX9 antibody in DU145 cells. A. DU145 cells were treated with 25 µM forskolin and 100 µM IBMX for 0, 3, or 10 minutes. Cells were stained for the membrane (green), phospho-DHX9 (red), and nucleus (blue), then visualised using the Zeiss LSM confocal microscope. B. The mean fluorescence intensity for phospho-DHX9 from each condition was measured. Data is presented as the mean ± SEM of n>6 cells. Statistical significance was determined using a One-Way Anova where p*=0.0255.

Phosphorylated DHX9 could be detected in DU15 by confocal microscopy. Treatment with forskolin-IBMX led to a visible increase in the detection of phospho-DHX9 after 3-minutes of treatment (Figure 4.14 A middle row). However, very little phospho-DHX9 could be detected in DU145 cells treated for

10-minutes (Figure 4.14 A bottom row). As in the HEK293 cells, phosphorylated DHX9 was mainly found in the cytoplasm where highest levels of cAMP and PKA can be found (Figure 4.14 A second column). Unlike in the HEK293 ICC staining (Figure 4.13), some phosphorylated DHX9 could be detected within the nuclear region of DHX9. This data is further supported by the fact that PLA signal between endogenously expressed DHX9 and phospho-PKA substrate could be found across the whole cell in LNCaP cells (Figure 4.9) When the MFI for phospho-DHX9 was measured from each condition, treatment with forskolin-IBMX did lead to an increase in phospho-DHX9 detection after three minutes. Although this was not shown to be significant when compared to the non-treated control, there was a significant increase in the detection of phospho-DHX9 when the 3-minute condition was compared to the 10-minute condition (Figure 4.14 B).

4.3.5 Disruption of the DHX9-PDE4D7 leads to an increase in DHX9 phosphorylation.

So far, my data has suggested that DHX9 can be readily phosphorylated by PKA at Ser^{449} and our newly synthesised antibody is able to detect it by western blotting and ICC with confocal microscopy. However, I was interested to know if PDE4D7 can influence the levels of DHX9 that can be phosphorylated *in vitro*. Previous work in chapter 3 has shown that PDE4D7 binds downstream of the newly identified PKA phosphorylation site. The interaction between PDE4D7 and DHX9 could potentially regulate the levels of DHX9 being phosphorylated by modulating the local levels of cAMP (Fertig and Baillie, 2018). The UCR1 disruptor peptide (described previously in chapter 3 and in Figure 3.20 A) was used in order to investigate how PDE4D7 can influence the phosphorylation of DHX9. To do so, HEK293 cells were transfected with VSV-tagged PDE4D7 for 24 hours. The cells were then treated for two hours with either DMSO, 10 μM scrambled peptide, or 10 μM UCR1 disruptor peptide, after which they were lysed, and total protein concentration was determined used a standard Bradford assay. The lysates were then subjected to IP, where they were incubated with DHX9 antibody and protein G sepharose beads overnight at 4˚C. The IPs were thoroughly washed the next day and boiled in sample buffer. IPs were run on an SDS-PAGE gel and protein expression was assessed by western blotting. The membranes were probed for total DHX9, phospho-PKA substrate, and VSV (Figure

4.15). The commercially available phospho-PKA substrate antibody was used here as the custom phospho-DHX9 antibody was not available at the time.

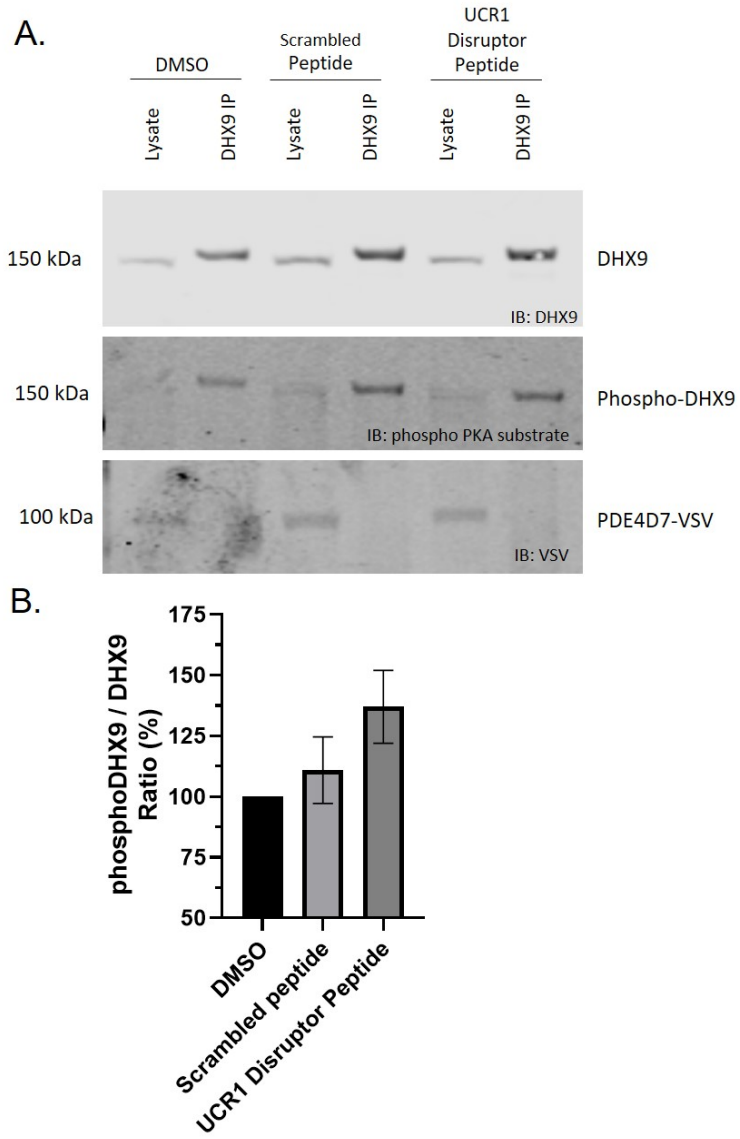

Figure 4.15 Disruption of the PDE4D7-DHX9 interaction leads to an increase in DHX9 phosphorylation A. IPs were run on an SDS-PAGE gel and protein expression was assessed by western blotting. Membranes were probed for DHX9 (top blot), phospho-PKA substrate (middle blot), and VSV (bottom blot). B. The ratio between DHX9 in the PKA substrate and DHX9 blot was measured. Data is presented as the mean ± SEM of three independent experiments. Statistical significance was determined using a One Way Anova.

I was able to successfully pull down DHX9 from transfected HEK293 cell lysate, and this was also detected in the phospho-PKA blot (Figure 4.15 A top and middle blot). PDE4D7-VSV was also successfully transfected into the cells (Figure 4.15 A bottom blot). Under basal conditions, disruption of the interaction between PDE4D7 and DHX9 led to an increase in the levels of phospho-DHX9 detected. However, this was not found to be significant when compared to the DMSO-treated condition (Figure 4.15 B). This data indicates that PDE4D7 acts as

a negative regulator of DHX9 phosphorylation. PDE4D7 can hydrolyse the cAMP located within close proximity to DHX9, and by doing so, it can inhibit the phosphorylation of DHX9, potentially regulating the helicase activity of DHX9. Loss of this interaction using our UCR1 disruptor peptide leads to a ~37.5% (Figure 4.15 B) increase in the levels of DHX9 being phosphorylated by PKA under basal conditions.

In order to provide further evidence that the decreased interaction between PDE4D7 and DHX9 leads to an increase in DHX9 phosphorylation, HEK293 cells were transfected with FLAG-tagged DHX9 and PDE4D7-VSV overnight on coverslips in a 12 well plate. The cells were then treated with the UCR1 disruptor peptide, or appropriate controls, as previously described. A subset of the UCR1 disruptor peptide, scrambled peptide and DMSO treated cells were further treated with 25 μM forskolin and 100 μM IBMX for 3-minutes in order to investigate if this could lead to any further increase in DHX9 phosphorylation. This timepoint was chosen as it was shown to lead to the highest detection of phospho-DHX9 by our custom-made antibody (Figure 4.13 and Figure 4.14). The cells were then stained for the membrane using wheat germ agglutinin, for phospho-DHX9 using our custom antibody, and for total DHX9. The cells were then fixed and visualised using a Zeiss LSM confocal microscope (Figure 4.16).

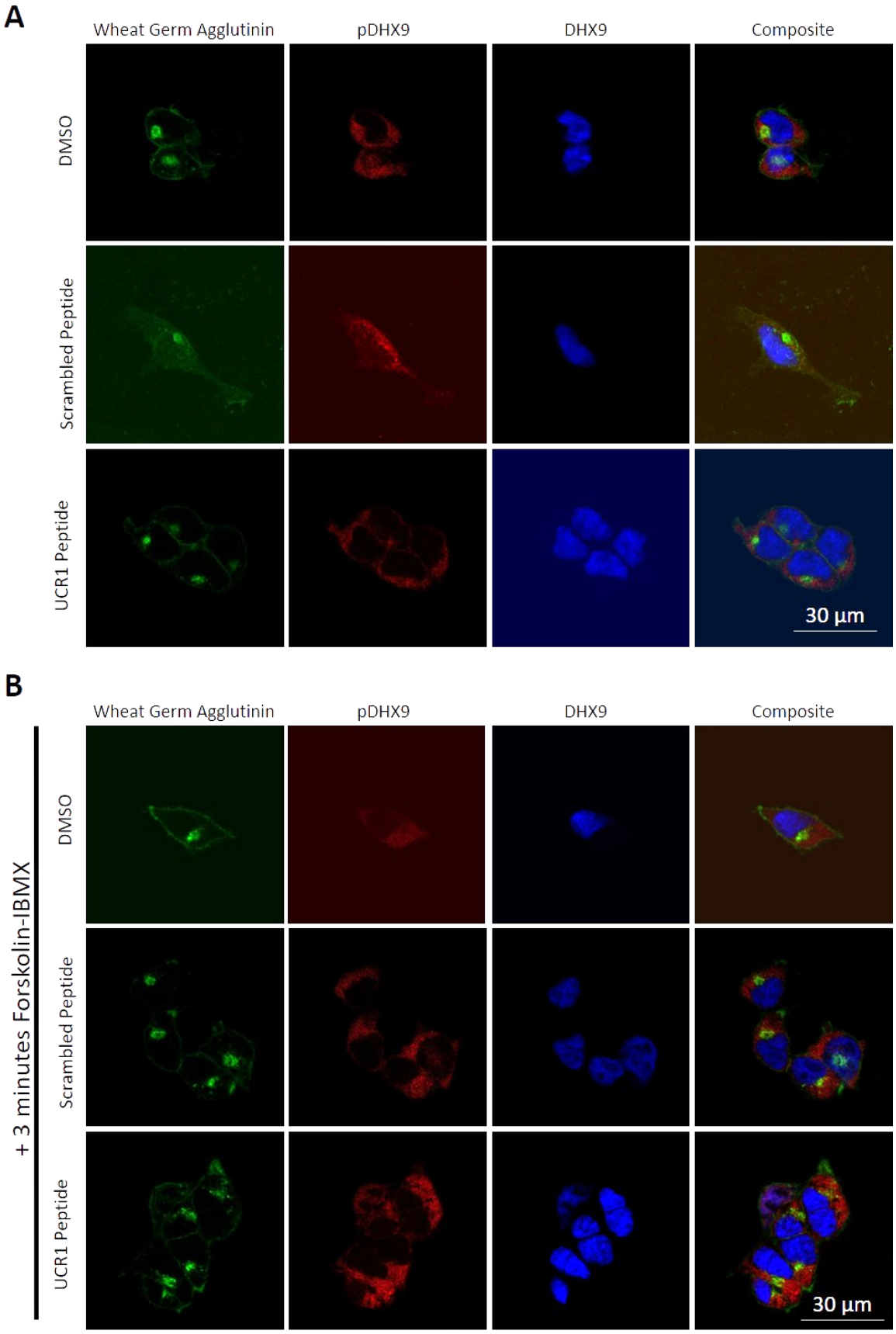

Figure 4.16 Detection of phosopho-DHX9 following UCR1 disruptor peptide treatment. A. HEK293 overexpressing Flag-tagged DHX9 and PDE4D7-VSV were stained with phospho-DHX9 and DHX9 following peptide treatment. B. HEK293 overexpressing Flag-tagged DHX9 and PDE4D7-VSV were stained with phospho-DHX9 and DHX9 following peptide and forskolin and IBMX treatment.

By staining for both phospho- and total-DHX9, it can be noted that the distribution of these two stains are completely different. Total DHX9 is found exclusively in nucleus, while phospho-DHX9 is only found within the cytoplasm (Figure 4.16). In order to investigate if peptide treatment led to any changes in the detection of phosopho-DHX9, the MFI from each condition was measured from each. The statistical significance of the mean was determined using a Two-Way Anova (Figure 4.17).

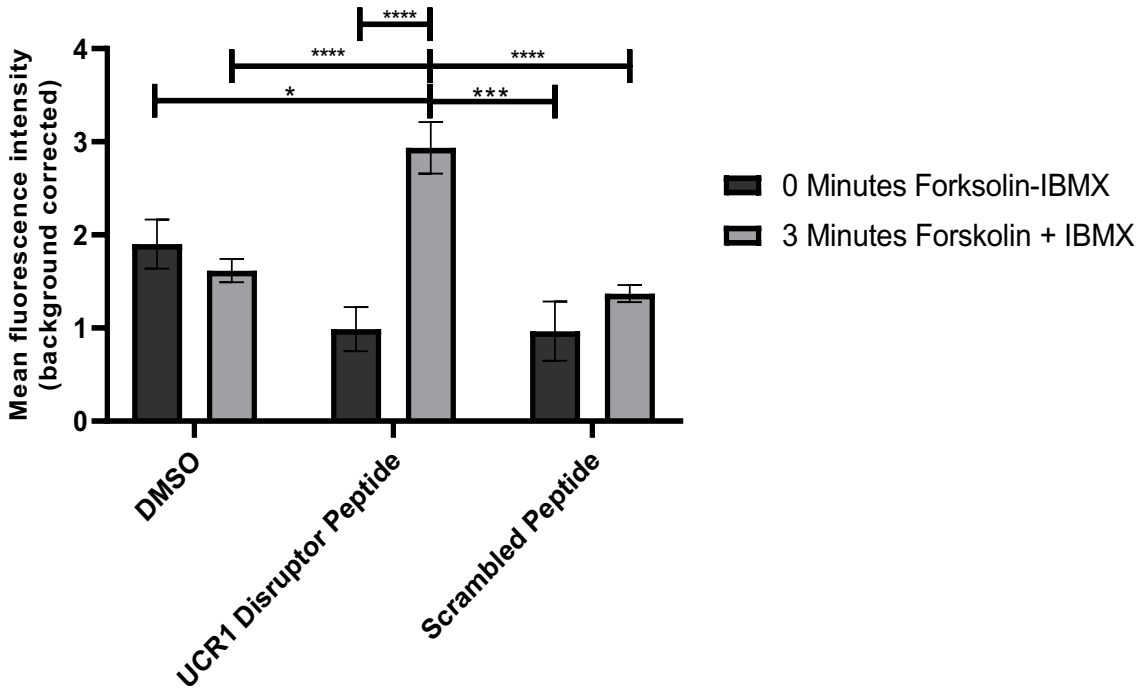

Figure 4.17 MFI of phosho-DHX9 from cells treated with UCR1 disruptor peptide and forskolin-IBMX. The MFI from cells stained with phospho-DHX9 in Figure 4.16 was determined. The data presented is representative of the mean ± SEM of N>14 cells from each condition. Statistical significance was determined using a Two-Way Anova, where p*=0.0138, p***=0.0007, and p****<0.0001.

Treatment with the UCR1 disruptor and scrambled peptide led to a slight non-significant decrease in the amount of phospho-DHX9 detected in the cells under basal conditions (Figure 4.16 A, last row, and Figure 4.17). However, a significant increase in levels of phospho-DHX9 could be detected in cells where the interaction between PDE4D7 and DHX9 was inhibited in conjunction with increased levels of intracellular cAMP due to the forskolin-IBMX treatment (Figure 4.16 B, last row, and Figure 4.17). Treatment of the cells with the UCR1 disruptor peptide and forskolin-IBMX led to a highly significant increase in levels of phospho-DHX9 detected when compared to all other conditions (Figure 4.17). Interestingly, this effect was not observed when the cells were pre-treated with

the scrambled peptide control. Although treatment of these cells with forskolin-IBMX did lead to a slight increase in the detection of phospho-DHX9, this was not to the same extent as the UCR1 disruptor peptide (Figure 4.16 A and B, middle row, and Figure 4.17). The increase in the levels of DHX9 phosphorylated can be attributed to the fact that DHX9 and PDE4D7 are no longer interacting with each other. This data provides further evidence that the binding of PDE4D7 to DHX9 gates DHX9 phosphorylation. PDE4D7 acts as a negative regulator of DHX9 phosphorylation, and dissociation of this complex leads to an increase in DHX9 phosphorylation by PKA.

4.4 Discussion

4.4.1 DHX9 PKA phosphorylation is regulated by PDE4D7

PTMs are known to be essential mechanisms in eukaryotic cells to diversify the function any single protein can have within the cells. Dynamic coordination of different signalling networks allows a single protein to respond to multiple extracellular signals. Reversible, or irreversible, biochemical reactions allow cells to regulate downstream signalling pathways and alter their physiological state (Wang, Peterson and Loring, 2014). Understanding the roles and mechanisms of PTMs is essential in biomedical sciences as certain PTMs are known to interfere with drug action. This in turn can influence different biochemical networks than can alter drug response (Brunk *et al.*, 2018).

Protein phosphorylation is one of the most important PTMs, with the ability to orchestrate a variety of cellular functions and processes (Gao *et al.*, 2008). This reversible reaction occurs through protein kinases that can mediate the addition of a phosphate group to the polar R group of various amino acids. This addition allows the protein to change its conformation when interacting with other molecules (Ardito *et al.*, 2017). The phosphate group has been shown to be used to regulate critical biological functions, as well as coordinate an appropriate drug response (Schwartz and Murray, 2011). Protein phosphatases are slowly being recognised as crucial regulators of signalling pathways (Reiterer *et al.*, 2020). The phosphorylation state of a single protein is a dynamic process that depends on the activities of both protein kinases and phosphatases acting on their appropriate substrate (Barford, Das and Egloff, 1998). PP1 is the major Ser/Thr phosphatase and it is expressed in all eukaryotic cells. This protein is involved in multiple cellular processes, including cell cycle regulation, highlighting its importance in maintaining normal cellular functions (Shi, 2009). Modification of proteins via their phosphorylation and subsequent dephosphorylation, is a critical function in multiple signalling pathways (Vitrac, Mallampalli and Dowhan, 2019).

In this chapter, I have shown that DHX9 is phosphorylated by PKA in biochemical assays and *in vitro* in cultured cells. Although DHX9 has previously been shown to be phosphorylated by DNA-PK and PI3KKs (Zhang *et al.*, 2004; Lin *et al.*, 2020),

this is the first study to show that DHX9 may be phosphorylated by PKA. Using PKA consensus site prediction software and peptide array technology, I was able to show that DHX9 can be phosphorylated at S^{449} in the helicase domain (Table 4.1 and Figure 4.3). Interestingly, loss of the PDE4D7-DHX9 interaction due to the UCR1 disruptor peptide treatment also led to an increase in DHX9 phosphorylation under basal conditions when investigated by IP (Figure 4.15). Further treatment by forskolin-IBMX lead to a highly significant increase in the detection of phospho-DHX9 (Figure 4.16). It is now widely accepted that compartmentalization of cAMP signalling and PKA action is regulated by localised pools of PDEs. The direct interaction between AKAP, PDEs, and PKA is complex and governs the dynamic signalling changes which in turn can direct down-stream signalling pathways and protein activity (Willoughby *et al.*, 2006). Interestingly, inhibition of PDEs using a combination of different inhibitors results in the global increase in levels of cellular cAMP (Beltejar *et al.*, 2017). Using a mass spectrometry-based phosphoproteomic analysis after treatment with various selective PDE inhibitors, Beltejar *et al.* (2017) attempted to characterise how PDEs can regulate the phosphoproteome in the Jurkat T-cell line. Using this approach, they were able to identify 3241 proteins that were phosphorylated when different PDEs were directly inhibited. Upon further inspection, phosphorylation of a subset of these proteins was directly mediated by PKA when PDE3 and PDE4 isoforms were directly inhibited. The proteins identified as being phosphorylated in this analysis were found to be associated with a wide range of biological functions, highlighting the ability of the cAMP to regulate multiple processes in T-cells (Beltejar *et al.*, 2017). Although this study was conducted in T-cells, it demonstrates the importance of PDEs in regulating the global phosphoproteome. However, interactions with specific PDE isoforms are known to regulate phosphorylation. The targeting of single PDE-protein interactions allows for the precise regulation of individual cAMP nanodomains (Blair and Baillie, 2019). Such is the case with the interaction between PDE4D and heat shock protein 20 (HSP20) in cardiac myocytes (Sin *et al.*, 2011). HSPs are a large family of molecular chaperones which have important roles in cell survival and development. While some HSPs are constitutively expressed, expression of certain Hsps are upregulated under stress conditions (Miller and Fort, 2018). The protective action of HSP20 is triggered following phosphorylation by PKA at S^{16}. Activation of ß-adrenergic stimulation and

increases in levels of intracellular cAMP leads to the phosphorylation of HSP20 by PKA, which is vital for cardioprotective actions of this protein (Edwards, Scott and Baillie, 2012). Using peptide array technology, Sin *et al.* (2011) were able to show that HSP20 binds to the catalytic region of PDE4D. Disruption of this interaction using cell permeable peptides was shown to increase the levels of PKA-mediated phosphorylation of HSP20 in neonatal rat cardiomyocytes. This in turn protected these cardiac cells against ß-adrenergic-induced hypertrophy (Sin *et al.*, 2011; Martin *et al.*, 2014).

Due to the importance of the cAMP/PKA pathway in multiple key processes, such as cell survival, proliferation, and differentiation (Palorini *et al.*, 2016), it is important that we identify novel proteins that can be phosphorylated by PKA. In this chapter, I suggest that disruption of the interaction between PDE4D7 and DHX9 leads to an increase in DHX9 phosphorylation detected by western blotting and ICC using an antibody directed towards a novel PKA phosphorylation site in DHX9 (S449) (Figure 4.15 and Figure 4.16). Future work into the functional implication of DHX9 phosphorylation is needed in order to understand how this change can alter its helicase activity. Previous work by Lin et al (2020) demonstrated that the inhibition of DHX9 phosphorylation by PI3KKs decreased the expression of oxaliplatin-induced circRNA expression, which in turn blocked the development of chemo-resistant cells (Lin *et al.*, 2020). It would be interesting to find out if DHX9 phosphorylation promotes the expression of circRNA that could lead to chemo-resistance. Inhibition of DHX9 PKA phosphorylation could potentially desensitize chemo-resistant cells, and potentially ameliorate treatment outcome of patients with hormone refractory or CRPC tumours.

Interestingly, other members of the helicase superfamily have been reported to be phosphorylated, which in turn affected their activity. The DDX1 helicase has recently been shown to be phosphorylated (Gustafson and Wessel, 2010). DDX1 is a member of the DEAD family of RNA helicases and its activity is associated with multiple aspects of cellular metabolism (Li, Monckton and Godbout, 2008). Research by Li *et al.* (2008) demonstrated that DDX1 colocalizes with ataxia telangiectasia mutated (ATM) kinase at DSBs within the nucleus following ionising radiation treatment . Interestingly, this co-localisation was associated with an increase in DDX1 phosphorylation *in vitro* and *in vivo*, suggesting that

DDX1 phosphorylation promotes DDX1 role in the repair (Li, Monckton and Godbout, 2008; Gustafson and Wessel, 2010). By identifying DHX9 as a novel PKA phospho-substrate is a step towards identifying a mechanism by which this protein is regulated.

4.4.2 DHX9 and other PTMs

Although I have shown that DHX9 is readily phosphorylated by PKA, DHX9 is known to be SUMOlyated at its N-terminus and methylated at its C-terminus (Fidaleo, De Paola and Paronetto, 2016). Many enzymes that are responsible for PTMs are able to recognise and modify multiples sites within the same target protein (Barber and Rinehart, 2018). Over 59% of proteins within the human genome are modified by more than one PTM (Woodsmith, Kamburov and Stelzl, 2013). Modified proteins are key regulators of signalling pathways and cellular homeostasis (Perchey *et al.*, 2019). PTMs represent a key mechanism by which a cell can regulate protein function (Beltrao *et al.*, 2013). Owing to the reversible nature of most PTMs, normal cells can use this switch in order to determine the resting and proliferative state of cells, enabling rapid and tight regulation of cell proliferation. However, in cancer cells, activation of oncogenes and loss of tumour suppressor genes provides continuous proliferative signals in part due to the changes in PTMs of effector proteins that are involved in proliferation (Hitosugi and Chen, 2014). Sustained proliferative signalling due to changes in PTMs and their downstream signalling pathways is recognised as one of the hallmarks of cancer, and understanding these changes is vital in order to find new therapeutic targets (Hanahan and Weinberg, 2011). In this chapter, DHX9 was shown to be by phosphorylated by PKA but I did not investigate whether this PTMs had any downstream effects on DHX9´s ability to mediate CREB transcription. Recent work in the Baillie lab used a PDE4D7 luciferase construct in order to investigate if AR signalling influenced PDE4D7 expression (Henderson et al., 2014). This assay could be adapted in order to investigate whether DHX9 phosphorylation by PKA alters PDE4D7 mRNA expression via its CREB sites. Not only would this experiment show that DHX9 has a role in PDE4D7 expression, it would also allow us to determine if PKA phosphorylation of DHX9 alters its transcriptional activity.

As previously mentioned, DHX9 has recently been shown to be SUMOylated by the SUMO-conjugating ubiquitin-conjugating enzyme 9 (UBC9) (Fidaleo, De Paola and Paronetto, 2016). SUMOylation is an evolutionarily conserved PTM, characterised by the covalent attachment of the small ubiquitin-like modifier (SUMO) to its target proteins (Li *et al.*, 2020). The SUMO conjugation pathway involves the use of three enzymes (E1-3), each having individual roles during the reaction (Hannoun *et al.*, 2010). The first step in this pathway is the activation of the mature SUMO protein at its C-terminus by a SUMO-specific E1 enzyme. The active SUMO protein is then transferred to an E2 conjugating enzyme UBC9, which can then transfer SUMO to its target protein. The transfer of the SUMO protein is mediated by a SUMO E3 ligase (Geiss-Friedlander and Melchior, 2007). Although several proteins have been reported to be SUMOylated, including PDE4D5 (X. Li *et al.*, 2010), SUMO modification is less commonly detected in cells when compared to other PTMs as it is more difficult to identify (Chen and Lu, 2015). Attachment of a SUMO peptide to its target protein has been implicated in numerous cellular processes, including DNA repair and cell cycle regulation (Andreou and Tavernarakis, 2009).

Recent studies have shown that transcription factors can be modified by SUMOylation, affecting target gene expression (Rosonina, 2019). Therefore, it comes as no surprise that DHX9 has been shown to be a substrate for SUMO modification. Work by Argasinska et al. (2004) recently showed that the N-terminal region of DHX9 (amino acids 1-37) can interact with UBC9. This in turn led to the attachment of a Sumo-1 complex to DHX9, both *in vitro* and *in vivo*. Interestingly, the interaction between UBC9 and DHX9 was shown to mediate CREB transcription by DHX9. However, DHX9 does not need to be SUMOylated to mediate CREB transcription. They suggested that although DHX9 has been shown to be SUMOylated in the presence of UBC9, this modification is not necessary in regulating DHX9 helicase activity (Argasinska *et al.*, 2004). However, DHX9 SUMOylation may have an impact on disease progression. Using mass spectroscopy analysis from Kaposi's sarcoma-associated herpesvirus (KSHV) cell lysate, DHX9 was recently found to contain a SUMO interacting motif (SIM). This SIM was shown to potentially regulate virus-mediated gene expression through SUMOylation of DHX9, therefore having an important role in KHSV persistence and pathogenesis (Gan *et al.*, 2015). The GPS-SUMO website can predict the

potential SUMOylation sites and SIMS within a protein of interest (Zhao *et al.*, 2014). The SUMOylation sites were classified into two groups (consensus and non-consensus) based on the canonical ψ-K-X-E, where ψ is a hydrophobic amino acid (I, V, L, A, P, or M), K is lysine and x is an arbitrary amino acid (Zhao *et al.*, 2014; Chang *et al.*, 2018). SUMOylation at a non-consensus site refers to the fact that a Lysine residue can be phosphorylated despite not being flanked by a hydrophobic amino acid (Impens *et al.*, 2014). By using the GPS-SUMO predictor site (http://sumosp.biocuckoo.org/online.php) I was able to identify 5 potential SIMs and SUMOylation consensus sites within DHX9 (Table 4.2).

Table 4.2 Identification of multiple SIMs and SUMOylation sites within DHX9.

Position	Peptide	Type
54	GMGNSTNKKDAQSNA	Sumoylation Nonconcensus
69 - 73	ARDFVNYLVRINEIKSEEV	SUMO Interaction
76	LVRINEIKSEEVPAF	Sumoylation Concensus
120	LPPHLALKAENNSEV	Sumoylation Concensus
152	LKDYYSRKEEQEVQA	Sumoylation Nonconcensus
365	EQISMDLKNELMYQL	Sumoylation Concensus
406 - 410	EAISQNSVVIIRGATGCGK	SUMO Interaction
560 - 564	EYFFNCPIIEVYGRTYPVQ	SUMO Interaction
596	KDKKKKDKDDDGGED	Sumoylation Nonconcensus
725 - 729	TSITINDVVYVIDSCKQKV	SUMO Interaction
1081 - 1085	KVQSDGQIVLVDDWIKLQI	SUMO Interaction
1111 - 1115	RAAMEALVVEVTKQPAIIS	SUMO Interaction

Interestingly, the GPS-SUMO analysis identified a SUMOylation non-consensus site within the PDE4D7 binding domain (Table 4.2 Position 596). This could suggest that binding between PDE4D7 and DHX9 could be further regulated by the SUMOylation status of DHX9. Interestingly, a study by Li *et al.* (2010) revealed that inhibiting the interaction between two interacting protein by blocking SUMOylation of a target protein, using a synthetic SIM peptide, inhibits DNA repair and increases cancer cell sensitivity to radiation (Y.-J. Li *et al.*, 2010). By treating cells with a SIM peptide designed to compete with SIM sites within a protein, they were able to inhibit SUMO-dependent protein-protein interactions. They were then able to test the effects of the disruption of these interactions on the cellular DNA damage response. Following SIM or control peptide treatment,

the cells were treated with the chemotherapeutic drug doxorubicin. Interestingly, treatment with the SIM peptide increased the sensitivity to doxorubicin treatment when compared to the control peptide (Y.-J. Li *et al.*, 2010). Inhibiting SUMO-mediated PPI are of pharmaceutical interest as an increasing number of studies have revealed that disruption of these interactions could potentially alter chemo- and drug sensitivity (Voet *et al.*, 2014).

Interestingly, protein phosphorylation and SUMOylation are known to be linked to one another. Rather than modification at a single site, a protein is dynamically altered at multiple sites by an array of modifications, including phosphorylation and SUMOylation (Yang and Grégoire, 2006) Studies have revealed that certain lysine residues are flagged for SUMOylation following the phosphorylation of a serine/threonine immediately downstream of the SUMO consensus sequence (Anckar and Sistonen, 2007). In addition to the ψ–K–X–E SUMO consensus site, a second phosphorylation-dependent SUMOylation motif (PDSM), composed of a SUMO and a proline-directed phosphorylation site (Ψ-K-x-E-x-x-S-P) has been identified. This motif has been involved in the phosphorylation-dependent SUMOylation of transcription factors nuclear factor erythroid-derived 2 (NF-E2) and shown to alter their activity (Hietakangas *et al.*, 2006). Work by Su *et al.* (2012) demonstrated that the transcriptional activity of NF-E2 was increased following SUMOylation and PKA-mediated phosphorylation. By purifying recombinant NF-E2 protein, they showed that PKA phosphorylation increased protein SUMOylation, which in turn promoted the dimerization of NF-E2 which in turn regulated its activity (Su *et al.*, 2012). Although not studied here, it would be interesting to investigate if the SUMOylation of DHX9 is dependent on DHX9 phosphorylation.

In addition to being PKA phosphorylated and SUMOylated, DHX9 is also methylated at its C-terminal end (Fidaleo, De Paola and Paronetto, 2016). Proteins can be methylated on the sidechain nitrogen of arginine and lysine residues on their C-terminal ends. This PTM subtly changes their primary protein structure in order to encode more information (Bedford, 2006). Interestingly, arginine methylation is associated with gene regulation, including regulating the binding between DNA and transcriptional activators (Lee *et al.*, 2005). DHX9 has recently been shown to be methylated within its RGG-box at its C-terminal domain (Smith *et al.*, 2004). Methylation of DHX9 was found to be crucial in its

ability to localise to the nucleus. Inhibition of DHX9 methylation using protein arginine methyltransferase (PRMT) inhibitors led to the accumulation of DHX9 in the cytoplasm when visualised by confocal microscopy. However, when a methylated DHX9 was expressed in Hela cells, this led to the immediate expression of DHX9 within the nuclear region, indicating that DHX9 methylation is crucial for its nuclear import (Smith *et al.*, 2004). Interestingly, the data presented in this chapter shows that PKA phosphorylation of DHX9 appears to lead to the accumulation of DHX9 within the cytoplasm when investigated by ICC with confocal microscopy (Figure 4.13, Figure 4.14 and Figure 4.16). Unlike protein methylation, phosphorylation of DHX9 by PKA could potentially act as an inhibitor of DHX9 import in order to sequester the protein within the cytoplasm to promote DHX9's translational activity. Multiple mRNA structures relies on DHX9 for efficient folding and unfolding (Murat *et al.*, 2018). Therefore, PKA phosphorylation of DHX9, and its sequestering in the cytoplasm, could promote the unwinding of aberrant mRNA structures in order to initiate protein translation. Translation initiation is known to play an important role in PC tumorigenesis and hyperactivation of the mTOR pathway in PC is often associated with increased translational output (Hernández *et al.*, 2019). In order to confirm that this is the case, further investigation such as subcellular fractionation need to be performed. If DHX9 phosphorylation does lead to its accumulation in the cytoplasm, we would expect to see a band representing phospho-DHX9 in the cytoplasmic fraction and unphosphorylated DHX9 within the nuclear fraction. DHX9 has recently been shown to be recruited by the mTOR pathway to promote the translation of specific mRNA (Nandagopal and Roux, 2015). Therefore, the accumulation of DHX9 in the cytoplasm as a result of PKA phosphorylation could lead to an increase in mRNA translation via the mTOR pathway.

4.4.3 Can DHX9 phosphorylation promote PC progression?

Protein phosphorylation is one of the most important mechanisms by which different cellular processes are regulated. Many enzymes and receptors are activated and deactivated by the reversible action of phosphorylation (Ardito *et al.*, 2017). Although protein phosphorylation is essential for normal cellular processes, abnormal phosphorylation is one of the main PTMs that causes structural and functional changes that lead to disease (Singh *et al.*, 2017).

Although the AR is activated by ligand binding, it is known to be phosphorylated at least 15 different sites, most of which are found within the N-terminal region. Phosphorylation of AR leads to an increase in its transcriptional activity, increased expression of AR, and changes in cell growth. Activation of AR has been identified as one of the mechanisms by which a PC tumour can progress into the lethal CRPC phenotype. Despite ADT lowering the levels of androgens, AR phosphorylation by PKA has been identified as a key mechanism by which PC can progress via the cross talk with the cAMP-PKA pathway (Daniels *et al.*, 2013). It is widely accepted that the PKA signalling pathway is highly involved in PC progression. Elevated levels of intracellular cAMP are known to increase the expression of PSA, highlighting the importance in PC (Sarwar *et al.*, 2014). This may potentially be due to the decrease in the global expression of PDE4 isoforms that has recently been reported by our group and others (R. Böttcher *et al.*, 2015; Böttcher *et al.*, 2016; van Strijp *et al.*, 2018).

The data presented in this chapter has shown that decreased interaction between PDE4D7 and DHX9 leads to an increase in DHX9 phosphorylation by PKA (Figure 4.15 and Figure 4.16). Although these experiments were performed in HEK293 cells overexpressing these proteins, we can suggest that the effect could be observed in PC cell lines. But this also poses the question: does DHX9 phosphorylation change depending on the stage of disease? Decreased expression of PDE4D7, and other PDE4D isoforms, could potentially contribute to an overall increase in intracellular levels of cAMP and PKA activation. This in turn could increase the amount of phosphorylation of DHX9 and other proteins such as AR *in vivo*. This could contribute to progression of the disease to the more lethal CRPC phenotype. In order to investigate if there is a difference in level of phospho-DHX9 between early and late stage disease, PC cells could be probed for phospho-DHX9 under basal conditions. We could also investigate if the interaction between DHX9 and other binding partners are also altered by PKA phosphorylation. Furthermore, by using our newly synthesised phospho-DHX9 antibody, we would be able to directly detect changes in levels of phosphorylated DHX9 from matched patient-derived tumours. These experiments could help us understand if DHX9 phosphorylation in crucial for PC progression.

4.4.4 Chapter summary

Data in this chapter has provided evidence that DHX9 is a novel substrate for PKA phosphorylation. Using PKA consensus site prediction software and peptide array technology, I was able to show that DHX9 is phosphorylated at Ser^{449} in the helicase domain of DHX9. Interestingly, this site is found upstream of PDE4D7's binding site. Loss of this serine by sequence substitutions and truncations shows that DHX9 phosphorylation is completely lost in biochemical assays, further providing evidence that DHX9 can be phosphorylated by PKA. Using the information obtained from the peptide array, a custom phospho-DHX9 antibody was synthesised. This antibody was able to successfully detect phospho-DHX9 by western blotting and confocal microscopy. Such a phosphorylation could potentially alter the activity of DHX9 and could contribute to a change in mRNA levels. The interaction between PDE4D7 and DHX9 was shown to be important in regulating the levels of DHX9 phosphorylation. Loss of this interaction was shown to increase the levels of PKA-mediated DHX9 phosphorylated. Unfortunately, the effects of DHX9 phosphorylation on its activity was not studied in this chapter. By performing a helicase assay using purified recombinant DHX9, we would be able to determine if DHX9 phosphorylation can increase its helicase activity. This assay directly looks at helicase activity by detecting levels of single stranded DNA or RNA by agarose gel electrophoresis following incubation with a helicase (Wang *et al.*, 2014). By phosphorylating DHX9 in the assay, we would be able to directly observe how this modification can affect DHX9 activity. This information could potentially provide us with information on whether DHX9 phosphorylation and activity contributes to PC disease progression.

Chapter 5 Characterising the role of DHX9 in Prostate Cancer

5.1 Introduction

5.1.1 DHX9 in prostate cancer

As PC is a mainly driven by testosterone and DHT, it is understandable that current research focuses on trying to find innovative ways to inhibit hormone production and initiation of hormone-activated signalling pathways (Crawford *et al.*, 2019). Although ADT is known to be a highly successful course of treatment, the mean progression time to CRPC was found to be 13.1 – 19.3 months under this regime. The majority of patients eventually progress into the more phenotypically lethal PC, with a significant proportion of their life span spent in this castration-resistant state (Damodaran, Kyriakopoulos and Jarrard, 2017). There is currently a need to find alternative targets that have the potential to supplement and strengthen therapies in use today. In recent years, the DNA damage response and repair mechanism has become a potential new therapeutic target. DNA helicases are found to be involved in every aspect of nucleic acid metabolism and are known to unwind alternate DNA structures and displace proteins bound to ssDNA/dsDNA. Mutations in these helicases are known to be associated with various cancers (Datta and Brosh, 2018).

In recent years, DHX9 has emerged as a potential new target in multiple cancers. Dysregulation of the mechanisms guiding cell death plays an important part in cancer. One of the hallmarks of cancer is the evasion of apoptosis leading to drug resistance and tumorigenesis. Genetic mutations and changes in DHX9 expression have been observed in different cancers, indicating that this protein may be involved in the development of disease. Work by Mills et al. (2013) has shown that suppression of DHX9 was able to reverse the resistance of Eμ-Myc/Bcl-2 lymphoma to the chemotherapeutic agent ABT-737. Loss of DHX9 expression in these cells was shown to lead to activation of the p53 apoptosis pathway via an increase in cellular stress (Mills *et al.*, 2013). Not only has it been observed that DHX9 increases cell sensitivity to chemotherapeutic agents but decreasing DHX9 levels also has profound cellular effects and can be lethal *in vitro*. Knockdown of DHX9 in a panel of cancer cells has a detrimental effect

on cell growth, and when suppressed in mice, it had not negative impact on their health (Lee *et al.*, 2016). YK-4279 has the unique ability to be lethal only to cancer cells, but not have any deleterious effects in animal models, thus demonstrating that DHX9 is new target in cancer treatment.

In prostate cancer, DHX9 has been shown to be a target gene of SOX4. The sex determining region Y (SOX), is a family of transcription factors that plays an important role in development. SOX4 is a 47 kDa protein that is overexpressed in multiple cancers, such as PC: increased expression at an mRNA and protein level is correlated with high Gleason scores and tumour grades (Liu *et al.*, 2006). Activation of the transcriptional activity of SOX4 via the Wnt pathway leads to an increase in the binding of SOX4 to the *DHX9* promoter (Lai *et al.*, 2011). Stimulation with recombinant WNT3A and leptomycin B (LMB) resulted in a decrease in the promoter binding (Lai *et al.*, 2011; Cai *et al.*, 2017). These studies suggest that DHX9 may play a role in the development of PC, however the direct mechanisms through which it contributes to the disease are still unknown (Lee and Pelletier, 2016). Current research suggests that DHX9 may be a contributor to tumorigenesis.

5.2 Chapter Aims

DHX9 is known to play a major role in cancer development and response to therapy. Although DHX9 maps to a PC susceptibility locus, its function in PC and cellular proliferation is currently undefined. Considering this, the aims of this chapter are as follows:

AIM 1: Determine if changes in DHX9 expression or its interaction with EWS-FL1 affects the proliferation of PC cells. Using the RTCA XCELLigence plate reader, the importance of DHX9 expression and its interactions with EWS-FL1 will be assessed. DHX9 expression will be suppressed using siRNA technology, while the interaction between DHX9 and EWS-FL1 will be disrupted using the small molecule YK-4-279.

AIM 2: Determine if disruption of the PDE4D7-DHX9 complex affects the proliferation of PC cells. Using the RTCA XCELLigence plate reader, the importance of PDE4D7-DHX9 complex will be assessed in order to understand if this interaction promotes or slow down PC cell growth.

AIM 3: Determine if the disruption of the PDE4D7-DHX9 complex affects the ability of DHX9 to unwind nascent RNA structures in order to promote R-loop formation. This will be assessed using ICC with confocal microscopy.

AIM 4: Determine if changes in DHX9 expression result in changes to downstream signalling pathways using Reverse Phase Protein Array (RPPA) technology. DHX9 expression will be suppressed using siRNA technology, and changes to any downstream signalling pathways can be reviewed using RPPA technology.

5.3 Results

5.3.1 siRNA-mediated knockdown of DHX9 leads to a decrease in cell proliferation in AS and CRPC cell lines

5.3.1.1 DuCaP growth is reduced in cells treated with siDHX9

The DuCap cell line was first established in 2001, DuCaP has since been used as a model for androgen sensitive PC (Lee *et al.*, 2001) . Interestingly, this cell line also harbours the *TMPRSS2-ERG* gene fusion, which results in the androgen-regulated expression of ERG (Pfeiffer, Mulders and Schalken, 2010). DuCaP were first derived from mouse SCID xenograft model (Sobel and Sadar, 2005) To determine if the cellular proliferation of prostate cancer cell lines is affected by decreased expression of DHX9, siRNA targeting DHX9 (and the controls GAPDH siRNA, and non-targeting siRNA) were transfected into DuCaP cells to check for siRNA efficiency. DuCaP cells were plated into six well plates, transfected with the appropriate siRNA the next day and left to incubate for 48 hours at 37˚C with 5% CO_2. Cell lysate was extracted and proteins separated on an SDS-PAGE gel. Protein expression was then assessed by western blotting. DHX9 expression in all samples were normalised to loading control, then compared to cells treated with non-targeting siRNA (Figure 5.1)

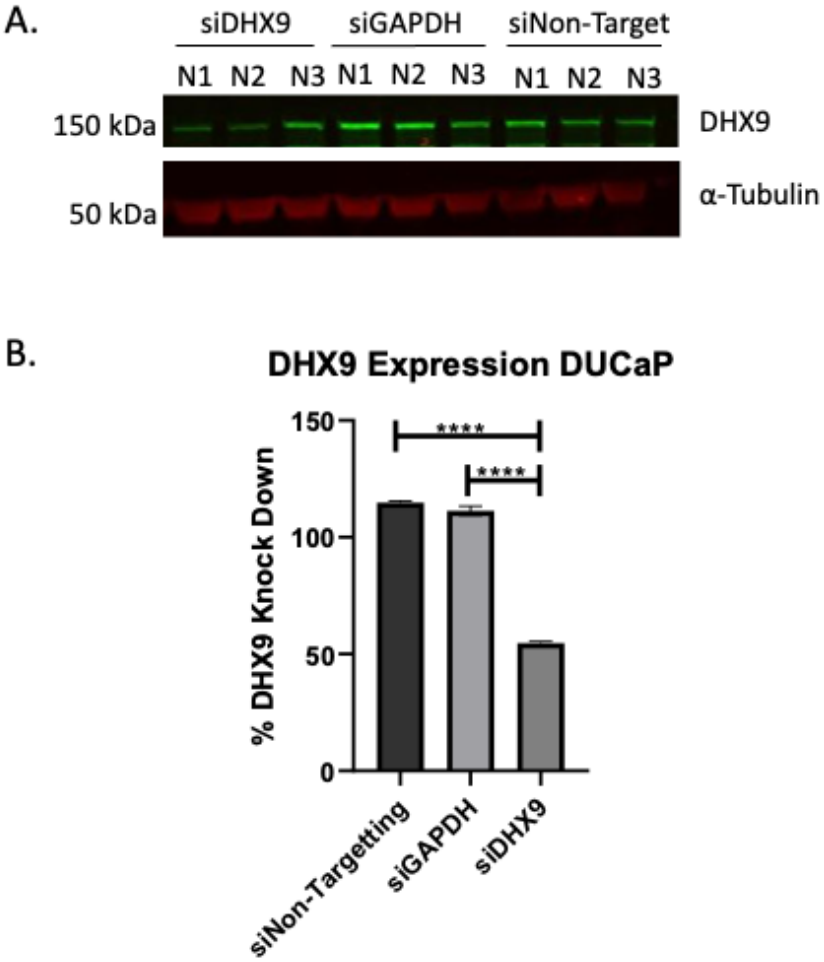

Figure 5.1 siRNA mediated knockdown of DHX9 in DuCaP cells. A. DuCaP cells were transfected with either siDHX9, siGAPDH, or siNon-Targeting. Protein expression was assessed by SDS-PAGE with western blotting. Membranes were probed with antibody against DHX9 and α-tubulin. B. DHX9 protein expression was normalised to α-tubulin, then normalised to the si Non-Targetting. Data is presented as the mean ± SEM from two separate experiments. Significance was determined using a One-Way Anova where $p<0.0001$. **This work was carried out by Jane Findlay.**

Transfection with the DHX9-specific siRNA led to a highly statistically significant 50% decrease in protein expression (Figure 5.1B). This siRNA was then used to investigate whether the decreased expression of DHX9 leads to a change in DuCaP proliferation. 10 000 cells were seeded into each well of the 96 well E-Plate and left to grow for 48 hours. They were then transfected with siRNA and left to grow for an additional five days (Figure 5.2). The cell growth of each condition was monitored using the RTCA software where cell growth is reported as the cell index (CI).

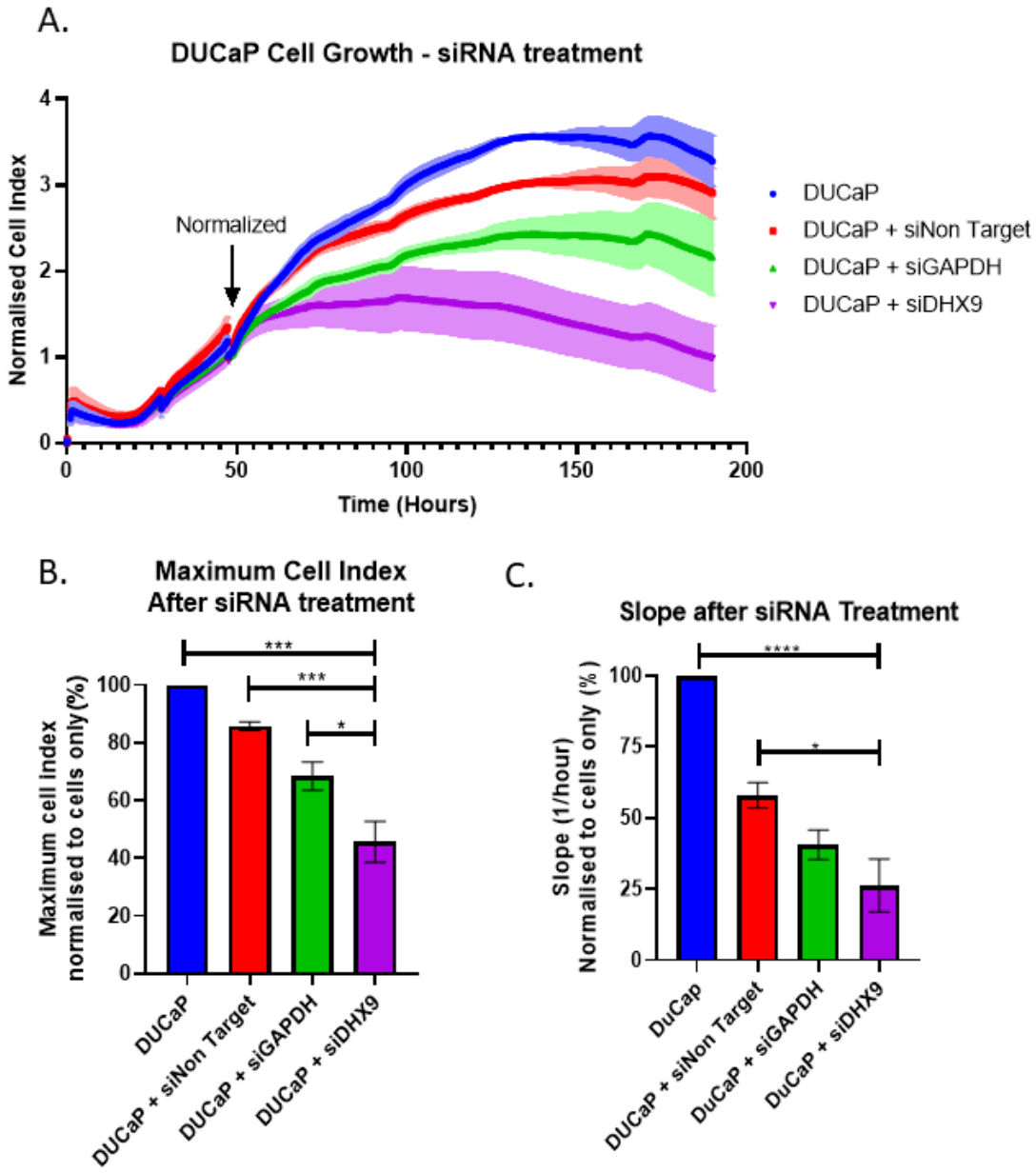

Figure 5.2 siRNA-mediated knockdown of DHX9 leads to a decrease in DuCaP cell proliferation. A. xCELLigence technology was used to measure proliferation of DuCaP cells transfected with siRNA against DHX9, GAPDH and Non-targeting. The cell index was normalised at the time of siRNA Transfection. Growth curves are represented as the mean ± SEM of three independent experiments. B. The maximum cell index for each growth curve was identified and represented as the mean ± SEM of three independent experiments. The maximum cell index was normalised to the cells-only condition and statistical significance was calculated using a One-Way Anova. C. The slope of each growth curve was calculated from the point of treatment to 100 hours. The slope is represented as the mean ± SEM of three independent experiments. The slope was normalised to the cells-only condition and statistical significance was calculated using a One-Way Anova. **This work was carried out by Jane Findlay.**

During the first 48 hours of the experiment, the CI is seen to steadily increase due to the cells coming out of suspension and adhering to the bottom of the well. When transfected with non-targeting siRNA and siGAPDH, the cells are seen to continue to increase over the 5 days of the experiment, indicating that cell growth is unaffected by these transfections (Figure 5.2 A, red and green traces).

However, when transfected with siDHX9, the CI steadily decreases when compared to the other conditions, indicating that decreased expression of DHX9 slows down DUCaP cell growth (Figure 5.2 A purple trace). Although in general, treatment with any siRNA reagents resulted in an overall reduction in cell growth (as assessed by the slope of exponential growth), growth of cells that were treated with siRNA specifically targeting DHX9 was significantly reduced when compared to the cells-only and siNon-Targeting conditions (Figure 5.2 C). A similar result was seen when the maximum cell index was evaluated (Figure 5.2 B). The maximum cell index represents the timepoint at which the cells have reached their maximum attachment strength and confluency. The maximum cell index of cells treated with siRNA against DHX9 was significantly reduced when compared to the other treatments and cells-only. The data presented here shows that expression of DHX9 is crucial for PC cell growth and proliferation. Previous work by Lee et al (2014) demonstrated that suppression of DHX9 expression in human fibroblast cells leads to an activation in the p53 pathway (Lee *et al.*, 2014), which is potentially what is observed in the cell growth curves.

5.3.1.2 LNCaP growth is reduced in cells treated with siDHX9

In order to investigate if this effect was also seen in other AS cell lines, a pilot study with AS VCaP and LNCaP cells was carried out.. This was to determine the best cell density and cell line to use in future experiments. 40 000, 20 000, 10 000 or 5 000 cells were plated into the 16 well E-P6ate, and their growth was monitored over 5 days (Figure 5.3). A pilot study was not conducted for the DuCaP experiments (Figure 5.2) as the optimum cell density was determined by previous members of the Baillie Lab.

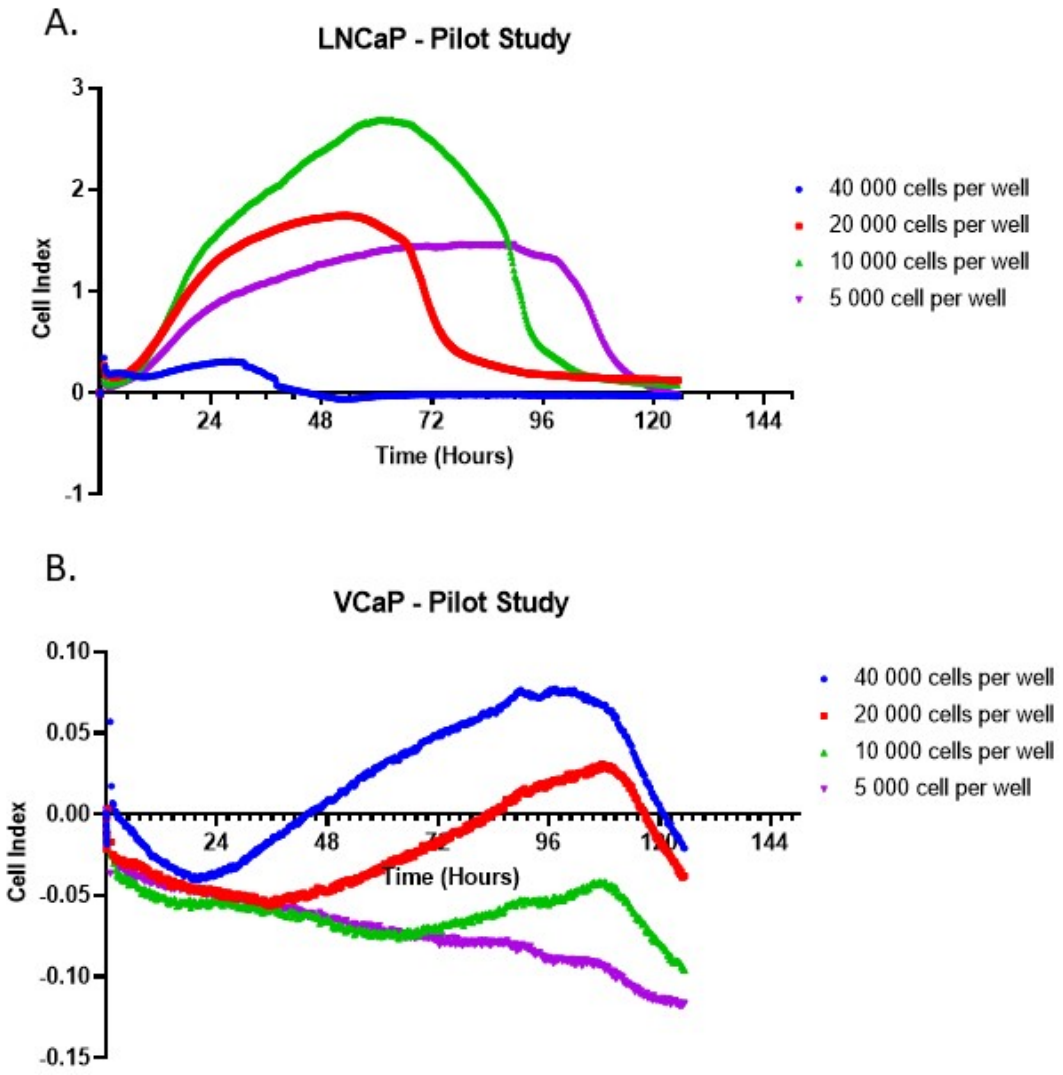

Figure 5.3 AS cell line pilot study. In order to use the correct cell line and cell density for future experiments, LNCaP (A) and VCaP (B) were plated at different densities and growth was monitored using the RTCA cell analyser over five days.

Based on the information obtained in Figure 5.3 A, I decided to use 5 000 LNCaP cells per well. This cell density provided three days of growth, giving us a large window of opportunity to study how growth can be affected by siRNA treatment. Although 10 000 and 20 000 LNCaP cells per well were able to show growth after seeding, they reached maximum cell index at 72 hours and 48 hours respectively. Unlike the other cell densities, when 40 000 LNCaP cells were seeded no growth was observed, potentially due to overcrowding of the well (Figure 5.3 A). VCaP cells were not chosen for any future experiments as most growth curves remained negative for 48 hours (Figure 5.3 B). Although VCaP have been used as a model for early stage PC, this cell line has a doubling time of 5-6 days (Cunningham and You, 2015), potentially explaining why it has taken them over 48 hours to recover from seeding. In order to use VCaP cells for future

xCELLigence experiments, more than 40 000 cells per well would be required in order to obtain an appropriate growth curve. Based on the information obtained in Figure 5.3 A, 5000 LNCaP cells per well was selected for future cell growth assays. siRNA transfection efficiency in LNCaP was then assessed by SDS-PAGE with western blotting (Figure 5.4) prior to starting xCELLigence experiments.

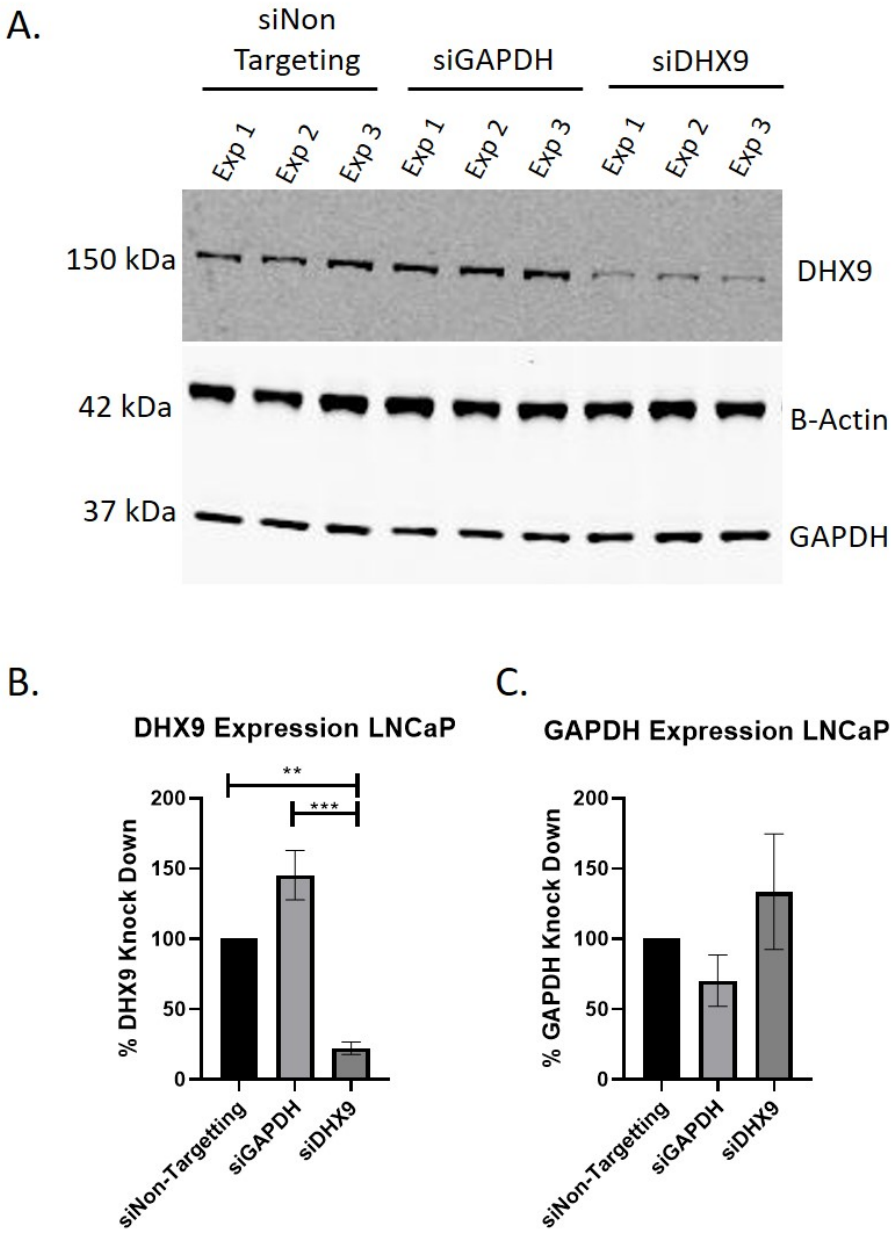

Figure 5.4 siRNA transfection efficiency in LNCaP cells. A. Lysates from three independent siRNA transfection reactions were separated by SDS-PAGE, and protein expression was assessed by western blotting. B. DHX9 expression in siRNA-transfected cells were normalised to the β-actin loading control, then to the siNon-Targeting control. Statistical significance was determined using a One-Way Anova. p**=0.0046 and p**=0.0004 C. GAPDH expression in siRNA-transfected cells were normalised to β-actin loading control, then to the siNon-Targeting control. Statistical significance was determined using a One-Way Anova.

Transfection of LNCaP with siRNA directly targeting DHX9 expression led to a visible reduction in protein expression as shown in Figure 5.4 A. When probed for DHX9 (Figure 5.4 A top membrane) DHX9 expression is visibly significantly reduced. When quantified and normalised to cells treated with non-targeting siRNA, DHX9 expression was shown to be statistically significantly reduced by approximately 75%. Although not significant, transfection with siRNA targeting GAPDH led to a 25% reduction in expression when compared to cells treated with non-targeting siRNA. Interestingly, treatment of LNCaP with siGAPDH increased the expression of DHX9 (Figure 5.4 A and C). GAPDH is widely used as a housekeeping gene. These genes are essential endogenous regulatory genes that are involved in various processes in the cell, such as metabolism, transcription, and homeostasis. The expression levels of references genes should remain constant between the cells of different tissues and under different experimental conditions in order to normalise the expression of the gene or protein of interest (Zainuddin *et al.*, 2010). Previous work by Phadke et al (2009) has shown that reduction of GAPDH protein in A549 human carcinoma cell lines arrested cell proliferation, and cells with reduced expressions of GAPDH accumulated in the G_0/G_1 phase of the cell cycle (Phadke *et al.*, 2009). DHX9 expression may have increased during this experiment due to the accumulation of cells in the G_0/G_1 phase. Work by Thacker et al (2020) has shown that DHX9 expression is required for the efficient progression of cells from G_1 to S phase of the cell cycle (Thacker *et al.*, 2020). Knockdown of GAPDH may have led to the increase in DHX9 expression due to its role in cell cycle progression. Using the information gained from figure 5.4, I can confidently say that the siDHX9 directly affects expression of the DHX9 protein (Figure 5.4 C). This siRNA was then used in a proliferation assay to investigate how the reduced expression of DHX9 affects LNCaP growth (Figure 5.5).

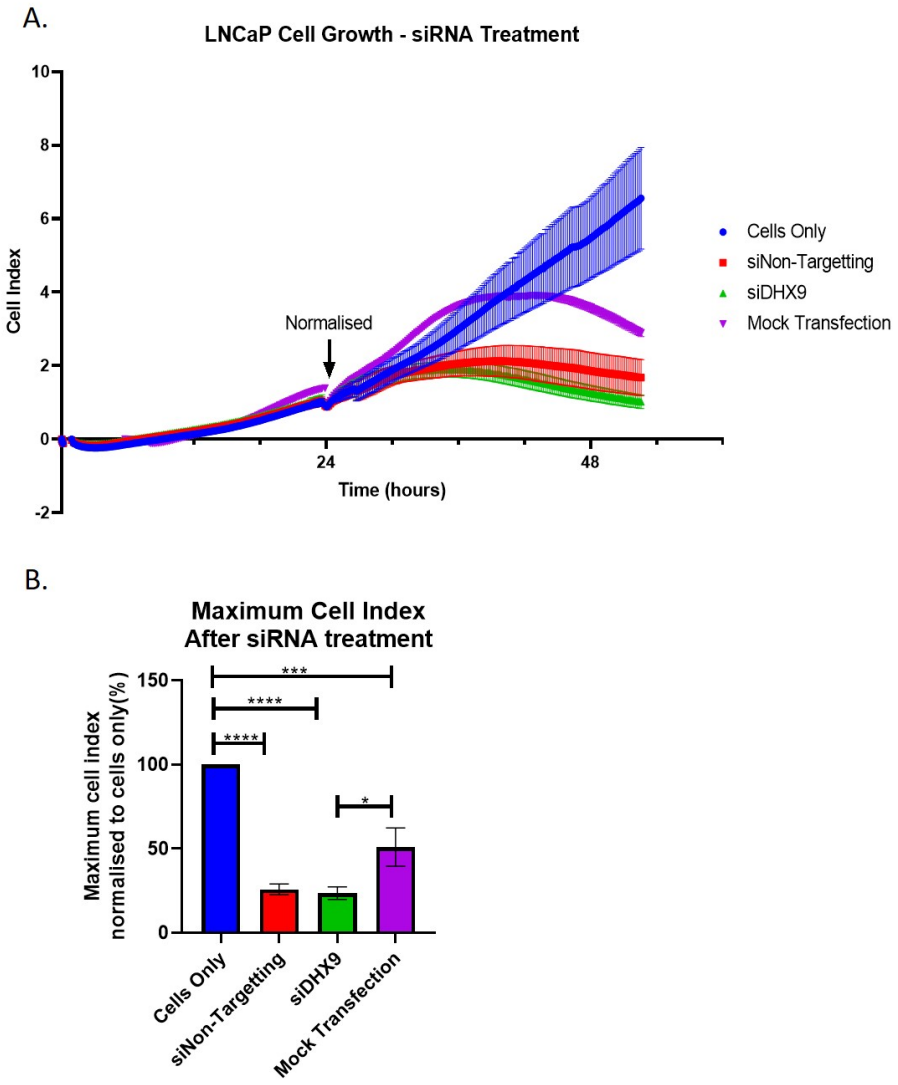

Figure 5.5 **siRNA-mediated knockdown of DHX9 in LNCaP cells.** A. xCELLigence technology was used to measure the proliferation of LNCaP cells transfected with siRNA against DHX9, Non-targeting, and mock transfection. The cell index was normalised at the time of siRNA transfection. Growth curves are represented as the mean ± SEM of three independent experiments. B. The maximum cell index for each growth curve was identified and presented as the mean ± SEM of three independent experiments. The maximum cell index was normalised to the cells only condition and statistical significance was calculated using a One-Way Anova, where p***=0.0006 and p****<0.001

Although I was able to achieve approximately 75% knockdown in DHX9 expression (Figure 5.4 B), siRNA treatment in this cell line led to an overall decrease in cellular growth. Treatment with the siRNA transfection reagent alone lead to a 50% decrease in cell growth, which was shown to be very significant when compared to the cells only condition (Figure 5.5 B purple bar). When the cells were treated with both non-targeting and DHX9 specific siRNA, this led to very significant decrease in cell growth when compared to the cells-only condition (Figure 5.5 B red and green bars). In addition, there was no significant difference in growth between these two conditions, indicating that this

reduction in cell growth is due to the treatment rather than the decreased expression of DHX9. Although the initial data from the DuCaP growth assay indicated that the decreased expression of DHX9 leads to a significant decrease in cellular proliferation, this observation cannot be made in LNCaP despite showing that the same siRNA can reduce DHX9 expression by western blot (Figure 5.4 B).

5.3.2 YK-4-279 inhibition of DHX9 leads to a decrease in PC cell proliferation

Many cancers, such as PC, carry non-random chromosomal translocations encoding tumour-specific fusion transcription factors that are essential for disease progression. Ewing's Sarcoma family tumours (ESFTs) express the EWS-FL1 fusion protein, which is known to interact with DHX9. This binding is important for oncogenic function of DHX9 in ESFT cells, and disruption of this interaction using the small molecule YK-4-279 induces apoptosis (Erkizan *et al.*, 2009). Disruption of PPI using small molecule inhibitors is a rapidly evolving field (Bhalla *et al.*, 2006) and disruption of the interactions of DHX9 with its interacting partners using disruptor peptides leads to a decrease in cell growth as demonstrated by Erzikan et al. (2009). YK-4-279 was initially identified from a library of over 3000 compounds after showing that it significantly reduced the interaction between the C-terminal end of DHX9 and EWS-FL1 without affecting expression levels of either protein. These authors also further showed that treatment of mouse ESFT xenograft models with 1.5 mg of YK-4-279 significantly reduced tumour growth when compared to PC3 prostate tumour xenografts that does no express EWS-FL1 protein. When tumours from DMSO- and YK-4-279-treated mice were stained for caspase-3 by immunohistochemistry, tumours from YK-4-279 mice had a threefold increase in caspase-3 staining when compared to control mice. Not only did YK-4-279 inhibit tumour growth, but it also increased apoptosis in this xenograft model (Erkizan *et al.*, 2009). Interestingly, this small molecule inhibitor is gaining the interest of PC researchers due to the fact that 40-70% of PC tumours have been shown to have gene rearrangements involving ETS transcription factors, with the most common of them being the *TMPRSS2-ERG* gene fusion (Rubin, 2012). Previous work by Rahim et al (2011) showed that growth of YK-4-279-treated LNCaP and VCaP PC cells was significantly reduced when compared with non-treated cells.

Furthermore, treatment with YK-4-279 reduced the invasive nature of LNCaP in a scratch assay (Rahim *et al.*, 2011). In order to confirm this, further xCELLigence studies were carried out with this DHX9-specific inhibitor. 5 000 LNCaP cells were plated in each well of the 96 E-plate and left to grow overnight. The cells were then treated with YK-4-279 over a range of concentrations to establish a dose response curve and determine an IC_{50} for LNCaP growth.

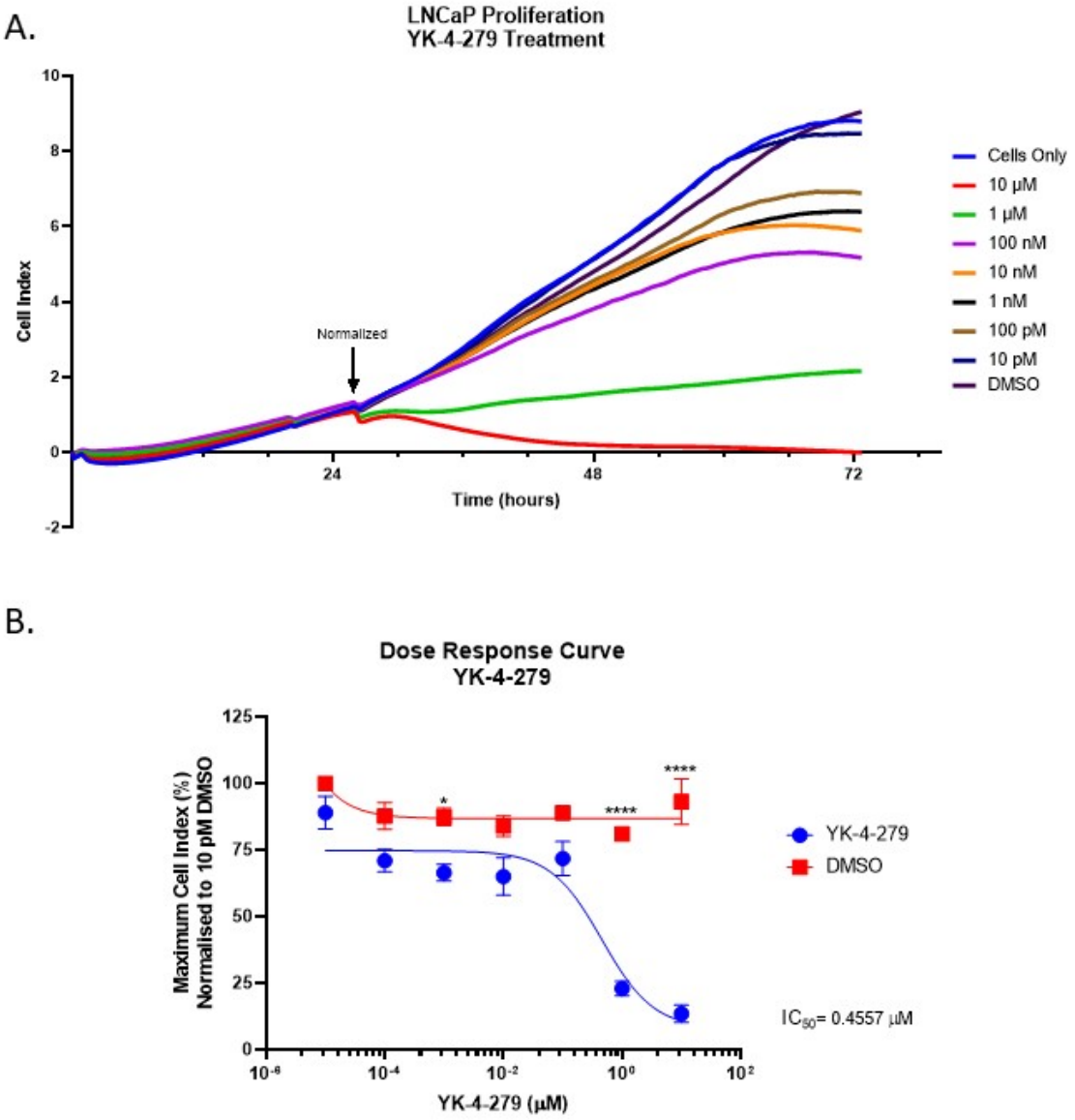

Figure 5.6 Growth of LNCaP cells following treatment with YK-4-279. A. xCELLigence technology was used to monitor the growth of LNCaP cells over the course of three days. Cells were treated with YK-4-279 at the indicated concentrations after 24 hours, and all growth curves were normalised to growth at this point. Growth curves are represented as means of four independent experiments. B. The maximum cell index was plotted as a dose response curve, and the IC50 was calculated using a non-linear regression. Data is presented as the mean ± SEM from four independent experiments.

YK-4-279 significantly reduced LNCaP cell growth at 10 µM and 1 µM after normalization when compared to the cells-only and DMSO controls (Figure 5.6 A). Interestingly, as the cells were exposed to lower concentrations of YK-4-279, the growth curve can be seen to increase up to basal levels in a dose-dependent manner (Figure 5.6 A). At 10 µM and 1 µM, we can assume that the treatment with YK-4-279 lead to the activation of caspase-3 as previously reported (Erkizan *et al.*, 2009). The maximum cell index for each growth curve was identified and plotted as a dose response curve in order to calculate the IC_{50} of YK-4-279 in this cell line. Using log (inhibitor) vs response model on GraphPad Prism, a non-linear

regression was plotted in order to determine the concentration at which a response halfway between the maximum response and the maximally-inhibited response. The IC_{50} of YK-4-279 was found to be 0.46 μM in LNCaP cells (Figure 5.6 B). Previous work by Sun et al (2017) showed that the IC_{50} of YK-4-279 in different neuroblastoma cells lines ranged from 0.218 μM to 2.255 μM (Sun *et al.*, 2017). VCaP cells, although they are known to harbour the *ERG* gene rearrangement, has been shown to have an IC_{50} of 16 μM (M. S. Butler *et al.*, 2017). Such large differences in YK-4-279 can be explained by the difference in cell doubling time. LNCaP are known to have a doubling time of 28-60 hours, compared to 5-6 days for VCaPs (Cunningham and You, 2015). IC_{50} values are thought to decrease with increasing numbers of cell doublings during the incubation period (Baguley, Hicks and Wilson, 2002). Within the same day, LNCaP can go through more cell doublings than VCaPs, indicating that lower concentrations of YK-4-279 are required to inhibit growth.

So far, I have been able to show that LNCaP growth is significantly affected by YK-4-279. We then investigated if growth of the AI cell line DU145 was affected by YK-4-279 . Previous work in our lab had determined that 10 000 cells per well is the most appropriate cell density for this cell line for xCELLigence experiments (Byrne, 2014). DU145 cells were seeded at the previously mentioned cell density and left to grow overnight. They were then treated with either 10 μM or1 μM of YK-4-279 or with DMSO vehicle control (Figure 5.7).

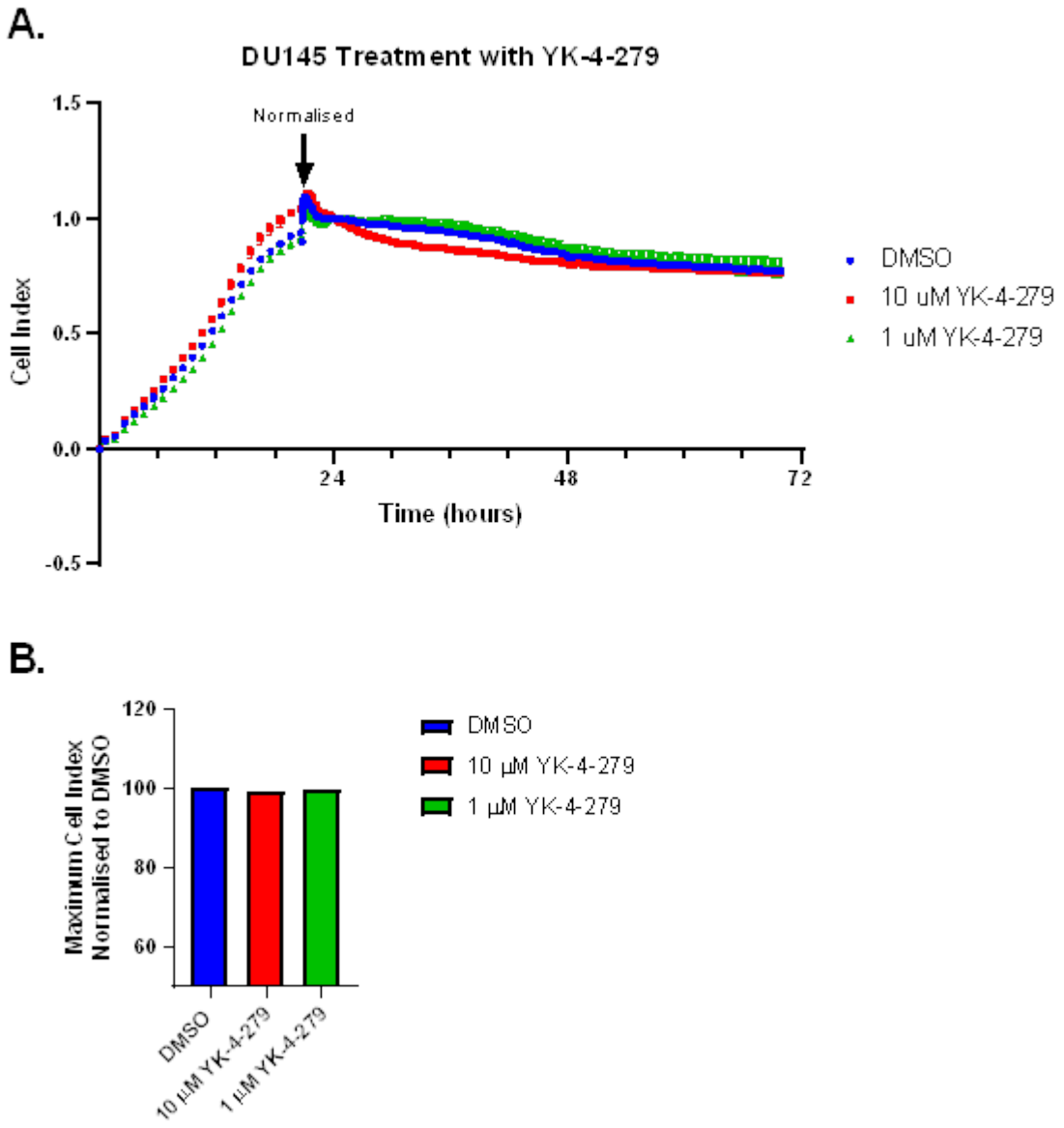

Figure 5.7 Treatment of DU145 cells with YK-4-279. A. xCELLigence technology was used to monitor the response of DU145 to YK-4-279. Cells were treated with either 10 µM or 1 µM of YK-4-279 24 hours after seeding and this was the point to which the growth curves were normalised to. B. The maximum cell index of each growth curve was measured, then normalised to the DMSO vehicle control. Data presented is N=1.

Unlike LNCaP cells, DU145 cells remained unaffected by the inhibitor. YK-4-279 did not significantly decrease the proliferation of DU145 cells at either of the concentrations used (Figure 5.7). DU145 is an AI cell line that is most commonly used as a model for aggressive PC. However, this cell line does not naturally express ETS fusion protein (Swanson *et al.*, 2011), explaining why this cell line remained unresponsive to the inhibitor. The data presented so far indicates that YK-4-279 is only able to target cells that express ETS fusion proteins that can bind to DHX9. Interruption of this DHX9-ETS interaction leads to an activation in

caspase-3 activity (Erkizan *et al.*, 2009), which in turn leads to a significant decrease in cell growth (Figure 5.6).

5.3.3 Disruption of the PDE4D7-DHX9 complex has no effect on cell proliferation

My data has so far shown that disruption of the interaction between DHX9 and EWS-FL1 protein significantly reduces cell growth. Not only did this indicate that DHX9 is important for cell growth but also showed that by disrupting of the interaction between DHX9 and its partners negatively impacts growth. With this in mind, I then investigated if disruption of PDE4D7 and DHX9 complex in PC cells has similar effects as YK-4-279. The same proliferation assay as used in Figure 5.7 was repeated with our newly designed disruptor peptides previously described in chapter 3. These peptides were designed to recognise the binding sites between DHX9 and PDE4D7 from peptide array data. The UCR1 disruptor peptide inhibits DHX9 binding to PDE4D7, whereas the DHX9 disruptor peptide inhibits PDE4D7 binding to DHX9 (Figure 3.20). The cell-permeable disruptor peptide was shown to be effective in pull-down and PLA imaging assays (Figure 3.21, Figure 3.22, and Figure 3.23). Therefore, I carried out these experiments to determine if disruption of this interaction by our newly synthesised peptides affected cell growth. 5000 LNCaP cells were seeded into each well of 96 well E-Plate, and the cells were left to grow for 24 hours. The cells were then treated with DMSO, scrambled peptide, or our disruptor peptides (UCR1 or DHX9 peptides), after which growth was monitored for 2 days (Figure 5.8).

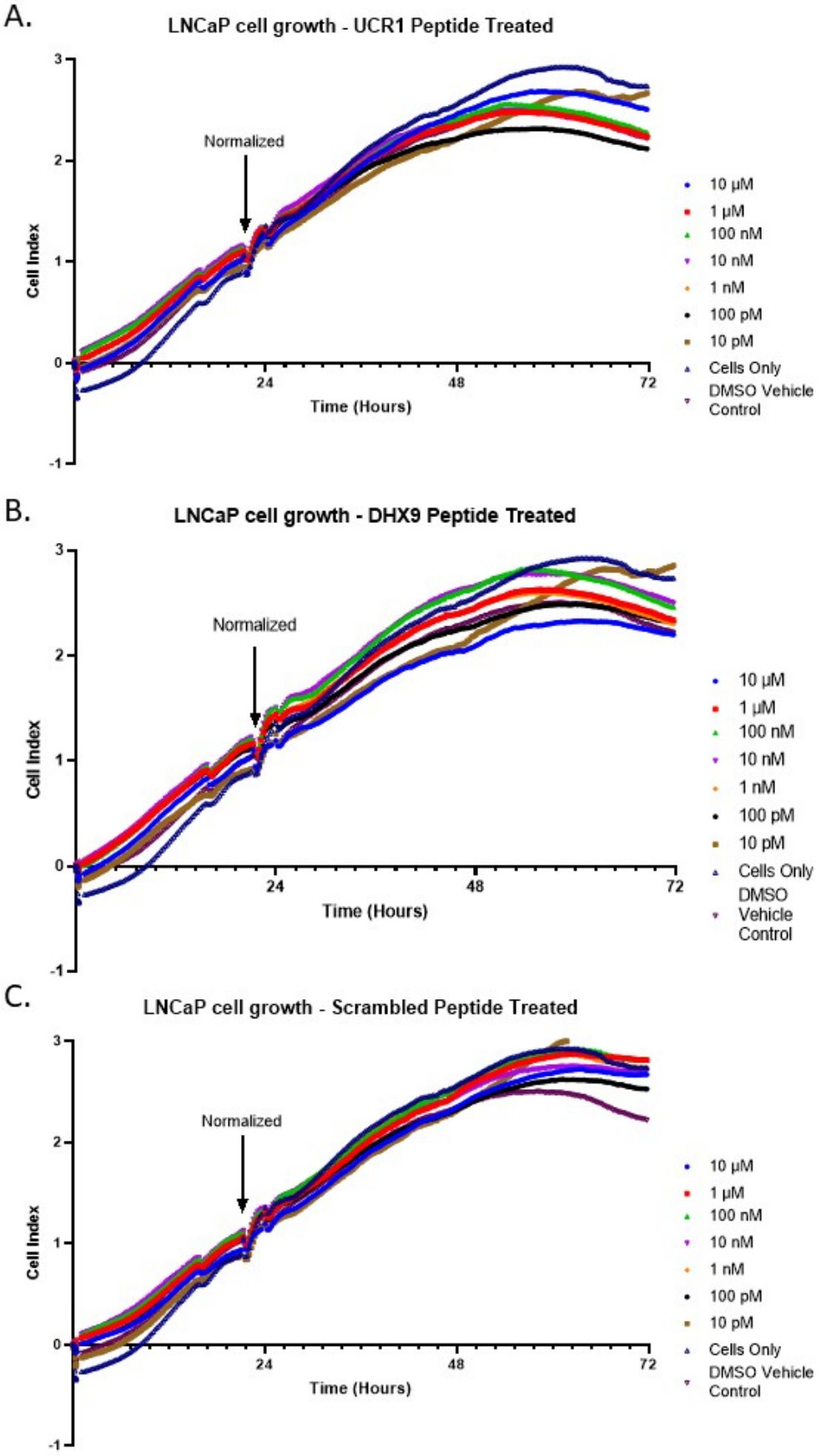

Figure 5.8 Growth of LNCaP cells following treatment with disruptor peptides. A. Cells were treated with UCR1 disruptor peptide at concentrations ranging from 10uM to 10pM. B. Cells were treated with DHX9 disruptor peptide at the same concentration as in A. C. Cells were treated with scrambled peptide at the same concentrations as in A. All data is representative of N=4 and were normalised to the point of treatment.

During the first 21 hours of the experiment, the CI of all the different conditions was shown to rapidly increase as the cells settled and adhered to the bottom of the well (Figure 5.8 A-C). After the cells were treated with the different peptides, all cells continued to grow as shown by the steady increase in CI over the 2 days of the experiment (Figure 5.8 A-C). However, a small dip in the CI can be seen between the time of treatment and 26 hours. In order to investigate whether there was a dose-response effect in the growth curves, the growth between the 20 and 26 hours was plotted for further analysis. (Figure 5.9).

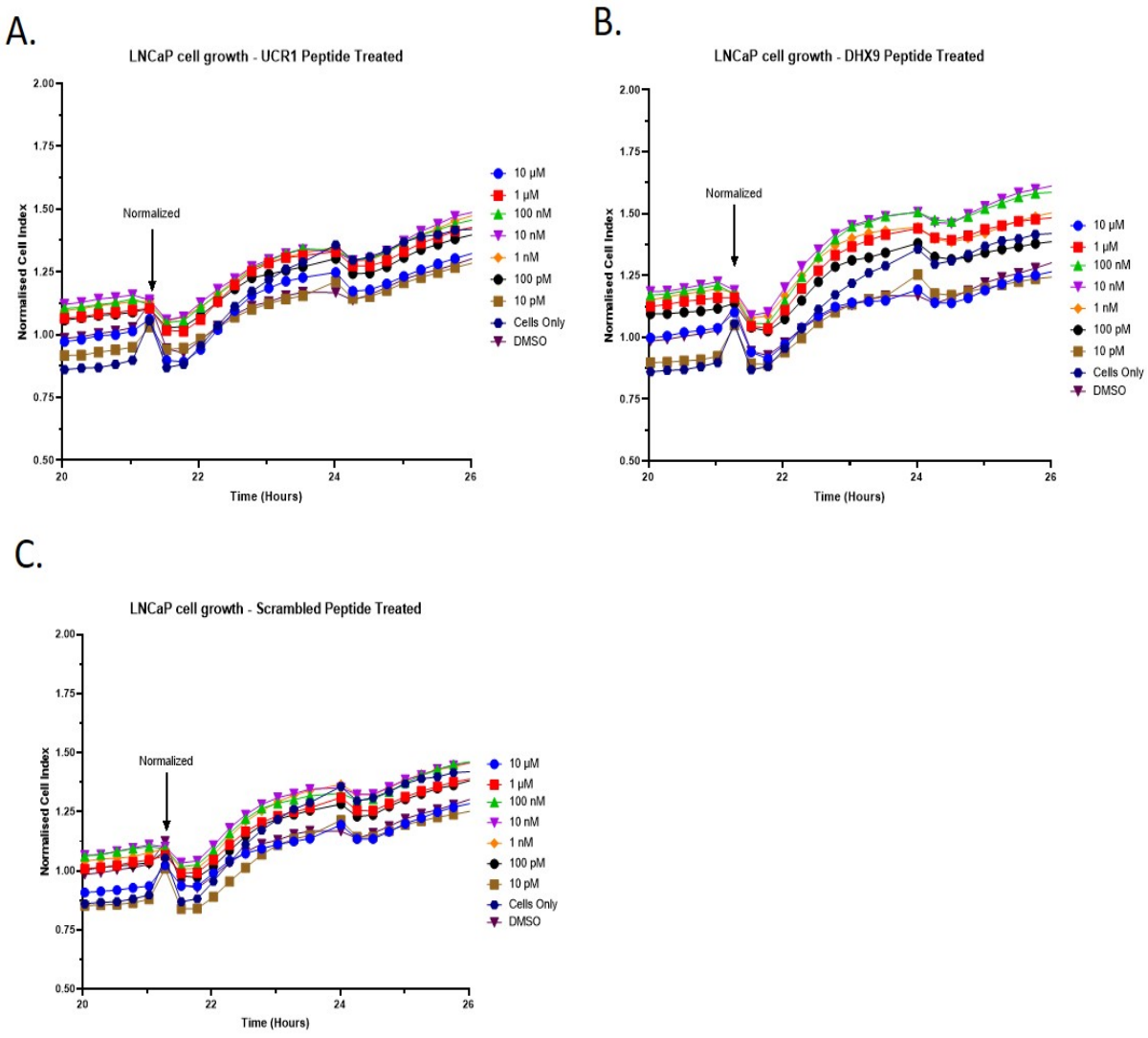

Figure 5.9 LNCaP growth between 20 and 26 hours. A. Cells were treated with UCR1 disruptor peptide. B. Cells were treated with DHX9 disruptor peptide. C. Cells were treated with scrambled peptide. All data is representative of N=4 and were normalised to the point of treatment.

Interestingly, cell growth can be seen to be briefly interrupted after the addition of the UCR1 and DHX9 disruptor peptides. During the first two hours of peptide incubation, all growth curves can be seen to decrease (Figure 5.9). Unfortunately, this decrease was not shown to be statistically different between

our two disruptor peptides and the scrambled peptide control, indicating that this effect may not be due to the disruption between PDE4D7 and DHX9 (Figure 5.9). Furthermore, unlike with YK-4-279, treatment with our disruptor peptide did not lead to any significant decrease in cell growth when looking at the traces over the two-day peptide incubation. Instead, LNCaP cells can be seen to continue to grow after the 26 hour time point in all peptide treatments (Figure 5.8 and Figure 5.9). Unfortunately, the disruption of the interaction between PDE4D7 and DHX9 does not affect long-term PC cell growth. This interaction, unlike the DHX9-EWS-FL1 interaction, may not be essential for cell growth and our disruptor peptides may not be a viable tool to slow disease progression. In order to evaluate the effects of peptides at early timepoints, the normalised cell index at the 24 hour “peak” was measured and normalised to the DMSO vehicle control (Figure 5.10).

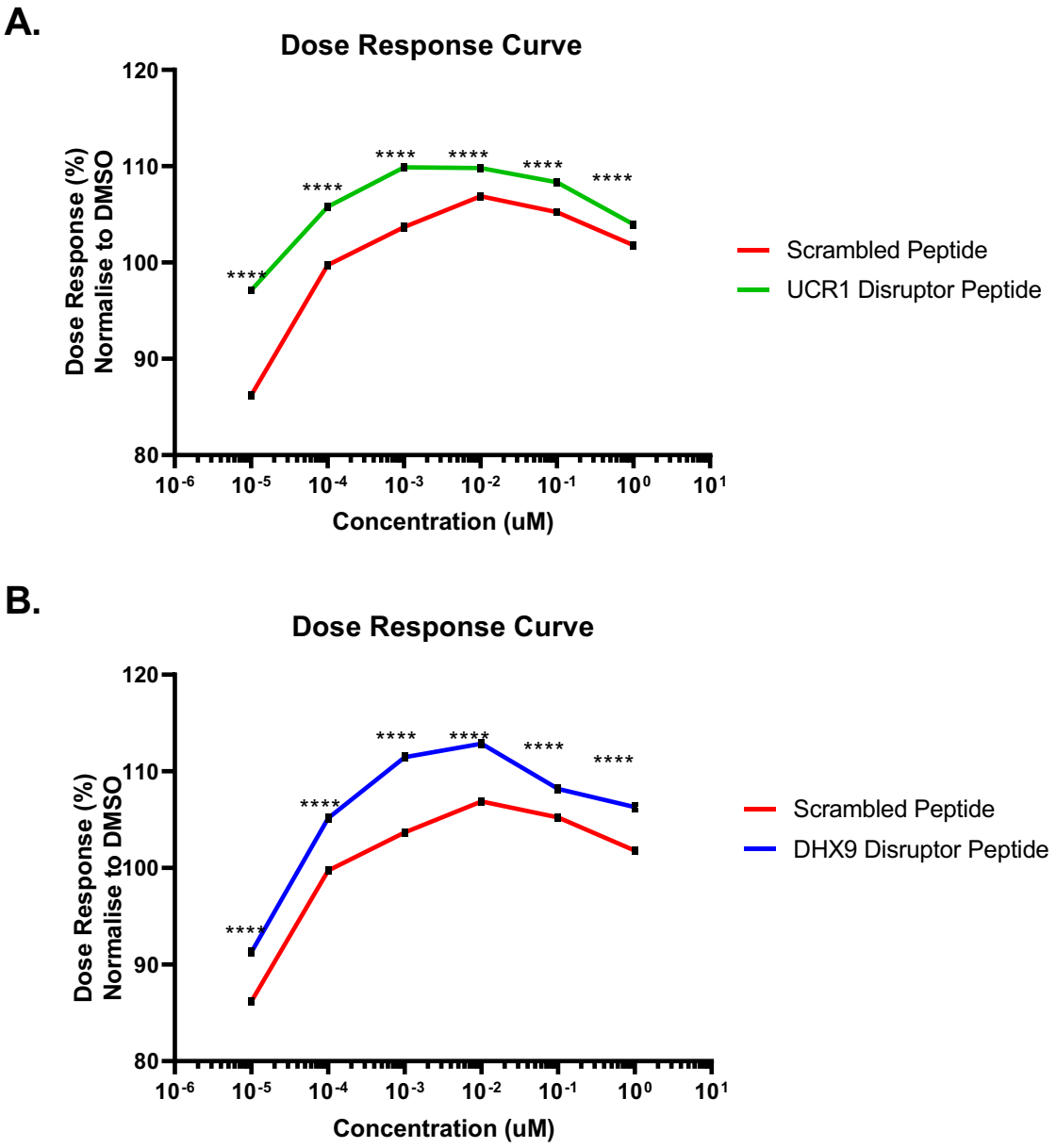

Figure 5.10 Dose response of UCR1 and DHX9 disruptor peptides at the 24-hour peak. A+B. The cell index of LNCaP at the 24 hour peak was measured and compared to the scrambled peptide. The data presented here is the mean ± SEM of four independent experiments. Cell index of all points was normalised to the DMSO vehicle control-treated cells. Statistical significance was determined using a Two-Way Anova with multiple comparisons, where p****>0.0001.

Unlike YK-4-279, both newly designed disruptor peptide significantly increased cell growth during the first two hours of treatment when compared to the scrambled peptide control (Figure 5.10). However, the cells were able to recover from peptide treatment as reflected by the increase in all growth curves after two hours of peptide treatment (Figure 5.8 and 5.10). In order to consider these peptides as “proof of concept” novel therapeutics, any changes in cell growth must be observed over a longer period of time. The ideal scenario in cancer drug development is to kill all tumour cells, while leaving the healthy

cells intact so that the patients survive treatment (Eastman, 2017). Additionally, measuring the potency of small molecule drugs is a critical step in the development of novel therapeutic agents (Niepel *et al.*, 2017). Unfortunately, the disruptor peptide developed in this thesis did not have any long-term effects on the growth of PC cells. Although an initial decrease in growth can be observed during the first two hours of treatment, the cells eventually were able to overcome this and continue to grow over the three days of this experiment (Figure 5.8). Although I have shown that our disruptor peptides are able to disassemble the PDE4D7-DHX9 complex in an IP and PLA (Figure 3.21, Figure 3.22,Figure 3.23), this does not lead to any changes in LNCaP cells growth. However, this assay does provide us with a platform to test other therapeutic agents that could potentially lead to a decrease in PC cell growth.

5.3.4 Disruption of PDE4D7-DHX9 complex alters DHX9 activity

The data in this thesis so far has shown that disruption of the PDE4D7-DHX9 complex only leads to a short-term decrease in cell growth during the first two hours of peptide treatment. Although promising, this did not lead to any long-term changes in LNCaP cell growth. However, I was interested to see if the disruption of this interaction could affect DHX9's helicase activity. Previous peptide array data showed that PDE4D7 binds within the helicase domain of DHX9 (Figure 3.16), suggesting that it may play a role in regulating its activity. Recent work by Chakraborty et al (2018) has shown that DHX9 activity can be studied by looking at levels of specific DNA-RNA hybrids known as R-loops. R-loops are three-stranded nucleic acid structures that include an RNA strand hybridized with the DNA template, leaving the non-template DNA single stranded (Figure 1.14). These structures occur naturally during transcription, however the prolonged formation of these structures can have deleterious effects on genome integrity (Skourti-Stathaki and Proudfoot, 2014). DHX9 has recently been shown to promote the formation of R-loops in cells that are deficient for the Splicing Factor Proline and Glutamine rich (SFPQ). In the absence of SFPQ, there is a prolonged interaction between DHX9 and RNA polymerase II (RNA pol II) leading to increased production of R-loops (Chakraborty, Huang and Hiom, 2018). In order to investigate if the activity of DHX9 is affected by dissociation from PDE4D7, the same R-Loop assay was repeated. In order to ensure that SFPQ

could be successfully knocked down in LNCaP cells, SFPQ protein expression was first assessed by western blotting after siRNA treatment (Figure 5.11).

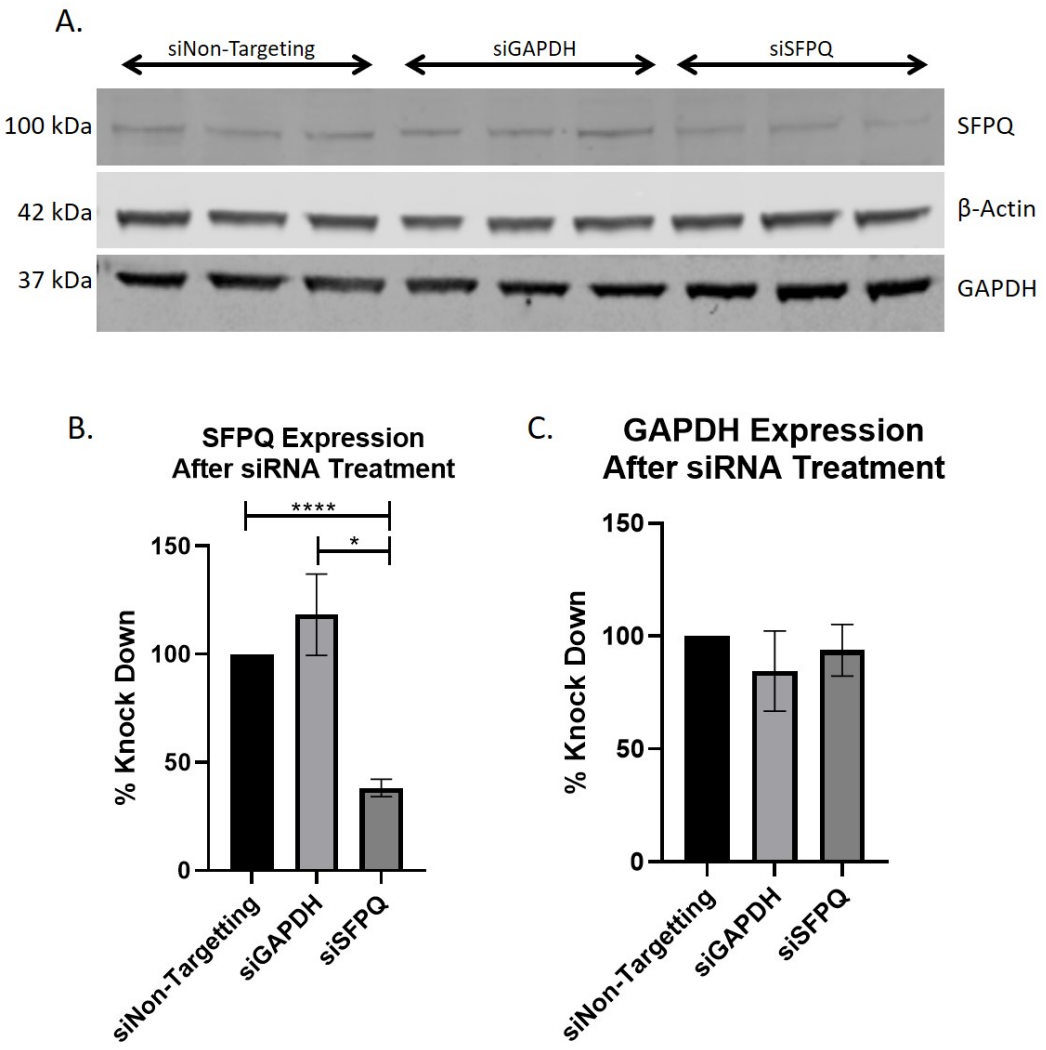

Figure 5.11 LNCaP siSFPQ treatment efficiency. A. SFPQ protein expression was assessed by SDS-PAGE with western blotting. B. SFPQ expression was normalised to β-actin loading control. Percentage knockdown was then determined by normalising protein expression to cells treated with non-targeting siRNA. Data is presented as the mean ± SEM of three independent experiments. C. GAPDH expression was normalised to β-actin loading control. Percentage knockdown was then determined by normalising protein expression to cells treated with non-targeting siRNA. Data is presented as the mean ± SEM of three independent experiments. Statistical significance was determined using a One-Way Anova, where p*>0.01 and p****>0.00001.

Transfection with siRNA targeting SFPQ expression led to a visible decrease in protein expression (Figure 5.11 A top membrane). When quantified and normalised to the loading control, SFPQ expression was significantly reduced by approximately 60% when compared to the non-targeting siRNA control (Figure 5.11 B). Although GAPDH expression did not seem to be visible decreased (Figure 5.11 last membrane), its expression was reduced by 15% when compared to the non-targeting siRNA control (Figure 5.11 C). As siRNA against SFPQ was so

efficient, I can then attribute any changes in R-loops formation to the reduction of expression of this specific splicing factor. LNCaPs were plated onto sterile glass coverslips and treated with siRNA against SFPQ alone, or in combination with siRNA against PDE4D7. siRNA PDE4D7 was previously designed by Dr Ashleigh Byrne and shown to significantly decrease its expression in PC cell lines (Byrne, 2014). The cells treated with siSFPQ alone were then treated with either UCR1 or DHX9 disruptor peptide, the scrambled control peptide, or DMSO vehicle control. Following fixing and blocking of the coverslips, the cells were stained for nucleolin and for DNA-RNA hybrids using the S9.6 antibody overnight. In recent years, the monoclonal S9.6 antibody has been used to purify, analyse and quantify R-loop structures in cells (König, Schubert and Längst, 2017). After counter staining with the appropriate secondary antibodies, the coverslips were mounted cell side down and imaged using a confocal microscope (Figure 5.12 and Figure 5.12).

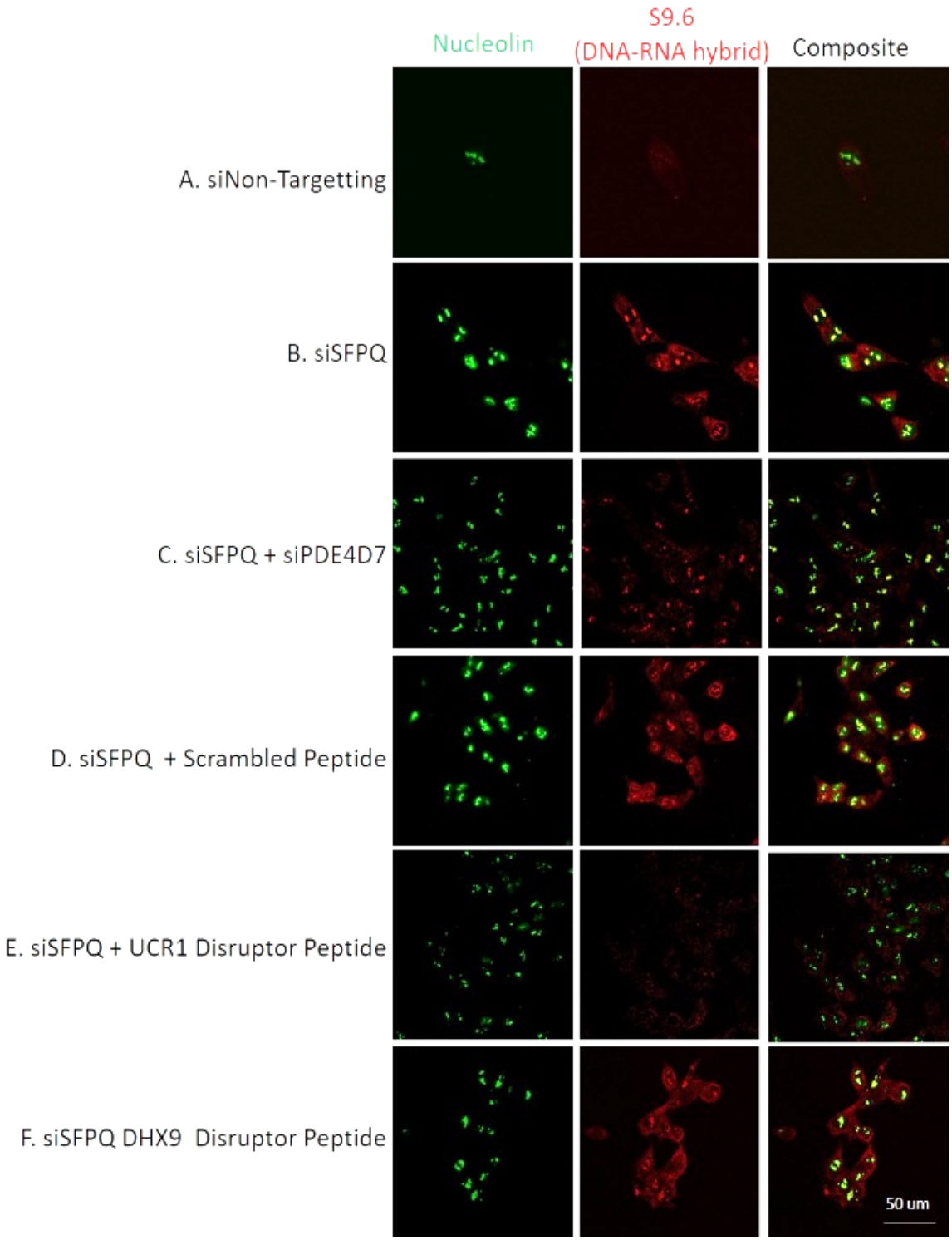

Figure 5.12 Staining for R-loops in LNCaP cells following treatment with siRNA and disruptor peptide. Representative images showing immunostaining for R-loops using the S96 antibody (red) and nucleolin (green). LNCaP were transfected with siNon-targeting (A) or siSFPQ (B) as indicated. Certain cells were also transfected with siPDE4D7 (C), or treated with scrambled peptide (D), or disruptor peptide (E+F). S9.6 staining from 30 different individual cells were measured as described in Figure 5.13. This work was performed in collaboration with Prof Kevin Hiom, University of Dundee.

In order to measure the levels of R-loops formed directly due to DHX9 helicase activity, the S9.6 staining from the regions stained with anti-nucleolin was subtracted from the S9.6 staining in the nucleus, as described in Figure 5.13.

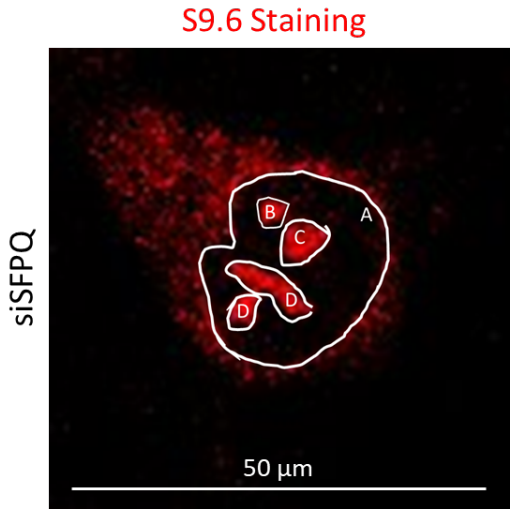

Figure 5.13 Determining R-loop staining in the nucleus following siRNA and peptide treatment. In order to determine if there were any changes in formation of R-loops due to siRNA transfection or peptide treatment, the mean fluorescence intensity (MFI) of the nucleolin regions (B-D) was subtracted from the total nuclear S9.6 staining (A). All data acquisition was performed on Image J and analysed using GrahphPad Prism 8.

S9.6 staining from at least 30 individual cells was measured from each condition. The mean S9.6 staining was then plotted, and any statistical difference in staining was determined using a One-Way Anova with multiple comparisons (Figure 5.14).

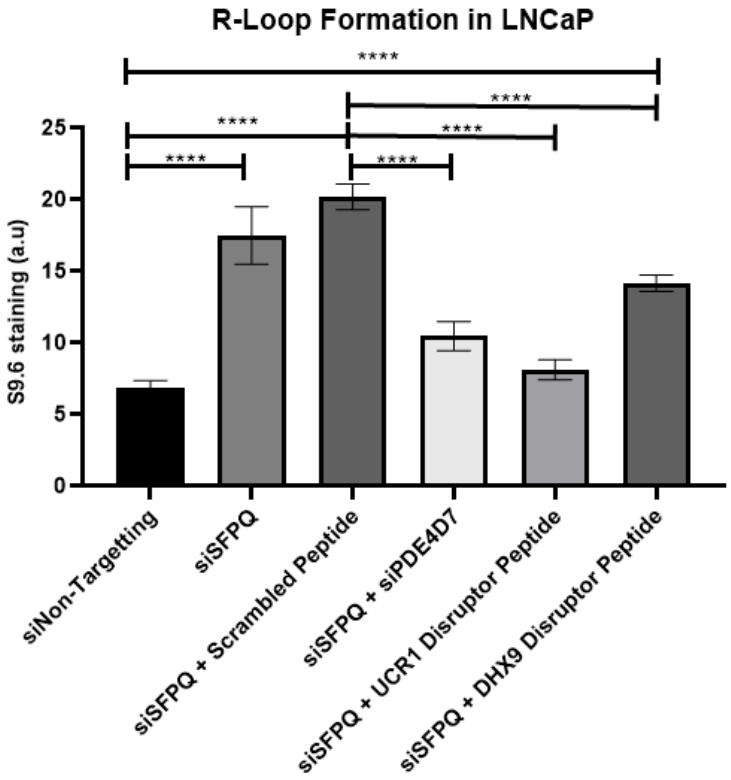

Figure 5.14 Quantification of R-loop staining following siRNA and peptide treatment. R-loop staining in LNCaP cells following siRNA and disruptor peptide. Data is presented as the mean ± SEM of at least 30 individual cells per treatment. Statistical significance was determined using a One-Way Anova with multiple comparisons where p****>0.0001. This work was performed in collaboration with Prof Kevin Hiom, University of Dundee.

When LNCaPs were treated with non-targeting siRNA, R-loop staining is low as splicing factors are still able to bind to nascent RNA structures, physically preventing R-loop formation (Figure 5.12 A and Figure 5.14). R-loop formation is normally protected by splicing factors which coat the nascent mRNA, which in turn allows for normal transcription to take place (Crossley, Bocek and Cimprich, 2019). However, when treated with siSFPQ alone and siSFPQ with scrambled peptide, S9.6 staining in these cells increased significantly by three-fold and four-fold respectively (Figure 5.12 B+D and Figure 5.14). However, when LNCaP cells were treated with siSFPQ and the UCR1 disruptor peptide, this led to a significant decrease in R-loop detection when compared to the scrambled peptide control. Interestingly, levels of R-loops detected in these cells were not significantly different from those in cells treated with non-targeting siRNA, indicating that R-loop formation had returned to normal levels (Figure 5.12 E and 5.14). This same response was seen in cells transfected with siFPQ and siPDE4D7 (Figures 5.12 C and 5.14). My results suggest that the interaction between DHX9 and PDE4D7 is required for DHX9 to unwind nascent RNA structures within the nucleus. Loss of this interaction leaves DHX9 unable to

unwind nascent RNA structures, leading to a decrease in R-loop formation and detection. Interestingly treatment with siSFPQ and our DHX9 disruptor peptide also led to a significant decrease in R-loop detection when compared to the scrambled peptide treated cells (Figure 5.12 F and 5.14). However, there was still a two-fold increase in R-loops when compared to the non-targeting siRNA treated control. Although my DHX9 disruptor peptide was able to lower R-loop formation, it is possible that not all DHX9-PDE4D7 complexes were disrupted within the nucleus. This could lead to continued DHX9 helicase activity and R-loop formation. The data presented here suggests that disruption of the interaction between PDE4D7 and DHX9 using our cell penetrating peptides inhibits DHX9's ability to promote R-loop formation.

5.3.5 Decreased expression of DHX9 leads to changes of downstream signalling pathways.

Although DHX9 is known to be involved in multiple signalling pathways, such as the p53 pathway (Lee and Pelletier, 2017), little is known about how changes in DHX9 protein expression can alter different downstream signalling pathways. Reverse phase protein array (RPPA) is a high throughput antibody-based proteomic technique which enables the concomitant quantification of multiple proteins and post-translational modifications of these proteins in multiple samples. Proteins extracted from cultured cells are denatured by SDS treatment and spotted onto nitrocellulose-coated glass slides. Using over 60 highly validated antibodies (Figure 5.16), these slides can measure changes in levels of total or post translationally modified proteins from the whole proteome available in the cell lysate (Creighton and Huang, 2015; Macleod, Serrels and Carragher, 2017). In this instance, RPPA was used to investigate how the decreased expression of DHX9 can affect linked signalling cascades by looking at the total levels and phosphorylation state of signalling intermediates. In this way, novel roles for DHX9 can be identified in PC cells. AI cells (DU145) were treated with siRNA against DHX9, GAPDH, or non-targeting control. Protein expression was assessed by SDS-PAGE with western blotting in order to ensure decreased protein expression (Figure 5.15). DU145 cells were used for this experiment as they had the highest endogenous level of DHX9 expression out of the three PC cell lines used in this thesis (Figure 3.1).

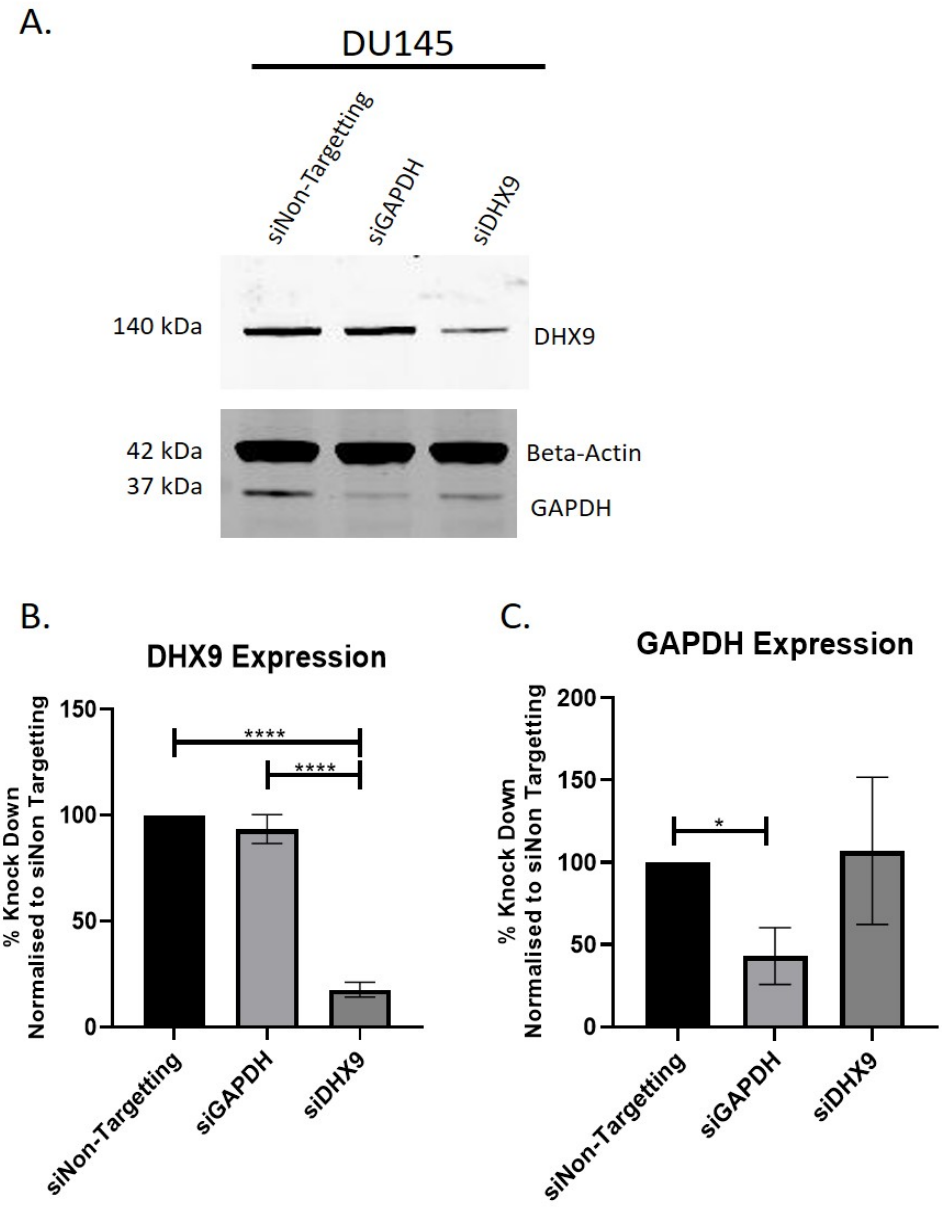

Figure 5.15 DHX9 expression in DU145 for RPPA analysis. A. DHX9 protein expression was assessed by SDS-PAGE with western blotting. B. DHX9 expression was normalised to β-actin loading control. Percentage knockdown was then determined by normalising protein expression to cells treated with non-targeting siRNA. Data is presented as the mean ± SEM of three independent experiments. C. GAPDH expression was normalised to β-actin loading control. Percentage knockdown was then determined by normalising protein expression to cells treated with non-targeting siRNA. Data is presented as the mean ± SEM of three independent experiments. Statistical significance was determined using a One-Way Anova, where p*>0.01 and p****>0.00001.

When treated with siDHX9, this led to a visible decrease in DHX9 expression by western blotting (Figure 5.15 A, top membrane). When quantified and normalised against the non-targeting siRNA control, DHX9 expression was significantly decreased when transfected with siDHX9 (Figure 5.15 B). Furthermore, western blotting and densitometry analysis showed that GAPDH expression was significantly decreased after siRNA transfection (Figure 5.15 A, bottom membrane, and Figure 5.15 C). Knowing that DHX9 expression is

significantly decreased when treated with siDHX9, this sample, as well as the lysate treated with non-targeting siRNA, were sent to the Edinburgh Cancer Research Centre for RPPA analysis. Spot and initial data analysis was performed by Kenneth Macleod at the University of Edinburgh (Figure 5.16).

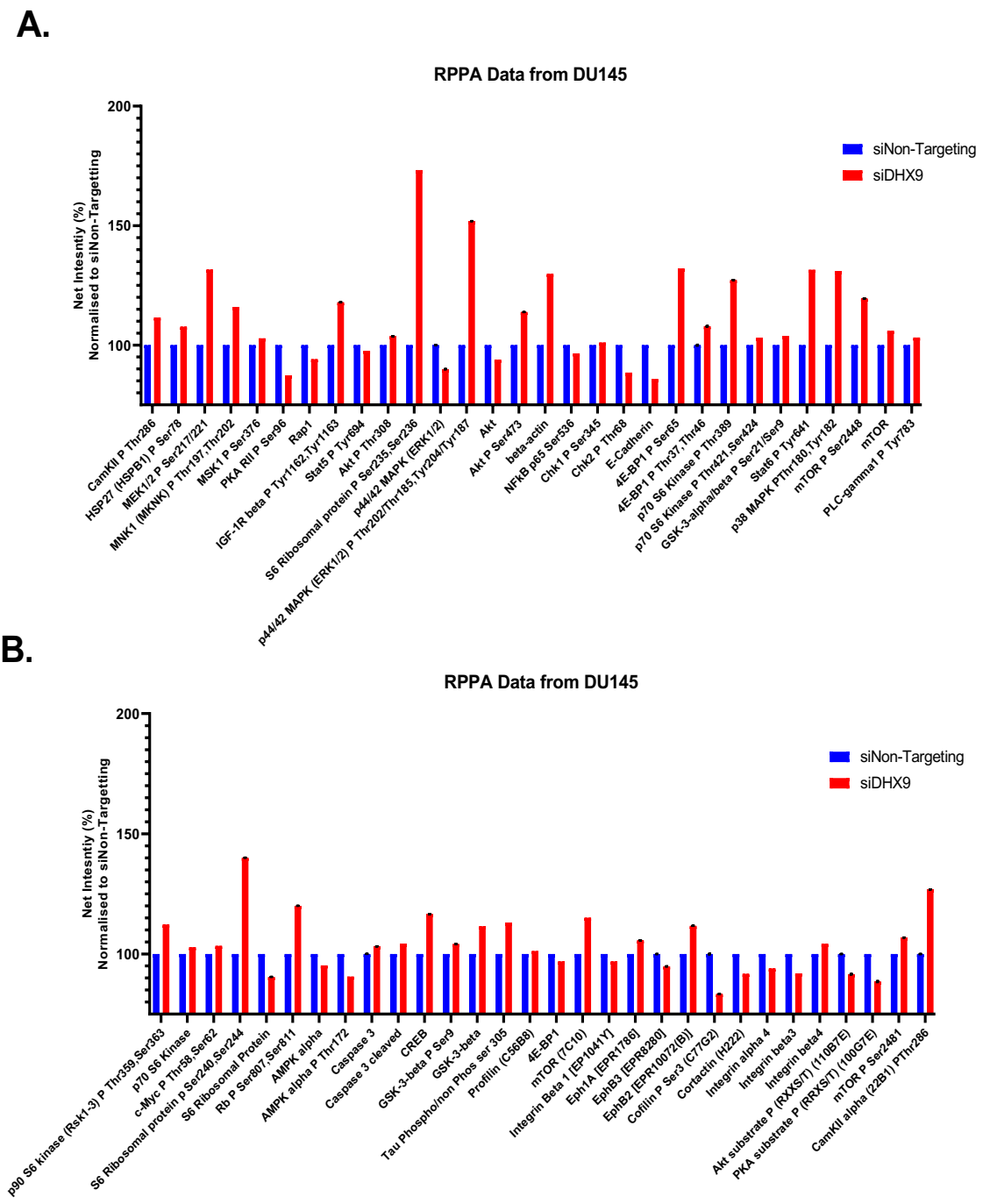

Figure 5.16 **RPPA data from DU145 cells treated with siNon-target or siDHX9.** A+B. Over 60 antibodies were tested. Arrays were scanned using a slide scanner and adjusted for maximal signal in order to avoid saturation. This data was generated by Kenneth Macleod at the University of Edinburgh.

Interestingly, the RPPA analysis revealed that the Mitogen-Activated Protein Kinase (MAPK) pathway (Figure 5.16 A) and the mTOR pathway (Figure 5.16 A and B) were altered after DHX9 knockdown. HSP27 pSer78, MEK1/2 pSer 217, MNK1 pThr197, Thr202 from the MAPK pathway, and 4E-BP1 P Ser65, p70 S6 Kinase P Thr389, mTOR (7C10), from the mTOR pathway, were all shown to increase in expression following siDHX9 transfection. Interestingly, these two pathways are often associated with each other in prostate cancer. Work by Kinkade et al (2008) showed that inhibition of the mTOR pathway by rapamycin and inhibition of the MAPK pathway using MEK inhibitor significantly inhibits cell growth in PC cell lines and AI PC tumours in mouse models (Kinkade *et al.*, 2008). Furthermore, inhibition of the mTOR pathway has been shown to activate the MAPK pathway as compensation (D. E. Butler *et al.*, 2017). The data here suggests that these two pathways may be reliant on DHX9 expression in order to successfully allow signalling via these pathways. In addition to the MAPK and mTOR pathways, phosphorylation of S6 Ribosomal protein P Ser235, Ser236 and S6 Ribosomal protein p Ser240, Ser244 expression increased following siDHX9 transfection. The ribosomal protein is an important component of the 40S ribosomal subunit (Puighermanal *et al.*, 2017) as it has the ability to bind to mRNA, tRNA, and initiation factors (Williams *et al.*, 2003). Phosphorylation of this protein is known to promote mRNA translation (Williams *et al.*, 2003) under the regulation of the mTOR pathway (Ruvinsky and Meyuhas, 2006). Initial RPPA analysis potentially suggests that knockdown of DHX9 expression can potentially affect the mTOR pathway, either by altering the phosphorylation of downstream proteins or by altering the translational activity of the cell.

It should also be noted that the decrease in DHX9 expression also led to the decreased detection of Cofilin pSer 3. Cofilin is an F-actin severing protein required for the reorganization of the cytoskeleton, which in turn drives cell migration. Cytoskeletal rearrangement is regulated by the phosphorylation of cofilin at Ser 3 in response to growth factor stimulation (Collazo *et al.*, 2014). The RPPA analysis presented here shows that total cofilin expression remains unchanged but cofilin pSer 3 expression decreases following siDHX9 transfection (Figure 5.16 B). Phosphorylation of cofilin abolishes its actin-binding activity, thereby reducing filament breakdown and promoting cell migration (Lee and Dominguez, 2010). This could indicate a role for DHX9 in regulating levels of

phosphorylated cofilin, thus regulating cellular migration and invasion. In addition to cofilin, DHX9 knockdown also led to a decrease in Chk1 P Ser345 and Chk2 P Thr68 detection. Chk1 and Chk2 are both kinases that play an important role in genome integrity and cell cycle control. Although these two proteins are structurally unrelated to each other, both play a role in relaying the checkpoint signals in response to DNA damage. Phosphorylation of these proteins promotes activation of DNA repair pathways (Bartek and Lukas, 2003). Interestingly, inhibition of CHK1 can promote tumour cell killing by different genotoxic agents (Smith *et al.*, 2010). This could mean that by decreasing phosphorylation of these two proteins by suppressing DHX9 expression, we could potentially increase the potential for PC cells to succumb to different anti-cancer drugs.

In order to further validate the RPPA analysis, the proteins presented in Figure 5.17 were selected for western blot analysis. These proteins were selected as the initial RPPA analysis showed that their expression was altered following siDHX9 transfection. Unfortunately, I was unable to further validate the other proteins above due to antibody availability and time constraints.

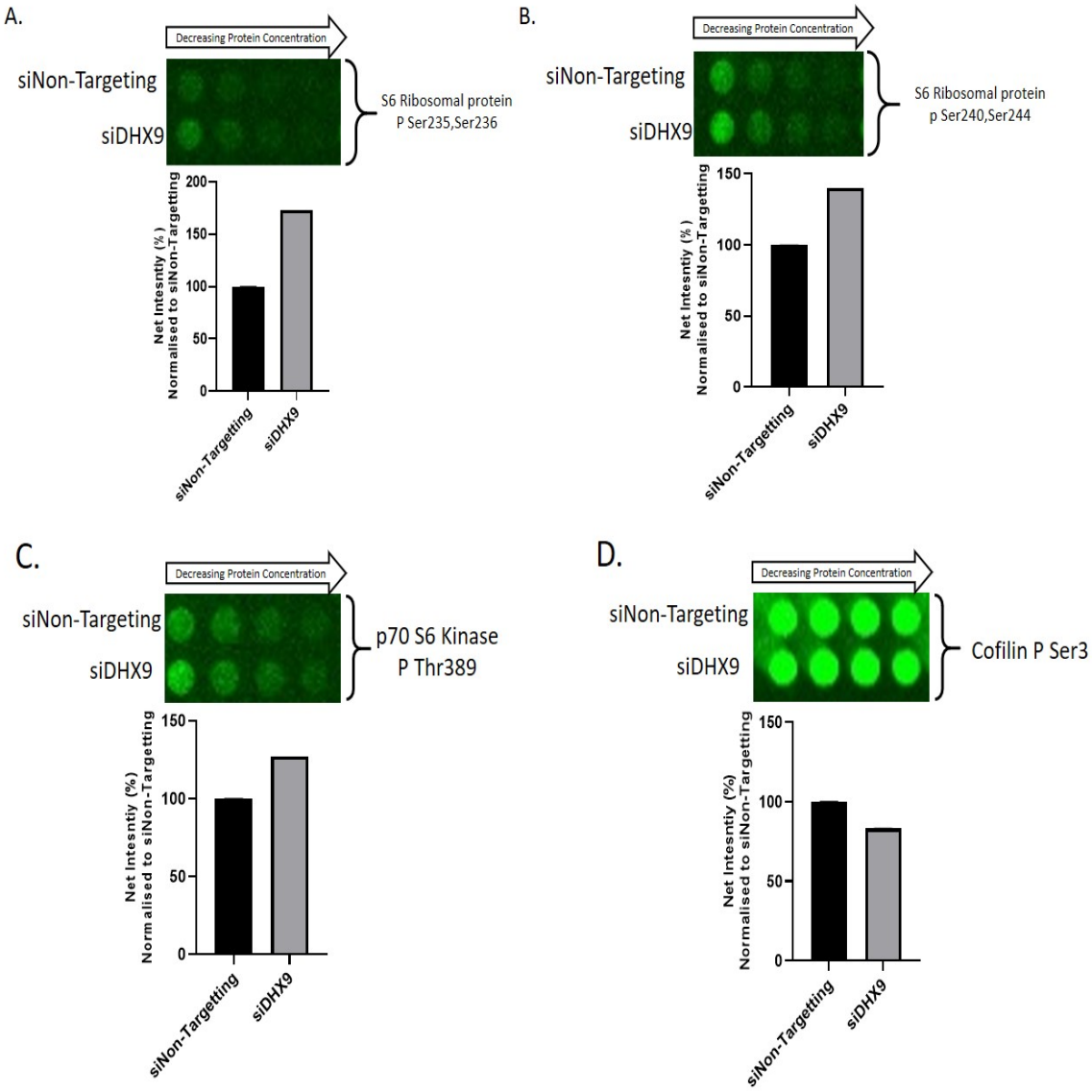

Figure 5.17 RPPA proteins selected for further validation. DU145 cells were treated with either siNon-targeting or siDHX9 for 48 hours. Cells were then lysed and the lysates were spotted onto glass nitrocellulose slides. Lysates were serially diluted 1:2 four times from a starting concentration of 1.5 mg/mL, then spotted in triplicate. The data presented here is the representative spot images and the net intensity following normalisation to loading control and siNon-targeting control. Data is presented as the mean ± standard deviation of the triplicate data. N=1. A+B+C. S6 Ribosomal protein P Ser235,Ser236, S6 Ribosomal protein p Ser240,Ser244, and p70 S6 Kinase P Thr389 expression increases following siDHX9 transfection. D. Cofilin pSer 3 expression decreases following siDHX9 transfection.

As previously described, the expression S6 Ribosomal protein P Ser235, Ser236, S6 Ribosomal protein p Ser240, Ser244, and p70 S6 Kinase P Thr389 increased after siDHX9 transfection (Figure 5.17 A-C). This could suggest that decreased expression of DHX9 could lead to changes in mTOR signalling. Additionally, expression of cofilin pSer 3 decreased following siDHX9 transfection. DHX9 could potentially have a role in mediating its phosphorylation, in turn regulating cell migration (Figure 5.17 D). The expression of the proteins mentioned in Figure 5.17 was then further validated by western blotting. DU145 cells were treated

with either siNon-targeting, siGAPDH, or siDHX9 for 48 hours, then lysed. The expression of the proteins of interest was then assessed by SDS-PAGE with western blotting (Figure 5.18) in order to validate the original RPPA analysis (Figure 5.16).

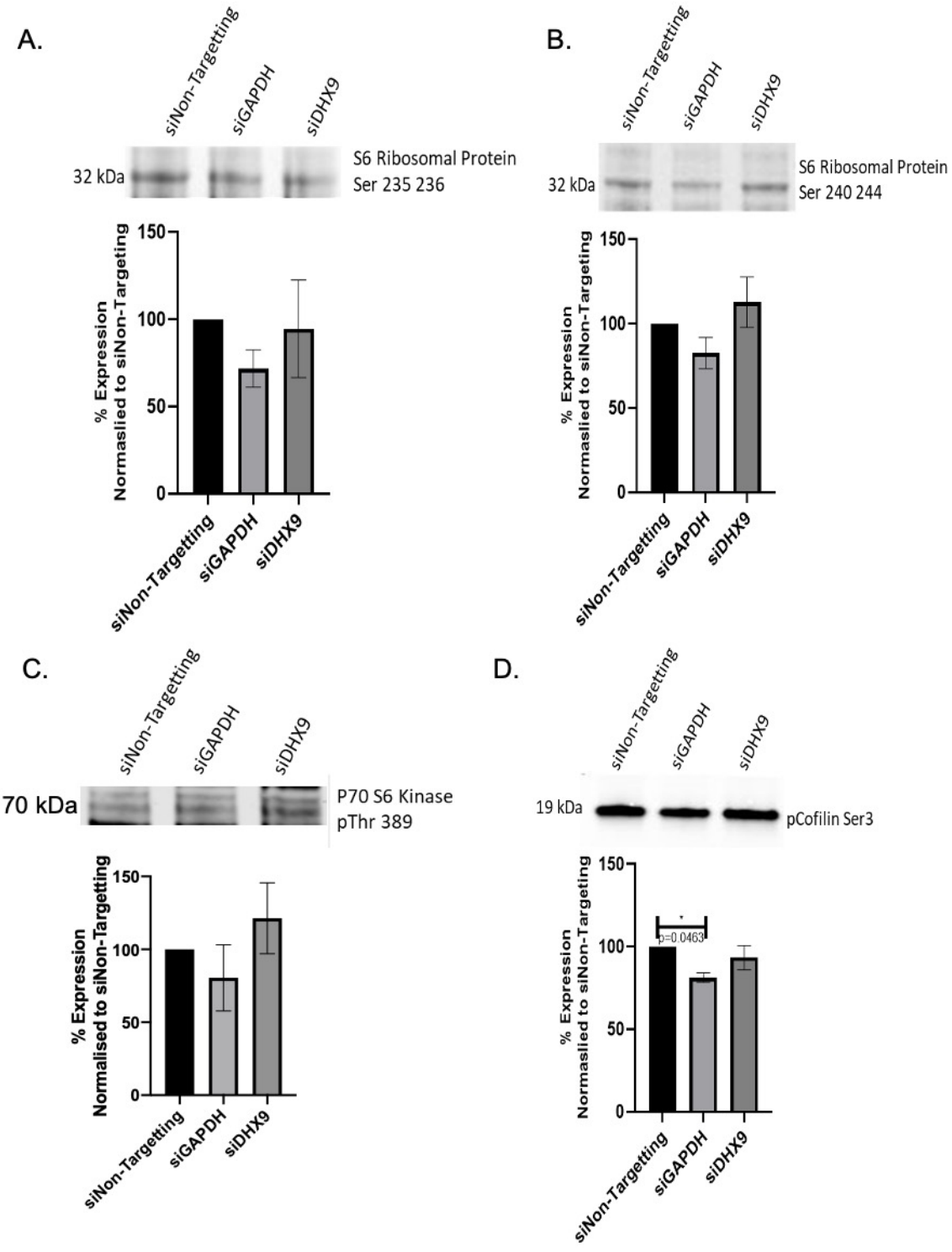

Figure 5.18 **Effects of DHX9 knockdown on the phosphorylation of downstream proteins.** Western blot analysis of the levels of phosphorylated proteins in cells treated with siRNA against, DHX9, GAPDH, or non-targeting control. The data is presented as the mean ± SEM of three independent experiments. Statistical significance was determined using a One-Way Anova.

Unlike in Figure 5.17 A, the expression of S6 Ribosomal protein pSer 235 236 and cofilin pSer 3 do not significantly change following siDHX9 transfection (Figure 5.18 A and D). However, S6 Ribosomal protein pSer 240 244 expression was increased following siDHX9 transfection (Figure 5.18 B). Interestingly, p70 S6 Kinase P Thr389 expression doubled following siDHX9 transfection (Figure 5.18 C), but it was not statistically significant due to high variability between experiments. Although these increases were not significant when compared to the non-targeting siRNA control, this data further validates the initial RPPA analysis from Figure 5.16 and 5.17. Interestingly, DHX9 has been shown to be an interactor of p70 S6 kinase (p70S6K) as well as a new possible target to regulate p70S6K activity (Pavan *et al.*, 2016). Although I was only able to validate a handful of proteins from the initial 60 from the RPPA analysis, this novel interaction as well as its role in the mTOR pathway could be of interest in order to identify alternate signalling pathways that are dysregulated in PC.

5.4 Discussion

5.4.1 Suppression of DHX9 leads to cell death

Cancer cells are reliant on the cell's transcriptional machinery for protein synthesis and translation of specific mRNA that promote tumour cell survival. Therefore, targeting this machinery has increasingly become a potential new target for cancer therapies. DHX9, as well as other members of the DEAD/H helicases, are involved in almost all steps of RNA metabolism and this process is thought to mediate oncogenic transformation of cancer cells (Heerma van Voss, van Diest and Raman, 2017). DHX9 thus may play a critical role in cellular metabolism and in cellular proliferation / neoplastic transformation (Fuller-Pace, 2013).

Part of this chapter's aim was to understand how DHX9 influences the proliferation of PC cells. When expression of DHX9 was knocked down using siRNA in AS and AI PC cell lines, proliferation of these cells was significantly affected (Figure 5.2 and Figure 5.5). Interestingly, this effect was most significant in the AI cell line highlighting the importance of DHX9 in promoting oncogenic growth. The loss of cancer cell proliferation can be partially explained by the potential activation of p53. P53 is a nuclear transcription factor and is known to activate numerous target genes involved in the induction of cell cycle arrest and apoptosis. In conditions where DNA damage is detected, p53 is activated and induces the activation of the pro-apoptotic pathway (Ozaki and Nakagawara, 2011). Suppression of DHX9 has been shown to lead to changes in cell cycle and DNA damage response protein expression. Suppression of DHX9 in MRC-5 cells resulted in a moderate increase in p53 expression. Interestingly, senescence was not induced in MRC-5 cells where both DHX9 and p53 expression were suppressed (Lee *et al.*, 2014). However, when repeated in p53 null mice and cell lines, DHX9 suppression led to cell death (Lee and Pelletier, 2017). Decreased proliferation of DUCaP and LNCaP cells in our experiments after knock-down of DHX9 may be due to the activation of the p53 pathway. Both DUCaP and LNCaP cells are known to express p53 (van Bokhoven *et al.*, 2003; Chappell *et al.*, 2012), providing a potential mechanism to explain why a decrease in cell proliferation was observed in PC cells. The DHX9-p53 "pathway" may be a potential new target for drug development. In cases where classic

chemotherapy targeting the p53 pathway is no longer a feasible option, p53-deficient cells expressing functional DHX9 can be a possible new target to suppress tumour growth (Lee and Pelletier, 2017). In order to confirm that this was the case, expression levels of p53 could be investigated by western blotting. Previous work by Lee et al (2017) showed that the suppression of DHX9 led to an increase in expression of p53 as well as its downstream effector protein (Lee and Pelletier, 2017).

5.4.2 YK-4-279 significantly inhibits cell growth in AS cell lines

YK-4-279 has quickly emerged as a new small molecule drug that can specifically target the oncogenic fusion protein EWS-FL1. This fusion protein is only expressed after chromosomal translocation, making it specific to tumour cells and a potential new therapeutic target in Ewing's Sarcoma. YK-4-279 can block the interaction of DHX9 and EWS-FL1 in ESFT cell lines, leading to a decrease in cell growth. Since its initial discovery in 2009, YK-4-279 has the potential to become a new therapeutic agent to target cancers that are known to express ERG fusion proteins, such as PC or Ewing's Sarcoma (Erkizan *et al.*, 2009). 50-70% of prostate tumours are characterised by the expression of ETS gene fusion proteins, with the most common one being the *TMPRSS2-ERG* fusion which occurs in 50% of tumours. Fusion proteins involving other members of the ETS gene family, such as FL1, have only been identified in less than 2% of cases (Kedage *et al.*, 2016). Currently, ETS transcription factors are grouped into four classes (I-IV) according to their sequence homology (Poon and Kim, 2017). FL1 and ERG are both part of Class I ETS factors and share more than 80% homology in their amino acid sequences. In this chapter, I show that disruption of the interaction between DHX9 and EWS-FL1, using YK-4-279, leads to a significant decrease in LNCaP proliferation. At the highest concentrations (10 μM and 1μM), YK-4-279 was shown to almost immediately alter cell growth (Figure 5.6). Although I did not investigate if LNCaP expresses the EWS-FL1 protein, YK-4-279 has previously been used to study how this drug can affect the efficacy of docetaxel in the treatment of PC (Yu *et al.*, 2017). Treatment of these cells with 10 μM and 1μM of drug led to a 75% decrease in the maximum cell index. My data suggests that the interaction between EWS-FL1 and DHX9 is required for oncogenic cell growth in LNCaP cells, and disruption of this interaction retards cellular proliferation. When repeated in the AI cell line (DU145), growth was not affected (Figure 5.7)

as they do not naturally express ETS fusion proteins (Swanson *et al.*, 2011). My data and conclusion are supported by the 2011 study by Rahim et al. who also looked at the effects of YK-4-279 on PC cells lines. YK-4-279 reduced the motility of PC lines in a scratch test as well as inhibiting the invasive nature of LNCaP cells. When the AI cell line PC3 was treated with YK-4-279, they remained unresponsive as they do not express ETS fusion proteins (Rahim *et al.*, 2011). This result was very similar to that reported in my thesis as I provide more evidence showing how YK-4-279 is dependent on the expression of ETS fusions proteins and inhibits the growth of LNCaP cells (Figure XX?).

YK-4-279 has the potential to become a new inhibitor of ETS-positive PC growth and metastasis. This small molecule has already been shown to be effective in slowing down the growth of primary tumours in mouse xenograft models (Rahim *et al.*, 2011). Severe combined immunodeficient mice (SCID) were subcutaneously transplanted with ETS fusion positive LNCaP and fusion negative PC3. These animals were then treated with YK-4-279, and primary tumour growth was evaluated. Treatment with YK-4-279 resulted in a decrease in the growth of primary tumours only in LNCaP-transplanted mice. Interestingly, YK-4-279 also inhibited metastasis to the lungs in these mice, indicating that this small molecule could be a powerful new therapeutic tool for treatment of PC at different stages of disease (Rahim *et al.*, 2014). Interestingly, when YK-4-279 was administered to SCID mice subcutaneously inoculated with lymphoma cells, this did not alter tumour volume, but the drug itself was well tolerated by all mice (Chung *et al.*, 2017). Recent work by Yu et al (2017) suggested that YK-4-279 can also be used as a combination therapy with docetaxel. The chemotherapeutic agent docetaxel is currently the first line treatment for CRPC patients. However, it is currently used as a monotherapy and is associated with high toxicity and resistance. Yu et al. has shown that YK-4-279 may have a synergistic effect with docetaxel. LNCaP cells were treated with low-dose docetaxel and YK-4-279, and the combination of these two drugs significantly decreased the expression of AR, PSA and ETV1. The use of YK-4-279 and docetaxel could permit the decrease in docetaxel dose necessary for patients with CRPC and lower its toxicity (Yu *et al.*, 2017). However, this would limit the treatment to tumours that are known to express the EWS-FL1 fusion protein.

As YK-4-279 has the potential to become the next cell growth inhibitor, alternative PPI disruption strategies need to be investigated in order to find alternative targets to inhibit growth. This is clear from my data, which shows that DU145 cells did not react to YK-4-279 as there was no change in cell growth. Other protein complexes could be targeted to halt AI PC cell growth.

5.4.3 Disruption of the PDE4D7-DHX9 complex does not change cell growth, but affects DHX9 activity

Due to the success of YK-4-279, a small molecule PPI inhibitor, we were interested to determine if the interaction between PDE4D7-DHX9 is crucial for cell growth. Previous work by Henderson et al. (2014) showed that PDE4D7 mediates the proliferation of PC cells. Using a dominant-negative approach, wild type PDE4D7 was displaced from endogenous anchoring sites and this resulted in an accumulation of cellular cAMP. Expression of the catalytically inactive PDE4D7 also led to an increase in cellular proliferation, a result that was confirmed using siRNA-mediated knockdown of global PDE4D7. Suppression of PDE4D7 was found to lead to an increase in the rate of proliferation. Interestingly, re-expression of PDE4D7 in AI PC3 cells lead to a significant decrease in proliferation (Henderson *et al.*, 2014). In this chapter I show that displacement of PDE4D7 from DHX9 using our new cell penetrating peptides does not affect LNCaP proliferation (Figure 5.8). Both UCR1- and DHX9-directed peptides significantly increased the normalised cell index two hours after treatment when compared to the scrambled peptide (Figure 5.10), indicating that the disruption of this interaction leads to a short-term increase in proliferation when compared to the scrambled peptide control. However, this did not lead to a change in cellular proliferation over the following three days. Unlike YK-4-279, our new cell penetrating peptides did not lead to an overall change in cell growth suggesting that the interaction between PDE4D7-DHX9 is not crucial for cell growth.

However, the disruption of the interaction between PDE4D7-DHX9 leads to a significant decrease in DHX9 activity as shown by the R-loop staining (Figure 5.12 and Figure 5.14). R-loops are transient, reversible structures that form in many parts of the genome. These structures facilitate transcription by regulating DNA methylation, which then promotes or inhibits gene expression (Crossley, Bocek

and Cimprich, 2019; Hegazy, Fernando and Tran, 2019). R-loops are generally formed during transcription. As the RNA polymerase moves along the DNA double helix, the newly formed RNA strand threads back to hybridise with the transiently accessible template strand and this displaces the non-template strand, which can be between 100-200 base pairs in length (Figure 5.19) (Allison and Wang, 2019). R-loops are generally formed by RNA polymerase II transcribing a cytosine (C)-rich template so that a guanine (G)-rich transcript is generated, and initial formation of this structure is favoured by G clusters and DNA nicks downstream from the promoter of the non-template strand (Skourti-Stathaki and Proudfoot, 2014). Once formed, R-loops are thermodynamically stable due to the formation of G quadruplexes formed in the single-stranded exposed RNA strand (Skourti-Stathaki and Proudfoot, 2014). Currently, the most widely used antibody to detect and understand R-loops is the monoclonal hybrid-specific S9.6 antibody (Boguslawski *et al.*, 1986; Niehrs and Luke, 2020). Genomic instability remains one of the hallmarks of cancer with replication stress and genome instability contributing to cancer development. Inappropriate accumulation of R loops is thought to play a role in a number of human cancers (Richard and Manley, 2017).

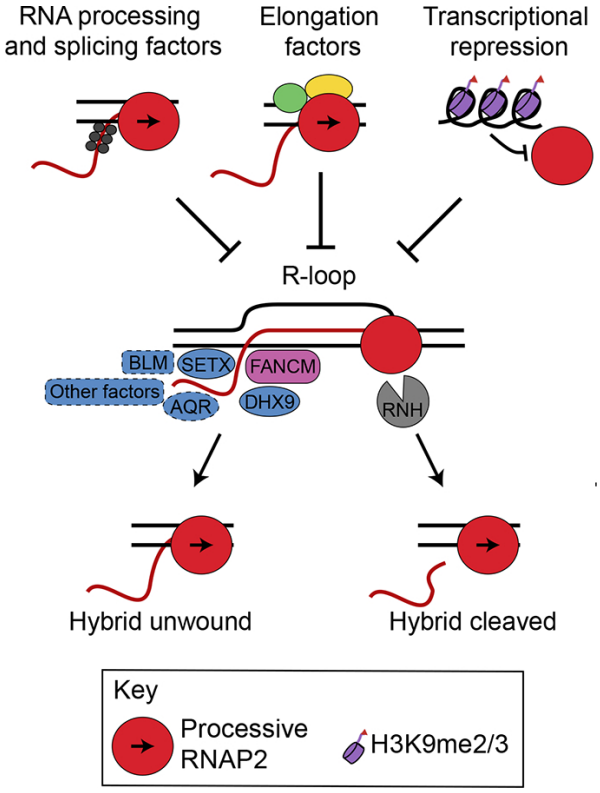

Figure 5.19 Model of R-loop formation and suppression. R-loops form during transcription when a nascent RNA hybridizes with DNA, generating and DNA-RNA hybrid. R-loops are suppressed by splicing factors which coat the nascent RNA structure, allowing for progression of transcription. Currently, DHX9 is thought to resolve these structures, releasing the nascent RNA for processing. (Figure taken from Crossley, Bocek and Cimprich, 2019).

Recent work by Chakrabortty et al (2018) showed that defects in the SFPQ splicing factor can cause R-loop formation and DNA replication stress. Defects in RNA splicing factors leads to an increase in genomic instability due to the formation of R-loops. Using siRNA technology, they observed that loss of SFPQ expression led to a significant increase in R-loops staining using the S9.6 antibody. They then showed that expression of DHX9 is needed to promote the formation of R-loops. In cells that are defective for splicing factors, such as SFPQ, formation of R-loops is dependent on DHX9 as shown by the significant increase in S9.6 staining (Chakraborty, Huang and Hiom, 2018). However, this concept is directly opposed to that published by others in the field. Other researchers have proposed that DHX9 is required for the suppression of R-loops. Work by Cristini et al (2018) initially identified DHX9 as one of the main proteins involved in the suppression of R-loop formation. DHX9 was shown to interact with R-loops by IP, and this interaction was shown to be reduced following treatment with a transcriptional inhibitor. By using DNA/RNA IPs, they were able to investigate how this interaction could affect the transcription of the *β-actin* and *γ-actin* genes in HeLa cells following siRNA transfection. This experiment revealed that the loss of DHX9 expression lead to an accumulation of R-loops within the transcription termination region of each gene when compared to the control siRNA condition. They suggested that the normal expression of DHX9 promotes the suppression of R-loops formed within the genome, allowing for successful gene transcription termination. Suppression of DHX9 within these cells also led to an accumulation of read-through transcripts, which results from continuous transcription of adjacent genes (Pintarelli *et al.*, 2016), due to the increased presence of R-loops at the termination region (Cristini *et al.*, 2018). Unlike Chakrabroty et al (2018), Cristini et al. (2018) conclude that DHX9 is needed to supress R-loop formation within the genome in order to limit R-loop associated DNA damage (Cristini *et al.*, 2018).

Using the newly developed method by the Hiom lab outlined above, we wanted to understand if the interaction between PDE4D7-DHX9 could modulate DHX9 R-loop formation. This work was carried out in collaboration with Prof Kevin Hiom's laboratory at the University of Dundee where I undertook a placement. My data (Figure 5.12 and Figure 5.14) showed that the disruption of PDE4D7-DHX9 using our cell penetrating peptides resulted in a significant decrease in

DHX9 activity with respect to R-loop formation (Figure 5.14). My conclusion is that the interaction between DHX9-PDE4D7 is essential for DHX9 to resolve secondary structures in RNA. As such, when this interaction is interrupted by our custom peptides and with siRNA targeting PDE4D7, DHX9 is no longer able to resolve secondary structures in the nascent RNA, inhibiting R-loop formation. When LNCaP cells were treated with siRNA against SFPQ alone, this led to a significant increase in S9.6 staining in the nucleus as DHX9 is able to unwind abnormal RNA structures (Figure 5.12 B and Figure 5.20 B). However, when the cells were depleted for SFPQ and treated with the UCR1 cell penetrating disruptor peptide, S9.6 staining significantly decreased and was comparable to the level of staining in the non-targeting siRNA control (Figure 5.12 E and F, Figure 5.20 C). This effect was also observed in cells treated with the DHX9 peptide and siRNA against PDE4D7 (Figure 5.12 C). My data further supports the idea that normal DHX9 expression is required in the formation to RNA-DNA hybrids as the protein can resolve secondary structures in the nascent RNA strand.

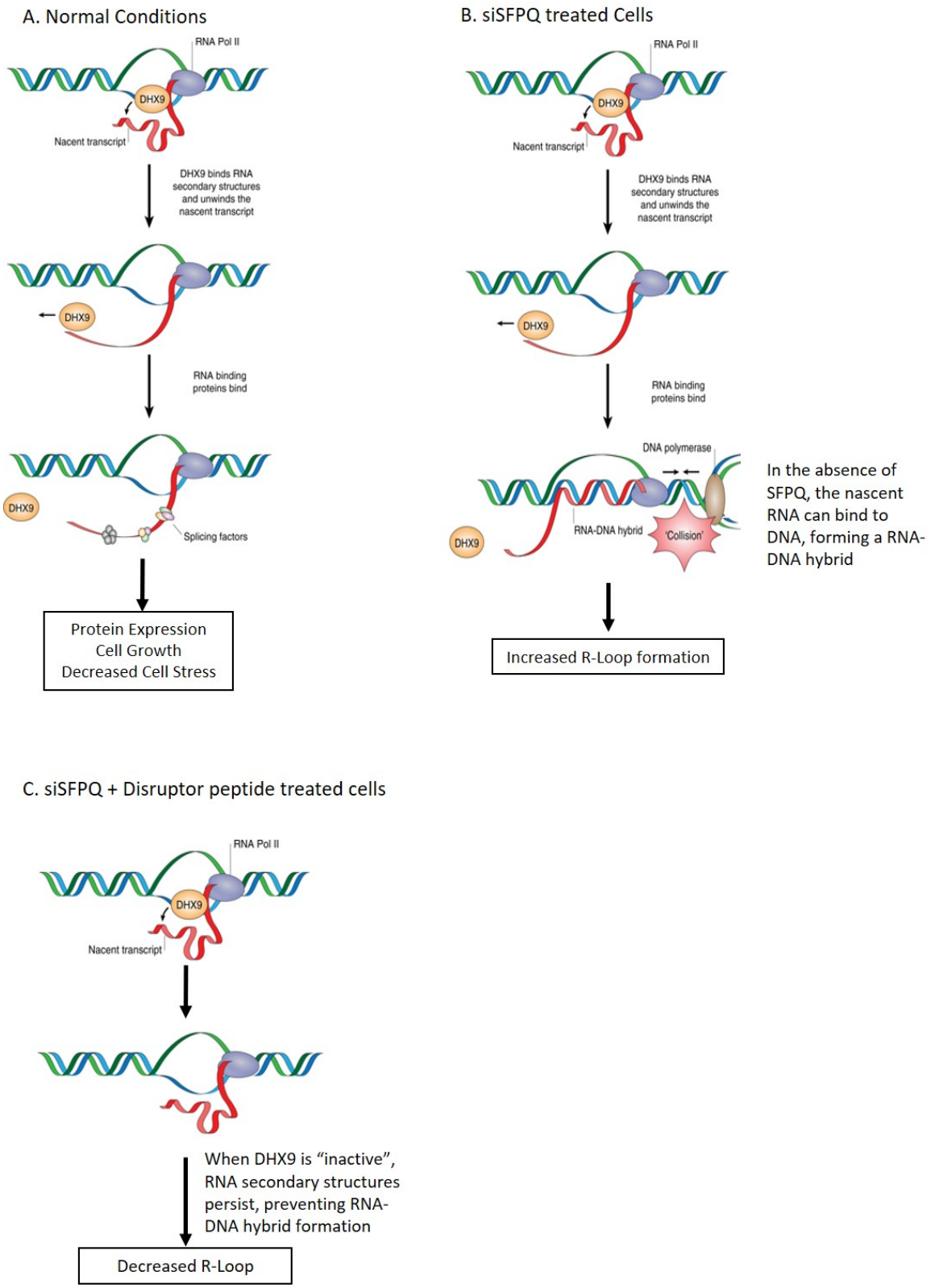

Figure 5.20 DHX9 promotes the generation of R-loops. A. Formation of R-loops in cells with impaired splicing factors can be due to a prolonged association of DHX9 with RNA Pol II during transcription. In normal cells, DHX9 can bind to RNA Pol II during the early phases of transcription, but this interaction in absent during elongation. The dissociation of DHX9 from RNA Pol II is dependent on the presence of SFPQ. SFPQ stabilizes the nascent RNA strand, preventing the formation of secondary structures. B. In the absence of these splicing factors, DHX9 remains bound to the transcription complex where it can then bind to the nascent RNA strand. These RNA strands are then able to invade DNA duplexes where it can form RNA-DNA hybrids. C. In cells deficient for splicing factors and decreased DHX9 activity, the nascent RNA remains in its secondary structures, leading to a decreased in RNA-DNA hybrid. Figure is adapted from Chakraborty, Huang and Hiom, 2018.

As previously mentioned, the role that DHX9 plays in R-loop formation is controversial as several groups have suggested that DHX9 promotes the suppression of R-loops in cells. Work by Cristinin et al. (2018) showed that DHX9 directly binds to these DNA-RNA hybrids and promotes the suppression of R-loops. DHX9 was also shown to be important in maintaining genome stability in response to camptothecin, a topoisomerase inhibitor, by preventing the accumulation of R-loops in the genome (Cristini *et al.*, 2018). Additionally, DHX9 has been identified as a protein that is involved in preventing and suppressing the formation of R-loops (Skourti-Stathaki and Proudfoot, 2014). Here we show that the interaction between PDE4D7-DHX9 is required in the formation of R-loops as the loss of this interaction is detrimental to DHX9 activity. Although it was not investigated here, the R-loop assay developed by the Hiom lab would have allowed us to understand how the inhibition or activation of these different pathway could affect DHX9 activity. LNCaP could have been treated with an array of inhibitors or activators, such as enzalutamide or rapamycin, and DHX9 activity could be assessed using this assay. This would have allowed us to understand how these different pathways can affect DHX9 activity.

The assay developed by the Hiom Lab, although effective, also presents with its own limitations. The main limitation is the reliance on the levels of SFPQ expressed in the cells. Although we have been able to show that SFPQ expression can be reduced in LNCaPs, the expression of this protein was very low to start with. Furthermore, the relationship between DHX9 and R-loops remains controversial between lab groups. Therefore, other methods need to be used in order to determine whether or not PDE4D7 does in fact have a role in regulating DHX9 activity. One such assay is the helicase assay, which has been previously used to show that DHX9 unwinds triplex DNA. This assay requires full length purified DHX9 protein and DNA substrates that have the ability to form triplex structures. DHX9 activity can be measured by the extent of strand displacement from the triplex DNA substrates. Briefly, purified DHX9 protein is incubated with 5 nM of specific DNA substrate in assay buffer containing DTT and ATP. The reaction is then placed in a temperature-controlled PCR machine at 32˚C for 20 minutes. The products can then be resolved by DNA agarose gel electrophoresis (Jain *et al.*, 2010, 2013). This method could potentially be modified in order to investigate if the interaction of PDE4D7 increases the helicase activity of DHX9.

We can also potentially hyper-phosphorylate DHX9 in order investigate how PKA phosphorylation alters its activity. Although this assay would be considered as an *in vitro* assay, it may be more accurate and reliable than the R-loop assay used in this chapter. The helicase assay was initially considered as a method to evaluate DHX9 activity in my thesis; however due to the complex nature of the purification of full length DHX9, we were unable to perform this assay. Full length protein is required for this assay as the HA2 region of DHX9 is required for helicase activity. Commercially available protein was therefore not an option as these only sold truncated versions of the protein.

5.4.4 p70 S6 Kinase P Thr389 in prostate cancer

RPPA based analysis has increasingly become a useful and highly efficient tool to quantify protein analytes with high precision, sensitivity, throughput and robustness. Due to its large antibody database, RPPA can assess a large number of proteins in many samples in a cost-effective and sensitive matter (Akbani *et al.*, 2014). Recently, the Cancer Genome Atlas group has employed this technology to characterise patients samples across a broad range of cancers, generating expression data of over 200 total and phosphorylated protein markers in major signalling pathways (Li *et al.*, 2017). Using RPPA, we were able to show that the levels of p70 S6 Kinase pThr 389 increases in DU145 cells with suppressed expression of DHX9. As total levels of p70 S6 kinase remained unchanged in the experiment, the data suggests that DHX9 may have a role in regulating p70 S6 kinase activity via its phosphorylation (Figure 5.17 and Figure 5.18).

p70S6K is a 85 kDa ribosomal protein that is a member of the AGC subfamily of serine/threonine protein kinases (Bahrami-B *et al.*, 2014). AGC kinases include more than 60 proteins in the genome and this group is highly expressed in eukaryotic cells. AGC kinases are involved in diverse cellular functions and have become potential targets in human diseases such as cancer. The AGC kinase was named after 3 representative families: the cAMP dependent PKA, the cGMP dependent protein kinase G (PKG), and protein kinase C (PKC) (Arencibia *et al.*, 2013). For many AGC proteins, activation requires the phosphorylation of two highly conserved regulatory motifs. This includes the activation segment, which can be located in the protein's catalytic domain, and the hydrophobic motif,

which is found in a non-catalytic region following the kinase domain (Pearce, Komander and Alessi, 2010) (Figure 5.21).

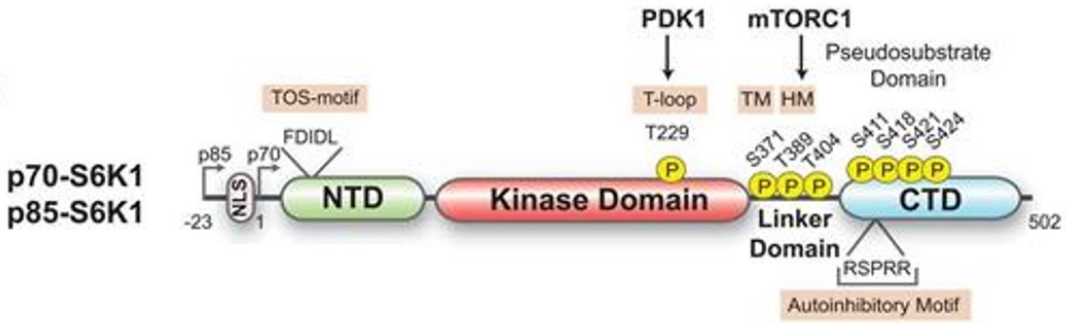

Figure 5.21 Domain structures of p70 S6 Kinase. P70SK contains an acidic N-terminal region, a kinase domain, a linker region, and an acidic C-terminal region. Figure taken from Magnuson, Ekim and Fingar, 2011.

In recent years, efforts have been made to map to the interactome of p70S6K involved in the regulation of multiple cellular processes. These newly identified interactors could represent new regulators or targets of p70S6K, furthering the understanding of this family of kinases. Such efforts have revealed that DHX9 is a novel interactor of p70S6K, and can potentially regulate its activity (Pavan *et al.*, 2016). Our data suggests that DHX9 could play an important role in regulating the phosphorylation of p70SK. Knockdown of DHX9 using target specific siRNA revealed that levels of phosphorylation of p70S6K at Thr389 were increased in both our RPPA and western blot analysis. This is further supported by levels of total p70S6K remaining unchanged in the RPPA analysis after DHX9 suppression. Interestingly, an increase in the levels of 4E-BP1 pSer 65 was also observed. These two proteins are both downstream effectors of the mammalian target of rapamycin (mTOR) complex 1 (mTORC1). Activation of mTORC1 results in the phosphorylation of 4E-BP1 and p70S6K which results in the initiation of protein synthesis (Choo *et al.*, 2008).

The mammalian target of rapamycin (mTOR) is a an evolutionarily conserved phosphatidylinositol 3-kinase (PI3K)-related Ser/Thr kinase that can integrate signals from nutrients, energy sufficiency, and growth factors to regulate cell growth as well as organ and body size. mTOR forms two distinct complexes, complex 1 which is rapamycin sensitive and complex 2 which is insensitive (Julien *et al.*, 2010). Currently, the most accepted models is that mTOR complex

1 phosphorylates p70S6K hydrophobic motif at Thr 389, and the process can be reversed by rapamycin (Zhang *et al.*, 2019) (Figure 5.22 panel A). P70S6K is one of the predominant effectors of the mTOR complex 1, and this pathway is known to play an important role in regulating protein synthesis, cell growth, metabolism, and aging (Laplante and Sabatini, 2009; Doscas *et al.*, 2014).

The mTORC1 substrate 4E-BP1, which is unrelated to p70S6K, inhibits translation by binding and sequestering the translation initiation factor eIF4E to prevent the formation of the eIF4F complex (Saxton and Sabatini, 2017). When 4E-BP1 is phosphorylated at serine 65 by mTOR complex 1, it no longer sequesters eIF4E, allowing formation of the eIF4F complex initiating cap-dependent translation. When mTORC1 is inhibited, 4E-BP1 becomes dephosphorylated, increasing its affinity for eIF4E (Sun *et al.*, 2019). Interestingly, DHX9 has recently been shown to be recruited by mTOR to a 5'mRNA cap structure following its activation. DHX9 was shown to assist eIF4A in the unwinding of secondary structures with the 5'UTR of mRNAs (Nandagopal and Roux, 2015). In recent years, mTOR signalling has been shown to be dysregulated during disease progression. Upregulation of mTOR signalling can promote tumour growth and progression through multiple mechanisms (Hua *et al.*, 2019). mTOR has specifically been implicated in PC metastasis via the regulation of HIFα and the inhibition of transforming growth factor ß1 (TGFß1) (Kremer *et al.*, 2006). Furthermore, PDE4D has recently been shown to be regulate mTORC1 transcriptional activity via Rheb. mTORC1 is a direct substrate of Rheb, a small GTPase. The direct binding of Rheb and mTORC1 allows for the activation of mTORC1 and activates pathways that are downstream of this activation (Long *et al.*, 2005). Under basal conditions, PDE4D binds to Rheb which in turn inhibits activation of the pathway. However, when cAMP levels are elevated, the interaction between PDE4D and Rheb is disrupted, inducing activation of mTORC1 and cap-dependent translation (Kim *et al.*, 2010). This could potentially mean that in late stage disease, where global PDE4D expression is low, disease progression could be initiated through mTORC1-p70S6-RHEB1 pathway. Our data suggests that the suppression of DHX9 in DU145 cells would potentially lead to an increase in translational activity via the mTORC1 pathway. Human mRNA translation requires DHX9 for folding / unfolding within their 5'UTR region. If these remain unresolved, the mRNA is unable to be read by ribosomal structures and inhibits the translation of

downstream open reading frames (Murat *et al.*, 2018). It can therefore be proposed that the normal expression of DHX9 is required to maintain normal protein expression as well as PC progression. Suppression of DHX9 can then lead to the accumulation of mRNA structures leading to the formation of aggregates in the cell (Figure 5.22 panel B). These aggregates create stress granules, and can potentially initiate the apoptotic pathway and decrease cellular proliferation (Khong *et al.*, 2017; Falcone and Mazzoni, 2018).

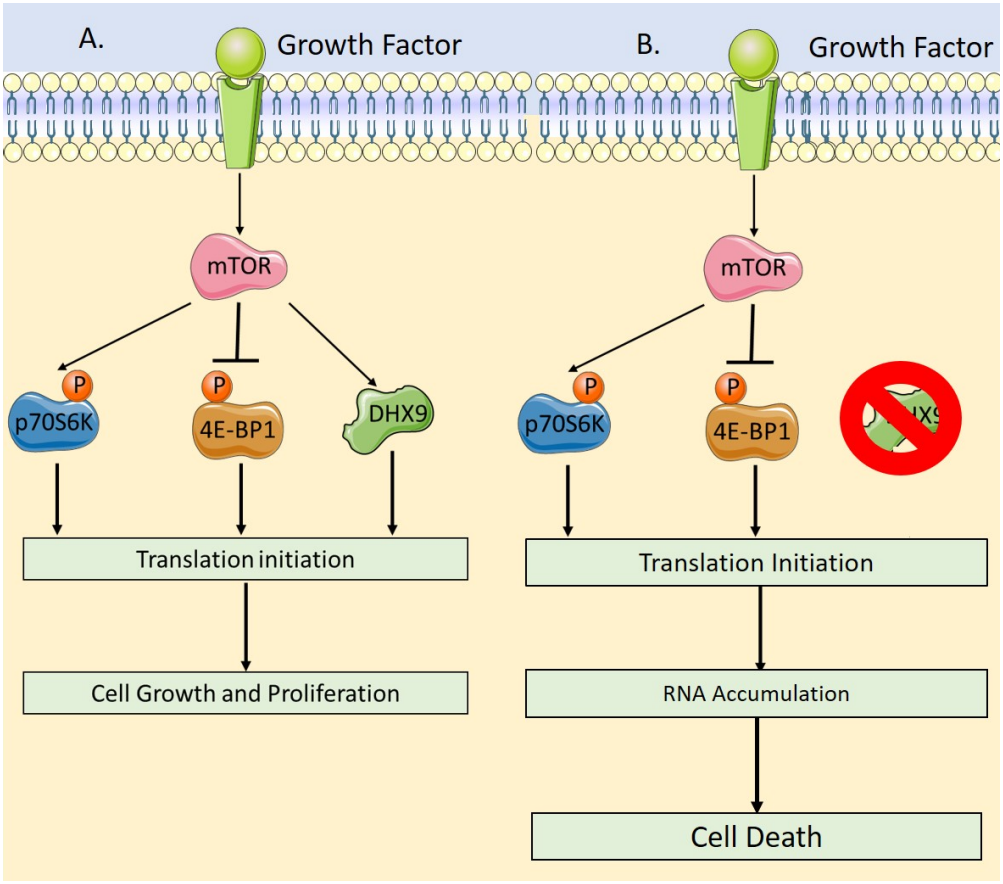

Figure 5.22 Schematic diagram illustrating the proposed interaction between DHX9 and the mTOR pathway. A. Activation of mTOR pathway leads to the phosphorylation of p70 S6 Kinase at threonine 389 and of 4E-BP1 at serine 65. DHX9 is also recruited to the pathway, and these three proteins promote the initiation of translation, allowing for cell growth and proliferation. B. Here, we propose that the decreased expression of DHX9 leads to an increase in phosphorylation of p70 S6 Kinase at threonine 389 and of 4E-BP1 at serine 65. Translation is still able to occurs, but due to the absence of DHX9, secondary RNA are not resolved and this leads to the accumulation of RNA that cannot be correctly translated into protein. This can then lead to the formation of stress granules and cell death. (Laplante and Sabatini, 2009; Pavan *et al.*, 2016; Khong *et al.*, 2017)

Various *in vitro* models have been used in PC in order to understand the mechanisms that leads to treatment resistance and disease progression. DU145 was once considered as the "gold standard" of PC cell lines. DU145 was first isolated from a brain metastatic prostate tumour, and no longer expresses mRNA or protein for AR or PSA. This observation has since cast doubts on this cell line as a true model for PC (Cunningham and You, 2015). Due to the absence of AR,

this cell line is most commonly used as an AR^- control or to study AR singling by ectopic expression (Sampson *et al.*, 2013). Most PC tumours still express AR, further supporting the idea that DU145 is not a true representation of late stage PC (Heinlein and Chang, 2004). As such, in order to ensure that the mTOR-DHX9 signalling axis is worth investigating, this RPPA should be repeated in other PC cell lines such as VCaPs or PC3. If RPPA results in these other cell lines indicate that the same signalling axis is altered, then further work on how PDE4D7-DHX9 is involved in this pathway should be carried out.

Although RPPA remains a very useful tool in cancer biology, it can only look at changes in protein levels. However, DHX9 is involved in RNA processing, biogenesis and processing. Increasing evidence has shown that different RNA markers are differentially expressed in PC and such is the case with circular RNA (cRNA). cRNA are a novel type of non-coding RNA (ncRNA) which can regulate the function of microRNA (miRNA), and can play a key role in the development of drug resistance in PC (Greene *et al.*, 2019). Furthermore, long-noncoding RNA (lncRNA) are known to bind to DHX9 and mediate cell invasion and angiogenesis of cervical cancer (Ding *et al.*, 2019). These two types of ncRNA have important functional roles and are frequently dysregulated in PC. There is evidence showing that these RNAs are responsible for oncogenesis and tumour progression (Hua, Chen and He, 2019). It would be interesting to investigate if the suppression of DHX9 could also alter the levels of ncRNA or cRNA in PC cell lines or patient samples. These changes could indicate which ncRNA plays a critical role in the progression of PC, potentially revealing new drug targets of DHX9 interactors. Unfortunately, RPPA does not have the ability to look at levels of RNA, therefore other approaches such as RNA-Sequencing could be used to look at changes in RNA levels due to decreased DHX9 expression.

5.4.5 Chapter Summary

The data presented in this chapter has provided further support to the current literature. I have shown that reduced expression of DHX9 in PC cell lines leads to a decrease in cellular proliferation. This supports the idea that DHX9 can be considered an oncogenic protein, and its increased expression in late-stage cancers further promotes disease progression. Disruption of the interaction between EWS-FL1-DHX9 also leads to very significant decrease in cell growth,

however this was not seen in the fusion negative cell line DU145. YK-4-279 has the potential to be a successful drug in treating fusion positive tumours and slowing the progression of disease. Unfortunately, our novel disruptor peptides targeting the interaction between PDE4D7-DHX9 did not have the same effect as YK-4-279, and instead showed that this interaction is not essential for cell growth or a viable target to slow down disease. Instead, this interaction has been shown to be important in DHX9's helicase activity. Disruption of PDE4D7-DHX9 interaction significantly reduced R-loop formation in cells that are deficient for splicing factors. This was also observed in cells that were co-treated with siRNA against PDE4D7. In order to confirm that this was the case, alternative DHX9 helicase activity assays need to performed using purified protein. Our RPPA analysis confirmed that DHX9 plays an important role in the mTORC1 signalling pathway, and PDE4D isoforms plays a role in regulating the activation of this pathway. Increasing evidence has implicated this pathway in the progression of disease, and DHX9 is known to be recruited by mTOR to mediate 5'UTR cap dependent translation. However, further validation in AS cell lines is needed in order to confirm that the pathways affected in DU145 is also seen in either LNCaP or VCaP. If the mTOR pathway in both these cell models is affected by DHX9 knockdown, this could be a potentially new pathway to investigate.

Chapter 6 Final Discussion

6.1 DNA/RNA helicases in PC

RNA/DNA helicases are ubiquitous enzymes that are involved in many different aspects of nucleic acid function. They utilise energy, derived from the hydrolysis of ATP, to unwind abnormal DNA or RNA structures such as R-loops. Due to the importance of helicases in different cellular functions, mutations in these helicases are linked to hereditary diseases or associated with various cancers (Datta and Brosh, 2018). Changes in expression levels, mutations in human tumours, and roles in different signalling pathways that alter tumour growth are all ways in which cancerous cells utilise helicases in order to initiate disease (Robert and Pelletier, 2013).

In recent years, members of the DExD/H and DEAD helicase family have emerged as having a role in the progression of PC. DDX5, also known as p68, has recently been shown to be a novel AR transcriptional co-activator that is overexpressed in PC (Clark *et al.*, 2008). DDX5, like DHX9, is an RNA-dependent ATPase capable of unwinding abnormal RNA structures (Dai *et al.*, 2014). DDX5 is thought to be involved in cellular proliferation and early organ maturation, as well as transcriptional regulation of multiple genes. Like DHX9, it is mainly expressed in the nucleus, but can be shuttled in and out of this compartment via RanGTPase-dependent pathways (Wang *et al.*, 2009). DDX5 was identified as a novel interactor of AR by yeast-two-hybrid screening by Clark et al. (2003). This interaction was further verified by ICC and IPs in LNCaP. Interestingly, DDX5 was found to contain the LXXLL motif that can be seen in cofactors that interact with hormone receptors. The LXXLL motif is a multifunctional binding sequence that participates in several protein-protein interactions between transcription factors and their cofactors. This binding sequence mediates these interactions in order to activate or repress the transcription of specific genes (Plevin, Mills and Ikura, 2005). DDX5 was found to contain this motif between amino acid 146 and 150. Using chromatin-immunoprecipitation (ChIP) assays, DDX5 was shown to interact with AR at ARE within the promoter and enhancer regions of the PSA gene. This interaction at the ARE region was enhanced following prolonged activation of the AR by androgens. Suppression of DDX5 using siRNA technology reduced the expression of PSA and AR mRNA and protein, indicating the DDX5 is an important

co-activator of AR mediated gene expression. DDX5 expression was also seen to be increased when compared to benign tissue (Clark *et al.*, 2008).

In addition to DDX5, DHX15 is also known to be involved in PC. DHX15 is another member of the DExD/H helicase family and shares many of the same functions as DHX9. Additionally, DHX15 mediates the innate immune system in sensing of viral RNA (Murakami *et al.*, 2017). DHX15 was identified as another AR co-activator, and this interaction is required to regulate AR activity by modulation E3 ligase Siah2 AR ubiquitination (Jing *et al.*, 2018). The E3 ligase Siah2 is thought to target chromatin-bound inactive AR, which in turn can regulate the expression of genes that control growth, survival, and tumorigenic abilities of PC cell (Qi *et al.*, 2013). Work by Jing et al (2018) has shown that DHX15 promotes the binding of Siah2 to the AR, which in turn regulates its ubiquitination. DHX15 was found to stabilize the interaction between Siah2 and AR, allowing for the activation of AR transcriptional activity (Jing *et al.*, 2018). Furthermore, DHX15 expression was found to be upregulated in CRPC samples. This increased expression was suggested to be protective towards these CRPC cells. Using a CRPC cell line model, the knockdown of DHX15 using siRNA technology reduced AR sensitivity to DHT and inhibited cell growth as well as increasing sensitivity to enzalutamide. Increased DHX15 could contribute to PC progression into CRPC (Xu *et al.*, 2019).

Many parallels between DDX5, DHX15, and DHX9 can be found. Data in this thesis has shown that the expression of DHX9 was increased in DU145 cells, which is currently used as a model for late stage disease (Figure 3.1). Multiple studies have shown that DHX9 is required for the appropriate expression of multiple genes via its interaction with different transcription factors (Lee and Pelletier, 2016). Like DHX15, DHX9 could potentially play a role in regulating AR activity by modulating the interaction of AR with different co-activators. This could be the case with CBP. CBP is known to be a co-activator of AR, and this interaction is thought to play a role in prostate tumorigenesis. CBP alters chromatic structures, allowing for the binding of transcription factors such as AR (Debes *et al.*, 2005). CBP is also known to form a complex with RNA polymerase II and DHX9 in order to mediate the targeting of genes activated by CREB (Nakajima, Uchida, Anderson, *et al.*, 1997). It could be possible that these three proteins could form a complex within the nucleus in order to promote the expression of

different ARE genes that could promote the progression of disease. Increased expression of DHX9 could further promote such activities. Owing to the highly conserved nature of the DExD/H helicase family (Jankowsky, 2000), it can be proposed that DHX9 could potentially interact with AR. Interestingly, a study conducted by Heemers et al (2009) has identified DHX9 as a coregulator of AR activity. By using a cDNA-mediated annealing, selection, extension, and ligation (DASL) RNA profiling array, a tool designed to monitor gene expression from tissues or cells, they were able to identify DHX9 as a coregulator of AR in LNCaP cells. However, treatment with R1881, a synthetic form of androgens, did not change DHX9 expression after 48 hours (Heemers and Tindall, 2007). Furthermore, recent work by Chen et al (2020) has shown that although the AR has a role in regulating the expression of multiple RNA editing genes, AR was not reported to alter DHX9 mRNA expression in cells (Chen *et al.*, 2020). Although these studies indicate that DHX9 can act as a coregulator of AR, no studies have further investigated whether DHX9 activity it required for AR's transcriptional activity. DHX9 has often been described as a transcriptional coactivator that acts a bridging factor between transcription factors (Fuller-Pace, 2006). As DHX9 expression increases at later stages of disease, it could potentially act as a co-activator of AR transcription despite low levels of circulating androgens.

6.2 PDE4D7 regulates DHX9 phosphorylation and helicase activity

Experimental work reported in this thesis has provided extensive evidence that PDE4D7 and DHX9 are novel interactors in prostate cancer. By using extensive biochemical and peptide array techniques, not only was I able to show that the two proteins were interacting (Figure 3.6-3.9), but I was able to map where this interaction took place (Figure 3.11 and 3.16). DHX9 binds within the UCR1 domain of PDE4D7, and this binding site contains the previously reported FLY PDE4 multi-docking site. On the other hand, PDE4D7 binds within the helicase core domain of DHX9, downstream of Ser^{449} that is readily phosphorylated by PKA (Figure 4.1). Treatment of HEK293 and PC cells with the UCR1 disruptor peptide led to a reduction in PDE4D7-DHX9 interaction (Figure 3.19 and 3.21). This interaction could potentially take place in the nucleus due to the expression of NLS in both proteins (Figure 3.5, Lee and Pelletier, 2016). Bioinformatic analysis showed that PDE4D7 potentially has a novel NLS sequence between its

linker and UCR2 domain (Figure 3.5), whereas DHX9 is known to have an NLS/NES sequence within its C-terminal domain (Lee and Pelletier, 2016; Ng *et al.*, 2018). Interestingly, this loss of interaction also leads to an increase in DHX9 phosphorylation by PKA under basal conditions (Figure 4.12) as well as a decrease in DHX9's helicase activity (Figure 5.13). This could be due to the sequestering of phosphorylated DHX9 in the cytoplasm (Figure 4.10), inhibiting its ability to unwind nascent mRNA that are found within the nuclear region, therefore decreasing R-loop formation.

Modulation of RNA structures by members of the DExD/H family of helicases is a crucial step for many fundamental cellular processes (Sheng *et al.*, 2006). In addition to their important cellular roles, subtle changes in their shape or activity can result in altered development, uncontrolled growth, or adaptation to environmental changes (Linder and Fuller-Pace, 2013). Therefore, it is important that these helicases are appropriately regulated via PTMs. Based on the data presented in this chapter, PKA phosphorylation of DHX9 could act as a negative regulator of its helicase activity within the nucleus owing to its translocation into the cytoplasm. It can be suggested that PKA phosphorylation has a role in modulating DHX9's subcellular location and PDE4D7 prevents DHX9 accumulation in the cytoplasm. Such protective interactions have been seen in the NF-κB signalling pathway. NF-κB is a family of transcription factors that plays an important role in inflammation, immunity, cellular proliferation, differentiation and survival. PKA is known to phosphorylate the NF-κB protein p65 in order to increase its transcriptional activity (Oeckinghaus and Ghosh, 2009). However, PKA phosphorylation of NF-κB has also been shown to regulate its ability to translocate into the nucleus. Recent work by King et al (2011) has shown that the complex between A kinase interacting protein 1 (AKIP1), the catalytic PKA subunit (PKAc), and p65 regulates the rate at which p65 translocates to the nucleus. P65 was found to be phosphorylated at Ser^{276}, and inhibition of its ability to be phosphorylated by PKA by creation of a phospho-null mutant lead to the accumulation of p65 in the nucleus. Furthermore, increased nuclear expression of p65 was observed when PKAc expression was suppressed using siRNA technology. This translocation was found to be mediated by AKIP1, where PKAc overexpression in cells resulted in increased expression of p65 in the nucleus. It was suggested AKIP1 protects p65 from PKA

phosphorylation, allowing p65 translocation into the nucleus and act as a transcription factor (King *et al.*, 2011).

Interestingly, the same observation was made in this thesis. The worked conducted in this thesis has shown that PKA phosphorylation directs the subcellular location of the proteins of DHX9. Conceptually, DHX9 phosphorylation by PKA should be "gated" by local PDE4D7 activity, allowing DHX9 to be mainly expressed in the nucleus. This interaction promotes DHX9's helicase activity allowing it to unwind RNA secondary structures. This in turn increases R-loop formation as explained in Figure 5.20 B. However, disruption of this interaction either using our cell permeable peptides or by lowering PDE4D7 expression using siRNA, resulted in a significant loss in R-loop detection as well as an increase in the level of phosphorylated DHX9. Like AKIP1, PDE4D7 activity can protect DHX9 phosphorylation and allow DHX9 to remain in the nucleus. PKA phosphorylation of DHX9 then leads to the translocation of DHX9 into the cytoplasm, which in turn leads to a decrease in its ability to unwind secondary RNA structures in the nucleus. Furthermore, phosphorylation of DHX9 could instead promote its translational activity. PKA phosphorylation not only promotes the enzymatic activity of certain proteins, but can also acts a molecular switch in order to promote other protein functions (Shwab *et al.*, 2017). Modification of DHX9 by PKA phosphorylation could potentially act as a way of promoting its translational activity. Phosphorylation of translation initiation factors can help reduce the amount of energy required for this process and provides a rapid way to adapt to cellular changes (Pierrat *et al.*, 2007). The majority of mRNA that exists in the cell are capped and polyadenylated, which requires unwinding prior to the initiation of translation (Marintchev, 2013). To date, the translation initiation factor eIF2 is the most well-known helicase to be recruited to these sites in order to unwind secondary structures, and failure to do so leads to inefficient translation initiation (Murat *et al.*, 2018). DHX9 is emerging as an additional helicase that has a role in translation initiation. For example, DHX9 has been shown to be required in the efficient translation of Type I collagen by unwinding its unique 5' stem-loop structure. siRNA mediated knockdown of DHX9 led to a significant loss in the synthesis of collagen protein, and has since been suggested to be an important factor in collagen synthesis in the human body (Manojlovic and Stefanovic, 2012). Therefore, the phosphorylation by PKA and loss of PDE4D7

could potentially promote DHX9's translational activity and initiate the translation of certain mRNAs.

6.3 DHX9 is involved in multiple signalling pathways

Initial ADT treatment has proven to be successful in PC, but it is widely accepted that the majority of men treated with either surgical or chemical ADT will develop disease progression due to the propagation of androgen-independent PC cells (Perlmutter and Lepor, 2007). Increasing evidence has shown that ADT for the treatment of PC carries significant health risks and some side effects, which is generally tolerated by the men receiving treatment (Fang, Merrick and Wallner, 2008). Furthermore, the age at which the men are being treated can affect the overall effect of ADT. A retrospective study by Keating et al. (2019) has shown that younger patients had no significant difference in overall survival between patients receiving active surveillance and ADT (Keating *et al.*, 2019). There is currently a need to find alternative therapies that could potentially be used in parallel with ADT in order to improve patient outcomes and limit the secondary effects associated with this course of treatment.

Considering the data presented here and that in the literature it could be considered that DHX9 has the potential to be an alternate target for the treatment of PC. Suppression of DHX9 expression using siRNA resulted in a significant decrease in DuCaP growth (Figure 5.2). Work by Lee et al (2014) has shown that this significant change in cellular growth rate can be attributed to the activation of the p53 apoptotic pathway (Lee *et al.*, 2014). However, using RPPA analysis, I was able to show that decreased expression of DHX9 by siRNA leads to an increase in p70 S6 Kinase phosphorylation at Thr^{389} and 4E-BP1 at Ser^{65} (Figure 5.15-17), both of which are known to be part of the mTOR signalling pathway. DHX9 has been shown to be recruited by mTOR to regulate the expression of specific mRNA (Nandagopal and Roux, 2015), and suppression of DHX9 could lead to the accumulation of these untranslated mRNA molecules. This in turn could potentially increase cellular stress, which could in turn activate pathways that activate cell death (Fulda *et al.*, 2010). These two signalling pathways are not mutually exclusive from each other, and research has shown that the mTOR and p53 pathways are needed in order to regulate their respective pathways. Work by Feng et al (2005) demonstrated that the

activation of the p53 pathway leads to an inhibition of the mTOR pathway through the activation of AMP kinase (AMPK) (Feng *et al.*, 2005). DHX9 could potentially act as protein that bridges these two signalling pathways in order to prevent the activation of the p53 pathway. In wild type cells, DHX9 could act as a negative regulator of p53 activation, which in turn allows for the activation of the mTOR pathway and translation of mRNA. However, when DHX9 is no longer expressed at normal levels, this leads to the activation of the p53 pathway and the inhibition of mTOR pathway. A potential way this can be studied is by looking at the expression of IGF-BP3, PTEN, TSC2, AMPK ß1, Sestrin1, and Sestrin2. The expression of these proteins are only induced following p53 activation and directly suppress the mTOR pathway (Feng, 2010). We could design an experiment where the expression of these protein changes following modulation of DHX9 expression using siRNA. It can by hypothesised that expression of IGF-BP3, PTEN, TSC2, AMPK ß1, Sestrin1, and Sestrin2 increases following siDHX9 treatment due to the activation of the p53 pathway, which in turn can negatively regulate the mTOR pathway.

6.4 Clinical trials involving mTOR and ERK signalling pathways

Since the 1990s, great efforts have been made to increase the detections of prostate cancer while at the same time reducing the number of PC related deaths (Ahdoot *et al.*, 2019). Although ADT has been the primary treatment of early and late-stage PC, patients ultimately progress to CRPC where the cancer becomes resistant to ADT. As such, these tumours develop ways to grow, decreasing the rate of survival (Ritch and Cookson, 2018). As such, alternative targets are currently being investigated in order to overcome these challenges.

As previously discussed, the PI3K-mTOR signalling pathway is frequently altered in PC, facilitating tumour formation, disease progression and therapeutic resistance (Shorning *et al.*, 2020). Drugs that target and inhibit the mTOR- PI3K activity is expected to therefore provide therapeutic value in a number of cancer types, including PC (Don and Zheng, 2011). Recent work by Statz et al (2017) evaluated the results of clinical trials investigating mTOR inhibition in CRPC, and predicted the clinical outcomes using the preclinical data. A total of 14 studies were evaluated, all using mTOR inhibitors either as a monotherapy or

in combination. Most studies showed that PSA levels declined during treatment, but often increased shortly after (Statz, Patterson and Mockus, 2017). Furthermore, the use of the mTOR kinase inhibitor voxtalisib showed limited clinical efficacy in the treatment of CRPC due to the dose reductions secondary to toxicity. Treatment of CRPC patients with this drug resulted in poor mTOR and signalling target inhibitions, which in turn led to increased AR Activation and PSA expression (Graham *et al.*, 2018). Work by George et al (2020) have also shown that the treatment of CRPC with the FDA approved mTOR inhibitor Everolimus has no clinical effect on CRPC treatment. Out of 35 men enrolled in this phase 2 trial, no changes in PSA levels were observed while patients were taking everolimus. Instead, several patients had declines in PSA levels following cessation of everolimus treatment (George *et al.*, 2020). Although promising, mTOR is still yet to become an effective drug target in PC. Despite mTOR inhibitors being used in the treatment of different cancers, such as pancreatic and breast cancer (Hua *et al.*, 2019), mTOR inhibitors are yet to be used in the treatment of CRPC.

In addition to the mTOR pathway, the ERK pathway is frequently altered in PC. In recent years, an increasing number of clinical trials are being performed on ERK inhibitors (Georgi *et al.*, 2014). Recent work by Nickols et al (2019) has shown that the ERK pathway may be a viable treatment strategy for patients suffering from CRPC. They compared the differential phosphorylation of key downstream kinases between metastatic and localised CRPC, as well as the expression of mRNA, in order to infer differential ERK activity. From this study, 32% of patients showed signs of amplified ERK pathway as well as increased levels of phosphorylated ERK1/2 when comparing CRPC to untreated primary PC (Nickols *et al.*, 2019). Currently, the only approved ERK inhibitor is trametinib, which is commonly used for the treatment for metastatic melanoma showing favourable safety profile (Georgi *et al.*, 2014). Work by Li et al (2019) has shown that inhibition of ERK using trametinib suppresses the growth of enzalutamide-resistant CRPC (Li *et al.*, 2019). Trametinib is currently in phase 2 clinical trial in order to study how this drug can help treat patients suffering from metastatic CRPC. Unfortunately, there is no data to date to indicate how efficacious trametinib was in treating these patients as the study is due to be completed in January 2022 (Retting, 2020).

6.5 DHX9 – A new druggable target?

Although the disruption of the interaction between DHX9 and PDE4D7 using our cell permeable disruptor peptide did not lead to any long-term effects on cell growth (Figure 5.8-5.10), the YK-4-279 DHX9 inhibitor significantly decreased the growth of AS LNCaP cells (Figure 5.6). Disruption of the interaction between DHX9-EWS-FLI1 using this compound significantly decreased the growth of LNCaP cells, but not in DU145 cells (Figure 5.7). Treatment with YK-4-279 is selective for cells expressing the EWS-FL1 fusion protein (Erkizan *et al.*, 2009) which is mainly detected in early stages of PC (Gierisch *et al.*, 2016). Interestingly, YK-4-279 is gaining clinical interest as this small molecule is currently being used in early-phase human trials for the treatment of Ewing Sarcoma (ES). Original work by Erkizan et al (2009) demonstrated that YK-4-279 was specific for ES due to the presence of the of the fusion protein (Erkizan *et al.*, 2009). By using an oral formulation of YK-4-276, Lamhamedi-Cherradi et al (2015) were able to use this inhibitor in order to slow tumour growth. When murine models of ES were administered daily with the oral formulation of YK-4-279, this led to a significant delay in ES tumour growth when compared to mice receiving a placebo drug. Daily dosing with YK-4-279 was required in order to achieve tumour regression and slower growth rates. Interestingly, all 7 mice receiving this oral formulation showed no signs of toxicity or weight change, indicating that this drug regiment was well tolerated (Lamhamedi-Cherradi *et al.*, 2015).

Most of the work on YK-4-279 has mainly looked at its use in the treatment of Ewing's Sarcoma and there is growing interest in using this small molecule drug in the treatment of other cancers that are known to be driven by ERG fusion proteins. Work by Winter et al (2017) showed that mouse xenograft models of ERG positive PC patient derived tumours were greatly affected by YK-4-279 treatment. YK-4-279 was administered subcutaneously to these mice, which resulted in the reduction of tumour volume, decreased tumour progression, and decreased levels of PSA (Winters *et al.*, 2017). Interestingly, work by Kollareddy et al. (2017) showed that YK-4-279 is able to overcome drug resistance in two different neuroblastoma cell lines (Kollareddy *et al.*, 2017). Most patients who have progressed to the lethal CRPC phenotype have very little treatment options due drug resistance and clinical complications (Semenas *et al.*, 2012). YK-4-279 could be a potential new treatment for patients in the later stages of disease.

Due to its ability to only target cells expressing the fusion protein, and its ability to overcome drug resistance, YK-4-279 could potentially lead to decrease PC metastasis and could be considered as a putative curative treatment.

6.6 Thesis limitations and future work

Using a range of biochemical techniques, the work in this thesis has demonstrated that DHX9 is a novel interactor of PDE4D7 in PC cells. I was able to show that DHX9 binds within PDE4D7's UCR1 region, and this interaction can be disrupted using a competing, custom-made, cell penetrating peptide. Although IPs are most commonly used technique in studying PPI, some may argue that this technique may force the interaction between two proteins when IPs are performed using tagged proteins. Therefore, other methods should have been used in order to provide stronger evidence of PDE4D7-DHX9 interaction. One such way that we could have studied PDE4D7-DHX9 interaction is through the use of Fluorescence Resonance Energy Transfer (FRET) imaging, a method that is routinely used in the Baillie lab (Di Benedetto *et al.*, 2008). FRET is a distance-dependent physical process by which energy is transferred from one fluorophore (the donor) to another fluorophore (the acceptor). This technique can measure the molecular proximity between two proteins that are within 3-6 nm of each other. FRET microscopy is also reliant on the ability to capture fluorescent signals from single living cells. If FRET occurs, the donor channel signal will be quenched, while the acceptor channel increases. Not only does this technique allow the user to visualise colocalization between the donor and acceptor labelled probes, but is also allows the user to verify the molecular association between two proteins (Sekar and Periasamy, 2003; Rainey and Patterson, 2019). Such approaches have already been used to study the interaction between the oestrogen receptor and transcription co-activators. Gunther et al (2009) were able to design a FRET assay where they were able to monitor ER interaction with steroid receptor coactivators. This assay was then used to identify small molecules inhibitors to disrupt this interaction (Gunther *et al.*, 2009). Knowing that multiple FRET probes are available in the Baillie lab, we could potentially create FRET probes in order to study the interaction between PDE4D7 and DHX9 in live cells. We can then also monitor the dissociation of this interaction following peptide treatment. Alternatively, surface plasmon resonance (SPR) could be another way to study PPI. SPR is a powerful tool to study PPI and

quantify binding affinities. SPR allows the use to investigate PPI without having to label the proteins of interest (Nikolovska-Coleska, 2015). SPR depends on the binding of a molecule to a bait molecule that is immobilised onto a thin metal film. Binding between these two molecules then leads to a change in the refractive index. This information can then be used to determine binding affinities in order to characterize PPIs (Drescher, Ramakrishnan and Drescher, 2009). We could potentially immobilize PDE4D7 onto SPR metals film and investigate if DHX9 binds directly to it.

Like in FRET, FP can also be used to find small molecules that can enhance or disrupt PPI (Hall *et al.*, 2016). Although I attempted to establish an FP assay to study the PDE4D7 and DHX9 interaction, I was unable to unable to obtain proteins that were pure enough to obtain any binding information. In vast majority of cases, purified recombinant GST tagged proteins can be purified from bacterial lysates under non-denaturing conditions by affinity chromatography (Smith and Johnson, 1988). Although GST protein purification is a technique that is commonly used in the Baillie lab, successful GST protein purification relies on optimization of the methods and conditions for each protein (Harper and Speicher, 2011). Once the target protein has been cloned in the appropriate vectors, the optimization of protein expression conditions, such as *E.Coli* host strain, temperature, IPTG concentration, and length of induction should be optimized. (Harper and Speicher, 2011). Unfortunately, due to time constraints, I was unable to determine the optimal condition for the purification of GST tagged PDE4D-UCR1 or full length DHX9. Although I was able to purify this fragment, the eluate was highly degraded and of low yield (Figure 3.16). More time should have been invested in order to find the best conditions to purify this protein. Perhaps this would have enabled us to establish an FP assay that would have allowed me to determine the binding constant between PDE4D7 and DHX9.

Using peptide array technology, IPs, and PLA technology, I was able to show that DHX9 is readily phosphorylated at Ser^{449}. This information was used in order to generate a custom antibody which was able to specifically detect phospho-DHX9 by western blotting and ICC. However, more effort should have been made to further validate the newly identified PKA phosphorylation site. Unfortunately, I was unable to make a phospho-null DHX9 construct where Ser^{449} could be substituted with an alanine. By substituting this serine with and alanine, we

would expect to see a significant decrease in DHX9 phosphorylation in PKA pull down assays. This approach has previously been used by Byrne et al (2015) in order to validate that Ser^{42} within the unique N-terminal region of PDE4D7 can be PKA phosphorylated. By creating a phospho-null mutant using site directed mutagenesis, they were able to demonstrate that the $S^{42}A$ mutant led to an ablation of PDE4D7 phosphorylation at this site (Byrne *et al.*, 2015). Furthermore, most of the work relating to validating the newly synthesised phospho-DHX9 was performed in HEK293 cells. In recent years, HEK293 cell lines has been used as a tool to easily express a range of proteins (Chin *et al.*, 2019). Ideally, the expression of phospho-DHX9 should have been studied in PC related cell lines in order to ensure that this antibody is able to detect phospho-DHX9 in disease related cells. The most commonly used cell line for this could be PC3, DU145, LNCaP, and VCaP cells (Wu *et al.*, 2013). Additionally, expression of phospho-DHX9 and total DHX9 should also be investigated in non-tumour prostatic cell lines. These cells are models for normal prostate cell growth, and the prostatic intraepithelial neoplasia (PIN) is the most commonly used cell line to investigate oncogenic processes prior to disease formation (Cunningham and You, 2015). Ideally, the expression of phospho- and total-DHX9 should have been investigated in all these cell lines in order to see if expression of phospho-DHX9 changes during the progression of disease. When phosphorylated, DHX9 is sequestered in the cytoplasm (Figure 4.13), suggesting that this PTM not only regulates the subcellular location of the helicase but potentially also its cellular function. DHX9 is known to be involved in the translation machinery by unwinding different RNA structures in the cytoplasm (Lai *et al.*, 2011; Murat *et al.*, 2018; Ding *et al.*, 2019). Furthermore, the interaction between PDE4D7 and DHX9 was shown to be important in regulating the levels of DHX9 phosphorylated by PKA. Loss of this interaction led to an increase in DHX9 phosphorylation under basal conditions (Figure 4.15 and Figure 4.16). It would be interesting to investigate if the interaction, and phosphorylation of DHX9, is needed to promote DHX9's translational activity. This could be investigated by looking at the change in mRNA expression using RNA-Sequencing. RNA sequencing is now a commonly used tool to analyse gene expression, allowing the user to identify any changes in RNA biogenesis and metabolism (Hrdlickova, Toloue and Tian, 2017).

One of the biggest limitations in this thesis is the lack of specificity testing of the newly synthesised phospho-DHX9 antibody. Although I was able to detect a band at the molecular weight representing DHX9 using this new antibody (Figure 4.9), By BLASTing the antibody epitope without a phosphorylated serine (TQPRRISAVS) (https://blast.ncbi.nlm.nih.gov/) revealed that the epitope can be found in other members of the DExD/H helicase family such as DHX36, DHX57, and DHX16 (Figure 6.1). However, there is no information addressing whether these other isoforms can be phosphorylated by PKA. Interestingly, the BLAST sequence revealed that only DHX57 and DHX8 are similar in amino acid length when compared to DHX9 (Table 6.1). All other isoforms were less than 1000 amino acids in length; therefore, we can assume that the band identified in our western blots were not these isoforms.

Table 6.1 Amino Acid length of DHX57, DHX8 and DHX9.

Protein	Length (AA)
DHX57_HUMAN	1,386
DHX8_HUMAN	1,220
DHX9_HUMAN	1,270

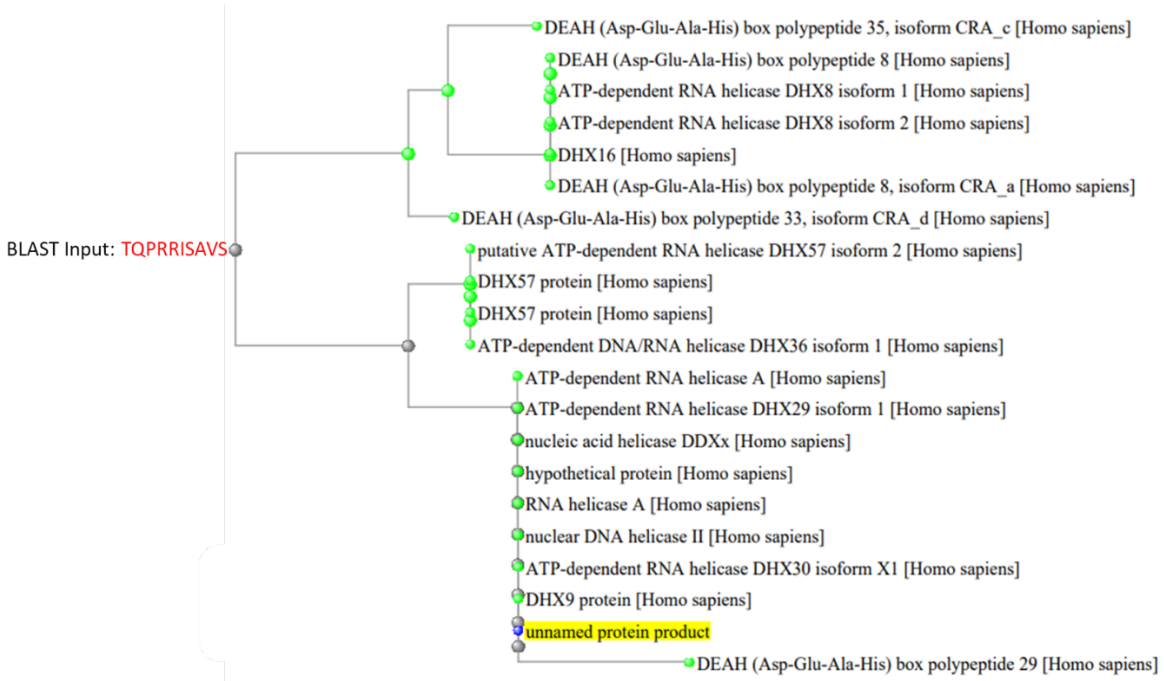

Figure 6.1 BLAST of the phospho-DHX9 epitope.

In order to confirm that the band seen in the western blots, and the signal detected in the ICC experiments, further siRNA experiments should be carried

out. Cells could be transfected with siDHX9, or other DExD/helicase isoforms, then treated with forskolin-IBMX for 3 minutes. In order to ensure that our new phospho-DHX9 antibody is detecting its unique antigen, we would only expect to see a decrease in phospho-DHX9 detection only in cells transfected with siDHX9. Furthermore, peptide arrays against other members of the DExD/H helicase family could have been synthesised and incubated with the phospho-DHX9 antibody. If this antibody could only specifically detect phosphorylated DHX9, we would not expect to see any spots in these other peptide arrays.

In addition to confirming that these two proteins are novel interactors, my thesis has also provided some information on how this interaction can influence DHX9's activity. By adapting the R-loop assay from the Hiom lab, I was able to demonstrate that the loss of PDE4D7-DHX9 interaction, either by decreasing PDE4D7 expression using siRNA or using our newly synthesised disruptor peptide, significantly decreased DHX9's ability to unwind the nascent RNA structure. However, for this assay to work correctly, it is reliant on the knockdown of SFPQ using siRNA. Unfortunately, theirs is no way of ensuring that the expression of this protein is sufficiently decreased before proceeding with ICC staining and confocal microscopy. Alternative assay should have been performed in order to further determine how PDE4D7 binding can affect DHX9 activity. Previous studies by Jain et al (2010) have used helicase assay in order to study DHX9 activity. This assay relies on the purification of recombinant DHX9, which is then incubated with DNA substrates and ATP. The reaction mix is then run on a DNA agarose gel to visualise how DHX9 can displace a strand of DNA (Jain *et al.*, 2010). Alternatively, other groups have used ATPase assays to study helicase activity. DHX9, like other members of the DExD/H helicase family, are ATPase dependent helicases and this is has been shown to be important in helicase activity (Ng *et al.*, 2018). ATPase assays have been used to characterize the helicase activity of UAP56, which is also a member of the DExD/H helicase family (Shen, Zhang and Zhao, 2007). ATPase assays rely on the incubation of the purified recombinant ATPase proteins with ATP, which in turn leads to the release of inorganic phosphate. The amount of phosphate released due to ATPase activity can be quantified using a colorimetric assay (Rule, Patrick and Sandkvist, 2016). Unfortunately, I was not able to use either of these two methods as I was unable to purify DHX9 from bacterial cells. Although I was able

to express the N-terminal and helicase fragments of DHX9, these remained stuck to the beads (Figure 3.14 D) and therefore not suitable for these assays. Future work for this project needs to include the optimization of the purification of GST-tagged DHX9. Not only would I be able to use this protein for helicase and ATPase assay, but we would be able to study how the interaction between PDE4D7 and DHX9 can affect DHX9's helicase activity. Furthermore, PDE4D7 and DHX9 purified protein can be used to further validate PDE4D7-DHX9 interaction by performing pure-protein IPs. The information collected from all these assays could provide us with invaluable information on how the interaction between PDE4D7 and DHX9 is important in the progression of disease.

6.7 Thesis conclusion

To conclude, the data presented in this thesis has shown that DHX9 is a novel interacting partner for PDE4D7 *in vitro*. DHX9 binds to PDE4D7 within its UCR1 domain, while PDE4D7 binding to DHX9 within its helicase domain. This interaction can be disrupted using the newly designed cell permeable disruptor peptides, which enabled me to confirm where the binding sites were. Interestingly, peptide array analysis revealed that DHX9 is readily phosphorylated by PKA at Ser^{449}, which can be found upstream of the PDE4D7 binding sequence. Disruption of the PDE4D7-DHX9 complex leads to the increase in the phosphorylation of DHX9 under basal conditions, suggesting that PDE4D7 plays an important role in regulating the phosphorylation of DHX9. The interaction between PDE4D7 and DHX9 was shown to be needed in order to unwind nascent RNAs when studied using an R-loop assay. Finally, using RPPA analysis, I was able to show that DHX9 is potentially part of the mTOR pathway. Research into DHX9, and other DExD/H helicases, is crucial in order to understand how this large family of proteins contributes to disease progression. My thesis has only scratched the surface on how DHX9 is involved in PC.

References

Adamo, P. and Ladomery, M. R. (2016) 'The oncogene ERG: A key factor in prostate cancer', *Oncogene*. Nature Publishing Group, 35(4), pp. 403–414. doi: 10.1038/onc.2015.109.

Agemy, L. *et al.* (2011) 'Targeted nanoparticle enhanced proapoptotic peptide as potential therapy for glioblastoma', *Proceedings of the National Academy of Sciences*, 108(42), pp. 17450 LP – 17455. doi: 10.1073/pnas.1114518108.

Ahdoot, M. *et al.* (2019) 'Contemporary treatments in prostate cancer focal therapy', *Current Opinion in Oncology*, 31(3), pp. 200–206. doi: 10.1097/CCO.0000000000000515.

Akbani, R. *et al.* (2014) 'Realizing the promise of reverse phase protein arrays for clinical, translational, and basic research: a workshop report: the RPPA (Reverse Phase Protein Array) society', *Molecular & cellular proteomics : MCP*. 2014/04/28. The American Society for Biochemistry and Molecular Biology, 13(7), pp. 1625–1643. doi: 10.1074/mcp.O113.034918.

Alasbahi, R. H. and Melzig, M. F. (2012) 'Forskolin and derivatives as tools for studying the role of cAMP.', *Die Pharmazie*. Germany, 67(1), pp. 5–13.

Albala, D. M. (2017) 'Imaging and treatment recommendations in patients with castrate-resistant prostate cancer.', *Reviews in urology*, 19(3), pp. 200–202. doi: 10.3909/riu193PracticeProfile.

Allison, D. F. and Wang, G. G. (2019) 'R-loops: formation, function, and relevance to cell stress', *Cell Stress*, 3(2), pp. 38–46. doi: 10.15698/cst2019.02.175.

Alquicer, G. *et al.* (2012) 'Development of a high-throughput fluorescence polarization assay to identify novel ligands of glutamate carboxypeptidase II', *Journal of biomolecular screening*. 2012/06/29, 17(8), pp. 1030–1040. doi: 10.1177/1087057112451924.

Altavilla, A. *et al.* (2012) 'Medical strategies for treatment of castration resistant prostate cancer (CRPC) docetaxel resistant', *Cancer Biology and Therapy*, 13(11), pp. 1004–1008. doi: 10.4161/cbt.21188.

Altschul, S. F. *et al.* (1997) 'Gapped BLAST and PSI-BLAST: a new generation of protein database search programs', *Nucleic acids research*, 25(17), pp. 3389–3402. doi: 10.1093/nar/25.17.3389.

Alvarez, M. G. and Besa, P. C. (2000) 'MOLECULAR BASIS OF CANCER AND CLINICAL APPLICATIONS', *Surgical Clinics of North America*, 80(2), pp. 443–457. doi: https://doi.org/10.1016/S0039-6109(05)70194-8.

Amunjela, J. N. and Tucker, S. J. (2016) 'POPDC proteins as potential novel therapeutic targets in cancer', *Drug Discovery Today*, 21(12), pp. 1920–1927. doi: https://doi.org/10.1016/j.drudis.2016.07.011.

Anassi, E. and Ndefo, U. A. (2011) 'Sipuleucel-T (provenge) injection: the first immunotherapy agent (vaccine) for hormone-refractory prostate cancer', *P & T : a peer-reviewed journal for formulary management*. MediMedia USA, Inc., 36(4), pp. 197–202. Available at: https://pubmed.ncbi.nlm.nih.gov/21572775.

Anckar, J. and Sistonen, L. (2007) 'SUMO: getting it on', *Biochemical Society Transactions*, 35(6), pp. 1409–1413. doi: 10.1042/BST0351409.

Andreou, A. M. and Tavernarakis, N. (2009) 'SUMOylation and cell signalling', *Biotechnology Journal*. John Wiley & Sons, Ltd, 4(12), pp. 1740–1752. doi: 10.1002/biot.200900219.

Arap, W. *et al.* (2002) 'Targeting the prostate for destruction through a vascular address', *Proceedings of the National Academy of Sciences of the United States of America*. The National Academy of Sciences, 99(3), pp. 1527–1531. doi: 10.1073/pnas.241655998.

Aratani, S. *et al.* (2001) 'Dual roles of RNA helicase A in CREB-dependent transcription', *Molecular and cellular biology*. American Society for Microbiology, 21(14), pp. 4460–4469. doi: 10.1128/MCB.21.14.4460-4469.2001.

Ardito, F. *et al.* (2017) 'The crucial role of protein phosphorylation in cell signaling and its use as targeted therapy (Review)', *International journal of molecular medicine*. 2017/06/22. D.A. Spandidos, 40(2), pp. 271–280. doi: 10.3892/ijmm.2017.3036.

Arencibia, J. M. *et al.* (2013) 'AGC protein kinases: From structural mechanism of regulation to allosteric drug development for the treatment of human

diseases', *Biochimica et Biophysica Acta (BBA) - Proteins and Proteomics*, 1834(7), pp. 1302–1321. doi: https://doi.org/10.1016/j.bbapap.2013.03.010.

Argasinska, J. *et al.* (2004) 'A functional interaction between RHA and Ubc9, an E2-like enzyme specific for Sumo-1', *Journal of Molecular Biology*, 341(1), pp. 15–25. doi: 10.1016/j.jmb.2004.06.004.

Arkin, M. R. *et al.* (2004) 'Inhibition of Protein-Protein Interactions: Non-Cellular Assay Formats', *Assay Guidance Manual*, (Md), pp. 1–23. Available at: http://www.ncbi.nlm.nih.gov/pubmed/22553871.

Armstrong, C. M. and Gao, A. C. (2019) 'Current strategies for targeting the activity of androgen receptor variants', *Asian Journal of Urology*. Elsevier Ltd, 6(1), pp. 42–49. doi: 10.1016/j.ajur.2018.07.003.

Aschoff, P. *et al.* (2011) *Clinical MRI of the abdomen: Why,how,when*, *Clinical MRI of the Abdomen: Why,How,When*. doi: 10.1007/978-3-540-85689-4.

Attard, G. *et al.* (2018) 'Abiraterone alone or in combination with enzalutamide in metastatic castration-resistant prostate cancer with rising prostate-specific antigen during enzalutamide treatment', *Journal of Clinical Oncology*, 36(25), pp. 2639–2646. doi: 10.1200/JCO.2018.77.9827.

Augello, M. ., Den, R. . and Knudsen, K. E. (2014) 'AR function in promoting metastatic prostate cancer', *Cancer Metastasis Rev*, 33(0), pp. 399–411. doi: 10.1016/j.physbeh.2017.03.040.

Autenrieth, K. *et al.* (2016) 'Defining A-Kinase Anchoring Protein (AKAP) Specificity for the Protein Kinase A Subunit RI (PKA-RI)', *Chembiochem : a European journal of chemical biology*. 2015/12/17, 17(8), pp. 693–697. doi: 10.1002/cbic.201500632.

Baguley, B. C., Hicks, K. O. and Wilson, W. R. (2002) 'Chapter 15 - Tumour cell cultures in drug development', in Baguley, B. C. and Kerr, D. J. B. T.-A. D. D. (eds). San Diego: Academic Press, pp. 269-cp1. doi: https://doi.org/10.1016/B978-012072651-6/50016-4.

Bahrami-B, F. *et al.* (2014) 'p70 Ribosomal protein S6 kinase (Rps6kb1): an update', *Journal of Clinical Pathology*, 67(12), pp. 1019 LP – 1025. doi: 10.1136/jclinpath-2014-202560.

Baillie, G. S. *et al.* (2000) 'Sub-family selective actions in the ability of Erk2 MAP kinase to phosphorylate and regulate the activity of PDE4 cyclic AMP-specific phosphodiesterases', *British Journal of Pharmacology*, 131(4), pp. 811–819. doi: 10.1038/sj.bjp.0703636.

Baillie, G. S., Tejeda, G. S. and Kelly, M. P. (2019a) 'Therapeutic targeting of 3′,5′-cyclic nucleotide phosphodiesterases: inhibition and beyond', *Nature Reviews Drug Discovery*, 18(10), pp. 770–796. doi: 10.1038/s41573-019-0033-4.

Baillie, G. S., Tejeda, G. S. and Kelly, M. P. (2019b) 'Therapeutic targeting of 3′,5′-cyclic nucleotide phosphodiesterases: inhibition and beyond', *Nature Reviews Drug Discovery*. Portland Press Ltd., 47(5), pp. 770–796. doi: 10.1038/s41573-019-0033-4.

Barber, K. W. and Rinehart, J. (2018) 'The ABCs of PTMs', *Nature chemical biology*, 14(3), pp. 188–192. doi: 10.1038/nchembio.2572.

Barford, D., Das, A. K. and Egloff, M.-P. (1998) 'The structure and mechanism of protein phosphatases: Insights into Catalysis and Regulation', *Annual Review of Biophysics and Biomolecular Structure*. Annual Reviews, 27(1), pp. 133–164. doi: 10.1146/annurev.biophys.27.1.133.

Bartek, J. and Lukas, J. (2003) 'Chk1 and Chk2 kinases in checkpoint control and cancer', *Cancer Cell*, 3(5), pp. 421–429. doi: https://doi.org/10.1016/S1535-6108(03)00110-7.

Beard, M. B. *et al.* (2000) 'UCR1 and UCR2 domains unique to the cAMP-specific phosphodiesterase family form a discrete module via electrostatic interactions', *The Journal of biological chemistry*. United States, 275(14), pp. 10349–10358. doi: 10.1074/jbc.275.14.10349.

Bedford, M. T. (2006) 'Methylation of Proteins BT - Encyclopedic Reference of Genomics and Proteomics in Molecular Medicine', in. Berlin, Heidelberg: Springer Berlin Heidelberg, pp. 1070–1075. doi: 10.1007/3-540-29623-9_2780.

Beebe-Dimmer, J. L. *et al.* (2018) 'Patterns of Bicalutamide Use in Prostate Cancer Treatment: A U.S. Real-World Analysis Using the SEER-Medicare Database', *Advances in therapy*. 2018/06/26. Springer Healthcare, 35(9), pp. 1438–1451. doi: 10.1007/s12325-018-0738-5.

Beltejar, M.-C. G. *et al.* (2017) 'Analyses of PDE-regulated phosphoproteomes reveal unique and specific cAMP-signaling modules in T cells', *Proceedings of the National Academy of Sciences of the United States of America*. 2017/06/20. National Academy of Sciences, 114(30), pp. E6240–E6249. doi: 10.1073/pnas.1703939114.

Beltrao, P. *et al.* (2013) 'Evolution and functional cross-talk of protein post-translational modifications', *Molecular systems biology*. European Molecular Biology Organization, 9, p. 714. doi: 10.1002/msb.201304521.

Di Benedetto, G. *et al.* (2008) 'Protein kinase A type I and type II define distinct intracellular signaling compartments.', *Circulation research*. United States, 103(8), pp. 836–844. doi: 10.1161/CIRCRESAHA.108.174813.

Bennett, N. C. *et al.* (2010) 'Molecular cell biology of androgen receptor signalling', *International Journal of Biochemistry and Cell Biology*. Elsevier Ltd, 42(6), pp. 813–827. doi: 10.1016/j.biocel.2009.11.013.

Berglund, L. *et al.* (2008) 'A genecentric Human Protein Atlas for expression profiles based on antibodies.', *Molecular & cellular proteomics : MCP*. United States, 7(10), pp. 2019–2027. doi: 10.1074/mcp.R800013-MCP200.

Bhalla, J. *et al.* (2006) 'Local Flexibility in Molecular Function Paradigm', *Molecular & Cellular Proteomics*, 5(7), pp. 1212 LP – 1223. doi: 10.1074/mcp.M500315-MCP200.

Biron, E. and Bédard, F. (2016) 'Recent progress in the development of protein–protein interaction inhibitors targeting androgen receptor–coactivator binding in prostate cancer', *The Journal of Steroid Biochemistry and Molecular Biology*, 161, pp. 36–44. doi: https://doi.org/10.1016/j.jsbmb.2015.07.006.

Blair, C. M. *et al.* (2019) 'Targeting B-Raf inhibitor resistant melanoma with novel cell penetrating peptide disrupters of PDE8A – C-Raf', *BMC Cancer*, 19(1), p. 266. doi: 10.1186/s12885-019-5489-4.

Blair, C. M. and Baillie, G. S. (2019) 'Reshaping cAMP nanodomains through targeted disruption of compartmentalised phosphodiesterase signalosomes', *Biochemical Society Transactions*, 47(5), pp. 1405–1414. doi: 10.1042/BST20190252.

Blom, N., Gammeltoft, S. and Brunak, S. (1999) 'Sequence and structure-based prediction of eukaryotic protein phosphorylation sites1 1Edited by F. E. Cohen', *Journal of Molecular Biology*, 294(5), pp. 1351–1362. doi: https://doi.org/10.1006/jmbi.1999.3310.

Bobrich, M. *et al.* (2013) 'PTPIP51: A new interaction partner of the insulin receptor and PKA in adipose tissue', *Journal of obesity*, 2013, p. 476240. doi: 10.1155/2013/476240.

Boccon-Gibod, L., Van Der Meulen, E. and Persson, bo E. (2011) 'An update on the use of gonadotropin-releasing hormone antagonists in prostate cancer', *Therapeutic Advances in Urology*, 3(3), pp. 127–140. doi: 10.1177/1756287211414457.

Boguslawski, S. J. *et al.* (1986) 'Characterization of monoclonal antibody to DNA · RNA and its application to immunodetection of hybrids', *Journal of Immunological Methods*, 89(1), pp. 123–130. doi: https://doi.org/10.1016/0022-1759(86)90040-2.

van Bokhoven, A. *et al.* (2003) 'Molecular characterization of human prostate carcinoma cell lines', *The Prostate*. John Wiley & Sons, Ltd, 57(3), pp. 205–225. doi: 10.1002/pros.10290.

Boohaker, R. J. *et al.* (2012) 'The use of therapeutic peptides to target and to kill cancer cells', *Current medicinal chemistry*, 19(22), pp. 3794–3804. doi: 10.2174/092986712801661004.

Böttcher, R. *et al.* (2015) 'Human phosphodiesterase 4D7 (PDE4D7) expression is increased in TMPRSS2-ERG-positive primary prostate cancer and independently adds to a reduced risk of post-surgical disease progression', *British Journal of Cancer*, 113(10), pp. 1502–1511. doi: 10.1038/bjc.2015.335.

Böttcher, R *et al.* (2015) 'Human phosphodiesterase 4D7 (PDE4D7) expression is increased in TMPRSS2-ERG-positive primary prostate cancer and independently adds to a reduced risk of post-surgical disease progression', *British Journal of Cancer*, 113(10), pp. 1502–1511. doi: 10.1038/bjc.2015.335.

Böttcher, R. *et al.* (2016) 'Human PDE4D isoform composition is deregulated in primary prostate cancer and indicative for disease progression and development

of distant metastases', *Oncotarget*. Impact Journals LLC, 7(43), pp. 70669–70684. doi: 10.18632/oncotarget.12204.

Brand, T. (2018) 'The Popeye Domain Containing Genes and Their Function as cAMP Effector Proteins in Striated Muscle', *Journal of cardiovascular development and disease*. MDPI, 5(1), p. 18. doi: 10.3390/jcdd5010018.

Bray, F. *et al.* (2018) 'Global cancer statistics 2018: GLOBOCAN estimates of incidence and mortality worldwide for 36 cancers in 185 countries.', *CA: a cancer journal for clinicians*. United States, 68(6), pp. 394–424. doi: 10.3322/caac.21492.

Brenner, J. C. *et al.* (2011) 'Mechanistic rationale for inhibition of poly(ADP-ribose) polymerase in ETS gene fusion-positive prostate cancer', *Cancer cell*, 19(5), pp. 664–678. doi: 10.1016/j.ccr.2011.04.010.

Brosh, R. M. (2013) 'DNA helicases involved in DNA repair and their roles in cancer', *Nature Reviews Cancer*, 13(8), pp. 542–558. doi: 10.1038/nrc3560.

Brown, R. L. *et al.* (2006) 'The pharmacology of cyclic nucleotide-gated channels: emerging from the darkness', *Current pharmaceutical design*, 12(28), pp. 3597–3613. doi: 10.2174/138161206778522100.

Brunk, E. *et al.* (2018) 'Characterizing posttranslational modifications in prokaryotic metabolism using a multiscale workflow', *Proceedings of the National Academy of Sciences*, 115(43), pp. 11096 LP – 11101. doi: 10.1073/pnas.1811971115.

Bul, M. *et al.* (2013) 'Active surveillance for low-risk prostate cancer worldwide: The PRIAS study', *European Urology*, 63(4), pp. 597–603. doi: 10.1016/j.eururo.2012.11.005.

Burnstein, K. L. (2005) 'Regulation of androgen receptor levels: Implications for prostate cancer progression and therapy', *Journal of Cellular Biochemistry*, 95(4), pp. 657–669. doi: 10.1002/jcb.20460.

Butler, D. E. *et al.* (2017) 'Inhibition of the PI3K/AKT/mTOR pathway activates autophagy and compensatory Ras/Raf/MEK/ERK signalling in prostate cancer', *Oncotarget*. Impact Journals LLC, 8(34), pp. 56698–56713. doi: 10.18632/oncotarget.18082.

Butler, M. S. *et al.* (2017) 'Discovery and characterization of small molecules targeting the DNA-binding ETS domain of ERG in prostate cancer', *Oncotarget*. Impact Journals LLC, 8(26), pp. 42438–42454. doi: 10.18632/oncotarget.17124.

Byrne, A. M. (2014) 'Functional Characterisation of Phosphodiesterase 4D7 in Prostate Cancer A Thesis Presented by'.

Byrne, A. M. *et al.* (2015) 'The activity of cAMP-phosphodiesterase 4D7 (PDE4D7) is regulated by protein kinase A-dependent phosphorylation within its unique N-terminus', *FEBS letters*. 2015/02/11. Elsevier Science B.V, 589(6), pp. 750–755. doi: 10.1016/j.febslet.2015.02.004.

Cai, C. *et al.* (2009) 'Reactivation of Androgen Receptor Regulated TMPRSS2:ERG Gene Expression in Castration Resistant Prostate Cancer', *Cancer Research*, 69(15), pp. 6027–6032. doi: 10.1158/0008-5472.CAN-09-0395.Reactivation.

Cai, W. *et al.* (2017) 'Wanted DEAD/H or Alive: Helicases Winding Up in Cancers', *JNCI: Journal of the National Cancer Institute*, 109(6). doi: 10.1093/jnci/djw278.

Calebiro, D., Nikolaev, V. O. and Lohse, M. J. (2010) 'Imaging of persistent cAMP signaling by internalized G protein-coupled receptors', *Journal of Molecular Endocrinology*. Bristol, UK: Society for Endocrinology, 45(1), pp. 1–8. doi: 10.1677/JME-10-0014.

Capitanio, J. S., Montpetit, B. and Wozniak, R. W. (2017) 'Human Nup98 regulates the localization and activity of DExH/D-box helicase DHX9', *eLife*. eLife Sciences Publications, Ltd, 6, p. e18825. doi: 10.7554/eLife.18825.

Casey, R. G., Corcoran, N. M. and Goldenberg, S. L. (2012) 'Quality of life issues in men undergoing androgen deprivation therapy: a review', *Asian journal of andrology*. 2012/01/09. Nature Publishing Group, 14(2), pp. 226–231. doi: 10.1038/aja.2011.108.

Cato, L. *et al.* (2019) 'ARv7 Represses Tumor-Suppressor Genes in Castration-Resistant Prostate Cancer', *Cancer Cell*, 35(3), pp. 401-413.e6. doi: 10.1016/j.ccell.2019.01.008.

Cedervall, P. *et al.* (2015) 'Engineered stabilization and structural analysis of the autoinhibited conformation of PDE4', *Proceedings of the National Academy*

of Sciences of the United States of America. 2015/03/09. National Academy of Sciences, 112(12), pp. E1414–E1422. doi: 10.1073/pnas.1419906112.

Chakraborty, P., Huang, J. T. J. and Hiom, K. (2018) 'DHX9 helicase promotes R-loop formation in cells with impaired RNA splicing', *Nature Communications*, 9(1), p. 4346. doi: 10.1038/s41467-018-06677-1.

Chan, D. S.-H. *et al.* (2017) 'Effect of DMSO on Protein Structure and Interactions Assessed by Collision-Induced Dissociation and Unfolding', *Analytical Chemistry*. American Chemical Society, 89(18), pp. 9976–9983. doi: 10.1021/acs.analchem.7b02329.

Chandrasekaran, A. *et al.* (2008) 'Identification and characterization of novel mouse PDE4D isoforms: Molecular cloning, subcellular distribution and detection of isoform-specific intracellular localization signals', *Cellular Signalling*, 20(1), pp. 139–153. doi: https://doi.org/10.1016/j.cellsig.2007.10.003.

Chang, C.-C. *et al.* (2018) 'SUMOgo: Prediction of sumoylation sites on lysines by motif screening models and the effects of various post-translational modifications', *Scientific Reports*, 8(1), p. 15512. doi: 10.1038/s41598-018-33951-5.

Chappell, W. H. *et al.* (2012) 'p53 expression controls prostate cancer sensitivity to chemotherapy and the MDM2 inhibitor Nutlin-3', *Cell cycle (Georgetown, Tex.)*. 2012/11/27. Landes Bioscience, 11(24), pp. 4579–4588. doi: 10.4161/cc.22852.

Chen, C. *et al.* (2016) 'Construction and analysis of protein-protein interaction networks based on proteomics data of prostate cancer', *International journal of molecular medicine*. 2016/04/26. D.A. Spandidos, 37(6), pp. 1576–1586. doi: 10.3892/ijmm.2016.2577.

Chen, J. *et al.* (2020) 'Androgen receptor-regulated circFNTA activates KRAS signaling to promote bladder cancer invasion', *EMBO reports*. John Wiley & Sons, Ltd, 21(4), p. e48467. doi: 10.15252/embr.201948467.

Chen, N. and Zhou, Q. (2016) 'The evolving Gleason grading system', *Chinese journal of cancer research = Chung-kuo yen cheng yen chiu*. AME Publishing Company, 28(1), pp. 58–64. doi: 10.3978/j.issn.1000-9604.2016.02.04.

Chen, Y. W. *et al.* (2010) 'TMPRSS2, a serine protease expressed in the prostate on the apical surface of luminal epithelial cells and released into semen in prostasomes, is misregulated in prostate cancer cells', *American Journal of Pathology*, 176(6), pp. 2986–2996. doi: 10.2353/ajpath.2010.090665.

Chen, Z. and Lu, W. (2015) 'Roles of ubiquitination and SUMOylation on prostate cancer: mechanisms and clinical implications', *International journal of molecular sciences*. MDPI, 16(3), pp. 4560–4580. doi: 10.3390/ijms16034560.

Chin, C. L. *et al.* (2019) 'A human expression system based on HEK293 for the stable production of recombinant erythropoietin', *Scientific Reports*, 9(1), p. 16768. doi: 10.1038/s41598-019-53391-z.

Cho, Y. S. *et al.* (2000) 'Extracellular protein kinase A as a cancer biomarker: its expression by tumor cells and reversal by a myristate-lacking Calpha and RIIbeta subunit overexpression', *Proceedings of the National Academy of Sciences of the United States of America*. The National Academy of Sciences, 97(2), pp. 835–840. doi: 10.1073/pnas.97.2.835.

Choi, S. and Lee, A. K. (2011) 'Efficacy and safety of gonadotropin-releasing hormone agonists used in the treatment of prostate cancer', *Drug, Healthcare and Patient Safety*, 3(1), pp. 107–119. doi: 10.2147/dhps.s24106.

Choo, A. Y. *et al.* (2008) 'Rapamycin differentially inhibits S6Ks and 4E-BP1 to mediate cell-type-specific repression of mRNA translation', *Proceedings of the National Academy of Sciences*, 105(45), pp. 17414 LP – 17419. doi: 10.1073/pnas.0809136105.

Christian, F. *et al.* (2011) 'Small molecule AKAP-protein kinase A (PKA) interaction disruptors that activate PKA interfere with compartmentalized cAMP signaling in cardiac myocytes', *The Journal of biological chemistry*. 2010/12/22. American Society for Biochemistry and Molecular Biology, 286(11), pp. 9079–9096. doi: 10.1074/jbc.M110.160614.

Chung, E. Y. *et al.* (2017) 'The ETS Inhibitors Yk-4-279 and TK-216 Interfere with Spib and Synergize with Lenalidomide in Diffuse Large B Cell Lymphoma of the Activated B Cell-like Type (ABC DLBCL)', *Blood*, 130(Supplement 1), p. 2810. doi: 10.1182/blood.V130.Suppl_1.2810.2810.

Chung, S. *et al*. (2009) 'Overexpressing PKIB in prostate cancer promotes its aggressiveness by linking between PKA and Akt pathways', *Oncogene*, 28(32), pp. 2849–2859. doi: 10.1038/onc.2009.144.

Clark, E. L. *et al*. (2008) 'The RNA helicase p68 is a novel androgen receptor coactivator involved in splicing and is overexpressed in prostate cancer', *Cancer research*, 68(19), pp. 7938–7946. doi: 10.1158/0008-5472.CAN-08-0932.

Colla, E. *et al*. (2006) 'TonEBP is inhibited by RNA helicase A via interaction involving the E'F loop', *The Biochemical journal*. Portland Press Ltd., 393(Pt 1), pp. 411–419. doi: 10.1042/BJ20051082.

Collazo, J. *et al*. (2014) 'Cofilin drives cell-invasive and metastatic responses to TGF-ß in prostate cancer', *Cancer research*. 2014/02/07, 74(8), pp. 2362–2373. doi: 10.1158/0008-5472.CAN-13-3058.

Conley-LaComb, M. K. *et al*. (2013) 'PTEN loss mediated Akt activation promotes prostate tumor growth and metastasis via CXCL12/CXCR4 signaling', *Molecular Cancer*, 12(1), p. 85. doi: 10.1186/1476-4598-12-85.

Corbi-Verge, C. and Kim, P. M. (2016) 'Motif mediated protein-protein interactions as drug targets', *Cell communication and signaling : CCS*. BioMed Central, 14, p. 8. doi: 10.1186/s12964-016-0131-4.

Crawford, E. D. *et al*. (2018) 'FSH suppression and tumour control in patients with prostate cancer during androgen deprivation with a GnRH agonist or antagonist', *Scandinavian Journal of Urology*. Taylor & Francis, 52(5–6), pp. 349–357. doi: 10.1080/21681805.2018.1522372.

Crawford, E. D. *et al*. (2019) 'Androgen-targeted therapy in men with prostate cancer: evolving practice and future considerations', *Prostate Cancer and Prostatic Diseases*, 22(1), pp. 24–38. doi: 10.1038/s41391-018-0079-0.

Creighton, C. J. and Huang, S. (2015) 'Reverse phase protein arrays in signaling pathways: a data integration perspective', *Drug design, development and therapy*. Dove Medical Press, 9, pp. 3519–3527. doi: 10.2147/DDDT.S38375.

Cristini, A. *et al*. (2018) 'RNA/DNA Hybrid Interactome Identifies DXH9 as a Molecular Player in Transcriptional Termination and R-Loop-Associated DNA Damage', *Cell reports*. Cell Press, 23(6), pp. 1891–1905. doi:

10.1016/j.celrep.2018.04.025.

Croney, D. M. J. and J. C. (2003) 'Fluorescence Polarization: Past, Present and Future', *Combinatorial Chemistry & High Throughput Screening*, pp. 167–176. doi: http://dx.doi.org/10.2174/138620703106298347.

Crossley, M. P., Bocek, M. and Cimprich, K. A. (2019) 'R-Loops as Cellular Regulators and Genomic Threats', *Molecular cell*, 73(3), pp. 398–411. doi: 10.1016/j.molcel.2019.01.024.

Crumbaker, M., Khoja, L. and Joshua, A. M. (2017) 'AR Signaling and the PI3K Pathway in Prostate Cancer', *Cancers*. MDPI, 9(4), p. 34. doi: 10.3390/cancers9040034.

Culig, Z. *et al.* (2003) 'Androgen receptors in prostate cancer', *Journal of Urology*, 170(4 I), pp. 1363–1369. doi: 10.1097/01.ju.0000075099.20662.7f.

Cunningham, D. and You, Z. (2015) 'In vitro and in vivo model systems used in prostate cancer research', *Journal of biological methods*, 2(1), p. e17. doi: 10.14440/jbm.2015.63.

Cutress, M. L. *et al.* (2008) 'Structural basis for the nuclear import of the human androgen receptor', *Journal of Cell Science*, 121(7), pp. 957–968. doi: 10.1242/jcs.022103.

Dai, T.-Y. *et al.* (2014) 'P68 RNA helicase as a molecular target for cancer therapy', *Journal of Experimental & Clinical Cancer Research*, 33(1), p. 64. doi: 10.1186/s13046-014-0064-y.

Damodaran, S., Kyriakopoulos, C. E. and Jarrard, D. F. (2017) 'Newly Diagnosed Metastatic Prostate Cancer: Has the Paradigm Changed?', *The Urologic clinics of North America*, 44(4), pp. 611–621. doi: 10.1016/j.ucl.2017.07.008.

Daniels, G. *et al.* (2013) 'Mini-review: androgen receptor phosphorylation in prostate cancer', *American journal of clinical and experimental urology*. e-Century Publishing Corporation, 1(1), pp. 25–29. Available at: https://pubmed.ncbi.nlm.nih.gov/25374897.

Datta, A. and Brosh, R. M. (2018) 'New Insights Into DNA Helicases as Druggable Targets for Cancer Therapy', *Frontiers in Molecular Biosciences*, 5, p. 59. doi:

10.3389/fmolb.2018.00059.

Davenport, A. P. *et al*. (2020) ‘Advances in therapeutic peptides targeting G protein-coupled receptors’, *Nature Reviews Drug Discovery*, 19(6), pp. 389–413. doi: 10.1038/s41573-020-0062-z.

Davey, R. and Grossmann, M. (2016) ‘Androgen Receptor Structure, Function and Biology: From Bench to Bedside’, *The Clinical Biochemist Review*, 37(1), pp. 3–15. Available at: https://www.ncbi.nlm.nih.gov/pmc/articles/PMC4810760/.

David, M. K. and Gopal, S. (2020) ‘Prostate Specific Antigen (PSA).’, in. Treasure Island (FL).

Debes, J. D. *et al*. (2005) ‘p300 Regulates Androgen Receptor–Independent Expression of Prostate-Specific Antigen in Prostate Cancer Cells Treated Chronically with Interleukin-6’, *Cancer Research*, 65(13), pp. 5965 LP – 5973. doi: 10.1158/0008-5472.CAN-04-2837.

Deshayes, E. *et al*. (2017) ‘Radium 223 dichloride for prostate cancer treatment’, *Drug design, development and therapy*. Dove Medical Press, 11, pp. 2643–2651. doi: 10.2147/DDDT.S122417.

Ding, X. *et al*. (2019) ‘A DHX9-lncRNA-MDM2 interaction regulates cell invasion and angiogenesis of cervical cancer’, *Cell Death & Differentiation*, 26(9), pp. 1750–1765. doi: 10.1038/s41418-018-0242-0.

Don, A. S. A. and Zheng, X. F. S. (2011) ‘Recent clinical trials of mTOR-targeted cancer therapies.’, *Reviews on recent clinical trials*. United Arab Emirates, 6(1), pp. 24–35. doi: 10.2174/157488711793980147.

Doscas, M. E. *et al*. (2014) ‘Inhibition of p70 S6 kinase (S6K1) activity by A77 1726 and its effect on cell proliferation and cell cycle progress’, *Neoplasia (New York, N.Y.)*. Neoplasia Press, 16(10), pp. 824–834. doi: 10.1016/j.neo.2014.08.006.

Drescher, D. G., Ramakrishnan, N. A. and Drescher, M. J. (2009) ‘Surface plasmon resonance (SPR) analysis of binding interactions of proteins in inner-ear sensory epithelia’, *Methods in molecular biology (Clifton, N.J.)*, 493, pp. 323–343. doi: 10.1007/978-1-59745-523-7_20.

Dunn, K. W., Kamocka, M. M. and McDonald, J. H. (2011) 'A practical guide to evaluating colocalization in biological microscopy', *American journal of physiology. Cell physiology*. 2011/01/05. American Physiological Society, 300(4), pp. C723–C742. doi: 10.1152/ajpcell.00462.2010.

Eastman, A. (2017) 'Improving anticancer drug development begins with cell culture: misinformation perpetrated by the misuse of cytotoxicity assays', *Oncotarget*. Impact Journals LLC, 8(5), pp. 8854–8866. doi: 10.18632/oncotarget.12673.

Edwards, H. V, Scott, J. D. and Baillie, G. S. (2012) 'PKA phosphorylation of the small heat-shock protein Hsp20 enhances its cardioprotective effects', *Biochemical Society transactions*, 40(1), pp. 210–214. doi: 10.1042/BST20110673.

Edwards, J. *et al.* (2001) 'Amplification of the androgen receptor may not explain the development of androgen-independent prostate cancer', *BJU International*. John Wiley & Sons, Ltd, 88(6), pp. 633–637. doi: 10.1046/j.1464-410X.2001.02350.x.

Edwards, J. *et al.* (2003) 'Androgen receptor gene amplification and protein expression in hormone refractory prostate cancer', *British journal of cancer*. Nature Publishing Group, 89(3), pp. 552–556. doi: 10.1038/sj.bjc.6601127.

Edwards, J. and Bartlett, J. M. S. (2005) 'The androgen receptor and signal-transduction pathways in hormone-refractory prostate cancer. Part 1: modifications to the androgen receptor', *BJU International*. John Wiley & Sons, Ltd, 95(9), pp. 1320–1326. doi: 10.1111/j.1464-410X.2005.05526.x.

Eisermann, K. *et al.* (2013) 'Androgen receptor gene mutation, rearrangement, polymorphism', *Translational Andrology and Urology*, 2(3), pp. 137–147. doi: 10.3978/j.issn.2223-4683.2013.09.15.

Epstein, J. I. *et al.* (2016) 'A Contemporary Prostate Cancer Grading System: A Validated Alternative to the Gleason Score.', *European urology*, 69(3), pp. 428–435. doi: 10.1016/j.eururo.2015.06.046.

Erkizan, H. V *et al.* (2009) 'A small molecule blocking oncogenic protein EWS-FLI1 interaction with RNA helicase A inhibits growth of Ewing's sarcoma', *Nature*

medicine. 2009/07/05, 15(7), pp. 750–756. doi: 10.1038/nm.1983.

Falcone, C. and Mazzoni, C. (2018) 'RNA stability and metabolism in regulated cell death, aging and diseases', *FEMS Yeast Research*, 18(6). doi: 10.1093/femsyr/foy050.

Fang, J. *et al*. (2007) 'PI3K/PTEN/AKT signaling regulates prostate tumor angiogenesis', *Cellular signalling*. 2007/08/15, 19(12), pp. 2487–2497. doi: 10.1016/j.cellsig.2007.07.025.

Fang, L. C., Merrick, G. S. and Wallner, K. (2008) 'Androgen-deprivation Therapy— A Help or a Hindrance for Survival in High-risk Prostate Cancer?', *Oncology & Hematology Review (US)*, 04(01), p. 55. doi: 10.17925/ohr.2008.04.1.55.

Farkona, S., Diamandis, E. P. and Blasutig, I. M. (2016) 'Cancer immunotherapy: the beginning of the end of cancer?', *BMC Medicine*, 14(1), p. 73. doi: 10.1186/s12916-016-0623-5.

Fay, E. K. and Graff, J. N. (2020) 'Immunotherapy in Prostate Cancer', *Cancers*. MDPI, 12(7), p. 1752. doi: 10.3390/cancers12071752.

Feldman, B. J. and Feldman, D. (2001) 'ANDROGEN-INDEPENDENT PROSTATE CANCER', 1(October), pp. 34–45.

Feng, Z. *et al*. (2005) 'The coordinate regulation of the p53 and mTOR pathways in cells', *Proceedings of the National Academy of Sciences of the United States of America*. 2005/05/31. National Academy of Sciences, 102(23), pp. 8204–8209. doi: 10.1073/pnas.0502857102.

Feng, Z. (2010) 'p53 regulation of the IGF-1/AKT/mTOR pathways and the endosomal compartment', *Cold Spring Harbor perspectives in biology*. Cold Spring Harbor Laboratory Press, 2(2), pp. a001057–a001057. doi: 10.1101/cshperspect.a001057.

Ferre, S. (2015) 'The GPCR Heterotetramer: Challenging Classical Pharmacology', *Trends Pharmacol Sci*, 36(3), pp. 145–152. doi: doi:10.1016/j.tips.2015.01.002.

Fertig, B. A. and Baillie, G. S. (2018a) 'PDE4-Mediated cAMP Signalling', *Journal*

of cardiovascular development and disease. MDPI, 5(1), p. 8. doi: 10.3390/jcdd5010008.

Fertig, B. A. and Baillie, G. S. (2018b) 'PDE4-Mediated cAMP Signalling', *Journal of cardiovascular development and disease*. MDPI, 5(1), p. 8. doi: 10.3390/jcdd5010008.

Fidaleo, M., De Paola, E. and Paronetto, M. P. (2016) 'The RNA helicase A in malignant transformation', *Oncotarget*. Impact Journals LLC, 7(19), pp. 28711–28723. doi: 10.18632/oncotarget.7377.

Flück, C. E. and Pandey, A. V. (2014) 'Steroidogenesis of the testis - new genes and pathways', *Annales d'Endocrinologie*. Elsevier Masson SAS, 75(2), pp. 40–47. doi: 10.1016/j.ando.2014.03.002.

Formosa, R. and Vassallo, J. (2014) 'cAMP signalling in the normal and tumorigenic pituitary gland', *Molecular and Cellular Endocrinology*. Elsevier, 392(1–2), pp. 37–50. doi: 10.1016/J.MCE.2014.05.004.

Fosgerau, K. and Hoffmann, T. (2015) 'Peptide therapeutics: current status and future directions', *Drug Discovery Today*, 20(1), pp. 122–128. doi: https://doi.org/10.1016/j.drudis.2014.10.003.

Francis, S. H., Blount, M. A. and Corbin, J. D. (2011) 'Mammalian Cyclic Nucleotide Phosphodiesterases: Molecular Mechanisms and Physiological Functions', *Physiological Reviews*. American Physiological Society, 91(2), pp. 651–690. doi: 10.1152/physrev.00030.2010.

Franks, T. M. and Hetzer, M. W. (2013) 'The role of Nup98 in transcription regulation in healthy and diseased cells', *Trends in cell biology*. 2012/12/13, 23(3), pp. 112–117. doi: 10.1016/j.tcb.2012.10.013.

Freeman, E. R., Bloom, D. A. and McGuire, E. J. (2001) 'A brief history of testosterone', *Journal of Urology*, 165(2), pp. 371–373. doi: 10.1097/00005392-200102000-00004.

Fujimoto, N. *et al*. (2007) 'Prostate cancer cells increase androgen sensitivity by increase in nuclear androgen receptor and androgen receptor coactivators; a possible mechanism of hormone-resistance of prostate cancer cells', *Cancer Investigation*, 25(1), pp. 32–37. doi: 10.1080/07357900601130698.

Fujita, K. and Nonomura, N. (2018) ‘Role of Androgen Receptor in Prostate Cancer: A Review’, *The World Journal of Men’s Health*, 36. doi: 10.5534/wjmh.180040.

Fulda, S. *et al.* (2010) ‘Cellular stress responses: Cell survival and cell death’, *International Journal of Cell Biology*, 2010. doi: 10.1155/2010/214074.

Fuller-Pace, F. V (2006) ‘DExD/H box RNA helicases: multifunctional proteins with important roles in transcriptional regulation’, *Nucleic acids research*. 2006/08/25. Oxford University Press, 34(15), pp. 4206–4215. doi: 10.1093/nar/gkl460.

Fuller-Pace, F. V (2013) ‘DEAD box RNA helicase functions in cancer’, *RNA biology*. 2013/01/01. Landes Bioscience, 10(1), pp. 121–132. doi: 10.4161/rna.23312.

Gambardella, V. *et al.* (2020) ‘Personalized Medicine: Recent Progress in Cancer Therapy.’, *Cancers*, 12(4). doi: 10.3390/cancers12041009.

Gan, J. *et al.* (2015) ‘Proteomic profiling identifies the SIM-associated complex of KSHV-encoded LANA’, *PROTEOMICS*. John Wiley & Sons, Ltd, 15(12), pp. 2023–2037. doi: 10.1002/pmic.201400624.

Gao, X. *et al.* (2008) ‘Proteome-wide prediction of PKA phosphorylation sites in eukaryotic kingdom’, *Genomics*, 92(6), pp. 457–463. doi: https://doi.org/10.1016/j.ygeno.2008.08.013.

Gao, Y. *et al.* (2019) ‘Serum PSA levels in patients with prostate cancer and other 33 different types of diseases’, *Progress in Molecular Biology and Translational Science*, 162, pp. 377–390.

Gaudreau, P.-O. *et al.* (2016) ‘The Present and Future of Biomarkers in Prostate Cancer: Proteomics, Genomics, and Immunology Advancements’, *Biomarkers in Cancer*, 8s2, p. BIC.S31802. doi: 10.4137/BIC.S31802.

Geiss-Friedlander, R. and Melchior, F. (2007) ‘Concepts in sumoylation: a decade on’, *Nature Reviews Molecular Cell Biology*, 8(12), pp. 947–956. doi: 10.1038/nrm2293.

Gelman, I. H. (2016) ‘How the TRAMP Model Revolutionized the Study of Prostate

Cancer Progression', *Cancer Research*, 76(21), pp. 6137 LP – 6139. doi: 10.1158/0008-5472.CAN-16-2636.

George, D. J. *et al.* (2020) 'Phase 2 clinical trial of TORC1 inhibition with everolimus in men with metastatic castration-resistant prostate cancer.', *Urologic oncology*. United States, 38(3), pp. 79.e15-79.e22. doi: 10.1016/j.urolonc.2019.08.015.

Georgi, B. *et al.* (2014) 'Evolving therapeutic concepts in prostate cancer based on genome-wide analyses (Review)', *Int J Oncol*. Department of Urology, University of Heidelberg, 45(4), pp. 1337–1344. doi: 10.3892/ijo.2014.2567.

Gerber, D. E. (2008) 'EGFR Inhibition in the Treatment of Non-Small Cell Lung Cancer', *Drug development research*, 69(6), pp. 359–372. doi: 10.1002/ddr.20268.

Gierisch, M. E. *et al.* (2016) 'Proteasomal Degradation of the EWS-FLI1 Fusion Protein Is Regulated by a Single Lysine Residue', *The Journal of biological chemistry*. 2016/11/08. American Society for Biochemistry and Molecular Biology, 291(52), pp. 26922–26933. doi: 10.1074/jbc.M116.752063.

Gomella, L. G. (2003) 'Effective testosterone suppression for patients with prostate cancer: Is there a best castration?', *Urology*, 62(2), pp. 207–213. doi: 10.1016/S0090-4295(03)00331-5.

Gordetsky, J. and Epstein, J. (2016) 'Grading of prostatic adenocarcinoma: Current state and prognostic implications', *Diagnostic Pathology*. Diagnostic Pathology, 11(1), pp. 2–9. doi: 10.1186/s13000-016-0478-2.

Gottlieb, B. *et al.* (2012) 'The androgen receptor gene mutations database: 2012 update', *Human Mutation*, 33(5), pp. 887–894. doi: 10.1002/humu.22046.

Graham, L. *et al.* (2018) 'A phase II study of the dual mTOR inhibitor MLN0128 in patients with metastatic castration resistant prostate cancer.', *Investigational new drugs*, 36(3), pp. 458–467. doi: 10.1007/s10637-018-0578-9.

Green, S. M., Mostaghel, E. A. and Nelson, P. S. (2012) 'Androgen action and metabolism in prostate cancer', *Molecular and Cellular Endocrinology*, 360(0), pp. 3–13. doi: 10.1016/j.mce.2011.09.046.

Greene, J. *et al.* (2019) 'Circular RNAs are differentially expressed in prostate cancer and are potentially associated with resistance to enzalutamide', *Scientific Reports*, 9(1), p. 10739. doi: 10.1038/s41598-019-47189-2.

Gunther, J. R. *et al.* (2009) 'A set of time-resolved fluorescence resonance energy transfer assays for the discovery of inhibitors of estrogen receptor-coactivator binding', *Journal of biomolecular screening*. 2009/02/04, 14(2), pp. 181–193. doi: 10.1177/1087057108329349.

Guo, Z. *et al.* (2009) 'A novel androgen receptor splice variant is up-regulated during prostate cancer progression and promotes androgen depletion-resistant growth', *Cancer research*. 2009/02/24, 69(6), pp. 2305–2313. doi: 10.1158/0008-5472.CAN-08-3795.

Gustafson, E. A. and Wessel, G. M. (2010) 'DEAD-box helicases: posttranslational regulation and function', *Biochemical and biophysical research communications*. 2010/03/03, 395(1), pp. 1–6. doi: 10.1016/j.bbrc.2010.02.172.

Habault, J. and Poyet, J.-L. (2019) 'Recent Advances in Cell Penetrating Peptide-Based Anticancer Therapies', *Molecules (Basel, Switzerland)*. MDPI, 24(5), p. 927. doi: 10.3390/molecules24050927.

Hägglöf, C. *et al.* (2014) 'TMPRSS2-ERG expression predicts prostate cancer survival and associates with stromal biomarkers', *PLoS ONE*, 9(2). doi: 10.1371/journal.pone.0086824.

Hall, M. D. *et al.* (2016) 'Fluorescence polarization assays in high-throughput screening and drug discovery: a review', *Methods and applications in fluorescence*, 4(2), p. 22001. doi: 10.1088/2050-6120/4/2/022001.

Halpin, D. M. G. (2008) 'ABCD of the phosphodiesterase family: interaction and differential activity in COPD', *International journal of chronic obstructive pulmonary disease*. Dove Medical Press, 3(4), pp. 543–561. doi: 10.2147/copd.s1761.

Hanahan, D. and Weinberg, R. A. (2011) 'Hallmarks of Cancer: The Next Generation', *Cell*. Elsevier, 144(5), pp. 646–674. doi: 10.1016/j.cell.2011.02.013.

Hannoun, Z. *et al.* (2010) 'Post-translational modification by SUMO', *Toxicology*,

278(3), pp. 288–293. doi: https://doi.org/10.1016/j.tox.2010.07.013.

Hara, I. *et al.* (2018) 'Enzalutamide Versus Abiraterone as a First-Line Endocrine Therapy for Castration-Resistant Prostate Cancer: Protocol for a Multicenter Randomized Phase 3 Trial', *JMIR research protocols*. JMIR Publications, 7(7), pp. e11191–e11191. doi: 10.2196/11191.

Harper, S. and Speicher, D. W. (2011) 'Purification of proteins fused to glutathione S-transferase', *Methods in molecular biology (Clifton, N.J.)*, 681, pp. 259–280. doi: 10.1007/978-1-60761-913-0_14.

He, L. *et al.* (2020) 'Metastatic castration-resistant prostate cancer: Academic insights and perspectives through bibliometric analysis', *Medicine*, 99(15). Available at: https://journals.lww.com/md-journal/Fulltext/2020/04100/Metastatic_castration_resistant_prostate_cancer_.47.aspx.

He, Y. *et al.* (2018) 'Androgen receptor splice variants bind to constitutively open chromatin and promote abiraterone-resistant growth of prostate cancer', *Nucleic Acids Research*, 46(4), pp. 1895–1911. doi: 10.1093/nar/gkx1306.

Heemers, H. V. and Tindall, D. J. (2007) 'Androgen receptor (AR) coregulators: A diversity of functions converging on and regulating the AR transcriptional complex', *Endocrine Reviews*, 28(7), pp. 778–808. doi: 10.1210/er.2007-0019.

Heerma van Voss, M. R., van Diest, P. J. and Raman, V. (2017) 'Targeting RNA helicases in cancer: The translation trap', *Biochimica et biophysica acta. Reviews on cancer*. 2017/09/28, 1868(2), pp. 510–520. doi: 10.1016/j.bbcan.2017.09.006.

Hegazy, Y. A., Fernando, C. M. and Tran, E. J. (2019) 'The Balancing Act of R-loop Biology: The Good, the Bad, and the Ugly', *Journal of Biological Chemistry* . doi: 10.1074/jbc.REV119.011353.

Heidenreich, A. *et al.* (2014) 'EAU guidelines on prostate cancer. Part 1: Screening, diagnosis, and local treatment with curative intent - Update 2013', *European Urology*. European Association of Urology, 65(1), pp. 124–137. doi: 10.1016/j.eururo.2013.09.046.

Heidenreich, A. *et al.* (2019) 'Radium-223 in asymptomatic patients with

castration-resistant prostate cancer and bone metastases treated in an international early access program', *BMC Cancer*, 19(1), p. 12. doi: 10.1186/s12885-018-5203-y.

Heinlein, C. A. and Chang, C. (2002) 'Androgen receptor (AR) coregulators: An overview', *Endocrine Reviews*, 23(2), pp. 175–200. doi: 10.1210/edrv.23.2.0460.

Heinlein, C. A. and Chang, C. (2004) 'Androgen Receptor in Prostate Cancer', *Endocrine Reviews*, 25(2), pp. 276–308. doi: 10.1210/er.2002-0032.

Henderson, D. J. P. *et al.* (2014) 'The cAMP phosphodiesterase-4D7 (PDE4D7) is downregulated in androgen-independent prostate cancer cells and mediates proliferation by compartmentalising cAMP at the plasma membrane of VCaP prostate cancer cells', *British journal of cancer*. 2014/02/11. Nature Publishing Group, 110(5), pp. 1278–1287. doi: 10.1038/bjc.2014.22.

Henderson, D. J. P. *et al.* (2019) 'Creating a potential diagnostic for prostate cancer risk stratification (InformMDx™) by translating novel scientific discoveries concerning cAMP degrading phosphodiesterase-4D7 (PDE4D7)', *Clinical Science*, 133(2), pp. 269–286. doi: 10.1042/CS20180519.

Henninot, A., Collins, J. C. and Nuss, J. M. (2018) 'The Current State of Peptide Drug Discovery: Back to the Future?', *Journal of Medicinal Chemistry*. American Chemical Society, 61(4), pp. 1382–1414. doi: 10.1021/acs.jmedchem.7b00318.

Herden, J. and Weissbach, L. (2018) 'Utilization of Active Surveillance and Watchful Waiting for localized prostate cancer in the daily practice', *World Journal of Urology*. Springer Berlin Heidelberg, 36(3), pp. 383–391. doi: 10.1007/s00345-018-2175-0.

Hernández, G. *et al.* (2019) 'The Secret Life of Translation Initiation in Prostate Cancer', *Frontiers in genetics*. Frontiers Media S.A., 10, p. 14. doi: 10.3389/fgene.2019.00014.

Hessels, D. *et al.* (2007) 'Detection of TMPRSS2-ERG fusion transcripts and prostate cancer antigen 3 in urinary sediments may improve diagnosis of prostate cancer', *Clinical Cancer Research*, 13(17), pp. 5103–5108. doi: 10.1158/1078-0432.CCR-07-0700.

Hietakangas, V. *et al.* (2006) 'PDSM, a motif for phosphorylation-dependent

SUMO modification', *Proceedings of the National Academy of Sciences of the United States of America*, 103(1), pp. 45 LP – 50. doi: 10.1073/pnas.0503698102.

Hitosugi, T. and Chen, J. (2014) 'Post-translational modifications and the Warburg effect', *Oncogene*. Nature Publishing Group, 33(34), pp. 4279–4285. doi: 10.1038/onc.2013.406.

Hoffmann, K. *et al.* (2018) 'A platform for discovery of functional cell-penetrating peptides for efficient multi-cargo intracellular delivery', *Scientific Reports*, 8(1), p. 12538. doi: 10.1038/s41598-018-30790-2.

Hong, M. *et al.* (2020) 'RNA sequencing: new technologies and applications in cancer research.', *Journal of hematology & oncology*. England, 13(1), p. 166. doi: 10.1186/s13045-020-01005-x.

Hotte, S. J. and Saad, F. (2010) 'Current management of castrate-resistant prostate cancer', *Current Oncology*, 17(SUPPL. 2), pp. 72–79. doi: 10.3747/co.v17i0.718.

Houslay, K. F. *et al.* (2017) 'Identification of a multifunctional docking site on the catalytic unit of phosphodiesterase-4 (PDE4) that is utilised by multiple interaction partners', *Biochemical Journal*, 474(4), pp. 597–609. doi: 10.1042/BCJ20160849.

Houslay, K. F. *et al.* (2019) 'Phosphorylation of PDE4A5 by MAPKAPK2 attenuates fibrin degradation via p75 signalling', *The Journal of Biochemistry*, 166(1), pp. 97–106. doi: 10.1093/jb/mvz016.

Houslay, M. D. (2010) 'Underpinning compartmentalised cAMP signalling through targeted cAMP breakdown', *Trends in Biochemical Sciences*, 35(2), pp. 91–100. doi: https://doi.org/10.1016/j.tibs.2009.09.007.

Houslay, M. D. and Adams, D. R. (2003) 'PDE4 cAMP phosphodiesterases: modular enzymes that orchestrate signalling cross-talk, desensitization and compartmentalization', *The Biochemical journal*, 370(Pt 1), pp. 1–18. doi: 10.1042/BJ20021698.

Hrdlickova, R., Toloue, M. and Tian, B. (2017) 'RNA-Seq methods for transcriptome analysis', *Wiley interdisciplinary reviews. RNA*. 2016/05/19, 8(1), p. 10.1002/wrna.1364. doi: 10.1002/wrna.1364.

Hu, J. *et al*. (2010) 'Cellular cholesterol delivery, intracellular processing and utilization for biosynthesis of steroid hormones', *Nutrition and Metabolism*, 7(Table 1), pp. 7–9. doi: 10.1186/1743-7075-7-47.

Hua, H. *et al*. (2019) 'Targeting mTOR for cancer therapy', *Journal of Hematology & Oncology*, 12(1), p. 71. doi: 10.1186/s13045-019-0754-1.

Hua, J. T., Chen, S. and He, H. H. (2019) 'Landscape of Noncoding RNA in Prostate Cancer', *Trends in Genetics*. Elsevier, 35(11), pp. 840–851. doi: 10.1016/j.tig.2019.08.004.

Huang, Y. *et al*. (2018) 'Molecular and cellular mechanisms of castration resistant prostate cancer', *Oncology Letters*, 15(5), pp. 6063–6076. doi: 10.3892/ol.2018.8123.

Humphrey, P. A. (2004) 'Gleason grading and prognostic factors in carcinoma of the prostate', *Modern Pathology*, 17(3), pp. 292–306. doi: 10.1038/modpathol.3800054.

Humphrey, P. A. (2017) 'Histopathology of prostate cancer', *Cold Spring Harbor Perspectives in Medicine*, 7(10), pp. 1–21. doi: 10.1101/cshperspect.a030411.

Huppertz, I. *et al*. (2014) 'iCLIP: Protein–RNA interactions at nucleotide resolution', *Methods*, 65(3), pp. 274–287. doi: https://doi.org/10.1016/j.ymeth.2013.10.011.

Hussain, M. *et al*. (2015) 'Dichotomous role of protein kinase A type I (PKAI) in the tumor microenvironment: A potential target for "two-in-one" cancer chemoimmunotherapeutics', *Cancer Letters*, 369(1), pp. 9–19. doi: https://doi.org/10.1016/j.canlet.2015.07.047.

Hussain, M. *et al*. (2018) 'Enzalutamide in Men with Nonmetastatic, Castration-Resistant Prostate Cancer', *New England Journal of Medicine*. Massachusetts Medical Society, 378(26), pp. 2465–2474. doi: 10.1056/NEJMoa1800536.

Impens, F. *et al*. (2014) 'Mapping of SUMO sites and analysis of SUMOylation changes induced by external stimuli', *Proceedings of the National Academy of Sciences*, 111(34), pp. 12432 LP – 12437. doi: 10.1073/pnas.1413825111.

Ittmann, M. *et al*. (2013) 'Animal models of human prostate cancer: the

consensus report of the New York meeting of the Mouse Models of Human Cancers Consortium Prostate Pathology Committee', *Cancer research*. 2013/04/22, 73(9), pp. 2718–2736. doi: 10.1158/0008-5472.CAN-12-4213.

Ivanov, A. A., Khuri, F. R. and Fu, H. (2013) 'Targeting protein-protein interactions as an anticancer strategy', *Trends in pharmacological sciences*. 2013/05/29, 34(7), pp. 393–400. doi: 10.1016/j.tips.2013.04.007.

Jahn, J. L., Giovannucci, E. L. and Stampfer, M. J. (2015) 'The high prevalence of undiagnosed prostate cancer at autopsy: implications for epidemiology and treatment of prostate cancer in the Prostate-specific Antigen-era', *International journal of cancer*. 2015/01/08, 137(12), pp. 2795–2802. doi: 10.1002/ijc.29408.

Jain, A. *et al.* (2010) 'Human DHX9 helicase unwinds triple-helical DNA structures', *Biochemistry*, 49(33), pp. 6992–6999. doi: 10.1021/bi100795m.

Jain, A. *et al.* (2013) 'DHX9 helicase is involved in preventing genomic instability induced by alternatively structured DNA in human cells', *Nucleic Acids Research*, 41(22), pp. 10345–10357. doi: 10.1093/nar/gkt804.

Jamaspishvili, T. *et al.* (2018) 'Clinical implications of PTEN loss in prostate cancer', *Nature Reviews Urology*, 15(4), pp. 222–234. doi: 10.1038/nrurol.2018.9.

Jang, B.-C. *et al.* (2003) 'Leptomycin B, an Inhibitor of the Nuclear Export Receptor CRM1, Inhibits COX-2 Expression', *Journal of Biological Chemistry* , 278(5), pp. 2773–2776. Available at: http://www.jbc.org/content/278/5/2773.abstract.

Jankowsky, E. (2000) 'The DExH/D protein family database', *Nucleic Acids Research*, 28(1), pp. 333–334. doi: 10.1093/nar/28.1.333.

Jenster, G. (2000) 'Ligand-independent activation of the androgen receptor in prostate cancer by growth factors and cytokines', *The Journal of Pathology*. John Wiley & Sons, Ltd, 191(3), pp. 227–228. doi: 10.1002/1096-9896(200007)191:3<227::AID-PATH636>3.0.CO;2-3.

Jernberg, E., Bergh, A. and Wikström, P. (2017) 'Clinical relevance of androgen receptor alterations in prostate cancer', *Endocrine Connections*, 6(8), pp. R146–R161. doi: 10.1530/EC-17-0118.

Jing, Y. *et al.* (2018) 'DHX15 promotes prostate cancer progression by stimulating Siah2-mediated ubiquitination of androgen receptor', *Oncogene*. 2017/10/09, 37(5), pp. 638–650. doi: 10.1038/onc.2017.371.

Julien, L.-A. *et al.* (2010) 'mTORC1-Activated S6K1 Phosphorylates Rictor on Threonine 1135 and Regulates mTORC2 Signaling', *Molecular and Cellular Biology*, 30(4), pp. 908 LP – 921. doi: 10.1128/MCB.00601-09.

Kaarbø, M. *et al.* (2010) 'PI3K-AKT-mTOR pathway is dominant over androgen receptor signaling in prostate cancer cells', *Cellular Oncology*, 32(1–2), pp. 11–27. doi: 10.3233/CLO-2009-0487.

Kaarbø, M., Klokk, T. I. and Saatcioglu, F. (2007) 'Androgen signaling and its interactions with other signaling pathways in prostate cancer', *BioEssays*, 29(12), pp. 1227–1238. doi: 10.1002/bies.20676.

Kamran, S. C. and D'Amico, A. V. (2018) 'Radiation Therapy for Prostate Cancer', *Hematology/Oncology Clinics of North America*, 115(2), pp. 146–150. doi: 10.1016/j.hoc.2019.08.017.

Karamouzis, M. V, Konstantinopoulos, P. A. and Papavassiliou, A. G. (2007) 'Roles of CREB-binding protein (CBP)/p300 in respiratory epithelium tumorigenesis', *Cell Research*, 17(4), pp. 324–332. doi: 10.1038/cr.2007.10.

Karantanos, T., Corn, P. G. and Thompson, T. C. (2013) 'Prostate cancer progression after androgen deprivation therapy: mechanisms of', *Oncogene*, 32(49). doi: 10.1097/SPC.0b013e328363602e.

Kaufman, H. L., Kohlhapp, F. J. and Zloza, A. (2015) 'Oncolytic viruses: a new class of immunotherapy drugs.', *Nature reviews. Drug discovery*, 14(9), pp. 642–662. doi: 10.1038/nrd4663.

Kaupp, U. B. and Seifert, R. (2002) 'Cyclic Nucleotide-Gated Ion Channels', *Physiological Reviews*. American Physiological Society, 82(3), pp. 769–824. doi: 10.1152/physrev.00008.2002.

Keating, M. J. *et al.* (2019) 'Age-dependent overall survival benefit of androgen deprivation therapy for metastatic prostate cancer.', *Journal of oncology pharmacy practice : official publication of the International Society of Oncology Pharmacy Practitioners*. England, 25(8), pp. 1927–1932. doi:

10.1177/1078155219835597.

Kedage, V. *et al.* (2016) 'An Interaction with Ewing's Sarcoma Breakpoint Protein EWS Defines a Specific Oncogenic Mechanism of ETS Factors Rearranged in Prostate Cancer', *Cell reports*, 17(5), pp. 1289–1301. doi: 10.1016/j.celrep.2016.10.001.

Khong, A. *et al.* (2017) 'The Stress Granule Transcriptome Reveals Principles of mRNA Accumulation in Stress Granules', *Molecular cell*. 2017/11/09, 68(4), pp. 808-820.e5. doi: 10.1016/j.molcel.2017.10.015.

Khor, L.-Y. *et al.* (2008) 'Protein kinase A RI-alpha predicts for prostate cancer outcome: analysis of radiation therapy oncology group trial 86-10', *International journal of radiation oncology, biology, physics*. 2008/05/01, 71(5), pp. 1309–1315. doi: 10.1016/j.ijrobp.2007.12.010.

Kim, H. W. *et al.* (2010) 'Cyclic AMP controls mTOR through regulation of the dynamic interaction between Rheb and phosphodiesterase 4D', *Molecular and cellular biology*. 2010/09/13. American Society for Microbiology (ASM), 30(22), pp. 5406–5420. doi: 10.1128/MCB.00217-10.

Kim, M. *et al.* (2018) 'Androgen deprivation therapy during and after post-prostatectomy radiotherapy in patients with prostate cancer: a case control study', *BMC cancer*. BioMed Central, 18(1), p. 271. doi: 10.1186/s12885-018-4189-9.

Kim, T. H. *et al.* (2017) 'The role of CREB3L4 in the proliferation of prostate cancer cells', *Scientific Reports*. Nature Publishing Group, 7(March), pp. 1–11. doi: 10.1038/srep45300.

Kimmelman, J. and Tannock, I. (2018) 'The paradox of precision medicine.', *Nature reviews. Clinical oncology*. England, 15(6), pp. 341–342. doi: 10.1038/s41571-018-0016-0.

King, C. C. *et al.* (2011) 'The Rate of NF-κB Nuclear Translocation Is Regulated by PKA and A Kinase Interacting Protein 1', *PLOS ONE*. Public Library of Science, 6(4), p. e18713. Available at: https://doi.org/10.1371/journal.pone.0018713.

Kinkade, C. W. *et al.* (2008) 'Targeting AKT/mTOR and ERK MAPK signaling inhibits hormone-refractory prostate cancer in a preclinical mouse model', *The*

Journal of Clinical Investigation. The American Society for Clinical Investigation, 118(9), pp. 3051–3064. doi: 10.1172/JCI34764.

Kinsella, N. *et al.* (2018) 'Active surveillance for prostate cancer: A systematic review of contemporary worldwide practices', *Translational Andrology and Urology*, 7(1), pp. 83–97. doi: 10.21037/tau.2017.12.24.

Klaesson, A. *et al.* (2018) 'Improved efficiency of in situ protein analysis by proximity ligation using UnFold probes', *Scientific Reports*, 8(1), p. 5400. doi: 10.1038/s41598-018-23582-1.

Klussmann, E. (2016) 'Protein–protein interactions of PDE4 family members — Functions, interactions and therapeutic value', *Cellular Signalling*. Pergamon, 28(7), pp. 713–718. doi: 10.1016/J.CELLSIG.2015.10.005.

Knudsen, B. S. and Vasioukhin, V. (2010) *Mechanisms of Prostate Cancer Initiation and Progression*. 1st edn, *Advances in Cancer Research*. 1st edn. Elsevier Inc. doi: 10.1016/B978-0-12-380890-5.00001-6.

Knudsen, K. E., Arden, K. C. and Cavenee, W. K. (1998) 'Multiple G1 Regulatory Elements Control the Androgen-dependent Proliferation of Prostatic Carcinoma Cells ', *Journal of Biological Chemistry* , 273(32), pp. 20213–20222. Available at: http://www.jbc.org/content/273/32/20213.abstract.

Kohaar, I., Petrovics, G. and Srivastava, S. (2019) 'A Rich Array of Prostate Cancer Molecular Biomarkers: Opportunities and Challenges', *International Journal of Molecular Sciences*, 20(8), p. 1813. doi: 10.3390/ijms20081813.

Koivisto, P. *et al.* (1997) 'Androgen receptor gene amplification: A possible molecular mechanism for androgen deprivation therapy failure in prostate cancer', *Cancer Research*, 57(2), pp. 314–319.

Kollareddy, M. *et al.* (2017) 'The small molecule inhibitor YK-4-279 disrupts mitotic progression of neuroblastoma cells, overcomes drug resistance and synergizes with inhibitors of mitosis', *Cancer Letters*, 403, pp. 74–85. doi: https://doi.org/10.1016/j.canlet.2017.05.027.

König, F., Schubert, T. and Längst, G. (2017) 'The monoclonal S9.6 antibody exhibits highly variable binding affinities towards different R-loop sequences', *PLOS ONE*. Public Library of Science, 12(6), p. e0178875. Available at:

https://doi.org/10.1371/journal.pone.0178875.

Koryakina, Y., Ta, H. Q. and Gioeli, D. (2014) 'Androgen receptor phosphorylation: biological context and functional consequences', *Endocrine-related cancer*. 2014/01/14, 21(4), pp. T131–T145. doi: 10.1530/ERC-13-0472.

Koschinski, A. and Zaccolo, M. (2017) 'Activation of PKA in cell requires higher concentration of cAMP than in vitro: implications for compartmentalization of cAMP signalling', *Scientific Reports*, 7(1), p. 14090. doi: 10.1038/s41598-017-13021-y.

Kosugi, S. *et al.* (2009) 'Systematic identification of cell cycle-dependent yeast nucleocytoplasmic shuttling proteins by prediction of composite motifs', *Proceedings of the National Academy of Sciences of the United States of America*. 2009/06/11. National Academy of Sciences, 106(25), pp. 10171–10176. doi: 10.1073/pnas.0900604106.

Kovacs, A. and Pinkawa, M. (2019) 'Interventional therapy in malignant conditions of the prostate', *Radiologie*, 59(Suppl 1), pp. S28–S39. doi: 10.1007/s00117-019-00632-x.

Kremer, C. L. *et al.* (2006) 'Expression of mTOR signaling pathway markers in prostate cancer progression', *The Prostate*. John Wiley & Sons, Ltd, 66(11), pp. 1203–1212. doi: 10.1002/pros.20410.

Kron, K. J. *et al.* (2017) 'TMPRSS2-ERG fusion co-opts master transcription factors and activates NOTCH signaling in primary prostate cancer', *Nature Genetics*. Nature Publishing Group, 49(9), pp. 1336–1345. doi: 10.1038/ng.3930.

Krušlin, B., Ulamec, M. and Tomas, D. (2015) 'Prostate cancer stroma: An important factor in cancer growth and progression', *Bosnian Journal of Basic Medical Sciences*, 15(2). doi: 10.17305/bjbms.2015.449.

Krzyszczyk, P. *et al.* (2018) 'The growing role of precision and personalized medicine for cancer treatment', *Technology*. 2019/01/11, 6(3–4), pp. 79–100. doi: 10.1142/S2339547818300020.

Kudo, N. *et al.* (1998) 'Leptomycin B Inhibition of Signal-Mediated Nuclear Export by Direct Binding to CRM1', *Experimental Cell Research*, 242(2), pp. 540–547. doi: https://doi.org/10.1006/excr.1998.4136.

Kunath, F. *et al.* (2015) 'Gonadotropin-releasing hormone antagonists versus standard androgen suppression therapy for advanced prostate cancer A systematic review with meta-analysis', *BMJ open*, 5(11), p. e008217. doi: 10.1136/bmjopen-2015-008217.

de la Cruz, J., Kressler, D. and Linder, P. (1999) 'Unwinding RNA in Saccharomyces cerevisiae: DEAD-box proteins and related families', *Trends in Biochemical Sciences*, 24(5), pp. 192–198. doi: https://doi.org/10.1016/S0968-0004(99)01376-6.

Laakkonen, P. and Vuorinen, K. (2010) 'Homing peptides as targeted delivery vehicles', *Integrative Biology*, 2(7–8), pp. 326–337. doi: 10.1039/c0ib00013b.

Lai, Y.-H. *et al.* (2011) 'SOX4 interacts with plakoglobin in a Wnt3a-dependent manner in prostate cancer cells', *BMC cell biology*. BioMed Central, 12, p. 50. doi: 10.1186/1471-2121-12-50.

Lamhamedi-Cherradi, S.-E. *et al.* (2015) 'An Oral Formulation of YK-4-279: Preclinical Efficacy and Acquired Resistance Patterns in Ewing Sarcoma', *Molecular Cancer Therapeutics*, 14(7), pp. 1591 LP – 1604. doi: 10.1158/1535-7163.MCT-14-0334.

Lamoliatte, F. *et al.* (2014) 'Large-scale analysis of lysine SUMOylation by SUMO remnant immunoaffinity profiling', *Nature Communications*, 5(1), p. 5409. doi: 10.1038/ncomms6409.

Lampreht Tratar, U., Horvat, S. and Cemazar, M. (2018) 'Transgenic Mouse Models in Cancer Research', *Frontiers in oncology*. Frontiers Media S.A., 8, p. 268. doi: 10.3389/fonc.2018.00268.

Laplante, M. and Sabatini, D. M. (2009) 'mTOR signaling at a glance', *Journal of Cell Science*, 122(20), pp. 3589 LP – 3594. doi: 10.1242/jcs.051011.

Latorraca, N. R., Venkatakrishnan, A. J. and Dror, R. O. (2017) 'GPCR Dynamics: Structures in Motion', *Chemical Reviews*. American Chemical Society, 117(1), pp. 139–155. doi: 10.1021/acs.chemrev.6b00177.

Lau, J. L. and Dunn, M. K. (2018) 'Therapeutic peptides: Historical perspectives, current development trends, and future directions', *Bioorganic & Medicinal Chemistry*, 26(10), pp. 2700–2707. doi:

https://doi.org/10.1016/j.bmc.2017.06.052.

Lazarev, S. *et al.* (2018) 'Low-dose-rate brachytherapy for prostate cancer: outcomes at >10 years of follow-up', *BJU International*, 121(5), pp. 781–790. doi: 10.1111/bju.14122.

Le, T. and Gerber, D. E. (2019) 'Newer-Generation EGFR Inhibitors in Lung Cancer: How Are They Best Used?', *Cancers*. MDPI, 11(3), p. 366. doi: 10.3390/cancers11030366.

Lea, W. A. and Simeonov, A. (2011) 'Fluorescence polarization assays in small molecule screening', *Expert opinion on drug discovery*, 6(1), pp. 17–32. doi: 10.1517/17460441.2011.537322.

Lee, C. G. *et al.* (1999) 'The human RNA helicase a (DDX9) gene maps to the prostate cancer susceptibility locus at chromosome band Iq25 and its pseudogene (DDX9P) to 13q22, respectively', *Somatic Cell and Molecular Genetics*, 25(1), pp. 33–39. doi: 10.1023/b:scam.0000007138.44216.3a.

Lee, D. Y. *et al.* (2005) 'Role of Protein Methylation in Regulation of Transcription', *Endocrine Reviews*, 26(2), pp. 147–170. doi: 10.1210/er.2004-0008.

Lee, S. H. and Dominguez, R. (2010) 'Regulation of actin cytoskeleton dynamics in cells', *Molecules and cells*, 29(4), pp. 311–325. doi: 10.1007/s10059-010-0053-8.

Lee, T. *et al.* (2014) 'Suppression of the DHX9 Helicase Induces Premature Senescence in Human Diploid Fibroblasts in a p53-dependent Manner', *Journal of Biological Chemistry* , 289(33), pp. 22798–22814. doi: 10.1074/jbc.M114.568535.

Lee, T. *et al.* (2016) 'Tumor cell survival dependence on the DHX9 DExH-box helicase', *Oncogene*. 2016/03/14, 35(39), pp. 5093–5105. doi: 10.1038/onc.2016.52.

Lee, T. and Pelletier, J. (2016) 'The biology of DHX9 and its potential as a therapeutic target', *Oncotarget*, 7(27).

Lee, T. and Pelletier, J. (2017) 'Dependence of p53-deficient cells on the DHX9 DExH-box helicase', *Oncotarget*. Impact Journals LLC, 8(19), pp. 30908–30921.

doi: 10.18632/oncotarget.15889.

Lee, Y. G. *et al.* (2001) 'Establishment and characterization of a new human prostatic cancer cell line: DuCaP.', *In vivo (Athens, Greece)*. Greece, 15(2), pp. 157–162.

Lee, Y. H., Tan, H. T. and Chung, M. C. M. (2010) 'Subcellular fractionation methods and strategies for proteomics.', *Proteomics*. Germany, 10(22), pp. 3935–3956. doi: 10.1002/pmic.201000289.

Lenz, H.-J. (2006) 'Anti-EGFR mechanism of action: antitumor effect and underlying cause of adverse events.', *Oncology (Williston Park, N.Y.)*. United States, 20(5 Suppl 2), pp. 5–13.

Leon, E., Ranganathan, R. and Savoldo, B. (2020) 'Adoptive T cell therapy: Boosting the immune system to fight cancer', *Seminars in Immunology*, p. 101437. doi: https://doi.org/10.1016/j.smim.2020.101437.

Li, J. *et al.* (2017) 'Characterization of Human Cancer Cell Lines by Reverse-phase Protein Arrays', *Cancer cell*, 31(2), pp. 225–239. doi: 10.1016/j.ccell.2017.01.005.

Li, L., Monckton, E. A. and Godbout, R. (2008) 'A Role for DEAD Box 1 at DNA Double-Strand Breaks', *Molecular and Cellular Biology*, 28(20), pp. 6413 LP – 6425. doi: 10.1128/MCB.01053-08.

Li, N. *et al.* (2020) 'SUMOylation, a multifaceted regulatory mechanism in the pancreatic beta cells', *Seminars in Cell & Developmental Biology*. doi: https://doi.org/10.1016/j.semcdb.2020.03.008.

Li, S. *et al.* (2019) 'Activation of MAPK Signaling by CXCR7 Leads to Enzalutamide Resistance in Prostate Cancer', *Cancer Research*, 79(10), pp. 2580 LP – 2592. doi: 10.1158/0008-5472.CAN-18-2812.

Li, X. *et al.* (2010) 'Selective SUMO modification of cAMP-specific phosphodiesterase-4D5 (PDE4D5) regulates the functional consequences of phosphorylation by PKA and ERK', *Biochemical Journal*, 428(1), pp. 55–65. doi: 10.1042/BJ20091672.

Li, Y.-J. *et al.* (2010) 'Role of SUMO:SIM-mediated protein–protein interaction in

non-homologous end joining', *Oncogene*, 29(24), pp. 3509–3518. doi: 10.1038/onc.2010.108.

Lilja, H., Ulmert, D. and Vickers, A. J. (2008) 'Prostate-specific antigen and prostate cancer: Prediction, detection and monitoring', *Nature Reviews Cancer*, 8(4), pp. 268–278. doi: 10.1038/nrc2351.

Lin, H.-K. *et al.* (2004) 'Regulation of Androgen Receptor Signaling by PTEN (Phosphatase and Tensin Homolog Deleted on Chromosome 10) Tumor Suppressor through Distinct Mechanisms in Prostate Cancer Cells', *Molecular Endocrinology*, 18(10), pp. 2409–2423. doi: 10.1210/me.2004-0117.

Lin, Y.-C. *et al.* (2020) 'Oxaliplatin-Induced DHX9 Phosphorylation Promotes Oncogenic Circular RNA CCDC66 Expression and Development of Chemoresistance.', *Cancers*, 12(3). doi: 10.3390/cancers12030697.

Linder, P. and Fuller-Pace, F. V (2013) 'Looking back on the birth of DEAD-box RNA helicases', *Biochimica et Biophysica Acta (BBA) - Gene Regulatory Mechanisms*, 1829(8), pp. 750–755. doi: https://doi.org/10.1016/j.bbagrm.2013.03.007.

Liu, J.-M. *et al.* (2019) 'Androgen deprivation therapy for prostate cancer and the risk of autoimmune diseases', *Prostate Cancer and Prostatic Diseases*, 22(3), pp. 475–482. doi: 10.1038/s41391-019-0130-9.

Liu, P. *et al.* (2006) 'Sex-Determining Region Y Box 4 Is a Transforming Oncogene in Human Prostate Cancer Cells', *Cancer Research*, 66(8), pp. 4011 LP – 4019. doi: 10.1158/0008-5472.CAN-05-3055.

Loeb, S. *et al.* (2017) 'Active Surveillance Versus Watchful Waiting for Localized Prostate Cancer: A Model to Inform Decisions Stacy', *European Urology*, 72(6), pp. 899–907. doi: 10.1097/CCM.0b013e31823da96d.Hydrogen.

Lonergan, P. . and Donald, T. . (2011) 'Androgen receptor signaling in prostate cancer development and progression', *Journal of Carcinogenesis*, 10(20). Available at: https://www.ncbi.nlm.nih.gov/pmc/articles/PMC3162670/.

Long, X. *et al.* (2005) 'Rheb Binds and Regulates the mTOR Kinase', *Current Biology*, 15(8), pp. 702–713. doi: https://doi.org/10.1016/j.cub.2005.02.053.

Lu, S., Tsai, S. Y. and Tsai, M.-J. (1997) ‘Regulation of Androgen-dependent Prostatic Cancer Cell Growth: Androgen Regulation of CDK2, CDK4, and CKI p16 Genes’, *Cancer Research*, 57(20), pp. 4511 LP – 4516. Available at: http://cancerres.aacrjournals.org/content/57/20/4511.abstract.

Lundblad, J. R., Laurance, M. and Goodman, R. H. (1996) ‘Fluorescence polarization analysis of protein-DNA and protein-protein interactions.’, *Molecular Endocrinology*, 10(6), pp. 607–612. doi: 10.1210/mend.10.6.8776720.

Lyons, L. S. *et al.* (2008) ‘Ligand-independent activation of androgen receptors by Rho GTPase signaling in prostate cancer’, *Molecular Endocrinology*, 22(3), pp. 597–608. doi: 10.1210/me.2007-0158.

Ma, B. and Nussinov, R. (2014) ‘Druggable orthosteric and allosteric hot spots to target protein-protein interactions.’, *Current pharmaceutical design*, 20(8), pp. 1293–1301. doi: 10.2174/13816128113199990073.

Ma, X. *et al.* (2012) ‘Anti-Tumor Effects of the Peptide TMTP1-GG-D(KLAKLAK)2 on Highly Metastatic Cancers’, *PLOS ONE*. Public Library of Science, 7(9), p. e42685. Available at: https://doi.org/10.1371/journal.pone.0042685.

Mabonga, L. and Kappo, A. P. (2020) ‘Peptidomimetics: A Synthetic Tool for Inhibiting Protein–Protein Interactions in Cancer’, *International Journal of Peptide Research and Therapeutics*, 26(1), pp. 225–241. doi: 10.1007/s10989-019-09831-5.

MacKenzie, K. F. *et al.* (2011) ‘Phosphorylation of cAMP-specific PDE4A5 (phosphodiesterase-4A5) by MK2 (MAPKAPK2) attenuates its activation through protein kinase A phosphorylation’, *Biochemical Journal*, 435(3), pp. 755–769. doi: 10.1042/BJ20101184.

MacKenzie, S. J. *et al.* (2002a) ‘Long PDE4 cAMP specific phosphodiesterases are activated by protein kinase A-mediated phosphorylation of a single serine residue in Upstream Conserved Region 1 (UCR1)’, *British journal of pharmacology*, 136(3), pp. 421–433. doi: 10.1038/sj.bjp.0704743.

MacKenzie, S. J. *et al.* (2002b) ‘Long PDE4 cAMP specific phosphodiesterases are activated by protein kinase A-mediated phosphorylation of a single serine

residue in Upstream Conserved Region 1 (UCR1)', *British journal of pharmacology*, 136(3), pp. 421–433. doi: 10.1038/sj.bjp.0704743.

Macleod, K. ., Serrels, B. and Carragher, N. . (2017) 'Reverse Phase Protein Arrays and Drug Discovery', *Proteomics for Drug Discovery*, 1647, pp. 139–152. doi: 10.1007/978-1-4939-7201-2.

Magnuson, B., Ekim, B. and Fingar, D. C. (2011) 'Regulation and function of ribosomal protein S6 kinase (S6K) within mTOR signalling networks', *Biochemical Journal*, 441(1), pp. 1–21. doi: 10.1042/BJ20110892.

Makwana, K. M. and Mahalakshmi, R. (2015) 'Implications of aromatic–aromatic interactions: From protein structures to peptide models', *Protein Science*. John Wiley & Sons, Ltd, 24(12), pp. 1920–1933. doi: 10.1002/pro.2814.

Malinowski, B. *et al.* (2019) 'Previous, Current, and Future Pharmacotherapy and Diagnosis of Prostate Cancer-A Comprehensive Review.', *Diagnostics (Basel, Switzerland)*, 9(4). doi: 10.3390/diagnostics9040161.

Mangangcha, I. R. *et al.* (2019) 'Identification of key regulators in prostate cancer from gene expression datasets of patients', *Scientific Reports*, 9(1), p. 16420. doi: 10.1038/s41598-019-52896-x.

Manojlovic, Z. and Stefanovic, B. (2012) 'A novel role of RNA helicase A in regulation of translation of type I collagen mRNAs', *Rna*, 18(2), pp. 321–334. doi: 10.1261/rna.030288.111.

Marintchev, A. (2013) 'Roles of helicases in translation initiation: a mechanistic view', *Biochimica et biophysica acta*. 2013/01/19, 1829(8), pp. 799–809. doi: 10.1016/j.bbagrm.2013.01.005.

Marqus, S., Pirogova, E. and Piva, T. J. (2017) 'Evaluation of the use of therapeutic peptides for cancer treatment', *Journal of Biomedical Science*, 24(1), p. 21. doi: 10.1186/s12929-017-0328-x.

Marshall, J. C. and Kelch, R. P. (1986) 'Measurement of Prostate-Specific Antigen in Serum as a Screening Test for Prostate Cancer'.

Martin, T. P. *et al.* (2014) 'Targeted disruption of the heat shock protein 20-phosphodiesterase 4D (PDE4D) interaction protects against pathological cardiac

remodelling in a mouse model of hypertrophy', *FEBS open bio*. Elsevier, 4, pp. 923–927. doi: 10.1016/j.fob.2014.10.011.

Mason, M. *et al.* (2013) 'Neoadjuvant Androgen Deprivation Therapy for Prostate Volume Reduction, Lower Urinary Tract Symptom Relief and Quality of Life Improvement in Men with Intermediate- to High-risk Prostate Cancer: A Randomised Non-inferiority Trial of Degarelix versus Goser', *Clinical Oncology*. Elsevier Ltd, 25(3), pp. 190–196. doi: 10.1016/j.clon.2012.09.010.

McCall, P. *et al.* (2008) 'Is PTEN loss associated with clinical outcome measures in human prostate cancer?', *British journal of cancer*. Nature Publishing Group, 99(8), pp. 1296–1301. doi: 10.1038/sj.bjc.6604680.

Mellman, I., Coukos, G. and Dranoff, G. (2011) 'Cancer immunotherapy comes of age.', *Nature*, 480(7378), pp. 480–489. doi: 10.1038/nature10673.

Miliotou, A. N. and Papadopoulou, L. C. (2018) 'CAR T-cell Therapy: A New Era in Cancer Immunotherapy.', *Current pharmaceutical biotechnology*. Netherlands, 19(1), pp. 5–18. doi: 10.2174/1389201019666180418095526.

Miller, D. J. and Fort, P. E. (2018) 'Heat Shock Proteins Regulatory Role in Neurodevelopment', *Frontiers in Neuroscience*, 12, p. 821. doi: 10.3389/fnins.2018.00821.

Miller, W. L. (2002) 'Androgen biosynthesis from cholesterol to DHEA', *Molecular and Cellular Endocrinology*, 198(1–2), pp. 7–14. doi: 10.1016/S0303-7207(02)00363-5.

Miller, W. L. and Auchus, R. J. (2019) 'The "backdoor pathway" of androgen synthesis in human male sexual development', *PLoS Biology*, 17(4), pp. 2–7. doi: 10.1371/journal.pbio.3000198.

Mills, I. G. (2014) 'Maintaining and reprogramming genomic androgen receptor activity in prostate cancer', *Nature Reviews Cancer*. Nature Publishing Group, 14(3), pp. 187–198. doi: 10.1038/nrc3678.

Mills, J. R. *et al.* (2013) 'RNAi screening uncovers Dhx9 as a modifier of ABT-737 resistance in an Eμ-myc/Bcl-2 mouse model', *Blood*, 121(17), pp. 3402–3412. doi: 10.1182/blood-2012-06-434365.

Moerke, N. J. (2009) ‘Fluorescence Polarization (FP) Assays for Monitoring Peptide-Protein or Nucleic Acid-Protein Binding’, *Current Protocols in Chemical Biology*. John Wiley & Sons, Ltd, 1(1), pp. 1–15. doi: 10.1002/9780470559277.ch090102.

Mousavizadeh, A. *et al.* (2017) ‘Cell targeting peptides as smart ligands for targeting of therapeutic or diagnostic agents: a systematic review.’, *Colloids and surfaces. B, Biointerfaces*. Netherlands, 158, pp. 507–517. doi: 10.1016/j.colsurfb.2017.07.012.

Murakami, K. *et al.* (2017) ‘The crystal structure of human DEAH-box RNA helicase 15 reveals a domain organization of the mammalian DEAH/RHA family’, *Acta crystallographica. Section F, Structural biology communications*. 2017/05/25. International Union of Crystallography, 73(Pt 6), pp. 347–355. doi: 10.1107/S2053230X17007336.

Murat, P. *et al.* (2018) ‘RNA G-quadruplexes at upstream open reading frames cause DHX36- and DHX9-dependent translation of human mRNAs’, *Genome Biology*, 19(1), p. 229. doi: 10.1186/s13059-018-1602-2.

Nadiminty, N. and Gao, A. C. (2012) ‘Mechanisms of persistent activation of the androgen receptor in CRPC: Recent advances and future perspectives’, *World Journal of Urology*, 30(3), pp. 287–295. doi: 10.1007/s00345-011-0771-3.

Nakajima, T., Uchida, C., Anderson, Stephen F., *et al.* (1997) ‘RNA helicase A mediates association of CBP with RNA polymerase II’, *Cell*, 90(6), pp. 1107–1112. doi: 10.1016/S0092-8674(00)80376-1.

Nakajima, T., Uchida, C., Anderson, Stephen F, *et al.* (1997) ‘RNA Helicase A Mediates Association of CBP with RNA Polymerase II’, *Cell*, 90(6), pp. 1107–1112. doi: https://doi.org/10.1016/S0092-8674(00)80376-1.

Nandagopal, N. and Roux, P. P. (2015) ‘Regulation of global and specific mRNA translation by the mTOR signaling pathway’, *Translation (Austin, Tex.)*. Taylor & Francis, 3(1), pp. e983402–e983402. doi: 10.4161/21690731.2014.983402.

Nazareth, L. V and Weigel, N. L. (1996) ‘Activation of the Human Androgen Receptor through a Protein Kinase A Signaling Pathway’, *Journal of Biological Chemistry* , 271(33), pp. 19900–19907. doi: 10.1074/jbc.271.33.19900.

Ng, Y. C. *et al.* (2018) 'A DNA-sensing-independent role of a nuclear RNA helicase, DHX9, in stimulation of NF-κB-mediated innate immunity against DNA virus infection', *Nucleic acids research*. Oxford University Press, 46(17), pp. 9011–9026. doi: 10.1093/nar/gky742.

Nickols, N. G. *et al.* (2019) 'MEK-ERK signaling is a therapeutic target in metastatic castration resistant prostate cancer.', *Prostate cancer and prostatic diseases*, 22(4), pp. 531–538. doi: 10.1038/s41391-019-0134-5.

Niehrs, C. and Luke, B. (2020) 'Regulatory R-loops as facilitators of gene expression and genome stability', *Nature Reviews Molecular Cell Biology*, 21(3), pp. 167–178. doi: 10.1038/s41580-019-0206-3.

Niepel, M. *et al.* (2017) 'Measuring Cancer Drug Sensitivity and Resistance in Cultured Cells', *Current protocols in chemical biology*, 9(2), pp. 55–74. doi: 10.1002/cpch.21.

Nikolovska-Coleska, Z. (2015) 'Studying protein-protein interactions using surface plasmon resonance.', *Methods in molecular biology (Clifton, N.J.)*. United States, 1278, pp. 109–138. doi: 10.1007/978-1-4939-2425-7_7.

Nygren, P. J. and Scott, J. D. (2015) 'Therapeutic strategies for anchored kinases and phosphatases: exploiting short linear motifs and intrinsic disorder', *Frontiers in pharmacology*. Frontiers Media S.A., 6, p. 158. doi: 10.3389/fphar.2015.00158.

Oeckinghaus, A. and Ghosh, S. (2009) 'The NF-kappaB family of transcription factors and its regulation', *Cold Spring Harbor perspectives in biology*. Cold Spring Harbor Laboratory Press, 1(4), pp. a000034–a000034. doi: 10.1101/cshperspect.a000034.

Omar, F. *et al.* (2019) 'Small-molecule allosteric activators of PDE4 long form cyclic AMP phosphodiesterases', *Proceedings of the National Academy of Sciences*. National Academy of Sciences, 116(27), pp. 13320–13329. doi: 10.1073/PNAS.1822113116.

Ong, W. K. *et al.* (2009) 'The role of the PDE4D cAMP phosphodiesterase in the regulation of glucagon-like peptide-1 release', *British journal of pharmacology*. 2009/04/09. Blackwell Publishing Ltd, 157(4), pp. 633–644. doi: 10.1111/j.1476-

5381.2009.00194.x.

Osguthorpe, D. J. and Hagler, A. T. (2011) 'Mechanism of androgen receptor antagonism by bicalutamide in the treatment of prostate cancer', *Biochemistry*. 2011/04/25, 50(19), pp. 4105–4113. doi: 10.1021/bi102059z.

Ougolkov, A. *et al.* (2004) 'Associations Among β-TrCP, an E3 Ubiquitin Ligase Receptor, β-Catenin, and NF-κB in Colorectal Cancer', *JNCI: Journal of the National Cancer Institute*, 96(15), pp. 1161–1170. doi: 10.1093/jnci/djh219.

Ozaki, T. and Nakagawara, A. (2011) 'Role of p53 in cell death and human cancers', *Cancers*, 3(1), pp. 994–1013. doi: 10.3390/cancers3010994.

Palorini, R. *et al.* (2016) 'Protein Kinase A Activation Promotes Cancer Cell Resistance to Glucose Starvation and Anoikis', *PLOS Genetics*. Public Library of Science, 12(3), p. e1005931. Available at: https://doi.org/10.1371/journal.pgen.1005931.

Parikh, K. *et al.* (2009) 'Comparison of peptide array substrate phosphorylation of c-Raf and mitogen activated protein kinase kinase kinase 8', *PloS one*. Public Library of Science, 4(7), pp. e6440–e6440. doi: 10.1371/journal.pone.0006440.

Parisotto, M. and Metzger, D. (2013) 'Genetically engineered mouse models of prostate cancer', *Molecular oncology*. 2013/02/14. John Wiley and Sons Inc., 7(2), pp. 190–205. doi: 10.1016/j.molonc.2013.02.005.

Patek, S. *et al.* (2017) 'Androgen receptor phosphorylation status at serine 578 predicts poor outcome in prostate cancer patients', *Oncotarget*. Impact Journals LLC, 8(3), pp. 4875–4887. doi: 10.18632/oncotarget.13608.

Pavan, I. C. B. *et al.* (2016) 'Different interactomes for p70-S6K1 and p54-S6K2 revealed by proteomic analysis', *Proteomics*, 16(20), pp. 2650–2666. doi: 10.1002/pmic.201500249.

Pearce, L. R., Komander, D. and Alessi, D. R. (2010) 'The nuts and bolts of AGC protein kinases', *Nature Reviews Molecular Cell Biology*. Nature Publishing Group, 11(1), pp. 9–22. doi: 10.1038/nrm2822.

Peng, Y. *et al.* (2008) 'Distinct nuclear and cytoplasmic functions of androgen receptor cofactor p44 and association with androgen-independent prostate

cancer', *Proceedings of the National Academy of Sciences of the United States of America*, 105(13), pp. 5236–5241. doi: 10.1073/pnas.0712262105.

Perchey, R. T. *et al.* (2019) 'PTMselect: optimization of protein modifications discovery by mass spectrometry', *Scientific Reports*, 9(1), p. 4181. doi: 10.1038/s41598-019-40873-3.

Pérez-Ibave, D. C., Burciaga-Flores, C. H. and Elizondo-Riojas, M. Á. (2018) 'Prostate-specific antigen (PSA) as a possible biomarker in non-prostatic cancer: A review', *Cancer Epidemiology*, 54(December 2017), pp. 48–55. doi: 10.1016/j.canep.2018.03.009.

Perlmutter, M. A. and Lepor, H. (2007) 'Androgen deprivation therapy in the treatment of advanced prostate cancer', *Reviews in urology*. MedReviews, LLC, 9 Suppl 1(Suppl 1), pp. S3–S8. Available at: https://pubmed.ncbi.nlm.nih.gov/17387371.

Pfeiffer, M. J., Mulders, P. F. and Schalken, J. A. (2010) 'An in vitro model for preclinical testing of endocrine therapy combinations for prostate cancer', *Prostate*, 70(14), pp. 1524–1532. doi: 10.1002/pros.21187.

Phadke, M. S. *et al.* (2009) 'Glyceraldehyde 3-phosphate dehydrogenase depletion induces cell cycle arrest and resistance to antimetabolites in human carcinoma cell lines', *The Journal of pharmacology and experimental therapeutics*. 2009/07/23. The American Society for Pharmacology and Experimental Therapeutics, 331(1), pp. 77–86. doi: 10.1124/jpet.109.155671.

Pienta, K. J. *et al.* (2008) 'The current state of preclinical prostate cancer animal models', *The Prostate*, 68(6), pp. 629–639. doi: 10.1002/pros.20726.

Pierrat, O. A. *et al.* (2007) 'Control of protein translation by phosphorylation of the mRNA 5'-cap-binding complex.', *Biochemical Society transactions*. England, 35(Pt 6), pp. 1634–1637. doi: 10.1042/BST0351634.

Pintarelli, G. *et al.* (2016) 'Read-through transcripts in normal human lung parenchyma are down-regulated in lung adenocarcinoma', *Oncotarget*. Impact Journals LLC, 7(19), pp. 27889–27898. doi: 10.18632/oncotarget.8556.

Pippione, A. C. *et al.* (2017) 'Androgen-AR axis in primary and metastatic prostate cancer: chasing steroidogenic enzymes for therapeutic intervention',

Journal of Cancer Metastasis and Treatment, 3(12), p. 328. doi: 10.20517/2394-4722.2017.44.

Plevin, M. J., Mills, M. M. and Ikura, M. (2005) 'The LxxLL motif: a multifunctional binding sequence in transcriptional regulation', *Trends in Biochemical Sciences*, 30(2), pp. 66–69. doi: https://doi.org/10.1016/j.tibs.2004.12.001.

Podder, T. K., Fredman, E. T. and Ellis, R. J. (2018) 'Advances in Radiotherapy for Prostate Cancer Treatment', *Advances in experimental medicine and biology*. United States, 1096, pp. 31–47. doi: 10.1007/978-3-319-99286-0_2.

Poon, G. M. K. and Kim, H. M. (2017) 'Signatures of DNA target selectivity by ETS transcription factors', *Transcription*. 2017/03/16. Taylor & Francis, 8(3), pp. 193–203. doi: 10.1080/21541264.2017.1302901.

Powers, E. *et al.* (2020) 'Novel therapies are changing treatment paradigms in metastatic prostate cancer', *Journal of Hematology & Oncology*, 13(1), p. 144. doi: 10.1186/s13045-020-00978-z.

Prelich, G. (2012) 'Gene overexpression: uses, mechanisms, and interpretation', *Genetics*. Genetics Society of America, 190(3), pp. 841–854. doi: 10.1534/genetics.111.136911.

Prough, R. A., Clark, B. J. and Klinge, C. M. (2016) 'Novel mechanisms for DHEA action', *Journal of Molecular Endocrinology*, 56(3), pp. R139–R155. doi: 10.1530/JME-16-0013.

Pucci, C., Martinelli, C. and Ciofani, G. (2019) 'Innovative approaches for cancer treatment: current perspectives and new challenges', *Ecancermedicalscience*. Cancer Intelligence, 13, p. 961. doi: 10.3332/ecancer.2019.961.

Puighermanal, E. *et al.* (2017) 'Ribosomal Protein S6 Phosphorylation Is Involved in Novelty-Induced Locomotion, Synaptic Plasticity and mRNA Translation', *Frontiers in molecular neuroscience*. Frontiers Media S.A., 10, p. 419. doi: 10.3389/fnmol.2017.00419.

Qi, J. *et al.* (2013) 'The E3 ubiquitin ligase Siah2 contributes to castration-resistant prostate cancer by regulation of androgen receptor transcriptional activity', *Cancer cell*, 23(3), pp. 332–346. doi: 10.1016/j.ccr.2013.02.016.

Rahim, S. *et al*. (2011) 'YK-4-279 Inhibits ERG and ETV1 Mediated Prostate Cancer Cell Invasion', *PLOS ONE*. Public Library of Science, 6(4), p. e19343. Available at: https://doi.org/10.1371/journal.pone.0019343.

Rahim, S. *et al*. (2014) 'A small molecule inhibitor of ETV1, YK-4-279, prevents prostate cancer growth and metastasis in a mouse xenograft model.', *PloS one*, 9(12), p. e114260. doi: 10.1371/journal.pone.0114260.

Rahrmann, E. P. *et al*. (2009) 'Identification of PDE4D as a Proliferation Promoting Factor in Prostate Cancer Using a Sleeping Beauty Transposon-Based Somatic Mutagenesis Screen', *Cancer Research*, 69(10), pp. 4388 LP – 4397. doi: 10.1158/0008-5472.CAN-08-3901.

Rainey, K. H. and Patterson, G. H. (2019) 'Photoswitching FRET to monitor protein–protein interactions', *Proceedings of the National Academy of Sciences*, 116(3), pp. 864 LP – 873. doi: 10.1073/pnas.1805333116.

Ramaswami, R., Harding, V. and Newsom-Davis, T. (2013) 'Novel cancer therapies: treatments driven by tumour biology', *Postgraduate Medical Journal*, 89(1057), pp. 652 LP – 658. doi: 10.1136/postgradmedj-2012-131533.

Rathkopf, D. E. *et al*. (2017) 'Androgen receptor mutations in patients with castration-resistant prostate cancer treated with apalutamide', *Annals of Oncology*, 28(9), pp. 2264–2271. doi: 10.1093/annonc/mdx283.

Rawla, P. (2019) 'Epidemiology of Prostate Cancer', *World journal of oncology*. 2019/04/20. Elmer Press, 10(2), pp. 63–89. doi: 10.14740/wjon1191.

Rea, D. *et al*. (2016) 'Mouse Models in Prostate Cancer Translational Research: From Xenograft to PDX', *BioMed research international*. 2016/05/18. Hindawi Publishing Corporation, 2016, p. 9750795. doi: 10.1155/2016/9750795.

Rehman, Y. and Rosenberg, J. E. (2012) 'Abiraterone acetate: Oral androgen biosynthesis inhibitor for treatment of castration-resistant prostate cancer', *Drug Design, Development and Therapy*, 6, pp. 13–18. doi: 10.2147/DDDT.S15850.

Rehmann, H., de Rooij, J. and Bos, J. L. (2010) 'Epac, cAMP-Regulated Guanine Nucleotide Exchange Factors for Rap1 and Rap2', *Handbook of Cell Signaling*. Academic Press, pp. 1525–1529. doi: 10.1016/B978-0-12-374145-5.00186-8.

Reiterer, V. *et al*. (2020) 'The dead phosphatases society: a review of the emerging roles of pseudophosphatases', *The FEBS Journal*. John Wiley & Sons, Ltd, n/a(n/a). doi: 10.1111/febs.15431.

Retting, M. (2020) *Trametinib in Treating Patients With Progressive Metastatic Hormone-Resistant Prostate Cancer*. Available at: https://clinicaltrials.gov/ct2/show/NCT02881242.

Reynard, J. M., Peters, T. J. and Gillatt, D. (1995) 'Prostate-specific antigen and prognosis in patients with metastatic prostate cancer--a multivariable analysis of prostate cancer mortality.', *British journal of urology*. England, 75(4), pp. 507–515. doi: 10.1111/j.1464-410x.1995.tb07274.x.

Rice, M. A., Malhotra, S. V and Stoyanova, T. (2019) 'Second-Generation Antiandrogens: From Discovery to Standard of Care in Castration Resistant Prostate Cancer', *Frontiers in oncology*. Frontiers Media S.A., 9, p. 801. doi: 10.3389/fonc.2019.00801.

Richard, P. and Manley, J. L. (2017) 'R Loops and Links to Human Disease', *Journal of molecular biology*. 2016/09/04, 429(21), pp. 3168–3180. doi: 10.1016/j.jmb.2016.08.031.

Rinaldi, L. *et al*. (2019) 'Feedback inhibition of cAMP effector signaling by a chaperone-assisted ubiquitin system', *Nature Communications*, 10(1), p. 2572. doi: 10.1038/s41467-019-10037-y.

Rinken, A., Lavogina, D. and Kopanchuk, S. (2018) 'Assays with Detection of Fluorescence Anisotropy: Challenges and Possibilities for Characterizing Ligand Binding to GPCRs', *Trends in Pharmacological Sciences*. Elsevier, 39(2), pp. 187–199. doi: 10.1016/j.tips.2017.10.004.

Ritch, C. and Cookson, M. (2018) 'Recent trends in the management of advanced prostate cancer', *F1000Research*. F1000 Research Limited, 7, p. F1000 Faculty Rev-1513. doi: 10.12688/f1000research.15382.1.

Robert, F. and Pelletier, J. (2013) 'Perturbations of RNA helicases in cancer', *WIREs RNA*. John Wiley & Sons, Ltd, 4(4), pp. 333–349. doi: 10.1002/wrna.1163.

Robinson, J. L. *et al*. (2020) 'An atlas of human metabolism', *Science Signaling*, 13(624), p. eaaz1482. doi: 10.1126/scisignal.aaz1482.

Romanel, A. *et al.* (2015) 'Plasma AR and abiraterone-resistant prostate cancer', 7(312). doi: 10.1126/scitranslmed.aac9511.Plasma.

Rosenbaum, D. ., Rasmussen, S. G. . and Kobilka, B. . (2009) 'The structure and function of G-protein-coupled receptors', *Nature*, 459(7245), pp. 356–363. doi: 10.1038/nature08144.The.

Rosonina, E. (2019) 'A conserved role for transcription factor sumoylation in binding-site selection', *Current Genetics*, 65(6), pp. 1307–1312. doi: 10.1007/s00294-019-00992-w.

Rossi, A. M. and Taylor, C. W. (2011) 'Analysis of protein-ligand interactions by fluorescence polarization', *Nature Protocols*, 6(3), pp. 365–387. doi: 10.1038/nprot.2011.305.

Rubin, M. A. (2012) 'ETS rearrangements in prostate cancer', *Asian journal of andrology*. 2012/04/16. Nature Publishing Group, 14(3), pp. 393–399. doi: 10.1038/aja.2011.145.

Ruffalo, M. and Bar-Joseph, Z. (2019) 'Protein interaction disruption in cancer', *BMC Cancer*, 19(1), p. 370. doi: 10.1186/s12885-019-5532-5.

Rule, C. S., Patrick, M. and Sandkvist, M. (2016) 'Measuring In Vitro ATPase Activity for Enzymatic Characterization.', *Journal of visualized experiments : JoVE*, (114). doi: 10.3791/54305.

Russo, J. W. *et al.* (2018) 'Phosphorylation of androgen receptor serine 81 is associated with its reactivation in castration-resistant prostate cancer', *Cancer letters*. 2018/09/11, 438, pp. 97–104. doi: 10.1016/j.canlet.2018.09.014.

Russo, J. W. and Balk, S. P. (2018) 'Initiation and Evolution of Early Onset Prostate Cancer', *Cancer Cell*. Elsevier Inc., 34(6), pp. 874–876. doi: 10.1016/j.ccell.2018.11.010.

Ruvinsky, I. and Meyuhas, O. (2006) 'Ribosomal protein S6 phosphorylation: from protein synthesis to cell size', *Trends in Biochemical Sciences*, 31(6), pp. 342–348. doi: https://doi.org/10.1016/j.tibs.2006.04.003.

Sampson, N. *et al.* (2013) 'In vitro model systems to study androgen receptor signaling in prostate cancer', *Endocrine-Related Cancer*. Bristol, UK: Society for

Endocrinology, 20(2), pp. R49–R64. doi: 10.1530/ERC-12-0401.

Sarwar, M. *et al.* (2014) 'Protein kinase A (PKA) pathway is functionally linked to androgen receptor (AR) in the progression of prostate cancer', *Urologic Oncology: Seminars and Original Investigations*. Elsevier, 32(1), pp. 25.e1-25.e12. doi: 10.1016/J.UROLONC.2012.08.019.

Sassone-Corsi, P. (2012) 'The Cyclic AMP pathway', *Cold Spring Harbor Perspectives in Biology*, 4(12), pp. 3–5. doi: 10.1101/cshperspect.a011148.

Le Saux, O. *et al.* (2020) 'Neoadjuvant immune checkpoint inhibitors in cancer, current state of the art.', *Critical reviews in oncology/hematology*. Netherlands, 157, p. 103172. doi: 10.1016/j.critrevonc.2020.103172.

Saxton, R. A. and Sabatini, D. M. (2017) 'mTOR Signaling in Growth, Metabolism, and Disease', *Cell*, 168(6), pp. 960–976. doi: 10.1016/j.cell.2017.02.004.

Schächterle, C. *et al.* (2015) 'Screening for Small Molecule Disruptors of AKAP–PKA Interactions BT - cAMP Signaling: Methods and Protocols', in Zaccolo, M. (ed.). New York, NY: Springer New York, pp. 151–166. doi: 10.1007/978-1-4939-2537-7_12.

Schiewer, M. J., Augello, M. A. and Knudsen, K. E. (2012) 'The AR dependent cell cycle: mechanisms and cancer relevance', *Molecular and cellular endocrinology*. 2011/07/12, 352(1–2), pp. 34–45. doi: 10.1016/j.mce.2011.06.033.

Schilsky, R. L. *et al.* (2020) 'Progress in Cancer Research, Prevention, and Care', *New England Journal of Medicine*. Massachusetts Medical Society, 383(10), pp. 897–900. doi: 10.1056/NEJMp2007839.

Schindler, R. F. R. and Brand, T. (2016) 'The Popeye domain containing protein family - A novel class of cAMP effectors with important functions in multiple tissues', *Progress in Biophysics and Molecular Biology*. Elsevier Ltd, 120(1–3), pp. 28–36. doi: 10.1016/j.pbiomolbio.2016.01.001.

Schroeder, J. A. *et al.* (2012) 'The phosphodiesterase inhibitor isobutylmethylxanthine attenuates behavioral sensitization to cocaine', *Behavioural Pharmacology*, 23(3). Available at: https://journals.lww.com/behaviouralpharm/Fulltext/2012/06000/The_phospho

diesterase_inhibitor.10.aspx.

Schütz, P. *et al*. (2010) 'Crystal structure of human RNA helicase A (DHX9): Structural basis for unselective nucleotide base binding in a DEAD-box variant protein', *Journal of Molecular Biology*. Elsevier Ltd, 400(4), pp. 768–782. doi: 10.1016/j.jmb.2010.05.046.

Schwartz, P. A. and Murray, B. W. (2011) 'Protein kinase biochemistry and drug discovery', *Bioorganic Chemistry*, 39(5), pp. 192–210. doi: https://doi.org/10.1016/j.bioorg.2011.07.004.

Sekar, R. B. and Periasamy, A. (2003) 'Fluorescence resonance energy transfer (FRET) microscopy imaging of live cell protein localizations', *The Journal of cell biology*. The Rockefeller University Press, 160(5), pp. 629–633. doi: 10.1083/jcb.200210140.

Semenas, J. *et al*. (2012) 'Overcoming drug resistance and treating advanced prostate cancer', *Current drug targets*. Bentham Science Publishers, 13(10), pp. 1308–1323. doi: 10.2174/138945012802429615.

Shang, S., Hua, F. and Hu, Z.-W. (2017) 'The regulation of ß-catenin activity and function in cancer: therapeutic opportunities', *Oncotarget*. Impact Journals LLC, 8(20), pp. 33972–33989. doi: 10.18632/oncotarget.15687.

Shariff, A. I. *et al*. (2019) 'Novel cancer therapies and their association with diabetes', *Journal of Molecular Endocrinology*. Bristol, UK: Bioscientifica Ltd, 62(2), pp. R187–R199. doi: 10.1530/JME-18-0002.

Sharifi, N. (2013) 'Mechanisms of androgen receptor activation in castration-resistant prostate cancer', *Endocrinology*. 2013/09/03. Endocrine Society, 154(11), pp. 4010–4017. doi: 10.1210/en.2013-1466.

Sharp, A. *et al*. (2019) 'Androgen receptor splice variant-7 expression emerges with castration resistance in prostate cancer', *Journal of Clinical Investigation*, 129(1), pp. 192–208. doi: 10.1172/JCI122819.

Sharpless, N. E. and DePinho, R. A. (2006) 'The mighty mouse: genetically engineered mouse models in cancer drug development', *Nature Reviews Drug Discovery*, 5(9), pp. 741–754. doi: 10.1038/nrd2110.

El Sheikh, S. S. *et al*. (2008) ‘Predictive value of PTEN and AR coexpression of sustained responsiveness to hormonal therapy in prostate cancer--a pilot study’, *Neoplasia (New York, N.Y.)*. Neoplasia Press, 10(9), pp. 949–953. doi: 10.1593/neo.08582.

Shen, J., Zhang, L. and Zhao, R. (2007) ‘Biochemical characterization of the ATPase and helicase activity of UAP56, an essential pre-mRNA splicing and mRNA export factor’, *Journal of Biological Chemistry*, 282(31), pp. 22544–22550. doi: 10.1074/jbc.M702304200.

Shen, L. *et al*. (2019) ‘Probing the Druggablility on the Interface of the Protein-Protein Interaction and Its Allosteric Regulation Mechanism on the Drug Screening for the CXCR4 Homodimer’, *Frontiers in Pharmacology*, 10, p. 1310. doi: 10.3389/fphar.2019.01310.

Sheng, Y. *et al*. (2006) ‘Gonadotropin-regulated Testicular RNA Helicase (GRTH/Ddx25) Is a Transport Protein Involved in Gene-specific mRNA Export and Protein Translation during Spermatogenesis’, *Journal of Biological Chemistry* , 281(46), pp. 35048–35056. doi: 10.1074/jbc.M605086200.

Shi, C., Chen, X. and Tan, D. (2019) ‘Development of patient-derived xenograft models of prostate cancer for maintaining tumor heterogeneity’, *Translational andrology and urology*. AME Publishing Company, 8(5), pp. 519–528. doi: 10.21037/tau.2019.08.31.

Shi, Y. (2009) ‘Serine/Threonine Phosphatases: Mechanism through Structure’, *Cell*. Elsevier, 139(3), pp. 468–484. doi: 10.1016/j.cell.2009.10.006.

Shorning, B. Y. *et al*. (2020) ‘The PI3K-AKT-mTOR Pathway and Prostate Cancer: At the Crossroads of AR, MAPK, and WNT Signaling’, *International journal of molecular sciences*. MDPI, 21(12), p. 4507. doi: 10.3390/ijms21124507.

Shwab, E. K. *et al*. (2017) ‘A Novel Phosphoregulatory Switch Controls the Activity and Function of the Major Catalytic Subunit of Protein Kinase A in Aspergillus fumigatus’, *mBio*. Edited by T. L. A. Doering David Brakhage, Axel, 8(1), pp. e02319-16. doi: 10.1128/mBio.02319-16.

Sidelsky, S., Setia, S. and Vourganti, S. (2017) ‘Spatial Tracking of Targeted Prostate Biopsy Locations: Moving Towards Effective Focal Partial Prostate Gland

Ablation with Improved Treatment Planning', *Current Urology Reports*. Current Urology Reports, 18(12). doi: 10.1007/s11934-017-0741-4.

Sigismund, S., Avanzato, D. and Lanzetti, L. (2018) 'Emerging functions of the EGFR in cancer', *Molecular oncology*. 2017/11/27. John Wiley and Sons Inc., 12(1), pp. 3–20. doi: 10.1002/1878-0261.12155.

Silverman, E., Edwalds-Gilbert, G. and Lin, R.-J. (2003) 'DExD/H-box proteins and their partners: helping RNA helicases unwind', *Gene*, 312, pp. 1–16. doi: https://doi.org/10.1016/S0378-1119(03)00626-7.

Simonetta, K. R. *et al.* (2019) 'Prospective discovery of small molecule enhancers of an E3 ligase-substrate interaction', *Nature Communications*, 10(1), p. 1402. doi: 10.1038/s41467-019-09358-9.

Sin, Y. Y. *et al.* (2011) 'Disruption of the cyclic AMP phosphodiesterase-4 (PDE4)-HSP20 complex attenuates the β-agonist induced hypertrophic response in cardiac myocytes', *Journal of Molecular and Cellular Cardiology*, 50(5), pp. 872–883. doi: https://doi.org/10.1016/j.yjmcc.2011.02.006.

Singer, E. A. *et al.* (2008) 'Androgen deprivation therapy for prostate cancer', *Expert Opinion on Pharmacotherapy*, 9(2), pp. 211–228. doi: 10.1517/14656566.9.2.211.

Singh, A. S. *et al.* (2005) 'Mechanisms of disease: Polymorphisms of androgen regulatory genes in the development of prostate cancer', *Nature Clinical Practice Urology*, 2(2), pp. 101–107. doi: 10.1038/ncpuro0091.

Singh, V. *et al.* (2017) 'Phosphorylation: Implications in Cancer', *The Protein Journal*, 36(1), pp. 1–6. doi: 10.1007/s10930-017-9696-z.

Skourti-Stathaki, K. and Proudfoot, N. J. (2014) 'A double-edged sword: R loops as threats to genome integrity and powerful regulators of gene expression', *Genes and Development*, 28(13), pp. 1384–1396. doi: 10.1101/gad.242990.114.

Smith, D. B. and Johnson, K. S. (1988) 'Single-step purification of polypeptides expressed in Escherichia coli as fusions with glutathione S-transferase', *Gene*, 67(1), pp. 31–40. doi: https://doi.org/10.1016/0378-1119(88)90005-4.

Smith, F. D. and Scott, J. D. (2018) 'Protein kinase A activation: Something new

under the sun?', *Journal of Cell Biology*, 217(6), pp. 1895–1897. doi: 10.1083/jcb.201805011.

Smith, J. *et al*. (2010) 'Chapter 3 - The ATM–Chk2 and ATR–Chk1 Pathways in DNA Damage Signaling and Cancer', in Vande Woude, G. F. and Klein, G. B. T.-A. in C. R. (eds). Academic Press, pp. 73–112. doi: https://doi.org/10.1016/B978-0-12-380888-2.00003-0.

Smith, W. A. *et al*. (2004) 'Arginine Methylation of RNA Helicase A Determines Its Subcellular Localization', *Journal of Biological Chemistry* , 279(22), pp. 22795–22798. doi: 10.1074/jbc.C300512200.

Smits, A. H. and Vermeulen, M. (2016) 'Characterizing Protein–Protein Interactions Using Mass Spectrometry: Challenges and Opportunities', *Trends in Biotechnology*. Elsevier Ltd, 34(10), pp. 825–834. doi: 10.1016/j.tibtech.2016.02.014.

Sobel, R. E. and Sadar, M. D. (2005) 'Cell lines used in prostate cancer research: A compendium of old and new lines - Part 1', *The Journal of Urology*, 173(2), pp. 342–359. doi: https://doi.org/10.1097/01.ju.0000141580.30910.57.

Søberg, K. *et al*. (2017) 'Evolution of the cAMP-dependent protein kinase (PKA) catalytic subunit isoforms', *PloS one*. Public Library of Science, 12(7), pp. e0181091–e0181091. doi: 10.1371/journal.pone.0181091.

Soni, S., Anand, P. and Padwad, Y. S. (2019) 'MAPKAPK2: the master regulator of RNA-binding proteins modulates transcript stability and tumor progression', *Journal of Experimental & Clinical Cancer Research*, 38(1), p. 121. doi: 10.1186/s13046-019-1115-1.

Sousa, E. *et al*. (2013) 'Enoxacin inhibits growth of prostate cancer cells and effectively restores microRNA processing', *Epigenetics*. 2013/04/17. Landes Bioscience, 8(5), pp. 548–558. doi: 10.4161/epi.24519.

Speranzini, V., Fish, A. and Mattevi, A. (2014) 'Protein-ligand binding measurements using fluorescence polarization', *BMG LabTech*, 10, pp. 1–2. Available at: https://www.bmglabtech.com/fileadmin/06_Support/Download_Documents/Application_Notes/AN256.pdf.

Statz, C. M., Patterson, S. E. and Mockus, S. M. (2017) 'mTOR Inhibitors in Castration-Resistant Prostate Cancer: A Systematic Review', *Targeted Oncology*, 12(1), pp. 47–59. doi: 10.1007/s11523-016-0453-6.

Stavridis, S. *et al.* (2010) 'Screening for prostate cancer: a controversy or fact', *Hippokratia*. LITHOGRAPHIA Antoniadis I.-Psarras Th. G.P., 14(3), pp. 170–175. Available at: https://pubmed.ncbi.nlm.nih.gov/20981165.

van der Steen, T., Tindall, D. J. and Huang, H. (2013) 'Posttranslational modification of the androgen receptor in prostate cancer', *International Journal of Molecular Sciences*, 14(7), pp. 14833–14859. doi: 10.3390/ijms140714833.

Stish, B. J. *et al.* (2018) 'Low dose rate prostate brachytherapy', *Translational Andrology and Urology*, 7(3), pp. 341–356. doi: 10.21037/tau.2017.12.15.

van Strijp, D. *et al.* (2018) 'The Prognostic PDE4D7 Score in a Diagnostic Biopsy Prostate Cancer Patient Cohort with Longitudinal Biological Outcomes', *Prostate Cancer*, 2018, pp. 1–11. doi: 10.1155/2018/5821616.

Su, Y.-F. *et al.* (2012) 'Phosphorylation-Dependent SUMOylation of the Transcription Factor NF-E2', *PLOS ONE*. Public Library of Science, 7(9), p. e44608. Available at: https://doi.org/10.1371/journal.pone.0044608.

Suhasini, A. N. and Brosh Jr, R. M. (2013) 'DNA helicases associated with genetic instability, cancer, and aging', *Advances in experimental medicine and biology*, 767, pp. 123–144. doi: 10.1007/978-1-4614-5037-5_6.

Sun, A.-Q. *et al.* (2013) 'Identification of functionally relevant lysine residues that modulate human farnesoid X receptor activation', *Molecular pharmacology*. 2013/03/05. The American Society for Pharmacology and Experimental Therapeutics, 83(5), pp. 1078–1086. doi: 10.1124/mol.113.084772.

Sun, R. *et al.* (2019) 'Mitosis-related phosphorylation of the eukaryotic translation suppressor 4E-BP1 and its interaction with eukaryotic translation initiation factor 4E (eIF4E)', *The Journal of biological chemistry*. 2019/06/14. American Society for Biochemistry and Molecular Biology, 294(31), pp. 11840–11852. doi: 10.1074/jbc.RA119.008512.

Sun, W. *et al.* (2017) 'EWS-FLI1 and RNA helicase A interaction inhibitor YK-4-279 inhibits growth of neuroblastoma', *Oncotarget; Vol 8, No 55*. Available at:

https://www.oncotarget.com/article/21933/text/.

Sunassee, A., Al Sannaa, G. and Ro, J. (2019) ‘Intraductal carcinoma of prostate (IDC-P), grade group, and molecular pathology: recent advances and practical implication’, *Ann Urol Oncol*, 2(1), pp. 9–18.

Swanson, T. A. *et al*. (2011) ‘TMPRSS2/ERG fusion gene expression alters chemo- and radio-responsiveness in cell culture models of androgen independent prostate cancer’, *The Prostate*. John Wiley & Sons, Ltd, 71(14), pp. 1548–1558. doi: 10.1002/pros.21371.

Tan, M. E. *et al*. (2015) ‘Androgen receptor: Structure, role in prostate cancer and drug discovery’, *Acta Pharmacologica Sinica*. Nature Publishing Group, 36(1), pp. 3–23. doi: 10.1038/aps.2014.18.

Tanner, N. K. and Linder, P. (2001a) ‘DExD/H Box RNA Helicases: From Generic Motors to Specific Dissociation Functions’, *Molecular Cell*. Cell Press, 8(2), pp. 251–262. doi: 10.1016/S1097-2765(01)00329-X.

Tanner, N. K. and Linder, P. (2001b) ‘DExD/H Box RNA Helicases: From Generic Motors to Specific Dissociation Functions’, *Molecular Cell*, 8(2), pp. 251–262. doi: https://doi.org/10.1016/S1097-2765(01)00329-X.

Thacker, U. *et al*. (2020) ‘Identification of DHX9 as a cell cycle regulated nucleolar recruitment factor for CIZ1’, *Scientific Reports*, 10(1), p. 18103. doi: 10.1038/s41598-020-75160-z.

Thomas, B. C. and Neal, D. E. (2013) ‘Androgen deprivation treatment in prostate cancer’, *BMJ (Online)*, 346(7893), pp. 1–5. doi: 10.1136/bmj.e8555.

Thomas, C. *et al*. (2013) ‘Synergistic targeting of PI3K/AKT pathway and androgen receptor axis significantly delays castration-resistant prostate cancer progression in vivo’, *Molecular Cancer Therapeutics*, 12(11), pp. 2342–2355. doi: 10.1158/1535-7163.mct-13-0032.

Thompson, I. M. (2001) ‘Flare Associated with LHRH-Agonist Therapy.’, *Reviews in urology*, 3 Suppl 3, pp. S10-4. Available at: http://www.ncbi.nlm.nih.gov/pubmed/16986003%0Ahttp://www.pubmedcentral.nih.gov/articlerender.fcgi?artid=PMC1476081.

Thundimadathil, J. (2012) ‘Cancer Treatment Using Peptides: Current Therapies and Future Prospects’, *Journal of Amino Acids*, 2012, pp. 1–13. doi: 10.1155/2012/967347.

Tibbo, A. J., Tejeda, G. S. and Baillie, G. S. (2019) ‘Understanding PDE4’s function in Alzheimer’s disease; a target for novel therapeutic approaches’, *Biochemical Society transactions*. Portland Press Ltd., 47(5), pp. 1557–1565. doi: 10.1042/BST20190763.

Toivanen, R. and Shen, M. M. (2017) ‘Prostate organogenesis: tissue induction, hormonal regulation and cell type specification’, *Development*, 144(8), pp. 1382–1398. doi: 10.1242/dev.148270.

Tomlins, S. A. *et al.* (2009) ‘ETS Gene Fusions in Prostate Cancer: From Discovery to Daily Clinical Practice’, *European Urology*, 56(2), pp. 275–286. doi: 10.1016/j.eururo.2009.04.036.

Tompa, P. *et al.* (2014) ‘A Million Peptide Motifs for the Molecular Biologist’, *Molecular Cell*. Elsevier, 55(2), pp. 161–169. doi: 10.1016/j.molcel.2014.05.032.

Tsalkova, T. *et al.* (2009) ‘Mechanism of Epac activation: structural and functional analyses of Epac2 hinge mutants with constitutive and reduced activities’, *The Journal of biological chemistry*. 2009/06/24. American Society for Biochemistry and Molecular Biology, 284(35), pp. 23644–23651. doi: 10.1074/jbc.M109.024950.

Tuteja, N. (2009) ‘Signaling through G protein coupled receptors’, *Plant Signaling and Behavior*, 4(10), pp. 942–947. doi: 10.4161/psb.4.10.9530.

Uhlen, M. *et al.* (2017) ‘A pathology atlas of the human cancer transcriptome’, *Science*, 357(6352), p. eaan2507. doi: 10.1126/science.aan2507.

Valkenburg, K. C. and Williams, B. O. (2011) ‘Mouse models of prostate cancer’, *Prostate cancer*. 2011/02/23. Hindawi Publishing Corporation, 2011, p. 895238. doi: 10.1155/2011/895238.

Varenhorst, E. *et al.* (2016) ‘Predictors of early androgen deprivation treatment failure in prostate cancer with bone metastases’, *Cancer medicine*. 2016/01/14. John Wiley and Sons Inc., 5(3), pp. 407–414. doi: 10.1002/cam4.594.

Verze, P., Cai, T. and Lorenzetti, S. (2016) 'The role of the prostate in male fertility, health and disease', *Nature Reviews Urology*. Nature Publishing Group, 13(7), pp. 379–386. doi: 10.1038/nrurol.2016.89.

Virtanen, V. *et al.* (2019) 'PARP Inhibitors in Prostate Cancer—The Preclinical Rationale and Current Clinical Development', *Genes*. MDPI, 10(8), p. 565. doi: 10.3390/genes10080565.

Visakorpi, T. *et al.* (1995) 'In vivo amplification of the androgen receptor gene and progression of human prostate cancer', *Nature Genetics*, 9, pp. 401–406.

Vitkin, N. *et al.* (2019) 'The Tumor Immune Contexture of Prostate Cancer', *Frontiers in immunology*. Frontiers Media S.A., 10, p. 603. doi: 10.3389/fimmu.2019.00603.

Vitrac, H., Mallampalli, V. K. P. S. and Dowhan, W. (2019) 'Importance of phosphorylation/dephosphorylation cycles on lipid-dependent modulation of membrane protein topology by posttranslational phosphorylation', *Journal of Biological Chemistry* , 294(49), pp. 18853–18862. doi: 10.1074/jbc.RA119.010785.

Voet, A. R. D. *et al.* (2014) 'Discovery of small molecule inhibitors targeting the SUMO–SIM interaction using a protein interface consensus approach', *MedChemComm*. The Royal Society of Chemistry, 5(6), pp. 783–786. doi: 10.1039/C3MD00391D.

Volkmer, R., Tapia, V. and Landgraf, C. (2012) 'Synthetic peptide arrays for investigating protein interaction domains', *FEBS Letters*. John Wiley & Sons, Ltd, 586(17), pp. 2780–2786. doi: 10.1016/j.febslet.2012.04.028.

Wada, A. *et al.* (2019) 'Efficient Prostate Cancer Therapy with Tissue-Specific Homing Peptides Identified by Advanced Phage Display Technology', *Molecular therapy oncolytics*. American Society of Gene & Cell Therapy, 12, pp. 138–146. doi: 10.1016/j.omto.2019.01.001.

Waller, D. G. and Sampson, A. P. (2018) '46 - Androgens, antiandrogens and anabolic steroids', in Waller, D. G. and Sampson, A. P. B. T.-M. P. and T. (Fifth E. (eds). Elsevier, pp. 531–535. doi: https://doi.org/10.1016/B978-0-7020-7167-6.00046-4.

Walstrom, K. M. *et al.* (2005) 'RNA helicase A is important for germline transcriptional control, proliferation, and meiosis in C. elegans', *Mechanisms of Development*, 122(5), pp. 707–720. doi: https://doi.org/10.1016/j.mod.2004.12.002.

Wang, D. *et al.* (2003) 'Cloning and characterization of novel PDE4D isoforms PDE4D6 and PDE4D7', *Cellular Signalling*, 15(9), pp. 883–891. doi: https://doi.org/10.1016/S0898-6568(03)00042-1.

Wang, G. *et al.* (2006) 'Identification of genes targeted by the androgen and PKA signaling pathways in prostate cancer cells', *Oncogene*, 25(55), pp. 7311–7323. doi: 10.1038/sj.onc.1209715.

Wang, H. *et al.* (2009) 'P68 RNA helicase is a nucleocytoplasmic shuttling protein', *Cell Research*, 19(12), pp. 1388–1400. doi: 10.1038/cr.2009.113.

Wang, J. *et al.* (2006) 'Expression of variant TMPRSS2/ERG fusion messenger RNAs is associated with aggressive prostate cancer', *Cancer Research*, 66(17), pp. 8347–8351. doi: 10.1158/0008-5472.CAN-06-1966.

Wang, X. *et al.* (2014) 'Helicase Assays', *Bio-protocol*. 2014/03/20, 4(6), p. e1079. doi: 10.21769/bioprotoc.1079.

Wang, X. *et al.* (2017) 'Development of Peptidomimetic Inhibitors of the ERG Gene Fusion Product in Prostate Cancer', *Cancer cell*. 2017/03/23, 31(4), pp. 532-548.e7. doi: 10.1016/j.ccell.2017.02.017.

Wang, Y.-C., Peterson, S. E. and Loring, J. F. (2014) 'Protein post-translational modifications and regulation of pluripotency in human stem cells', *Cell Research*, 24(2), pp. 143–160. doi: 10.1038/cr.2013.151.

Wei, X. *et al.* (2004) 'Analysis of the RNA helicase A gene in human lung cancer', *Oncology Reports*, 11(1), pp. 253–258.

Wen, A. Y., Sakamoto, K. M. and Miller, L. S. (2010) 'The Role of the Transcription Factor CREB in Immune Function', *The Journal of Immunology*, 185(11), pp. 6413 LP – 6419. doi: 10.4049/jimmunol.1001829.

Whitmarsh, A. J. and Davis, R. J. (2000) 'Regulation of transcription factor function by phosphorylation', *Cellular and Molecular Life Sciences*, 57(8–9), pp.

1172–1183. doi: 10.1007/PL00000757.

Willder, J. M. *et al*. (2013) 'Androgen receptor phosphorylation at serine 515 by Cdk1 predicts biochemical relapse in prostate cancer patients', *British Journal of Cancer*. Nature Publishing Group, 108(1), pp. 139–148. doi: 10.1038/bjc.2012.480.

Williams, A. J. *et al*. (2003) 'Regulated phosphorylation of 40S ribosomal protein S6 in root tips of maize', *Plant physiology*. The American Society for Plant Biologists, 132(4), pp. 2086–2097. doi: 10.1104/pp.103.022749.

Willoughby, D. *et al*. (2006) 'An anchored PKA and PDE4 complex regulates subplasmalemmal cAMP dynamics', *The EMBO journal*. 2006/04/27, 25(10), pp. 2051–2061. doi: 10.1038/sj.emboj.7601113.

Wilt, T. J. (2003) 'Prostate cancer: epidemiology and screening', *Reviews in urology*. MedReviews, LLC, 5 Suppl 6(Suppl 6), pp. S3–S9. Available at: https://pubmed.ncbi.nlm.nih.gov/16985974.

WINTERS, B. *et al*. (2017) 'Inhibition of ERG Activity in Patient-derived Prostate Cancer Xenografts by YK-4-279', *Anticancer Research* , 37(7), pp. 3385–3396. Available at: http://ar.iiarjournals.org/content/37/7/3385.abstract.

Wolff, B., Sanglier, J. J. and Wang, Y. (1997) 'Leptomycin B is an inhibitor of nuclear export: Inhibition of nucleo-cytoplasmic translocation of the human immunodeficiency virus type 1 (HIV-1) Rev protein and Rev-dependent mRNA', *Chemistry and Biology*, 4(2), pp. 139–147. doi: 10.1016/S1074-5521(97)90257-X.

Woodsmith, J., Kamburov, A. and Stelzl, U. (2013) 'Dual Coordination of Post Translational Modifications in Human Protein Networks', *PLOS Computational Biology*. Public Library of Science, 9(3), p. e1002933. Available at: https://doi.org/10.1371/journal.pcbi.1002933.

Wu, X. *et al*. (2013) 'Current mouse and cell models in prostate cancer research', *Endocrine-related cancer*, 20(4), pp. R155–R170. doi: 10.1530/ERC-12-0285.

Xie, M. *et al*. (2014) 'The upstream conserved regions (UCRs) mediate homo- and hetero-oligomerization of type 4 cyclic nucleotide phosphodiesterases (PDE4s)', *The Biochemical journal*, 459(3), pp. 539–550. doi: 10.1042/BJ20131681.

Xu, D. *et al.* (2012) 'Sequence and structural analyses of nuclear export signals in the NESdb database', *Molecular biology of the cell*. 2012/07/25. The American Society for Cell Biology, 23(18), pp. 3677–3693. doi: 10.1091/mbc.E12-01-0046.

Xu, J. and Qiu, Y. (2016) 'Role of androgen receptor splice variants in prostate cancer metastasis', *Asian Journal of Urology*. Elsevier Ltd, 3(4), pp. 177–184. doi: 10.1016/j.ajur.2016.08.003.

Xu, Y. *et al.* (2006) 'Androgens Induce Prostate Cancer Cell Proliferation through Mammalian Target of Rapamycin Activation and Post-transcriptional Increases in Cyclin D Proteins', *Cancer Research*, 66(15), pp. 7783 LP – 7792. doi: 10.1158/0008-5472.CAN-05-4472.

Xu, Y. *et al.* (2019) 'DHX15 is up-regulated in castration-resistant prostate cancer and required for androgen receptor sensitivity to low DHT concentrations', *The Prostate*. 2019/02/03, 79(6), pp. 657–666. doi: 10.1002/pros.23773.

Yan, K. *et al.* (2016) 'The cyclic AMP signaling pathway: Exploring targets for successful drug discovery (Review)', *Molecular medicine reports*. 2016/03/18. D.A. Spandidos, 13(5), pp. 3715–3723. doi: 10.3892/mmr.2016.5005.

Yan, Xueli *et al.* (2019) 'DHX9 inhibits epithelial-mesenchymal transition in human lung adenocarcinoma cells by regulating STAT3', *American journal of translational research*. e-Century Publishing Corporation, 11(8), pp. 4881–4894. Available at: https://www.ncbi.nlm.nih.gov/pubmed/31497206.

Yang, H. and Yang, L. (2016) 'Targeting cAMP/PKA pathway for glycemic control and type 2 diabetes therapy', *Journal of Molecular Endocrinology*. Bristol, UK: Bioscientifica Ltd, 57(2), pp. R93–R108. doi: 10.1530/JME-15-0316.

Yang, X. J. and Grégoire, S. (2006) 'A Recurrent Phospho-Sumoyl Switch in Transcriptional Repression and Beyond', *Molecular Cell*, 23(6), pp. 779–786. doi: 10.1016/j.molcel.2006.08.009.

Yu, L. *et al.* (2017) 'The Effects and Mechanism of YK-4-279 in Combination with Docetaxel on Prostate Cancer', *International journal of medical sciences*. Ivyspring International Publisher, 14(4), pp. 356–366. doi: 10.7150/ijms.18382.

Zainuddin, A. *et al.* (2010) 'Effect of experimental treatment on GAPDH mRNA expression as a housekeeping gene in human diploid fibroblasts', *BMC Molecular Biology*, 11(1), p. 59. doi: 10.1186/1471-2199-11-59.

Zhang, K. Y. J. *et al.* (2005) 'Phosphodiesterase-4 as a potential drug target', *Expert Opinion on Therapeutic Targets*. Taylor & Francis, 9(6), pp. 1283–1305. doi: 10.1517/14728222.9.6.1283.

Zhang, P. *et al.* (2012) 'Structure and allostery of the PKA RIIß tetrameric holoenzyme.', *Science (New York, N.Y.)*, 335(6069), pp. 712–716. doi: 10.1126/science.1213979.

Zhang, S. *et al.* (2004) 'DNA-dependent protein kinase (DNA-PK) phosphorylates nuclear DNA helicase II/RNA helicase A and hnRNP proteins in an RNA-dependent manner', *Nucleic acids research*. Oxford University Press, 32(1), pp. 1–10. doi: 10.1093/nar/gkg933.

Zhang, S. *et al.* (2019) 'The Prognostic Role of Ribosomal Protein S6 Kinase 1 Pathway in Patients With Solid Tumors: A Meta-Analysis', *Frontiers in Oncology*, 9, p. 390. doi: 10.3389/fonc.2019.00390.

Zhang, S. and Grosse, F. (1997) 'Domain Structure of Human Nuclear DNA Helicase II (RNA Helicase A)', *Journal of Biological Chemistry* , 272(17), pp. 11487–11494. doi: 10.1074/jbc.272.17.11487.

Zhang, S. and Grosse, F. (2004) 'Multiple Functions of Nuclear DNA Helicase II (RNA Helicase A) in Nucleic Acid Metabolism', *Acta Biochimica et Biophysica Sinica*, 36(3), pp. 177–183. doi: 10.1093/abbs/36.3.177.

Zhao, Q. *et al.* (2014) 'GPS-SUMO: a tool for the prediction of sumoylation sites and SUMO-interaction motifs', *Nucleic Acids Research*, 42(W1), pp. W325–W330. doi: 10.1093/nar/gku383.

Zhou, F. *et al.* (2019) 'TMPRSS2-ERG activates NO-cGMP signaling in prostate cancer cells', *Oncogene*. Springer US, 38(22), pp. 4397–4411. doi: 10.1038/s41388-019-0730-9.

Zhou, H. *et al.* (2013) 'Toward a Comprehensive Characterization of a Human Cancer Cell Phosphoproteome', *Journal of Proteome Research*. American Chemical Society, 12(1), pp. 260–271. doi: 10.1021/pr300630k.

Zhu, W. *et al*. (2017) 'The cAMP-PKA Signaling Pathway Regulates Pathogenicity, Hyphal Growth, Appressorial Formation, Conidiation, and Stress Tolerance in Colletotrichum higginsianum', *Frontiers in Microbiology*, 8, p. 1416. doi: 10.3389/fmicb.2017.01416.